AYK SSI [Required SSSF / PCSRF form]

Final Report Summary Format: PART 1 OF 2

Project Number: 45491 and 45557

Project Title: AYK: Factors Affecting Chum Growth & Condition - Parts 1 and 2

Project Manager: Ed Farley
NOAA/NMFS AFSC, Auke Bay Laboratories
17109 Point Lena Loop Road
Juneau, AK 99801
Phone: (907) 789-6085
Email: ed.farley@noaa.gov

Duration of Project: May 1, 2006 – April 30, 2009

Abstract:

Our goal was to examine control of marine survival of salmon smolts within the context of the critical size and period hypothesis by examining trophic and bioenergetic processes influencing growth and survival of chum salmon during their juvenile life history stage.

Approach: *Detailed description of the work that was done, including (if applicable) methods or techniques, materials used, design of the study, sample sizes planned, kind of controls and proposed analysis for results. Project management, including list of individuals and/or organizations actually performing the work and how it was done.*

Obj.1:Development of the comprehensive database for chum salmon. The OCC/BASIS cruise data on size (length and weight), catch per unit effort, diet, condition, scale-based size-at-age (scale radius-at-circuli) of juvenile chum salmon (2001-2007) was assimilated into a comprehensive database. In addition, comparable data sets from OCC/BASIS oceanographic research (2001-2007, Eisner) on spatial-temporal distribution of water mass characteristics (e.g. temperature, salinity, nutrients, chlorophyll a), and zooplankton were completed, edited and assimilated into the comprehensive chum salmon data base.

Obj.2:Develop estimates for the density and biomass of exploitable forage available to salmon by processing and maintaining a database of prey size and species, and spatial-temporal patterns of prey availability to salmon when they are actively foraging. Plankton samples are collected at each station, and preserved in formalin. Zooplankton samples collected during OCC/BASIS research cruises (2005 – 2007) were processed (under contract) in accordance with protocols developed by the Alaska Fisheries Science Center for zooplankton collections in the North Pacific Ocean. Estimates of ichthyoplankton (i.e. age-0

pollock) biomass developed from surface trawl catches and determined following methods of Farley and Trudel (in press).

Obj.3:Compare outmigration timing, estuarine residency, and growth histories in marine habitats occupied by juvenile Yukon and Kuskokwim chum salmon using otolith chemistry. Reconstructing migration and habitat utilization patterns from otolith chemistry will improve our understanding of juvenile salmon ecology and linkages between salmon growth and bioenergetic models of consumption and growth efficiency (Objs. 4, 8). Strontium levels in otoliths vary with salinity (Figure 3) and can be used to identify transition of anadromous fish between freshwater to marine habitats (Kimura et al. 2000; Secor et al. 1995; Figure 4). We will attempt to combine otolith chemistry with daily age information to reconstruct migration timing and habitat utilization patterns between freshwater, estuarine, and marine habitats varying in salinity (Figure 5). Chum salmon otoliths collected during juvenile salmon surveys by the Alaska Fisheries Science Center will be sent to the otolith laboratory at the University of Alaska, Fairbanks (UAF) and methods for preparing otoliths and assaying otolith microchemistry will follow methods described by (Secor 2001). One of the sagittal otoliths will be assayed for microchemistry composition using a newly installed laser ablation system at the University of Alaska, Fairbanks. The second sagittal otolith will be thin-sectioned, digitized, and used for daily age and growth estimates. The UAF laser ablation (LA) system will be interfaced with an inductively coupled plasma mass-spectrometer (7500 ICP-MS, Agilent),. The LA-ICP-MS system is a relatively new technique that is particularly well suited to otolith chemistry assays. ICP-MS analysis can also assay inter-element ratios, such as Sr/Ca, with precision (0.05% relative standard deviation [RSD]) approaching that of thermal ionization mass spectrometry. Mg/Ca, Mn/Ca, Sr/Ca and Ba/Ca ratios in the otoliths will be assayed along with other trace elements that provide a distinguishable signature from the otolith core to edge.

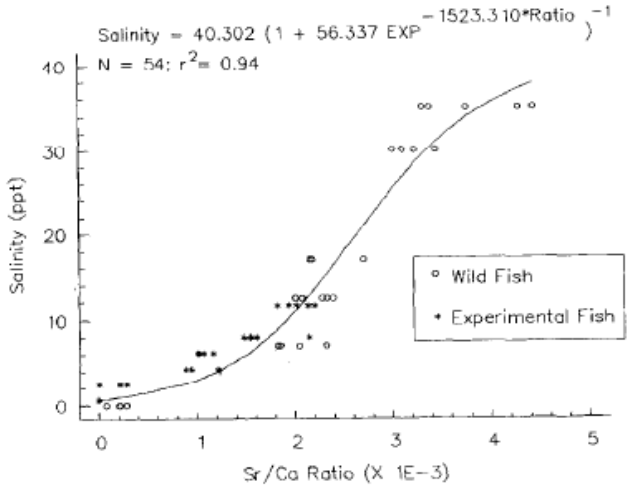

Figure 3 (from Secor et al. 1995). Logistic relationship between salinity and otolith Sr/Ca ratio for experimental and wild striped bass, *Morone saxatilis* (Walbaum).

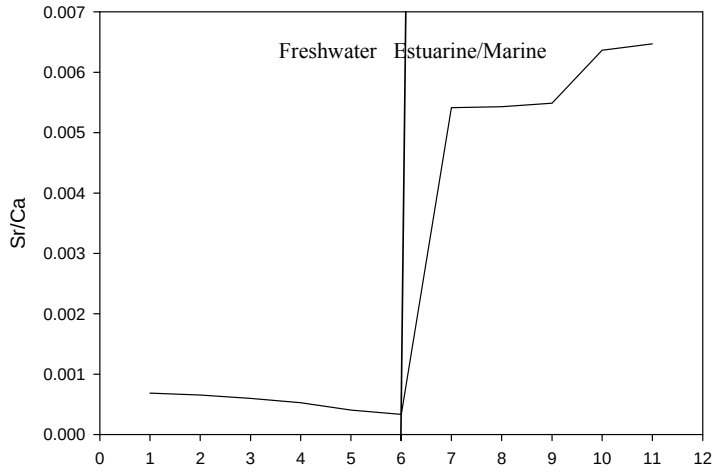

Figure 4. Sr/Ca ratios from a juvenile Chinook salmon otolith from the Bering Sea. Sr/Ca ratios track salinity and identify variable salinity habitats utilized by Chinook salmon.

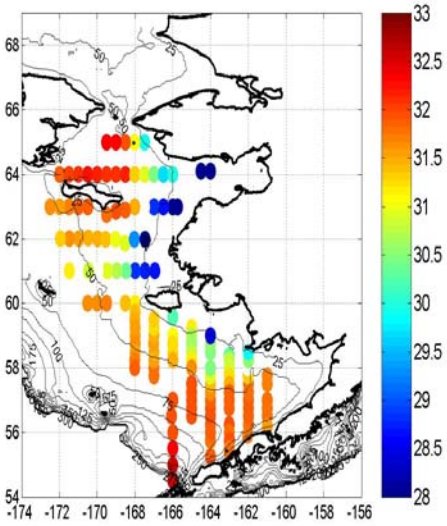

Figure 5. Sea surface salinities (PSU) collected a during the 2002 Bering-Aleutian Salmon International Survey by the Alaska Fisheries Science Center. Surface salinities identify the

location of the salinity front separating the low salinity coastal domain from higher salinity habitats on the eastern Bering Sea shelf.

Obj.4: Reconstruct growth histories of juvenile Yukon and Kuskokwim chum salmon in estuarine and marine habitats using otolith and scale growth patterns. A number of studies have examined the application of scale and otolith formation patterns to reconstructing growth histories in salmon (Wells et al. 2003; Courtney 2000; Fukuwaka 1988; Volk et at. 1984). These studies have shown that although otolith increment patterns are positively correlated with instantaneous growth rate, scale circuli patterns are more correlated to somatic growth than otolith increment patterns. This is due to the fact that scale formation is directly tied to body size whereas otolith formation is tied to metabolic activity (protein synthesis) of fish (Campana & Thorrold 2001). However, growth histories from scales are dependent on obtaining scales from the preferred body region and therefore can be impacted by capture methods. Otoliths may provide a more reliable measure of mean growth for sampling methods resulting in limited recovery of scales from the preferred body region. Due to scale loss of juvenile salmon in trawls used during our survey, less than 10% of chum salmon retain scales from the preferred region. This significantly reduces sample sizes for growth summaries and potentially biases the results to larger, faster growing individuals. The ability to link otolith growth with habitat utilization patterns (Obj. 3) from otolith chemistry can also increase the interpretive power of otolith over scale growth. Therefore, it is useful to apply both otolith and scale growth data to the reconstruction of growth histories in juvenile salmon.

Periodicity in otolith increment formation occurs at daily intervals during larval and early juvenile life-history stages of fish and can be used to estimate daily age and growth rates of fish (Campana and Neilson, 1985). Volk et al. (1984), and Fukuwaka (1988) validated daily periodicity in otolith increment formation in juvenile hatchery chum salmon; Courtney et al. (2000) validated daily increment formation during the first summer at sea in juvenile pink salmon in southeast Alaska. We will use thermally-marked juvenile chum salmon otoliths recovered by the Auke Bay Laboratory (Farley and Munk 1997) to validate periodicity in otolith increment formation.

Laboratory analysis of otoliths and scales will be completed as a collaborative effort between the National Marine Fisheries Service (NMFS), Alaska Dept. of Fish and Game (ADF&G), and the University of Alaska, Fairbanks (UAF). Scales from the preferred body region will be collected and mounted on scale gum-cards at sea. Acetate impressions of the scales will be made at the Auke Bay Laboratory, NMFS and digitized at the Mark, Tag, and Age Laboratory, ADF&G in Juneau Alaska following methods described in Hagen et al. (2001). Otoliths will be extracted from fish heads at the Auke Bay Laboratory and sent to the otolith laboratory at the University of Alaska for thin-sectioning and digitizing in a manner described by Courtney et al. (2000).

Obj.5: Map interannual variation in habitat (coastal, inner front, and middle domains) and ocean conditions along the eastern Bering Sea shelf. Vertical casts were conducted at all stations with a CTD (SBE19, SBE25 or SBE-911, Sea-Bird) with compact carousel. Additional sensors measure chlorophyll a fluorescence (WETStar, WET Labs), light transmission (C-Star, WET Labs), optical backscatter (turbidity measurement, D&A

Instruments), photosynthetic available radiation (PAR, LI-193 spherical quantum sensor, LI-COR), and dissolved oxygen (SBE-43, Sea-Bird). Surface (3 m) along track thermosalinograph (SBE-45, Sea-Bird) data were collected at 5 second intervals to evaluate fine scale changes in water mass (temperature, salinity) properties throughout the eastern Bering Sea. CTD and thermosalinograph data were processed using Sea-Bird data processing modules and stored in Access databases.

Water samples were collected with the CTD carousel system for salinity, nutrients, chlorophyll a, microzooplankton and phytoplankton species and High Performance Liquid Chromatography (HPLC). Salinity samples were collected at a limited number of stations and depths, focusing on the pycnocline where salinity spiking can occur. For nutrients and chlorophyll a (total and size fractionated for > 2, > 5, > 10 μm), samples were collected above and below the pycnocline at two-six depths and stored frozen until analysis. Nutrient samples were analyzed for nitrate, ammonium, phosphate and silicate at the University of Washington Marine Chemistry Laboratory (UNESCO, 1994). Chlorophyll a samples were analyzed using the fluorometric acidification method (Parsons et al. 1984) with a bench top fluorometer (Turner model TD-700) at Auke Bay Laboratory. Microzooplankton and phytoplankton species were collected at 5 m and at the chlorophyll maximum with the CTD carousel using 5 L Niskin bottles and preserved in 10% acid Lugols (Throndsen 1978). Phytoplankton species samples were also preserved in buffered (sodium borate) 1% formalin (Throndsen 1978) since some species (e.g. coccolithophores) were not well preserved in Lugols. All data were integrated into Access databases.

The southeastern Bering Sea shelf was differentiated into three bathymetrically fixed domains, including the Coastal Domain extending from near shore to approximately 50 m depth, the Middle Domain between 50 m and 100 m depth, and the Outer Domain (Coachman 1986).

Obj.6: Determine the interannual variation in diet composition of chum salmon among the coastal waters of western Alaska and oceanographic characteristics along the eastern Bering Sea shelf. Interannual (2002 – 2007) variation in diet composition of chum salmon within oceanographic water masses (based on temperature and salinity profiles) designated as the Coastal Domain, Inner Front, and Middle Domain. With each trawl station as the sampling unit, mean values for prey weight, diet composition, feeding intensity, and caloric value of the diet were calculated. Stations were grouped by oceanographic water mass, and stratified by region (Yukon and Kuskokwim), and year. To determine if there are significant regional and temporal differences in salmon diet among different water masses, data were analyzed using ANOVA (fixed effects) methods. Diet composition was expressed as mean percent prey by volume and weight, because these are the most energetically-relevant metrics. Relative caloric value of the diet was estimated by multiplying measured or published values of energy densities (e.g., Davis et al. 1998) of each prey category in the diet times the prey weight in each category, and summed across prey categories.

Obj.7: Parameterize chum salmon body size and temperature dependence on maximum consumption functions used in bioenergetics models.
Bioenergetics modeling is based on the laws of thermal dynamics where the energy consumed by a fish must balance with the energy lost through physiological processes and or is

assimilated into growth. The terms of the energy budget can be measured directly in laboratory experiments specifically designed to quantify metabolism and maximum consumption rate. The Wisconsin bioenergetics model (Hanson et al. 1997) is an energy balance equation wherein energy acquired through consumption C must equal the sum of metabolic costs (M), waste (W), and growth (G) (somatic and gonadal).

$$\mathbf{C = M + W + G}$$

For each term of this equation, there are formulae that describe the processes in units of energy (Joules·day^{-1}), with the form and parameterization of each term specific to the physiology or ontogenetic stage of a species. Previous analyses have indicated that functions describing the effect of body mass and temperature on maximum consumption and respiration contain the most sensitive parameters (Bartell et al. 1986). However, parameters are often borrowed from other species, resulting in reduced accuracy and confidence in predictions when employing this approach. Therefore, estimating parameters specific to juvenile chum salmon will enhance the performance of the model. Bioenergetics models have been used to quantify juvenile salmon growth (Cross et al. 2005) and consumption (Boldt and Haldorson 2002), however, despite many applications, relatively few models have been parameterized to the specific consumer species, life stages, and body sizes being investigated.

In the bioenergetics approach, consumption (C) is modeled as a function of consumer body mass and temperature, and is iteratively fit the proportion (P) of maximum consumption (C_{max}) required to satisfy the change in body mass observed over a specified time interval for fish of a given size experiencing a given thermal regime (Hanson et al. 1997). In order to parameterize the equations for C_{max}, a series of feeding-to-satiation experiments will be performed over a range of temperatures and body masses.

$$\mathbf{C = C_{max} * P * F(T)}$$

$$\mathbf{C_{max} = CA * W^{CB}}$$

C specific consumption rate ($g \cdot g^{-1} \cdot d^{-1}$)
C_{max} maximum specific feeding rate ($g \cdot g^{-1} \cdot d^{-1}$)
P proportion of maximum consumption
F(T) temperature dependence function
T water temperature (ºC)
W fish mass (g)
CA intercept of the allometric mass function ($g \cdot g^{-1} \cdot d^{-1}$)
CB slope of the allometric mass function

Juvenile chum salmon will be collected in Icy Strait, Alaska during June, July, and August using a midwater rope trawl aboard NOAA research vessel John N. Cobb. Specimens will be held in live tanks onboard the vessel and immediately transported to NOAA's Auke Bay Laboratory, Juneau, Alaska.

Maximum consumption experiments will occur over a 24-hour period in 5-gallon Plexiglas tanks. Juvenile chum salmon will be presented with an excess of live mysid shrimp prey during the feeding trials, and the amount of prey eaten calculated by subtracting the weight of uneaten mysid prey remaining at the cessation of the experiment from the weight of mysid prey added to the tank at the initiation of the experiment. Water temperature will be maintained at one of five experimental treatments (9º, 12º, 15º, 18ºC) throughout the course of the trial with the aid of water chillers. Maximum consumption parameter estimates generated from this experiment will be used to estimate juvenile chum salmon prey consumption (Obj. 8) and growth rate potential (Obj. 9).

Obj.8: Use bioenergetics models to estimate consumption and growth efficiency of Yukon and Kuskokwim chum salmon during estuarine and marine habitats, using scale and otolith-based growth trajectories.

Obj.9: Determine the inter-annual, and spatial variation in growth potential of chum salmon. The Wisconsin bioenergetics model for pink/sockeye salmon (Beauchamp et al. 1989, Hanson et al. 1997) and chum salmon was be applied to construct spatially-explicit models (SEM) of growth potential that accommodated different inputs for food supply and consumption rates. This was accomplished by calculating growth potentials for each sampling location from bioenergetics simulations based on the mean temperature in 0-10 m and diet composition for each site.

Model simulations will be limited to a single day, and by comparing inter-annual variation in growth potential, we can investigate how interannual and spatial variability in prey quality and water temperature affect growth and survival. Differences in the magnitude and heterogeneity of potential growth estimates will be related to stock-specific (Yukon vs. Kuskokwim) production by applying information from annual stock migration trajectories (Figure 7).

Results/Findings: *Actual accomplishments and findings. If there were significant problems that resulted in less than satisfactory or negative results that should be discussed. If results suggest further study, describe additional work needed.*

Anticipated products listed in our proposal include: 1) Improved mechanistic knowledge of the impact of climate variability on western Alaska chum salmon populations and ecosystems; 2) Input to a detailed, quality-controlled western Alaska chum salmon dataset; 3) New tools (chum salmon bioenergetic parameters, growth/survival indices) to aid in management of western Alaska salmon resources.

Oceanography

Abstract: Late summer and early fall temperature and salinity data collected by the Bering-Aleutian Salmon International Survey (BASIS) program are examined in order to better understand the dynamics controlling the temperature and salinity variability of the central eastern Bering Sea shelf waters. Decorrelation length scales are found to be on the order of 100-500 *km* and are generally longer (shorter) in the southern (northern) portion of the domain;

the changes from south to north reflect differences in the local circulation fields. Temperature decorrelation length scales are typically longer than the salinity length scales, reflecting differences between the sources and sinks for each parameter. Near surface and near bottom salinity anomalies tend to fluctuate in phase across the central shelf although temperature anomalies fluctuate in phase only in the weakly and unstratified inner shelf waters. Salinities exhibit a broadly weak but locally significant anti-correlation between the coastal and mid-shelf waters. Integrated heat content (HC) and fresh water content (FWC) parameters provide bulk measures of the fluxes required to raise or lower the multi-year mean shelf water temperature and salinity fields to the observed annual values. We find that the HC anomaly is primarily driven by variance in the along-shelf summertime flow field, while the bulk FW anomaly is set by wind-driven transport manifested over the course of the previous winter. In both seasons, the wind forcing is a consequence of the position and strength of the Aleutian Low. Evidence that both the Bering Sea heat and freshwater budgets are experiencing a period of multi-decadal changes comes from observations of significant (at the 99% level) 30 year increasing trends in the winter surface heat flux anomaly and the annual duration of ice-free waters.

Secondary Procuctivity

Abstract:The southeastern Bering Sea sustains one of the largest fisheries in the United States, as well as wildlife resources that support valuable tourist and subsistence economies. The fish and wildlife populations in turn are sustained by a food web linking primary producers to apex predators through the zooplankton community. Recent shifts in climate toward warmer conditions may threaten these resources by altering productivity and trophic relationships in the ecosystem on the southeastern Bering Sea shelf. We examined the zooplankton community near the Pribilof Islands and on the middle shelf of the southeastern Bering Sea in summer of 1999 and 2004 to document differences and similarities in species composition, abundance and biomass by region and year. Between August 1999 and August 2004, the summer zooplankton community of the middle shelf shifted from large to small species. Significant declines were observed in the biomass of large scyphozoans (Chrysaora melanaster), large copepods (Calanus marshallae), arrow worms (Sagitta elegans) and euphausiids (Thysanoessa raschii, T. inermis) between 1999 and 2004. In contrast, significantly higher densities of the small copepods (Pseudocalanus spp., Oithona similis) and small hydromedusae (Euphysa flammea) were observed in 2004 relative to 1999. Stomach analyses of young-of-the-year (age 0) pollock (Theragra chalcogramma) from the middle shelf indicated a dietary shift from large to small copepods in 2004 relative to 1999. The shift in the zooplankton community was accompanied by a 3-fold increase in water-column stability in 2004 relative to 1999, primarily due to warmer water above the thermocline, with a mean temperature of
7.3 1C in 1999 and 12.6 1C in 2004. The elevated water-column stability and warmer conditions may have influenced the zooplankton composition by lowering summer primary production and selecting for species more tolerant of a warm, oligotrophic environment. A time series of temperature from the middle shelf indicates that the warmer conditions in 2004 are part of a trend rather than an expression of interannual variability. These results suggest that if climate on the Bering Sea shelf continues to
warm, the zooplankton community may shift from large to small taxa which could strongly impact apex predators and the economies they support.

Western Alaska Juvenile Salmon Ecology

Abstract: During the past five years (2002 – 2006), the Auke Bay Laboratory's Ocean Carrying Capacity program conducted surveys of western Alaska juvenile salmon (*Oncorhynchus* spp.) along the eastern Bering Sea shelf. The goal of our juvenile salmon research is to understand mechanisms underlying the effects of environment on the distribution, migration, and growth of juvenile salmon in the eastern Bering Sea. The primary findings indicated that there were spatial variations in distribution among species; juvenile coho (*O. kisutch*) and Chinook (*O. tshawytscha*) salmon tended to be distributed nearshore and juvenile sockeye (*O. nerka*), chum (*O. keta*), and pink (*O. gorbuscha*) salmon tended to be distributed further offshore. In general, juvenile salmon were largest during 2002 and 2003 and smallest during 2006, particularly in the northeastern Bering Sea (NEBS) region. Fish, including age-0 pollock (*Theragra chalcogramma*) and Pacific sand lance (*Ammodytes hexapterus*) were important components of the diets for all species of juvenile salmon in some years, however, annual comparisons of juvenile salmon diet indicated a shift in primary prey for many of the salmon species during 2006 in both the NEBS and southeastern Bering Sea (SEBS) regions. In addition, the average CPUE of juvenile salmon fell sharply during 2006 in the SEBS region. We speculate that spring sea surface temperatures (SST's) on the eastern Bering Sea shelf impact the growth marine survival rates of juvenile western Alaska salmon through bottom-up control in the ecosystem. Cold spring SST's lead to lower growth and marine survival rates for juvenile western Alaska salmon; warm spring SST's have the opposite effect.

Juvenile chum salmon bioenergetic parameters

Temperature is a controlling factor that governs the rate of biochemical reactions and influences the activity level of fish. Little is currently know about the influence of temperature on the feeding rates of juvenile salmon; information which could provide insight into the influence of biophysical factors on feeding ecology and behavior. Utilizing bioenergetics models in research focused on understanding biophysical mechanisms that influence salmon ecology is growing, which has resulted in a need for species- and life stage-specific model parameters to generate accurate predictions. The effect of temperature and body size on the consumption rate of juvenile chum salmon (*Oncorhynchus keta*) was investigated for individuals of similar body size to those within their first summer in the marine environment to address these concerns. Juvenile chum salmon ranging 50–100mm (FL) in size were fed live mysid shrimp (*Mysidopsis bahia*) to satiation over a 24-hour period. Feeding trials were conducted across a range of temperatures (3.5–23.0º C), that were held constant during a given trial. Weight dependence on specific consumption took the form of a decreasing power function. Temperature dependence on specific maximum consumption took the form of a cool and coldwater species. Maximum consumption increased rapidly from 3-8.5 ºC, and demonstrated a slight decrease between 8.5-23 ºC. Bioenergetics model simulations run with the newly estimated parameters predicted lower growth rates than the existing model most commonly used to estimate growth for juvenile pink (*O. gorbuscha*), chum, and sockeye salmon (*O. nerka*).

Juvenile Chum Salmon Bioenergetics

Abstract: Spatial and temporal variation in growing conditions for juvenile salmon may determine the survival of salmon after their first year at sea. To assess this aspect of habitat quality, a spatially explicit bioenergetics model was used to predict juvenile chum salmon

(*Oncorhynchus keta)* growth rate potential (GRP) on the eastern Bering Sea shelf during years with cold and warm spring sea surface temperatures (SSTs). Annual averages of juvenile chum salmon GRP were generally lower among years and regions with cold spring SSTs. In addition, juvenile chum salmon GRP was generally higher in offshore than in nearshore regions of the eastern Bering Sea shelf during years with warm SSTs; however, the distribution (catch per unit effort) of juvenile chum salmon was not significantly ($p < 0.05$) related to GRP. Shifts from warm to cold SSTs in the northern region do not appear to affect summer abundance of juvenile Yukon River chum salmon, whereas the abundance of juvenile Kuskokwim River chum salmon drops precipitously during years with cold SSTs. From this result, we hypothesize that size-selective predation is highest on juvenile Kuskokwim chum salmon during cold years, but that predation is not as great a factor for juvenile Yukon River chum salmon. Although not addressed in this study, we also hypothesize that the smaller Yukon River chum salmon captured during years with cold SSTs likely incur higher size-selective mortality during winter.

Climate Change and Juvenile Salmon Ecology

Abstract: Loss of non-seasonal sea-ice and a general warming trend in the Bering Sea has altered the composition, distribution, and abundance of marine organisms inhabiting the region. Juvenile pink (*Oncorhynchus gorbusha*) and chum (*O. keta*) salmon were found in significant numbers throughout the Chukchi Sea and Bering Strait regions during early autumn 2007 reflecting significant utilization of Arctic marine habitat. Linear models of juvenile pink and chum salmon body size and day of year were parameterized to estimate daily growth rates, habitat specific differences in body size were calculated and contrasted, and growth trajectories for three distinct Arctic habitats simulated using a bioenergetics model. Juvenile Pink salmon inhabiting the eastern Bering Sea were estimated to grow at a rate of 1.17 $mm \cdot day^{-1}$ and juvenile chum salmon were estimated to grow at 1.21 $mm \cdot day^{-1}$. The largest juvenile pink and chum salmon that were encountered during 2007 were distributed in the northern Chukchi Sea. The second largest juvenile pink and chum salmon were located in the southern Chukchi Sea, and the smallest were located in the Bering Strait. Thermal conditions and prey quality the northern Chukchi Sea were most favorable for supporting pink and chum salmon growth, followed by the Bering Strait, and southern Chukchi Sea. The majority of chum salmon encountered in the Arctic were from Alaskan or Russian stocks, and results from this study suggest that these particular stocks will likely benefit from the loss of Arctic sea-ice through experiencing favorable growth rates that support over winter survival.

Abstract:Migratory patterns of western Alaska juvenile Chinook salmon (*Oncorhynchus tshawytscha*) are described using stock-structured distribution data from the United States Bering-Aleutian Salmon International Surveys (BASIS). Juvenile Chinook salmon were distributed within the coastal domain throughout their first summer at sea and the highest densities of juvenile Chinook salmon were found close to river mouths of primary Chinook salmon producing rivers in western Alaska. This reflects a lower marine dispersal pattern than typically found in Gulf of Alaska stream-type Chinook salmon. Stock mixtures of juvenile salmon in the northern shelf region (north of 60°N) did not support significant northward migration of stocks from the southern shelf, reflecting limited mixing of salmon from different production regions. Recoveries of coded-wire tagged Yukon River Chinook salmon near the Bering Strait provide evidence that Yukon River Chinook salmon distributions can extend

north into the Chukchi Sea. These data clarify and update migratory patterns of western Alaska juvenile Chinook salmon, which are essential to interpret abundance data from the BASIS survey and to define critical habitats of western Alaska Chinook salmon.

Evaluation: *Describe the extent to which the project objectives were attained. This description should address the following: were objectives attained? If so, how? If not, why not? Were modifications made to the objectives, if so explain.*

Obj.1:**Development of the comprehensive database for chum salmon**.

Fisheries and oceanographic data collected during the survey were entered into an ACCESS data base for storage. Because the datasets were large, three ACCESS data bases were created: a) to house the biological and physical oceanographic data, b) the species composition, abundance and biomass of zooplankton data, and c) information pertaining to the survey and fish catch and biological characteristics.

Obj.2:Estimate the density and biomass of exploitable zooplankton and ichthyoplankton taxa available to salmon.

The University of Alaska Fairbanks laboratory processed zooplankton samples collected during the surveys and provided the density and exploitable zooplankton biomass. The ichthyoplankton abundance and biomass were estimated when composition of these types of prey were found in the chum salmon stomach contents. See Farley and Moss (in press) for methods and estimates of exploitable prey biomass. No problems were encountered.

Obj.3:Compare outmigration timing, estuarine residency, and growth histories in marine habitats occupied by juvenile Yukon and Kuskokwim chum salmon using otolith microchemistry.

Otolith chemistry and microstructure were used to estimate ocean entry dates and marine growth rates of juvenile chum salmon in the northern and southern regions of the eastern Bering Sea shelf during 2006 and 2007.

Obj.4:Reconstruct growth histories of juvenile Yukon and Kuskokwim chum salmon in estuarine and marine habitats using otolith and scale growth patterns.

This objective was not completed due to high scale loss during 2006 to 2007 caused by high seas, there were a limited number of juvenile chum salmon with preferred scales (n=8) with matching otoliths.

Obj.5:Map interannual variation in habitat (coastal, inner front, and middle domains) and ocean conditions along the eastern Bering Sea sheld.

Oceanographic data (sea surface temperature) were utilized in bioenergetics models and to define the oceanographic domains for juvenile chum salmon growth rate potential and distributional characteristics described in Farley and Moss (in press). No problems were encountered.

Obj.6:Determine the interannual variation in diet composition of chum salmon with coastal waters of western Alaska and oceanographic characteristics along the eastern Bering Sea shelf.

Stomach contents analyses of juvenile chum salmon were performed on-board during the surveys. These data were summarized in two manuscripts: one by Farley et al. (in press) and the other in Farley and Moss (in press). Oceanographic data were also summarized in a draft manuscript by Danielson et al. (in prep). No problems were encountered.

Obj.7:Parameterize chum salmon body size and temperature dependence on maximum consumption functions used in bioenergetics models.

Laboratory experiments were completed to determine parameter estimates for body size and temperature dependence on maximum consumption functions for juvenile chum salmon bioenergetics models. These experiments were completed during the first two years of the project. A draft manuscript was completed describing the methods and results and parameter estimates were utilized in Farley and Moss (in press) for bioenergetics growth rate potential models.

Obj.8:Use bioenergetics models to estimate consumption and growth efficiency of juvenile Yukon and Kuskokwim chum salmon during estuarine and marine habitats, using scale and otolith-based growth trajectories.

The scale and otolith growth trajectories were not accomplished (see reasons why above), thus much of this objective was incorporated into Obj. 9 for bioenergetics growth rate potential models.

Obj.9:Map inter-annual and spatial variability in instantaneous growth potential for juvenile chum salmon at each sampling site within coastal waters of the eastern Bering Sea during August – October (2002 – 2007).

Bioenergetics growth rate potential models were created for data collected during 2004 to 2007 (Farley and Moss in press). The reason we did not incorporate 2002 and 2003 is that the surveys design changed during 2004 to 2007 as more money was brought in for more survey coverage in the northeastern Bering Sea. The data set utilized allowed us to test for significant differences in juvenile chum salmon growth rate potential between years with anomalously warm (2004 and 2006) and cold (2006 and 2007) sea temperatures. These analyses also included tests for variability in growth rate potential between the northeastern (Yukon chum salmon) and southeastern (Kuskokwim chum salmon) stocks and for variability among ocean habitats on the eastern Bering Sea shelf.

Project Products: *Explain, in detail, how the project results have been or will be disseminated. Include two copies of any results (reports, technical documents, web site addresses, etc.) with this final report. Title pages of publications should have sufficient information (author, title, key words, etc.) to facilitate cataloguing or information sharing.*

Project results were published in peer reviewed journals and within the peer reviewed, North Pacific Anadromous Fish Commission, Bulletin 5, BASIS Symposium proceedings,

Key Words: Juvenile salmon, bioenergetics, climate variability, western Alaska, eastern Bering Sea

Date Prepared: June 30, 2009

AYK SSI Final Product Format: PART 2 OF 2

OPTION A : IF MANUSCRIPT DRAFTS / AGENCY REPORT DRAFTS ARE SUBMITTED.

AYK SSI TITLE PAGE:

20__ Arctic Yukon Kuskokwim Sustainable Salmon Initiative Project Final Product[1]

Factors Affecting Juvenile AYK Chum Salmon Growth and Condition

by:

Edward V. Farley, Jr.[1], James Murphy[1], Jamal Moss[1], and Lisa Eisner[1]

[1] NOAA/NMFS Alaska Fisheries Science Center, Ted Stevens Marine Research Institute, Auke Bay Laboratories, 17109 Point Lena Loop Road, Juneau, AK 99801

June 30, 2009

1 Final products of AYK Sustainable Salmon Initiative-sponsored research are made available to the Initiatives Partners and the public in the interest of rapid dissemination of information that may be useful in salmon management, research, or administration. Sponsorship of the project by the AYK SSI does not necessarily imply that the findings or conclusions are endorsed by the AYK SSI.

ABSTRACT:

A spatially explicit bioenergetics model was used to predict juvenile chum salmon (*Oncorhynchus keta)* growth rate potential (GRP) offshore of the Yukon River and Kuskokwim River. Data for the GRP models come from ocean surveys conducted along the eastern Bering Sea shelf during 2002 to 2007. Data for the GRP models included spatial-temporal patterns in sea surface temperatures (deg C), salmon diet (% prey composition), salmon prey availability (grams/cm3), relative abundance (catch per unit effort), size (grams) and caloric content (cal/gram). These data were collected during years with anomalously cold (2006 and 2007) and warm (2002 – 2005) sea surface temperatures (SSTs) on the eastern Bering Sea shelf. Annual averages of juvenile chum salmon GRP were generally lower among years and regions with cold spring SSTs. In addition, juvenile chum salmon GRP was generally higher in offshore than in nearshore regions of the eastern Bering Sea shelf during years with warm SSTs; however, the distribution (catch per unit effort) of juvenile chum salmon was not significantly ($p < 0.05$) related to GRP. Shifts from warm to cold SSTs in the northern region do not appear to affect summer abundance of juvenile Yukon River chum salmon, whereas the abundance of juvenile Kuskokwim River chum salmon drops precipitously during years with cold SSTs. From this result, we hypothesize that size-selective predation is highest on juvenile Kuskokwim chum salmon during cold years, but that predation is not as great a factor for juvenile Yukon River chum salmon. Although not addressed in this study, we also hypothesize that the smaller Yukon River chum salmon captured during years with cold SSTs likely incur higher size-selective mortality during winter.

PRESS RELEASE:

Does Climate Variation Affect Marine Survival of Chum Salmon from the Yukon and Kuskokwim Rivers?

Every spring, chum salmon fry from the Yukon and Kuskokwim Rivers enter the eastern Bering Sea to begin their marine life history stage and an uncertain future.

The highest marine mortality rates for salmon occur during their first year in the ocean. Known as the "critical size and period" hypothesis, faster growing juvenile salmon escape predators early on after leaving freshwater, and larger fish after their first summer at sea are believed to be better fit to survive their first winter at sea.

"We are beginning to understand how climate variation affects the quantity and quality of food resources and thus impacts on growth rate potential of juvenile western Alaska chum salmon" says Ed Farley, a Fishery Research Biologist with the Alaska Fisheries Science Center in Juneau, Alaska.

From 2002 to 2007, Farley and a team of researchers from the Alaska Fisheries Science Center collected sea water temperature, estimated juvenile chum salmon prey quantity and quality, and determined the relative abundance of juvenile chum salmon from the Yukon and Kuskokwim Rivers during late summer and fall research surveys along the eastern Bering Sea

shelf. These data were used within bioenergetic models to predict the growth rate potential of juvenile chum salmon, an indicator for juvenile salmon marine survival.

"We were fortunate to be able to conduct annual surveys during a period of contrasting ocean sea temperature conditions, with unusually cold sea temperatures during 2006 and 2007 and unusually warm sea temperatures during 2002 to 2005," says Farley. "The bioenergetics models indicate that growth rate potential of juvenile chum salmon is much lower during years with cold sea temperatures, due mostly to the quantity of prey available to chum salmon. In addition, relative abundance of juvenile Kuskokwim River chum salmon and the size of juvenile Yukon River chum salmon are much lower during years with cold sea temperatures. All of these indices suggest that marine mortality for western Alaska chum salmon is highest during years with unusually cold sea temperatures."

Recent research suggests that the upper regions of the water column, where juvenile salmon are found, are more productive during years with warm spring and summer sea temperatures. It is natural then to think that under a warming climate scenario that western Alaska salmon should do better.

However, when examining the "sensitivity" of juvenile western Alaska sockeye salmon bioenergetic models to increased sea temperature, Farley found that growth rate potential can decline if sea temperatures increase by 2 deg C above the warmest sea temperatures found during the annual surveys.

"We are in uncharted waters here, where climate models predict further sea temperature warming in the Bering Sea as well as reduced marine productivity. Both of these variables could negatively impact growth rate potential for western Alaska salmon, thus increasing early marine mortality during years with highly unusual sea temperatures along the eastern Bering Sea shelf."

For more information on the research, contact Ed Farley at ed.farley@noaa.gov

This research is co-ordinated by the Alaska Fisheries Science Center in Juneau, Alaska with financial support from the Arctic-Yukon-Kuskokwim Sustainable Salmon Initiative.

[Provide a press release pertaining to the results of your project and potential applications of your results that would capture the interest of AYK salmon fishers, community residents, or fishery managers. Press release should not exceed 500 words.]

PROJECT EVALUATION:

[A summary statement should be added to the front of the report that compares the original proposal to what has been accomplished. This statement should 1); 2) indicate any problems encountered which may have affected completion of the original objectives; 3) describe how these problems were resolved or addressed. Reference all manuscript drafts to this statement.].

Obj.1:Development of the comprehensive database for chum salmon.

Fisheries and oceanographic data collected during the survey were entered into an ACCESS data base for storage. Because the datasets were large, three ACCESS data bases were created: a) to house the biological and physical oceanographic data, b) the species composition, abundance and biomass of zooplankton data, and c) information pertaining to the survey and fish catch and biological characteristics.

Obj.2:Estimate the density and biomass of exploitable zooplankton and ichthyoplankton taxa available to salmon.

The University of Alaska Fairbanks laboratory processed zooplankton samples collected during the surveys and provided the density and exploitable zooplankton biomass. The ichthyoplankton abundance and biomass were estimated when composition of these types of prey were found in the chum salmon stomach contents. See Farley and Moss (in press) for methods and estimates of exploitable prey biomass. No problems were encountered.

Obj.3:Compare outmigration timing, estuarine residency, and growth histories in marine habitats occupied by juvenile Yukon and Kuskokwim chum salmon using otolith microchemistry.

Otolith chemistry and microstructure were used to estimate ocean entry dates and marine growth rates of juvenile chum salmon in the northern and southern regions of the eastern Bering Sea shelf during 2006 and 2007.

Obj.4:Reconstruct growth histories of juvenile Yukon and Kuskokwim chum salmon in estuarine and marine habitats using otolith and scale growth patterns.

This objective was not completed due to high scale loss during 2006 to 2007 caused by high seas, there were a limited number of juvenile chum salmon with preferred scales (n=8) with matching otoliths.

Obj.5:Map interannual variation in habitat (coastal, inner front, and middle domains) and ocean conditions along the eastern Bering Sea sheld.

Oceanographic data (sea surface temperature) were utilized in bioenergetics models and to define the oceanographic domains for juvenile chum salmon growth rate potential and distributional characteristics described in Farley and Moss (in press). No problems were encountered.

Obj.6:Determine the interannual variation in diet composition of chum salmon with coastal waters of western Alaska and oceanographic characteristics along the eastern Bering Sea shelf.

Stomach contents analyses of juvenile chum salmon were performed on-board during the surveys. These data were summarized in two manuscripts: one by Farley et al. (in press) and

the other in Farley and Moss (in press). Oceanographic data were also summarized in a draft manuscript by Danielson et al. (in prep). No problems were encountered.

Obj.7:Parameterize chum salmon body size and temperature dependence on maximum consumption functions used in bioenergetics models.

Laboratory experiments were completed to determine parameter estimates for body size and temperature dependence on maximum consumption functions for juvenile chum salmon bioenergetics models. These experiments were completed during the first two years of the project. A draft manuscript was completed describing the methods and results and parameter estimates were utilized in Farley and Moss (in press) for bioenergetics growth rate potential models.

Obj.8:Use bioenergetics models to estimate consumption and growth efficiency of juvenile Yukon and Kuskokwim chum salmon during estuarine and marine habitats, using scale and otolith-based growth trajectories.

The scale and otolith growth trajectories were not accomplished (see reasons why above), thus much of this objective was incorporated into Obj. 9 for bioenergetics growth rate potential models.

Obj.9:Map inter-annual and spatial variability in instantaneous growth potential for juvenile chum salmon at each sampling site within coastal waters of the eastern Bering Sea during August – October (2002 – 2007).

Bioenergetics growth rate potential models were created for data collected during 2004 to 2007 (Farley and Moss in press). The reason we did not incorporate 2002 and 2003 is that the surveys design changed during 2004 to 2007 as more money was brought in for more survey coverage in the northeastern Bering Sea. The data set utilized allowed us to test for significant differences in juvenile chum salmon growth rate potential between years with anomalously warm (2004 and 2006) and cold (2006 and 2007) sea temperatures. These analyses also included tests for variability in growth rate potential between the northeastern (Yukon chum salmon) and southeastern (Kuskokwim chum salmon) stocks and for variability among ocean habitats on the eastern Bering Sea shelf.

DELIVERABLES:

[List deliverables resulting from the project, including annual progress reports, final reports, data sets, database systems, workshop reports, networking meetings, oral or poster presentations, and submission of journal papers. Explain how the project results have been, and will be, disseminated.]

Project results were published in peer reviewed journals and within the peer reviewed, North Pacific Anadromous Fish Commission, Bulletin 5, BASIS Symposium proceedings,

PROJECT DATA SUMMARY:

[A summary of the data collected during the project shall be provided in order to preserve the opportunity for other researchers and the public to access these data in the future. The summary shall: (1) describe the data; (2) indicate the format of the available data collections; (3) identify the archive in which the data have been stored or the custodian of the data

(including contact name, organization, address, phone/fax, e-mail, and web address where data may be acquired); and (4) indicate any access limitations placed on the data.]

An FGDC compliant metadata record was prepared for all active data sets for BASIS research. The records are available on the National Biological Information (NBII) metadata clearinghouse web site (web site below).

http://metadata.nbii.gov/portal/community/Communities/Toolkit/Metadata/FGDC_Metadata/Clearinghouse/

To access the metadata files, enter "juvenile salmon Alaska" in the search window and the records for BASIS should be in the first few hits returned.

APPENDIX 1

Farley, E. V., Jr., J. Murphy, J. Moss, A. Feldmann, and L. Eisner. In press. Marine ecology of western Alaska juvenile salmon. *In* C. C. Krueger and C. E. Zimmerman, editors. Pacific salmon: ecology and management of western Alaska's populations. American Fisheries Society, Symposium 70, Bethesda, Maryland.

Marine Ecology of Western Alaska Juvenile Salmon

EDWARD V. FARLEY, JR., JAMES MURPHY, JAMAL MOSS, ANGELA FELDMANN, AND LISA EISNER

National Marine Fisheries Service, Alaska Fisheries Science Center, Auke Bay Laboratories, 17109 Point Lena Loop Road, Juneau, AK 99801, USA
Corresponding author: email – ed.farley@noaa.gov, phone – (907) 789-6085; fax – (907) 789-6094

Abstract

During the past five years (2002 – 2006), the Auke Bay Laboratory's Ocean Carrying Capacity program conducted surveys of western Alaska juvenile salmon (*Oncorhynchus* spp.) along the eastern Bering Sea shelf. The goal of our juvenile salmon research is to understand mechanisms underlying the effects of environment on the distribution, migration, and growth of juvenile salmon in the eastern Bering Sea. The primary findings indicated that there were spatial variations in distribution among species; juvenile coho (*O. kisutch*) and Chinook (*O. tshawytscha*) salmon tended to be distributed nearshore and juvenile sockeye (*O. nerka*), chum (*O. keta*), and pink (*O. gorbuscha*) salmon tended to be distributed further offshore. In general, juvenile salmon were largest during 2002 and 2003 and smallest during 2006, particularly in the northeastern Bering Sea (NEBS) region. Fish, including age-0 pollock (*Theragra chalcogramma*) and Pacific sand lance (*Ammodytes hexapterus*) were important components of the diets for all species of juvenile salmon in some years, however, annual comparisons of juvenile salmon diet indicated a shift in primary prey for many of the salmon species during 2006 in both the NEBS and southeastern Bering Sea (SEBS) regions. In addition, the average CPUE of juvenile salmon fell sharply during 2006 in the SEBS region. We speculate that spring sea surface temperatures (SST's) on the eastern Bering Sea shelf impact the growth marine survival rates of juvenile western Alaska salmon through bottom-up control in the ecosystem. Cold spring SST's lead to lower growth and marine survival rates for juvenile western Alaska salmon; warm spring SST's have the opposite effect.

Introduction

Pacific salmon (*Oncorhynchus* spp.) returns (catch + escapement) to western Alaska have been inconsistent, and at times very weak. During 1998, low returns of Chinook (*O. tshawytscha*) and chum (*O. keta*) salmon to western Alaska prompted the State of Alaska to restrict commercial and subsistence fisheries and declare a fisheries disaster for the region (Kruse 1998). Low returns of sockeye (*O. nerka*) salmon to Bristol Bay, Alaska also occurred

during 1997 and 1998. The regional scale decline of these salmon stocks indicates that the marine environment may play a critical role in regulating survival of Pacific salmon.

Ocean conditions are known to significantly affect salmon survival, particularly during the first few months after leaving freshwater (Holtby et al. 1990; Friedland et al. 1996; Beamish et al. 2004). Growth rates of juvenile salmon in the estuarine and near shore marine environments are thought to be directly linked to their marine survival with larger fish having higher survival rates (Parker 1968; Pearcy 1992). Size-dependent mortality is believed to occur during two critical periods. The first period is predominated by predation based mortality occurring shortly after juvenile salmon leave freshwater. During the first critical period, smaller individuals are vulnerable to a broader spectrum of predators and experience higher size-selective predation (Parker 1968; Willette et al. 1999). The second period is controlled by energetic-based mortality occurring after the first summer at sea. During the second critical period, reduced storage capability of smaller individuals make them more vulnerable to overwinter mortality (Beamish and Mahnken 2001). Thus, years with favorable environmental conditions and increased growth rates of juvenile salmon may reduce susceptibility of the salmon to size-selective predation or improve survival during their first winter at sea.

Ecological processes affecting marine survival of eastern Bering Sea salmon stocks are poorly understood due to the lack of basic biological information about the early marine life history of salmon in this region. Until recently, studies of juvenile salmon migration in the eastern Bering Sea were generally focused within Bristol Bay (Hartt and Dell 1986; Isakson et al. 1986; Straty 1974). Information on juvenile salmon in the Arctic, Yukon, and Kuskokwim region was limited to a few studies of juvenile salmon within nearshore locations of Kotzebue Sound (Merritt and Raymond 1983; Raymond et al. 1984), Norton Sound (Nemeth et al. 2004), the Yukon River delta (Martin et al. 1986; 1987), and Kuskokwim Bay (Burril 2007; Hillgruber et al. 2007; Hillgruber and Zimmerman 200X). However, during 2002 scientists from Canada, Russia, Japan, South Korea, and the United States, member nations of the North Pacific Anadromous Fish Commission, cooperated in the design and execution of a field survey of salmon across the entire Bering Sea. The research, designated as Bering-Aleutian Salmon International Survey (BASIS), was developed to clarify the mechanisms of biological response by salmon to climate change.

In this paper, we summarize information on juvenile salmon ecology from the U.S. BASIS research cruises along the eastern Bering Sea shelf from August to October 2002 - 2006. We report new information on juvenile salmon distribution, size, and diet and provide relative abundance indices (catch per unit effort) for all five species of salmon. We also discuss ecological processes that may affect marine survival of western Alaska juvenile salmon during this critical life history period.

Methods

Survey

The Auke Bay Laboratory's Ocean Carrying Capacity (OCC) survey of the eastern Bering Sea was generally conducted from mid August to early October during 2002 to 2006 aboard the chartered fishing vessel *Sea Storm* (38 m in length) and *Northwest Explorer* (49 m in length, 2006 only). The area surveyed was along the eastern Bering Sea shelf (Figures 1a and b). During 2002 and 2003, survey stations were spaced every 15 degrees along latitudinal (60ºN to 65ºN) and longitudinal (161ºW to 168ºW) lines (Figure 1a). From 2004 to 2006, stations were spaced every 30 degrees, forming a grid along the eastern Bering Sea shelf

(Figure 1b). The eastern Bering Sea was separated into two regions based on distribution and probable stock- and species-specific migration routes for juvenile salmon (Farley et al. 2005). The southeastern Bering Sea (SEBS) region was defined as the area south of lat 60ºN (does not include catches made along 60ºN) to the Alaska Peninsula, and the area west of long 161ºW to 168ºW. The northeastern Bering Sea (NEBS) region was defined as the area between lat 60ºN (includes catches made along lat 60ºN) and lat 65ºN, and from the eastern shoreline of Alaska to long 173ºW or the U.S.-Russian border.

Fish were collected using midwater rope trawls, Model 400/580 and 300/450, made by Cantrawl Pacific Limited[1] of Richmond, British Columbia. Trawls were 198 m long, had hexagonal mesh in wings and body, and included a 1.2-cm mesh liner in the codend. Trawls were towed at the surface from 3.5 to 5 knots, with typical horizontal and vertical mouth dimensions of 50 m and 14 m, respectively. The trawls were fished with Noreastern Trawl Systems 5-m alloy doors, 60-m bridles, and 330-366 m of warp line behind the boat. Buoys were secured to the wing tips (2-A5 and 4-A4 buoys) and 2 buoys were attached to the net sounder to help maintain the headrope near the surface. Wing-tip buoys could be seen floating near the surface when trawling and were used to ensure the headrope was at the surface. A Simrad FS900 net sounder was used to determine dimensions of the trawl mouth opening during each trawl set.

Stations were generally sampled during daylight hours (0730 – 2100, Alaska Daylight Savings Time); tows before 0800 in September and October were in the dark. All tows lasted 30 min and covered approximately 2.8 to 4.6 km. Salmon and other fishes captured during the tow were sorted by species and counted. We tested for a correlation between catch per unit effort (number of salmon caught during a 30 minute tow) and time of day and found no relationship ($r = 0.00$; $P = 0.36$). Standard biological measurements including fork length (nearest 1.0 mm) and body weight (nearest 1.0 g) were taken on board. Diet analyses differed between years. During 2002 and 2003, subsamples of all juvenile salmon species were wrapped in a labeled plastic bag, frozen (-80°C), and shipped to the laboratory for further processing. In the laboratory, stomachs were removed from a random sample of approximately 10 juvenile salmon from each trawl station. Individual stomachs were preserved in 10% formalin and placed in an individually labeled vial. During 2004 through 2006, stomachs were removed from a random sample of approximately 10 juvenile salmon from each trawl station and analyzed on board.

Distribution of juvenile salmon

Cumulative frequency distributions of the percent total catch of juvenile salmon in relation to distance offshore (Latitudinal meridians in decimal degrees for the SEBS region and Longitudinal meridians in decimal degrees for the NEBS region) of the Alaska coastline were created to help in the discussion on the inter annual variation in distribution of juvenile salmon.

Size of juvenile salmon

Adjusted mean fish lengths were calculated to standardize size across years and regions. Mean length was standardized to September 10 assuming three different daily growth rates: (1) 0 mm/day, representing no daily growth at sea, (2) 0.3 mm/day, the lower end of published ranges for juvenile Pacific salmon, and (3) 1.7 mm/day, representing the upper end

[1] Reference to trade names does not imply endorsement by the National Marine Fisheries Service, NOAA.

of the range (see Fisher and Pearcy, 1988; Fukuwaka and Kaeriyama, 1994; Orsi et al., 2000 for daily growth rate ranges for juvenile Pacific salmon).

Analysis of variance tests (ANOVA, fixed effect) were used to examine interannual and regional differences in length for each daily growth rate (i.e., 0 mm, 0.3 mm, or 0.7 mm). The dependent variable in the ANOVA was fork length and the independent variables were year (2002 to 2006), region (SEBS and NEBS) and the interaction among year and region. Data were analyzed using S-Plus statistical software. If a significant difference ($P < 0.05$) occurred, a Sidak multiple comparison test was used to calculate the 95% ($\alpha = 0.05$, 0.01, 0.001) confidence intervals for all pairwise differences between the dependent variable means (Insightful, 2001). The level of significance between the pairwise differences was determined by examining those confidence intervals that excluded zero for the three values of α.

Diets of juvenile salmon

Diet composition, expressed as percent wet weight of stomach contents (%WT), was used as the primary metric in the annual diet analyses and was calculated as

$$\%WT_{i,f,s} = WT_{i,f,s} * (\sum_{i} WT_{i,f,s})^{-1} * 100 \qquad (1)$$

where $WT_{i,f}$ is the total weight of prey category i in the fth salmon stomach for each species (s = pink (*O. gorbuscha*), chum, sockeye, coho (*O. kisutch*), and Chinook) sampled for diet analysis. Stomach content weight was estimated by subtracting the empty stomach weight from the stomach weight with contents. Stomachs were blotted dry prior to weighing. Stomach contents were divided into major taxonomic groups including fish species such as Pacific sand lance (*Ammodytes hexapterus*), age-0 walleye pollock (*Theragra chalcogramma*), and capelin (*Mallotus villosus*) and invertebrate taxonomic groups such as amphipods, copepods, euphausiids, megalopa, and tunicates (Oikopleura). Two "other" categories were included and described by "other fish", composed of unidentified fish, and fish species that were less than 5% wet weight of the diet within each year (including cottids, clupeids, *Sebastes*, and pleuronectids) and "other zooplankton", composed of zooplankton species that were less than 5% wet weight of the diet (including arthropods, chaetognaths, *Limacina* spp., and mysids) for each year.

We also include information on average CPUE of age-0 walleye pollock (SEBS and NEBS regions) and sand lance (SEBS region only; very few sand lance were captured in the NEBS region) during 2002 – 2006 from our survey and an index of spring sea surface temperatures (SSTs) during May 2000 to 2006 in the southeastern Bering Sea (courtesy of http://www.beringclimate.noaa.gov) as references for discussion points on ecological processes affecting juvenile salmon survival. The May temperatures characterize SST during May in the southeastern Bering Sea that is calculated as mean monthly SSTs averaged over the area 54.3°N to 60°N, 161.2°W to 172.5°W. The data are from the NCEP/NCAR Reanalysis project (Kalnay et al. 1996). The index values are the deviations from the mean value (2.33°C) for the 1970 – 2000 period normalized by the standard deviation (0.76°C)

Results

Distribution and relative abundance (CPUE)

Offshore distribution and CPUE of juvenile salmon varied among species in the SEBS and NEBS regions (Figures 2a and b; 3a – e).

Juvenile sockeye salmon were mainly distributed offshore with nearly 65% captured between 56.5°N and 58°N in the SEBS region. Within the SEBS region, the average CPUE of juvenile sockeye salmon varied between 40 and 65 during 2002 to 2004, more than doubled to 140 during 2005, then fell to 20 during 2006 (Figure 3a). Juvenile sockeye salmon were also distributed offshore in the NEBS region with nearly 90% of the catch occurring west of 169°W. In general, catches of juvenile sockeye salmon in the NEBS region were low in all years (Figure 3a).

Nearly 80% of juvenile chum salmon in the SEBS region were distributed north of lat 58°N directly west of the Kuskokwim River. Within the NEBS region, 75% of the juvenile chum salmon were distributed from 166°W to 169°W. Most of the juvenile chum salmon were captured south and west of the Yukon River although catches do occur north of the Yukon River (Farley et al. 2005). Average CPUE for juvenile chum salmon was generally higher in the NEBS region than the SEBS region, especially during 2002, 2003 and 2006 (Figure 3b).

In contrast to the offshore distribution of sockeye salmon, juvenile Chinook salmon were mainly distributed nearshore. In the SEBS region, 80% of the juvenile Chinook salmon were distributed north of lat 57.5°N. Nearly 80% of the juvenile Chinook salmon were caught east of 169°W in the NEBS region; roughly 10% of the catch occurred between 163°W and 165°W, transects with stations located within Norton Sound. There were 3 coded-wire tag recoveries of juvenile Chinook salmon during 2002 that were from the Yukon Territory, Whitehorse Rapids Salmon Hatchery, 2 within Norton Sound at lat 64.06°N, long 164.31°W station, and 1 offshore of the Yukon River at lat 63.00°N, long 165.58°W. In addition, the average CPUE of juvenile Chinook salmon was similar for both regions for all years except 2006, where catches of juvenile Chinook in the SEBS region were near zero (Figure 3c).

Juvenile coho salmon in the SEBS region had a bimodal distribution with nearly 30% of the catch occurring south of 55.5°N and 60% captured north of 57.5°N. The average CPUE for coho salmon was higher in the SEBS region for all years except 2006 (Figure 3d). Most of the juvenile coho salmon (60%) were distributed east of 169W in the NEBS region, with roughly 10% distributed within Norton Sound (163°W to 165°W).

Juvenile pink salmon in the NEBS and SEBS regions had similar distributions to Chinook and chum salmon. The highest catches of juvenile pink salmon within the SEBS region occurred during 2003 to 2005; very few pinks were caught in this region during 2002 and 2006 (Figure 3e). In contrast, average CPUE for juvenile pinks in the NEBS region were high during all years with the highest average CPUE occurring in 2006 (Figure 3e).

Juvenile salmon size

Mean fork lengths at each daily growth rate for all five juvenile salmon species (see Tables 1 and 2) were significantly different among years ($P < 0.001$), between regions ($P < 0.001$; except coho salmon where $P = 0.006$), and between the interaction of regions and years ($P < 0.01$).

SEBS region

Juvenile sockeye salmon in the SEBS region were largest during 2003 and smallest during 2004 and 2005 (Table 1). The multiple comparison test indicated that juvenile sockeye salmon were significantly larger ($P < 0.001$) during 2003 than all other years for the three daily growth rates. Juvenile sockeye salmon were significantly larger ($P < 0.001$) during 2002 than

2004 and 2005 for all 3 daily growth rates. In addition, juvenile sockeye salmon were significantly larger during 2006 than 2004 ($P < 0.001$) and 2005 ($P < 0.001$ for 0 mm and 0.3 mm; $P < 0.01$ for 1.7 mm) for all 3 daily growth rates.

The smallest juvenile chum salmon were found during 2005 for all daily growth rates (Table 1). The largest juvenile chum salmon were found during 2003 for daily growth rates of 0 mm and 0.3 mm and during 2004 for daily growth rates of 1.7 mm. Juvenile chum salmon were significantly larger ($P < 0.001$) in 2004 than 2002, 2003, and 2005 and significantly smaller ($P < 0.001$) in 2005 than 2002 and 2003 for daily growth rates of 1.7 mm. Juvenile chum salmon were significantly smaller ($P < 0.001$) in 2005 than 2002, 2003 and 2004 for daily growth rates of 0.3 mm, and were significantly larger in 2003 than, 2002 ($P < 0.05$), 2004 ($P < 0.001$), and 2005 ($P < 0.001$), significantly larger ($P < 0.001$) in 2002 than 2004 and 2005, and significantly larger ($P < 0.001$) in 2004 than 2005 for daily growth rates of 0.0 mm.

The largest juvenile Chinook salmon were found during 2006 for all 3 daily growth rates, however, the small sample size ($n = 6$) limits inferences to the size of Chinook salmon in the region (Table 1). If data from 2006 are ignored, the largest average size of Chinook salmon occurred in 2003, significantly larger ($P < 0.001$) than 2002, 2004 and 2005 for daily growth rates of 0.0 and 0.3 mm and significantly larger ($P < 0.001$) than 2004 for daily growth rates of 1.7 mm. The smallest juvenile Chinook salmon were found during 2004 and were significantly smaller than fish sampled during all other years for each of the daily growth rates ($P < 0.001$ for growth rates of 0.0 and 0.3 mm; $P < 0.001$ for 2003 and 2005 and $P < 0.05$ for 2002 and 2006 for daily growth rates of 1.7 mm).

Juvenile coho salmon were largest during 2003 and smallest during 2005 for all 3 daily growth rates (Table 1). Juvenile coho salmon lengths in this region were significantly larger ($P < 0.001$) during 2003 than all other years for all 3 daily growth rates. Juvenile coho salmon collected during 2002 were significantly larger than those captured during 2004 ($P < 0.001$) and 2005 ($P < 0.001$) for daily growth rates of 0 mm and 2005 ($P < 0.01$) for daily growth rates of 0.3 mm.

The largest juvenile pink salmon occurred during 2002 and the smallest during 2006 for each of the 3 daily growth rates (Table 1). Juvenile pink salmon were significantly larger during 2002 than those captured during 2004 ($P < 0.01$), 2005 ($P< 0.001$), and 2006 ($P < 0.001$) for daily growth rates of 0 mm, 2005 ($P < 0.001$) and 2006 ($P < 0.001$) for daily growth rates of 0.3 mm, and 2003 ($P < 0.05$), 2005 ($P < 0.001$), and 2006 ($P < 0.001$) for daily growth rates of 1.7 mm. Juvenile pink salmon were also significantly larger ($P < 0.001$) during 2003 and 2004 than 2005 and 2006 for daily growth rates of 0 mm and 0.3 mm, and significantly larger during 2003 than 2005 ($P < 0.001$) and 2004 than 2005 ($P < 0.001$) and 2006 ($P < 0.01$) for daily growth rates of 1.7mm. Juvenile pink salmon were significantly larger ($P < 0.001$) during 2003 than 2004 for daily growth rates of 0 mm, but switched for daily growth rates of 1.7 mm where size of juvenile pink salmon was significantly larger ($P < 0.001$) during 2004 than 2003.

NEBS region

The largest and smallest juvenile chum salmon for all daily growth rates were found during 2004 and 2006, respectively (Table 2). The multiple comparison test indicated that juvenile chum salmon were significantly smaller ($P < 0.001$) during 2006 than the previous four years for each daily growth rate. Juvenile chum salmon during 2002 were significantly

larger than 2003 ($P < 0.05$ for 0 mm, $P < 0.01$ for 0.3 mm, $P < 0.001$ for 1.7 mm) and 2005 ($P < 0.001$) for each daily growth rate. Juvenile chum salmon were significantly larger ($P < 0.001$) during 2004 than 2003, 2005, and 2006 for each daily growth rate except 0.0 mm, where juvenile chum salmon during 2004 were significantly larger than 2005 ($P < 0.01$) and 2006 ($P < 0.001$) only.

The smallest juvenile Chinook salmon occurred during 2006 and these fish were significantly smaller ($P < 0.001$) than all other years for daily growth rates of 0.0 mm and 0.3 mm and for all years except 2003 for daily growth rate of 1.7 mm (Table 2). Juvenile Chinook salmon were significantly smaller during 2003 than 2002 ($P < 0.01$ for 0 mm, $P < 0.001$ for 0.3 mm and 1.7 mm), 2004 ($P < 0.001$) for daily growth rates of 0.3 mm and 1.7 mm, 2005 ($P < 0.001$) for all 3 daily growth rates. In addition, juvenile Chinook salmon were significantly larger during 2005 than 2004 ($P < 0.05$) for daily growth rates of 0 mm.

Juvenile coho salmon captured during 2006 were also significantly smaller than coho salmon captured during 2002 – 2004 ($P < 0.001$) and 2005 ($P < 0.05$) for daily growth rates of 0 mm, 2002 ($P < 0.001$), 2003 ($P < 0.05$), and 2004 ($P < 0.001$) for daily growth rates of 0.3 mm, and 2004 ($P < 0.001$) for daily growth rates of 1.7 mm (Table 2). Juvenile coho salmon were significantly larger during 2004 than 2003 ($P < 0.01$ for 0 mm; $P < 0.001$ for 0.3 mm and 1.7 mm) and 2005 ($P < 0.05$) for all 3 daily growth rates.

The largest juvenile pink salmon were found during 2002 and the smallest juvenile pink salmon were found during 2006 for all 3 daily growth rates (Table 2). Juvenile pink salmon were significantly larger ($P < 0.001$) during 2002 than all other years for each daily growth rate and significantly smaller ($P < 0.001$) during 2006 than all other years for each daily growth rate. In addition, juvenile pink salmon were significantly larger ($P < 0.001$) during 2004 than 2003 and 2005 for all 3 daily growth rates, and significantly larger ($P < 0.05$) during 2005 than 2003 for a daily growth rate of 1.7 mm.

Size between regions

Fork lengths of juvenile salmon varied between regions and among years (Tables 1 and 2). Lengths of juvenile chum salmon in the NEBS region were significantly larger ($P < 0.001$) during all years and daily growth rates than juvenile chum salmon captured in the SEBS region except for daily growth 1.7 mm during 2003. Juvenile Chinook salmon in the SEBS region were significantly larger ($P < 0.001$) than those captured in the NEBS region during 2003 and 2006 for daily growth rates of 0.3 mm and 1.7 mm. Juvenile coho salmon captured in the SEBS region were significantly larger than those caught in the NEBS region during 2003 ($P < 0.01$ for 0 mm; $P < 0.001$ for 0.3 mm and 1.7 mm) and 2006 ($P < 0.001$), and significantly smaller than those in the NEBS region during 2004 ($P < 0.001$ for 0 mm and 0.3 mm; $P < 0.01$ for 1.7 mm). Juvenile pink salmon were significantly larger ($P < 0.001$) in the NEBS region during 2002 – 2005 for a daily growth rate of 0.0 mm, significantly larger ($P < 0.001$) in the NEBS region during 2002, 2004, and 2005 for a daily growth rate of 0.3 mm, and significantly larger in the NEBS region during 2002 ($P < 0.001$), 2004 ($P < 0.01$), and 2005 ($P < 0.001$) for a daily growth rate of 1.7 mm. Juvenile pink salmon were significantly larger ($P < 0.001$) in the SEBS region than the NEBS region during 2003 for daily growth rate of 1.7mm.

Diet – SEBS Region

The prey items in juvenile salmon diets varied between years, but the most notable change in percent wet weight of diet items occurred during 2006 (Figures 4a – d). Age-0 pollock were the dominate prey item in sockeye salmon diets during 2002 through 2005 followed by other fish and sand lance (Figure 4a). However, during 2006 sand lance and euphausiids dominated the diet items followed by megalopa and other fish (Figure 4a). Fish consisting of age-0 pollock, other fish, and sand lance were prey items in the diet of juvenile chum salmon during all years except 2006 (Figure 4b). During 2006, euphausiids composed nearly 95% of the wet weight for the stomach contents of juvenile chum salmon. Juvenile Chinook salmon diets consisted mainly of fish including sand lance, age-0 pollock, and other fish (Figure 4c). Too few juvenile Chinook salmon were captured during 2006 for diet analyses in the SEBS region. The percent wet weight of diet items in juvenile coho salmon diets was similar during 2004 and 2005, consisting mainly of age-0 pollock and sand lance (Figure 4d). However the percent wet weight of juvenile coho salmon diets changed dramatically during 2006, consisting mainly of euphausiids (Figure 4d). Fish consisting of age-0 pollock and sand lance were important components of the diet items in juvenile pink salmon stomachs during 2004 and 2005, and zooplankton including amphipods, euphausiids, and other zooplankton were important components for the diet during 2006 (Figure 4e).

Diet – NEBS Region

The most notable change in percent wet weight of prey items of juvenile fish in the NEBS region occurred during 2006, where the percent wet weight of sand lance in the diets increased for all five species of salmon (Figures 5a – d). The percent wet weight of fish in the diet of juvenile chum salmon increased during the five year study (Figure 5a). For instance, amphipods and tunicates dominated the percent wet weight of prey of juvenile chum salmon during 2002; whereas, during 2004 and 2005, juvenile chum salmon diets where composed of approximately 50% fish and 50% zooplankton, increasing to nearly 70% wet weight of fish (50% wet weight of sand lance) by 2006 (Figure 5a). Fish were also important components of the juvenile Chinook salmon diet including sand lance, capelin, age-0 pollock, and other fish (Figure 5b). Juvenile coho salmon prey items consisted mainly of age-0 pollock, other fish, sand lance, and megalopa during 2004 (Figure 5c). However, during 2006, juvenile coho salmon diets consisted mainly of sand lance (nearly 60%), age-0 pollock, and other fish (Figure 5c). For juvenile pink salmon , fish and zooplankton were important components of the diet items during 2004 and 2005; whereas, fish consisting mainly of sand lance (50%), were the main component of the diet items in juvenile pink salmon stomachs in this region during 2006 (Figure 5d).

The average CPUE of important fish prey (age-0 pollock and sand lance) in salmon diets is shown in Figures 6a – b. Age-0 pollock increased from 2002 to 2005, then declined during 2006 in both regions (Figure 6a). The average CPUE of sand lance varied among years in the SEBS regions with the highest average CPUE's occurring during 2000 and 2004 (Figure 6b). Sand lance were not captured during 2003 in either region and the large CPUE during 2002 in the NEBS region comes from a single trawl haul.

Discussion

The first step toward understanding mechanisms associated with highly variable marine survival rates of Pacific salmon is to provide basic biological information during their most critical life history stages. This study presents an examination of the temporal and spatial variation in distribution, size, diet, and average CPUE of five species of juvenile salmon from a

systematic survey along the eastern Bering Sea shelf during fall (August – October) 2002 – 2006. In general, there were spatial variations in distribution among species; juvenile chum, coho and Chinook salmon tended to be distributed nearshore and juvenile sockeye salmon tended to be distributed further offshore. Juvenile salmon were largest during 2002 and 2003 and smallest during 2004 and 2005 in the SEBS region and 2006 in the NEBS region. Annual comparisons of juvenile salmon diet indicated a shift in primary prey for many of the salmon species during 2006 in both the NEBS and SEBS regions. In addition, the average CPUE of juvenile salmon fell sharply during 2006 in the SEBS region.

Can these data provide insight into ecological processes that affect marine survival of western Alaska juvenile salmon during this critical life history period? A recent critical-size and critical-period hypothesis for Pacific salmon that links climate to ecosystem productivity and marine survival of fish was proposed by Beamish and Mahnken (1999). For this hypothesis, Pacific salmon must achieve a sufficient size by the end of the first marine summer in order to survive the metabolic demands during a period of energy deficit in late fall and winter. The critical-size and critical-period hypothesis links natural mortality of salmon to the productivity of the ocean ecosystem via the availability of nutrients regulating the food supply and hence competition for food (i.e., bottom-up processes; Beamish and Mahnken 1999).

There are several relationships that appear to be important in governing production on the eastern Bering Sea shelf (Hunt et al. 2002). First, the onset of spring net primary production on the eastern Bering Sea shelf is linked to the timing and duration of ice cover and winter winds. Second, mesozooplankton production is higher when the spring bloom occurs in warm water than during years when the bloom occurs in cold water at the ice edge. From these relationships we would expect higher marine survival of juvenile western Alaska salmon during years with warm water spring blooms as there would be more food available to salmon possibly leading to high early marine growth rates and reduced size-selective mortality during summer and late fall/winter. Years with cold-water spring blooms should have the opposite effect; food limitation would lead to slower growth during the first year at sea and a higher percentage of fish from a particular brood year not reaching the critical size to survive fall and winter.

The climate record for the Bering Sea indicates the coldest spring sea surface temperatures in the last seven years occurred during 2000, 2001, and 2006; warmer spring temperatures occurred during 2002 – 2005 (Figure 7). Data presented in this paper represent fish captured during four warm years (2002 – 2005) and one cold year (2006). However, we do have survey data on juvenile Bristol Bay sockeye salmon collected during 2000 and 2001 on the eastern Bering Sea shelf, and recent analyses of these data (2000 to 2002) found that relative marine survival rates were lower for these salmon during 2000 and 2001 (cool) and higher during 2002 (warm; Farley et al. 2007a). Farley et al. (2007a) suggested that the lower relative marine survival rates of Bristol Bay sockeye salmon were attributed to the significantly smaller size of juvenile Bristol Bay sockeye salmon during 2000 and 2001, as these fish would have a higher probability of marine mortality after their first summer at sea due to size-selective mortality. The recent increase in adult returns (2004 – 2006; references) to western Alaska rivers also provides evidence that juvenile salmon may have higher marine survival rates during years with warm spring SSTs (2002 – 2004)

If there is a relationship between spring sea surface temperatures and ocean productivity on the eastern Bering Sea shelf, then we would predict lower growth rates and increased marine mortality rates for juvenile salmon during 2006, a year with cool spring sea

temperatures. Our data indicated that CPUE of all juvenile salmon species declined dramatically in the SEBS region during 2006. The average CPUE of many juvenile salmon species remained high in the NEBS region, however the fork length for all juvenile salmon species in the NEBS region was significantly lower than the previous years. It is likely that juvenile salmon in the SEBS region experienced lower growth rates after leaving freshwater, thus higher size-selective mortality due to predation during summer (Parker 1968; Willette et al. 1999) Although average CPUE of juvenile salmon was high in the NEBS region, we would expect that the significantly lower size of these fish would negatively impact marine survival during late fall and winter as it is likely that smaller fish have lower energy reserves and may have higher overwinter mortality due to starvation (Oliver et al. 1979; Henderson et al. 1988).

Also, if spring sea temperatures are driving pelagic production on the eastern Bering Sea shelf, then we should expect to see changes in relative abundance of pelagic forage fish species as well. With the exception of 2002, age-0 pollock were abundant during years with warm spring temperatures. In addition to being more abundant, age-0 pollock were important prey items for all juvenile salmon species in the SEBS region. A decline in their abundance during 2006 was reflected in a switch from age-0 pollock to zooplankton as dominant prey for juvenile salmon in that region. Unfortunately our survey does not provide good estimates of pelagic forage fish abundance in the NEBS region. We note that a mixture of age-0 pollock, capelin and sand lance were important components of the juvenile salmon diets during 2002 to 2005, whereas sand lance were the dominant prey item of juvenile chum, coho, and pink salmon in the NEBS region during 2006.

In conclusion, we believe our research on juvenile salmon ecology along the eastern Bering Sea shelf has added insight to our understanding of ecological processes that affect their early marine growth and survival rate. A recent study suggested that regional averages of summer sea surface temperature may be a useful predictor of marine survival rates for Pacific salmon; (i.e., warmer summer SSTs were positively correlated with higher marine survival rates for salmon (Mueter et al. 2002). Data presented here and prior publications on juvenile Bristol Bay sockeye salmon suggest that spring SSTs on the eastern Bering Sea shelf likely impact growth rate of juvenile western Alaska salmon through bottom-up control in the ecosystem (Straty 1974; Farley et al. 2007a; Farley et al. 2007b). Cold spring SSTs lead to lower growth and marine survival rates for juvenile western Alaska salmon; warm spring SSTs have the opposite effect.

Acknowledgments

We gratefully appreciate the help of the captains (M. Cavanaugh and S. Brandstitter) and the crew of the FV *Sea Storm* and captain S. O'Brien and the crew of the FV *Northwest Explorer* for their fine efforts and technical assistance in all aspects of the field surveys. We thank the Yukon River Drainage Fisheries Association for funding technician (T. Hamilton, G. Yaska, and H. George) support during the 2002 to 2005 research cruises. We also than the two anonymous reviewers, as their comments and suggestions greatly improved the manuscript.

References

Beamish, R. J., and C. Mahnken. 1999. Taking the next step in fisheries management. Pages 1 – 21 *in* Ecosystem approaches for fisheries management. Alaska Sea Grant College Program AK-SG-99-01.

Beamish, R. J., and C. Mahnken. 2001. A critical size and period hypothesis to explain natural regulation of salmon abundance and the linkage to climate and climate change. Progress in Oceanography 49: 423 – 437.

Beamish, R. J., C. Mahnken, and C. M. Neville. 2004. Evidence that reduced early marine growth is associated with lower marine survival of coho salmon. Transactions of the American Fisheries Society 133(1):26 – 33.

Burril, S. E. 2007. Feeding ecology and energy density of chum salmon, *Oncorhynchus keta*, from Kuskokwim Bay, western Alaska. Master's thesis. University of Alaska Fairbanks, Fairbanks, Alaska.

Farley, E. V., Jr., J. M Murphy, B. W. Wing, J. H. Moss, and A. Middleton. 2005. Distribution, migration pathways, and size of western Alaska juvenile salmon along the eastern Bering Sea shelf. Alaska Fisheries Research Bulletin 11(1): 15 – 26.

Farley, E. V., Jr., J. M. Murphy, M. D. Adkison, L. B. Eisner, J. H. Helle, J. H. Moss, and J. Nielsen. 2007a. Early marine growth in relation to marine stage survival rate for Alaska sockeye salmon (*Oncorhynchus nerka*). Fishery Bulletin 105:121 – 130.

Farley, E. V., Jr., J. M. Murphy, M. Adkison, and L. Eisner. 2007b. Juvenile sockeye salmon distribution, size, condition, and diet during years with warm and cool spring sea temperatures along the eastern Bering Sea shelf. Journal of Fish Biology 71:1145 – 1158.

Fisher, J. P., and W. G. Pearcy. 1988. Growth of juvenile coho salmon (Oncorhynchus kisutch) off Oregon and Washington, USA, in years of differing coastal upwelling. Canadian Journal of Fisheries and Aquatic Sciences 45:1036 – 1044.

Friedland, K. D., R. W. Hasas, and T. F. Sheehan. 1996. Post-smolt growth, maturation, and survival of two stocks of Atlantic salmon. Fishery Bulletin 94:654 – 663.

Fukuwaka, M., and M. Kaeriyama. 1994. A back-calculation method for estimating individual growth of juvenile chum salmon by scale analysis. Scientific Reports of the Hokkaido Salmon Hatchery. 48:1-9.

Hartt, A. C., and M. B. Dell. 1986. Early oceanic migrations and growth of juvenile Pacific salmon and steelhead trout. International North Pacific Fisheries Commission Bulletin 46.

Henderson, P. A., R. H. A. Holmes, and R. N. Bamber. 1988. Size-selective overwintering mortality in the sand smelt, *Atherina boyeri* Risso, and its role in population regulation. Journal of Fish Biology 33:221 – 233.

Hillbruber, N., C. E. Zimmerman, S. E. Burril, and L. J. Haldorson. 2007. Early marine ecology of juvenile chum salmon (*Oncorhynchus keta*) in Kuskokwim Bay, Alaska. Project R0327, Final Report, North Pacific Research Board, Anchorage, Alaska.

Hillgruber, N., and C. E. Zimmerman. 200**X**. Estuarine ecology of juvenile salmon in western Alaska: A review. Pages **X – Y** in CC. Krueger and C.E. Zimmerman, editors. **Title will be inserted by copy editor**. American Fisheries Society Symposium **X**, Bethesda, Maryland.

Holtby, L. B., B. C. Andersen, and R. K Kadawaki. 1990. Importance of smolt size and early ocean growth to interannual variability in marine survival of coho salmon

(Oncorhynchus kisutch). Canadian Journal of Fisheries and Aquatic Sciences 47:2181 – 2194.

Hunt, G. L, Jr., P. Stabeno, G. Walters, E. Sinclair, R. Brodeur, J. Napp, N. Bond. 2002. Climate change and control of the southeastern Bering Sea pelagic ecosystem. Deep-Sea Research II 49:5821 – 5853.

Insightful. 2001. S-Plus 6 for Windows guide to statistics. Insightful Corporation, Volume 1, Seattle, WA.

Isakson, J. S., J. P. Houghton, D. E. Rogers, and S. S. Parker. 1986. Fish use of inshore habitats north of the Alaska Peninsula June – September 1984 and June – July 1985. Final Report, Outer Continental Shelf Environmental Assessment Program, Research Unit 659.

Kalnay, E., M. Kanamitsu, R. Kistler, W. Collins, D. Deaven, L. Gandin, M. Iredell, S. Saha, G. White, J. Woollen, Y. Zhu, A. Leetmaa, B. Reynolds, M. Chelliah, W. Ebisuzaki, W. Higgens, J. Janowiak, K.C. Mo, C. Ropelewski, J. Wang, R. Jenne, and D. Joseph. 1996. The NCEP/NCAR 40-year reanalysis project. Bulletin of the American Meteorological Society 77(3)437-471.

Kruse, G. H. 1998. Salmon run failures in 1997 – 1998: A link to anomalous ocean conditions? Alaska Fishery Research Bulletin 5(1): 55 – 63.

Martin, D. J., C. A. Simenstad, D. A. Milward, E. C. Volk, M. L. Stevenson, P. Nunes, M. Savoie, and R. A. Grotefendt. 1986. Distribution, seasonal abundance, and feeding dependencies of juvenile salmon and non-salmonid fishes in the Yukon River Delta. Final Report, Outer Continental Shelf Environmental Assessment Program, Research Unit 660, Dames & Moore, Seattle.

Merritt, M. F., and J. A. Raymond. 1983. Early life history of chum salmon in the Noatak River and Kotzebue Sound. Alaska Department of Fish and Game, Division of Fisheries Rehabilitation, Enhancement, and Development Report #1, Juneau, Alaska.

Mueter, F. J., D. M. Ware, and R. M Peterman. 2002. Spatial correlation patterns in coastal environmental variables and survival rates of salmon in the north-east Pacific Ocean. Fisheries Oceanography 11(4):205 – 218.

Nemeth, M. J., B. Haley, S. Kinneen, and W. Griffiths. 2003. Ecology of juvenile chum salmon from Norton Sound, Alaska. Annual Report to the Norton Sound Disaster Relief Fund by the Norton Sound Economic Development Corporation and LGL Alaska Research Associates, Inc. Anchorage, Alaska.

Oliver, J. D., G. F. Holeton, and K. E. Chua. 1979. Overwinter mortality of fingerling smallmouth bass in relation to size, relative energy stores, and environmental temperature. Transactions of the American Fisheries Society 108:130 -136.

Orsi, J. A., M. V. Sturdevant, J. M. Murphy, D. G. Mortensen, and B. L. Wing. 2000. Seasonal habitat use and early marine ecology of juvenile Pacific salmon in southeastern Alaska. Pages 111 – 122 *in* J. H. Helle, Y. Ishida, D. Noakes, and V. Radchenko, editors. Recent changes in ocean production of Pacific salmon. North Pacific Anadromous Fish Commission Bulletin 2.

Parker, R. R. 1968. Marine mortality schedules of pink salmon of the Bella Coola River, Central British Columbia. Journal of the Fisheries Research Board Canada 25:757-794.

Pearcy, W. G. 1992. Ocean ecology of the North Pacific salmonids. University of Washington Press. Seattle, WA.

Raymond, J. A., M. Merritt, and C. Skaugstad. 1984. Nearshore fishes of Kotzebue Sound in summer. Alaska Department of Fish and Game, Division of Fisheries Rehabilitation, Enhancement, and Development Report #37, Juneau, Alaska.

Straty, R. R. 1974. Ecology and behavior of juvenile sockeye salmon (*Oncorhynchus nerka*) in Bristol Bay and the eastern Bering Sea. Pages 285 – 320 *in* D. W. Hood and E. J. Kelley, editors. Oceanography of the Bering Sea with emphasis on renewable resources. Proceedings of the International Symposium on Bering Sea Study, Institute of Marine Sciences Occasional Publication 2, University of Alaska, Fairbanks.

Willette, T. M., R. T. Cooney, and K. Hyer. 1999. Predator foraging mode shifts affecting mortality of juvenile fishes during the sub arctic spring bloom. Canadian Journal of Fisheries and Aquatic Sciences 56:364 – 376.

TABLE 1. Annual mean ± (SE) fork lengths for daily growth adjusted by 0.0, 0.3, and 1.7 (mm day^{-1}) for juvenile salmon collected in the SEBS region. Statistics include sample size (*n*).

Species	Year	*n*	Daily Growth (mm day^{-1})		
			0.0	0.3	1.7
Pink	2002	46	188.8 (4.6)	188.0 (4.4)	186.9 (4.1)
	2003	790	182.7 (0.5)	180.2 (0.5)	177.0 (0.5)
	2004	653	177.8 (0.7)	179.7 (0.7)	182.3 (0.6)
	2005	876	161.7 (1.0)	164.5 (0.9)	168.1 (0.8)
	2006	14	154.8 (5.0)	157.7 (4.3)	161.6 (3.6)
Chum	2002	1069	184.3 (0.7)	184.6 (0.6)	184.9 (0.6)
	2003	949	187.1 (0.8)	185.9 (0.7)	184.4 (0.7)
	2004	885	179.7 (0.8)	183.5 (0.7)	188.6 (0.6)
	2005	687	172.0 (0.9)	175.6 (0.7)	180.3 (0.6)
	2006	30	179.9 (3.0)	182.3 (3.0)	185.4 (3.2)
Sockeye	2002	2070	195.7 (0.8)	198.5 (0.7)	202.2 (0.7)
	2003	2168	208.1 (0.8)	208.0 (0.7)	207.9 (0.7)
	2004	1845	182.9 (0.7)	187.4 (0.7)	193.3 (0.6)
	2005	2265	185.9 (0.7)	189.9 (0.7)	195.2 (0.6)
	2006	614	192.8 (1.2)	195.9 (1.1)	200.1 (1.1)
Coho	2002	228	291.5 (1.7)	292.5 (1.6)	293.9 (1.5)
	2003	498	309.4 (1.1)	309.3 (1.1)	309.1 (1.1)
	2004	87	277.5 (2.9)	284.0 (2.8)	292.7 (2.8)
	2005	116	276.4 (2.4)	282.1 (2.4)	289.8 (2.4)
	2006	40	285.1 (5.4)	287.2 (5.4)	290.0 (5.5)
Chinook	2002	191	205.6 (1.5)	208.9 (1.4)	213.3 (1.3)
	2003	190	220.0 (1.4)	219.8 (1.4)	219.6 (1.4)
	2004	258	190.1 (1.3)	196.9 (1.2)	205.9 (1.2)
	2005	291	203.0 (1.2)	208.7 (1.1)	216.4 (0.9)
	2006	6	240.8 (15.6)	240.0 (16.9)	239.0 (18.8)

TABLE 2. Annual mean ± SE fork lengths for daily growth adjusted by 0.0, 0.3, and 1.7 (mm day^{-1}) for juvenile salmon collected in the NEBS region. Statistics include sample size (*n*).

Species	Year	*n*	Daily Growth (mm day^{-1})		
			0.0	0.3	1.7
Pink	2002	392	215.8 (0.8)	212.4 (0.8)	207.9 (0.8)
	2003	361	188.7 (0.8)	181.4 (0.8)	171.5 (0.8)
	2004	621	192.7 (0.9)	189.8 (0.9)	185.9 (0.9)
	2005	287	188.6 (1.2)	183.3 (1.2)	176.3 (1.2)
	2006	353	150.8 (0.6)	151.0 (0.6)	151.2 (0.6)
Chum	2002	1097	205.3 (0.5)	201.0 (0.4)	195.3 (0.4)
	2003	714	202.1 (0.7)	195.1 (0.7)	185.8 (0.7)
	2004	482	205.4 (0.9)	202.0 (0.9)	197.4 (0.9)
	2005	258	199.6 (1.1)	194.3 (1.1)	187.2 (1.1)
	2006	645	156.1 (0.5)	156.7 (0.5)	157.6 (0.6)
Sockeye	2002	56	241.7 (3.4)	238.4 (3.4)	234.0 (3.5)
	2003	29	238.0 (2.8)	230.4 (2.9)	220.2 (2.9)
	2004	352	216.7 (1.0)	212.9 (1.0)	207.8 (1.1)
	2005	12	239.9 (5.6)	233.6 (5.6)	225.1 (5.6)
	2006	2	178.5 (45.5)	180.1 (45.3)	182.4 (45.1)
Coho	2002	16	297.2 (4.4)	293.7 (4.4)	289.1 (4.5)
	2003	24	289.8 (4.8)	284.5 (4.7)	277.4 (4.7)
	2004	105	311.5 (2.0)	308.5 (1.9)	304.5 (1.8)
	2005	13	286.9 (6.0)	284.6 (5.9)	281.4 (5.7)
	2006	94	263.8 (2.6)	267.1 (2.9)	271.5 (3.5)
Chinook	2002	112	227.6 (3.1)	222.8 (3.2)	216.5 (3.3)
	2003	129	214.9 (2.7)	207.8 (2.7)	198.4 (2.7)
	2004	175	220.7 (2.0)	219.0 (2.0)	216.7 (2.0)
	2005	129	229.9 (2.7)	225.8 (2.6)	220.2 (2.5)
	2006	106	189.5 (2.2)	190.1 (2.2)	190.8 (2.2)

Figure Captions

FIGURE 1. Station locations for the U.S. Bering Aleutian Salmon International Survey during 2002 and 2003 (a) and 2004 – 2006 (b).

FIGURE 2. Percentage of total catch in relation to (a) latitudinal meridians in the SEBS region and (b) longitudinal meridians in the NEBS region for juvenile pink (– - –), chum (---), sockeye (—), coho (– – –), and Chinook (– - - –) salmon.

FIGURE 3. Relative abundance (catch per unit effort during a 30-minute trawl haul) of (a) sockeye, (b) chum, (c) Chinook, (d) coho, and (e) pink salmon in the SEBS and NEBS regions during August – October 2002 – 2006.

FIGURE 4. Interannual comparison of juvenile salmon diets in the SEBS region expressed as percent by prey weight for (a) sockeye, (b) chum, (c) Chinook, (d) coho, and (e) pink salmon collected along the eastern Bering Sea shelf during August – September 2002 – 2006. Other zooplankton (Ozoop) include arthropods, chaetognaths, *Limacina* spp., and mysids. Other fish (Ofish) include cottids, clupeids, *Sebastes*, and pleuronectids.

FIGURE 5. Interannual comparison of juvenile salmon diets in the NEBS region expressed as percent by prey weight for (a) chum, (b) Chinook, (c) coho, and (d) pink salmon collected along the eastern Bering Sea shelf during August – September 2002 – 2006. Other zooplankton (Ozoop) include arthropods, chaetognaths, *Limacina* spp., and mysids. Other fish (Ofish) include cottids, clupeids, *Sebastes*, and pleuronectids.

FIGURE 6. Relative abundance (catch per unit effort during a 30-minute trawl haul) of (a) age-0 pollock in the SEBS and NEBS regions and (b) sand lance in the SEBS region during August – October 2002 – 2006.

FIGURE 7. Index of May sea surface temperatures (SSTs) calculated as mean monthly SSTs averaged over the area 54.3°N to 60°N, 161.2°W to 172.5°W. The index values are the deviations from the mean value (2.33°C) for the 1970 – 2000 period normalized by the standard deviation (0.76°C). Data courtesy of http://www.berginclimate.noaa.gov.

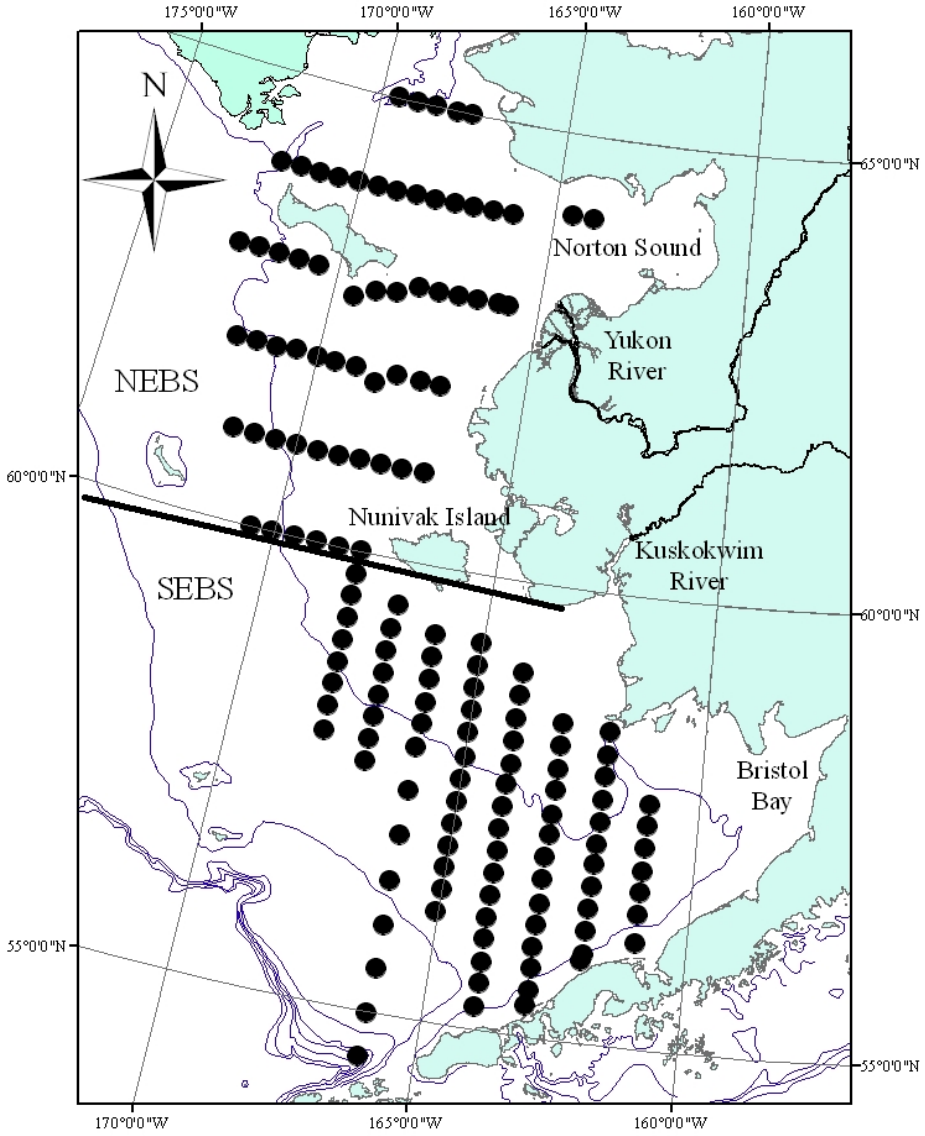
175°0'0"W
170°0'0"W
165°0'0"W
160°0'0"W
N
65°0'0"N
Norton Sound
Yukon
River
NEBS
60°0'0"N
Nunivak Island
Kuskokwim
River
SEBS
60°0'0"N
Bristol
Bay
55°0'0"N
55°0'0"N
170°0'0"W
165°0'0"W
160°0'0"W

Figure 1a.

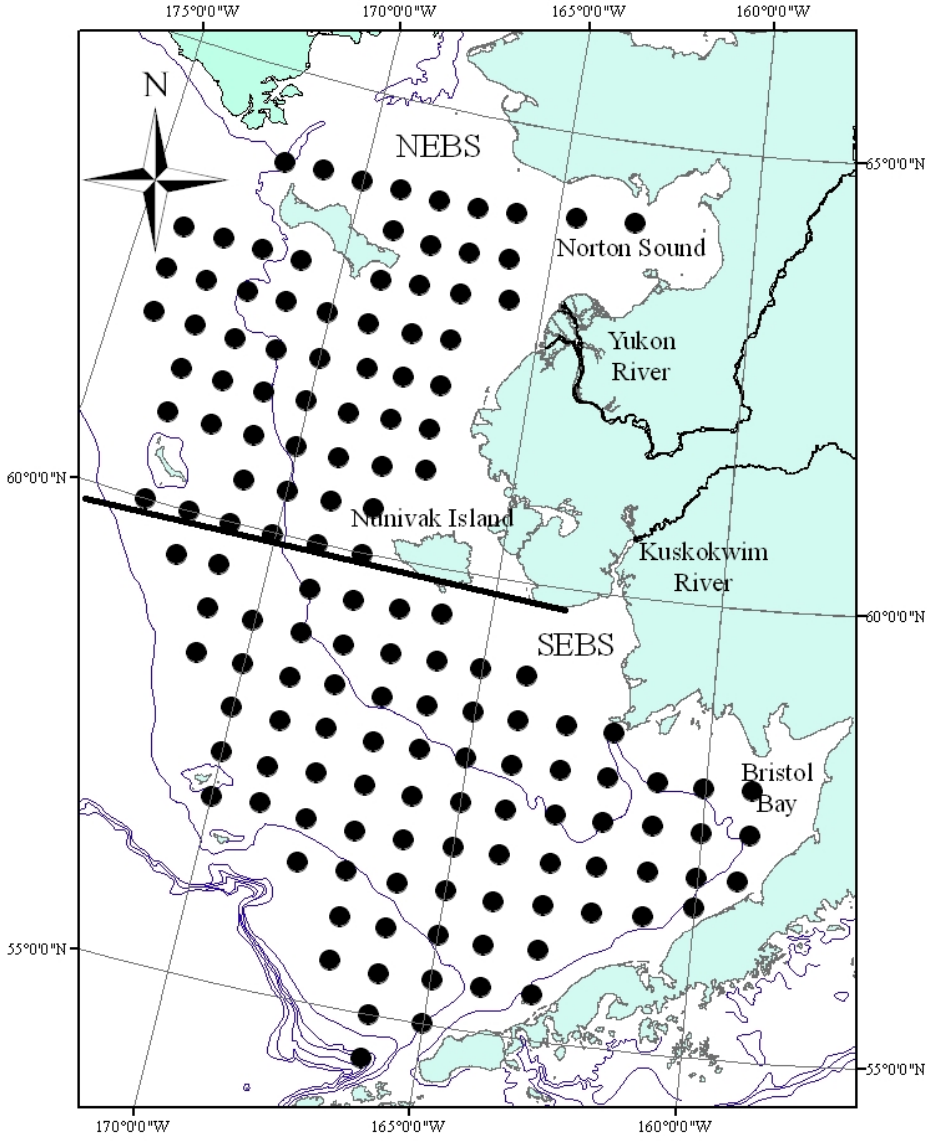
175°0'0"W
170°0'0"W
165°0'0"W
160°0'0"W
N
NEBS
65°0'0"N
Norton Sound
Yukon
River
60°0'0"N
Nunivak Island
Kuskokwim
River
60°0'0"N
SEBS
Bristol
Bay
55°0'0"N
55°0'0"N
170°0'0"W
165°0'0"W
160°0'0"W

Figure 1b.
a.

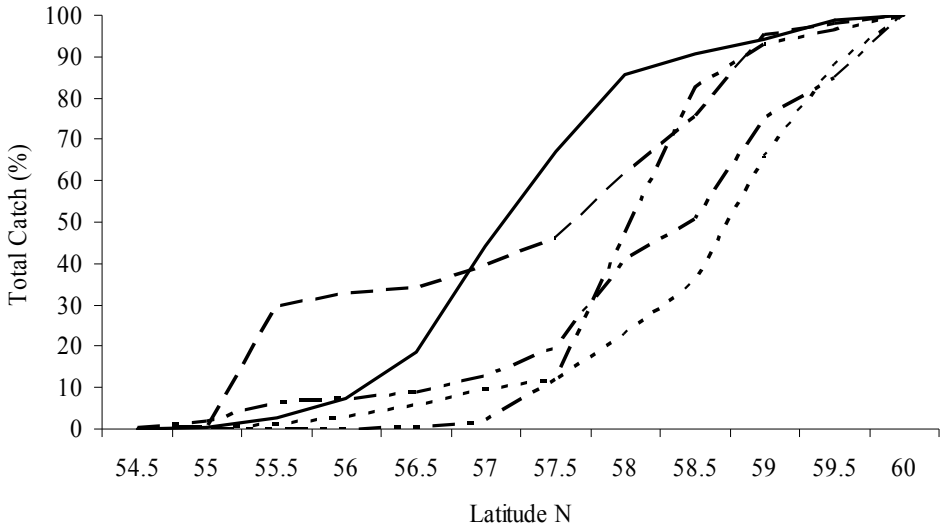
100
90
80
70
60
50
40
30
20
10
0
Total Catch (%)
54.5
55
55.5
56
56.5
57
57.5
58
58.5
59
59.5
60
Latitude N

b.

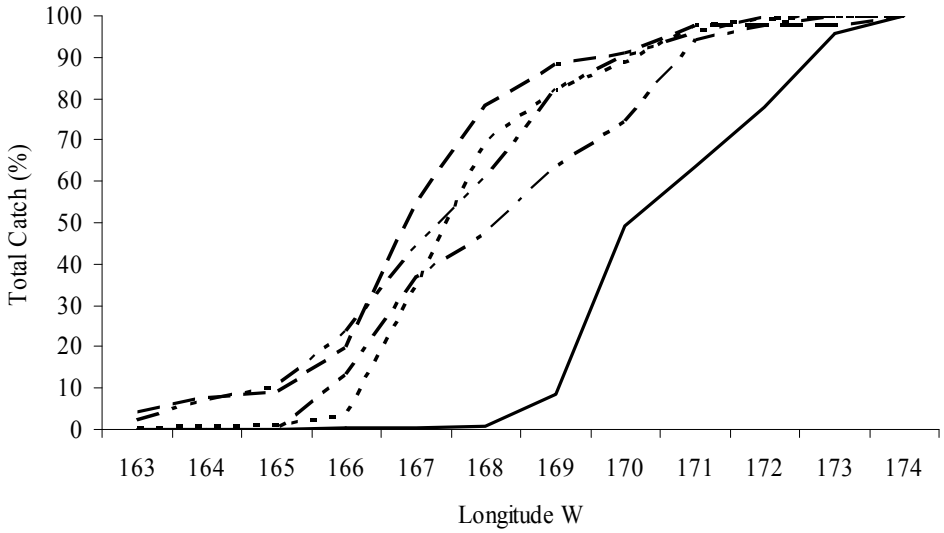
100
90
80
70
60
50
40
30
20
10
0
Total Catch (%)
163
164
165
166
167
168
169
170
171
172
173
174
Longitude W

Figure 2.

a

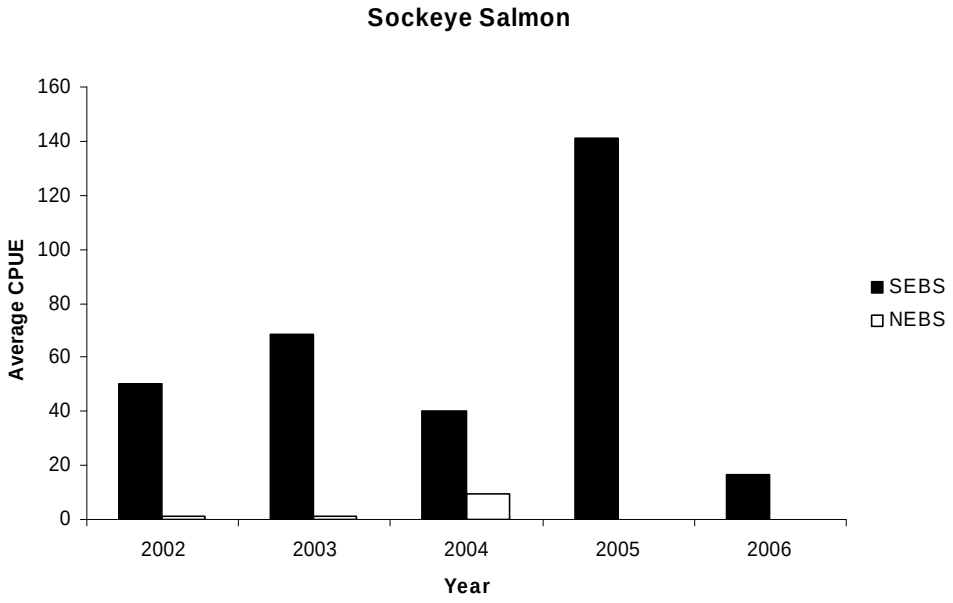
Sockeye Salmon
160
140
120
100
80
60
40
20
0
Average CPUE
2002
2003
2004
2005
2006
Year
SEBS
NEBS

b

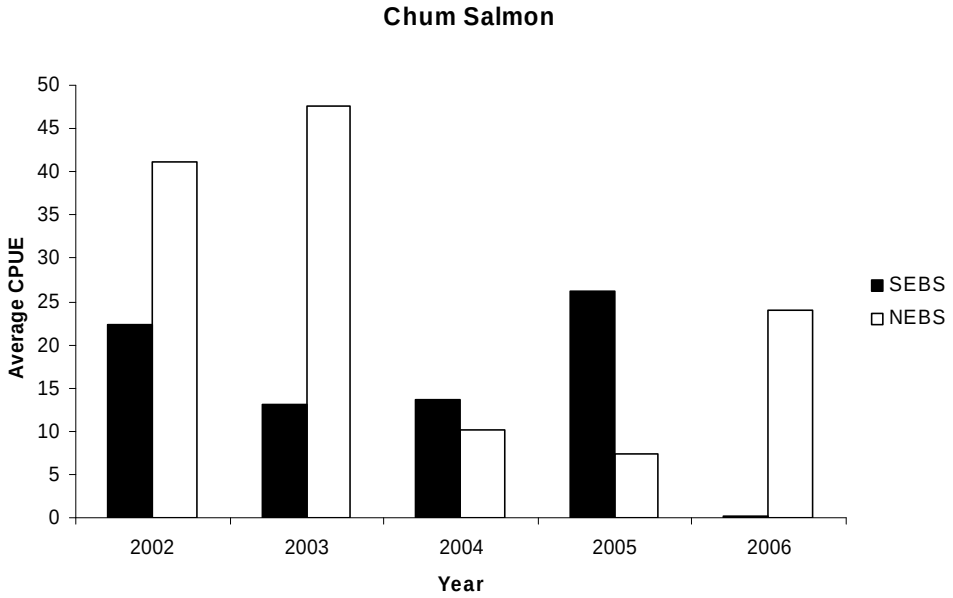
Chum Salmon
50
45
40
35
30
25
20
15
10
5
0
Average CPUE
2002
2003
2004
2005
2006
Year
SEBS
NEBS

Figure 3

c

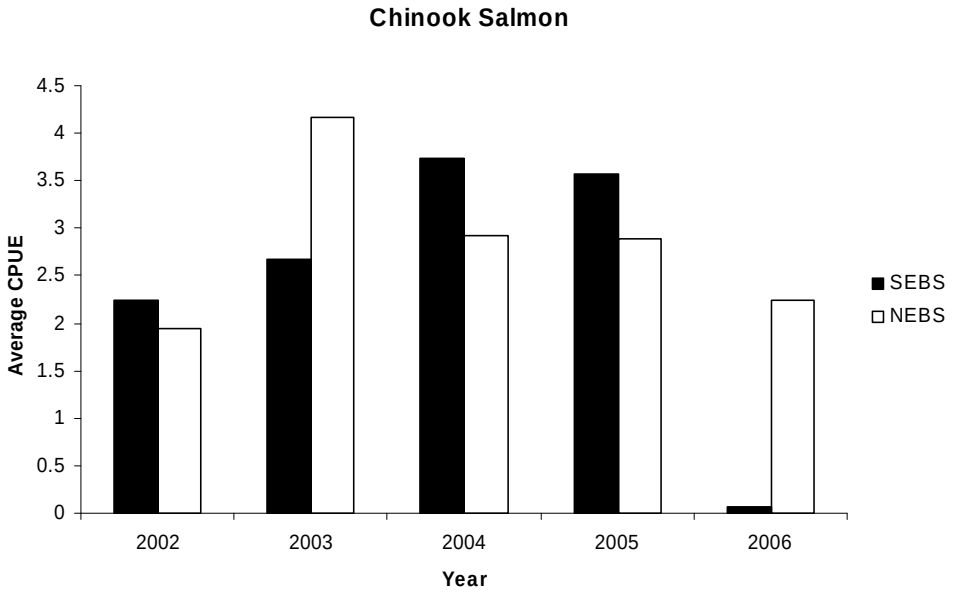
Chinook Salmon
Average CPUE
4.5
4
3.5
3
2.5
2
1.5
1
0.5
0
2002
2003
2004
2005
2006
Year
SEBS
NEBS

d

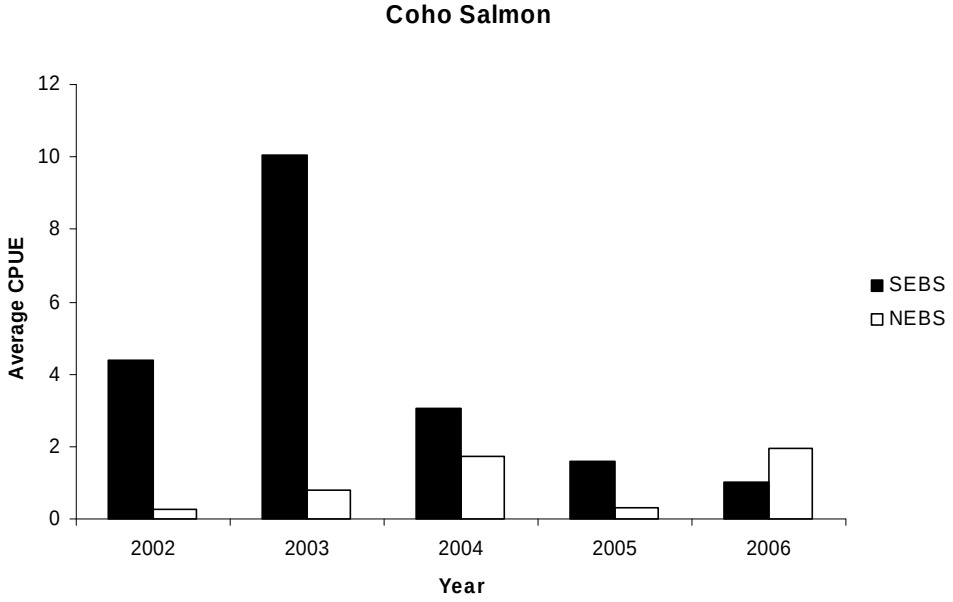
Coho Salmon
Average CPUE
12
10
8
6
4
2
0
2002
2003
2004
2005
2006
Year
SEBS
NEBS

Figure 3

e

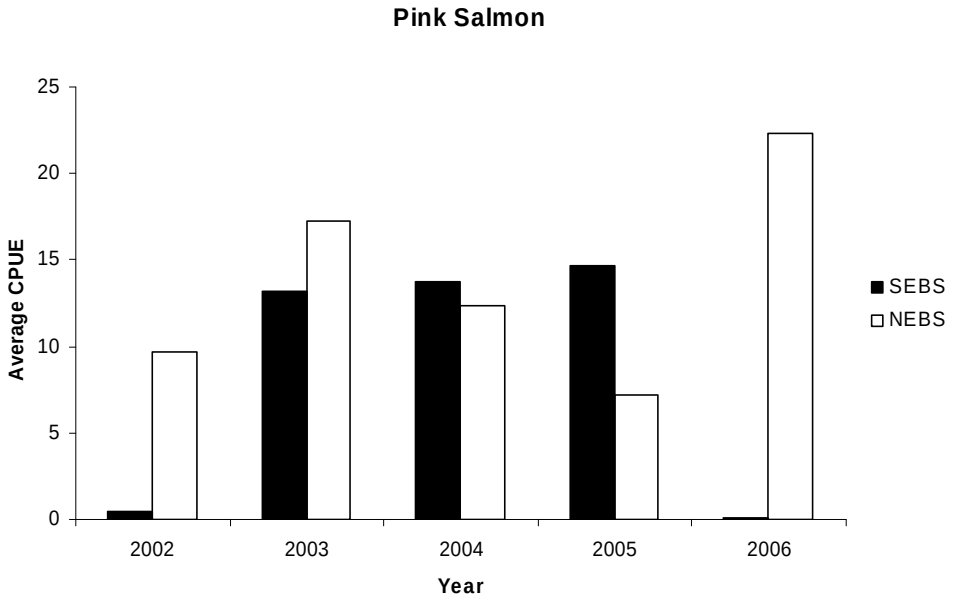
Pink Salmon
Average CPUE
25
20
15
10
5
0
2002
2003
2004
2005
2006
Year
SEBS
NEBS

Figure 3

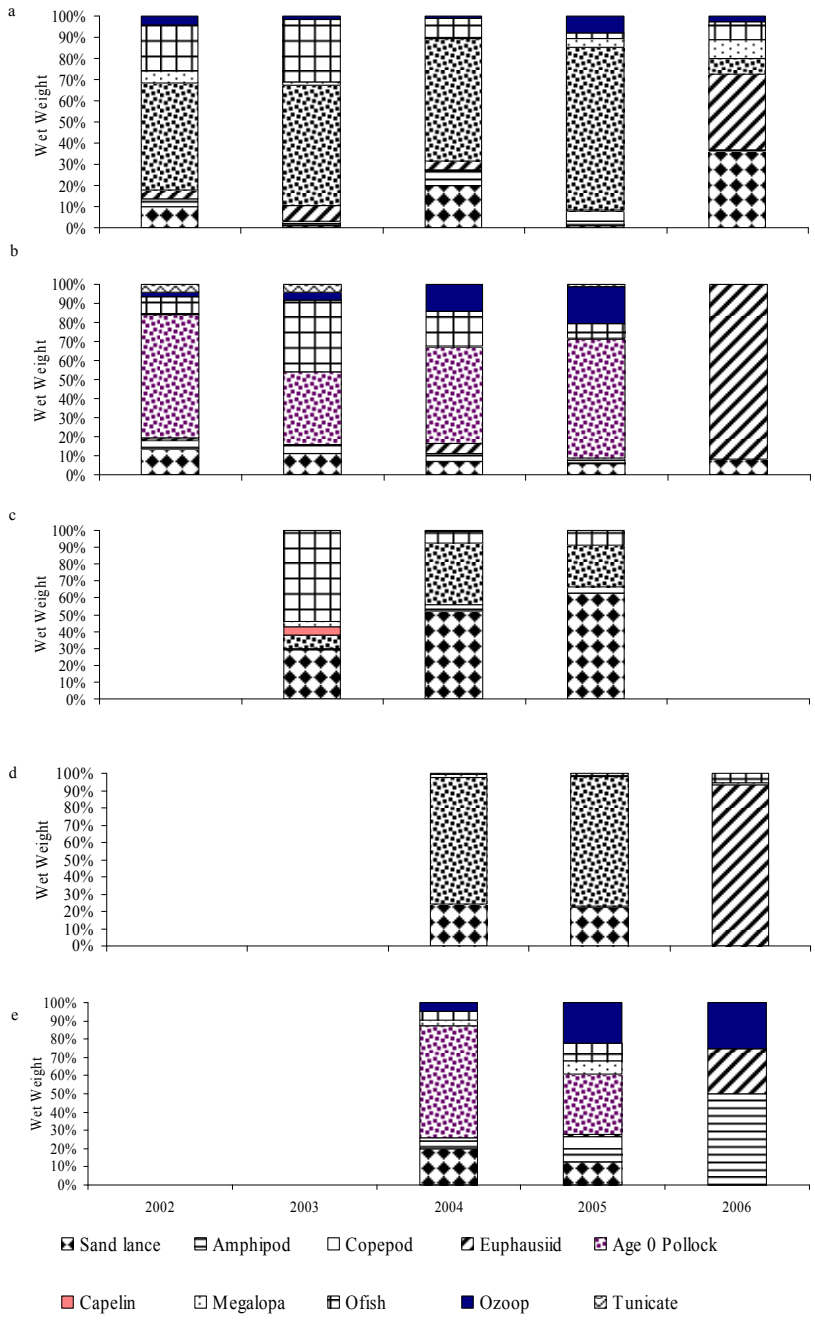
a
b
c
d
e
Wet Weight
100%
90%
80%
70%
60%
50%
40%
30%
20%
10%
0%
2002
2003
2004
2005
2006
Sand lance
Amphipod
Copepod
Euphausiid
Age 0 Pollock
Capelin
Megalopa
Ofish
Ozoop
Tunicate

Figure 4

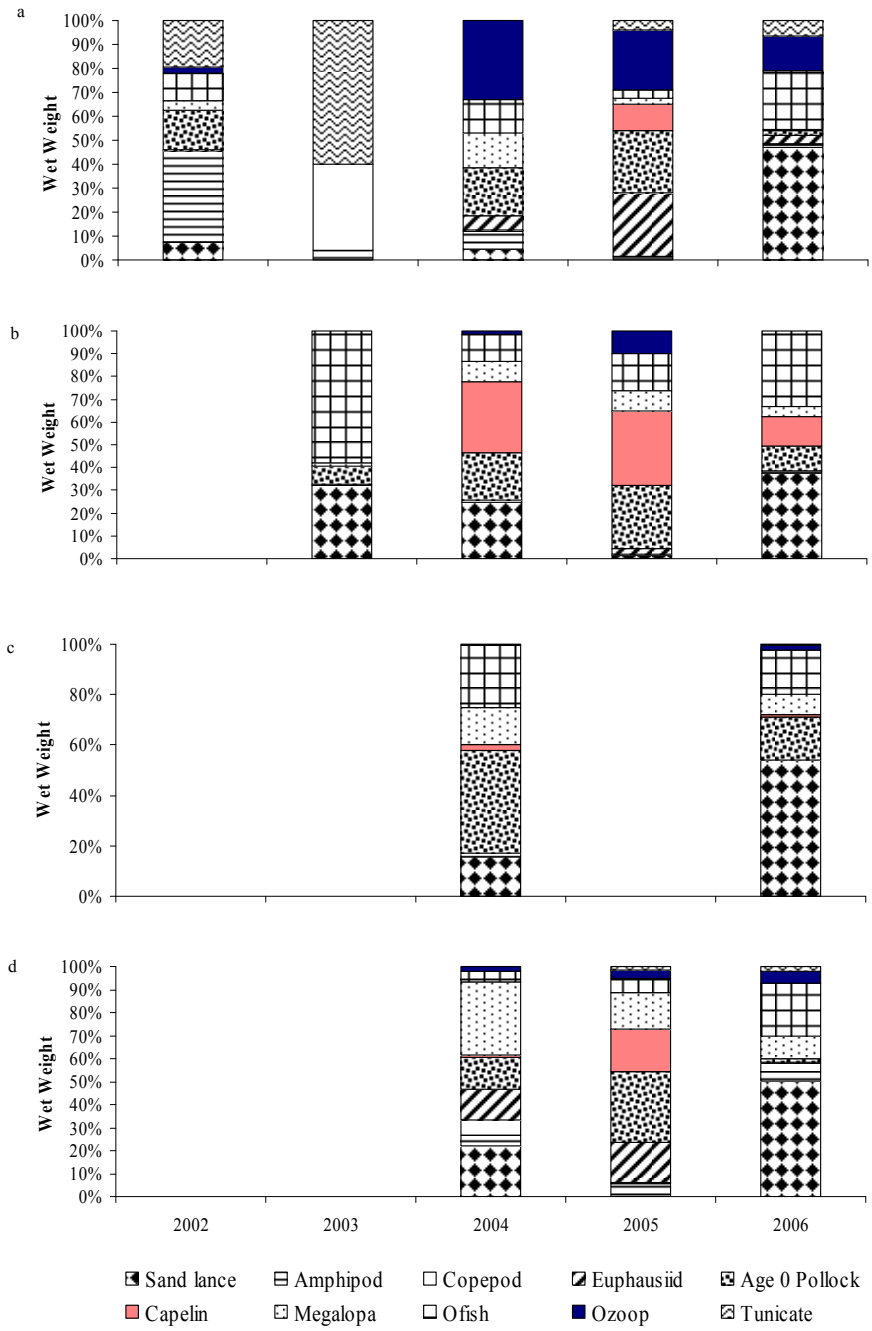
a
b
c
d
Wet Weight
100%
90%
80%
70%
60%
50%
40%
30%
20%
10%
0%
2002
2003
2004
2005
2006
Sand lance
Amphipod
Copepod
Euphausiid
Age 0 Pollock
Capelin
Megalopa
Ofish
Ozoop
Tunicate

Figure 5

a

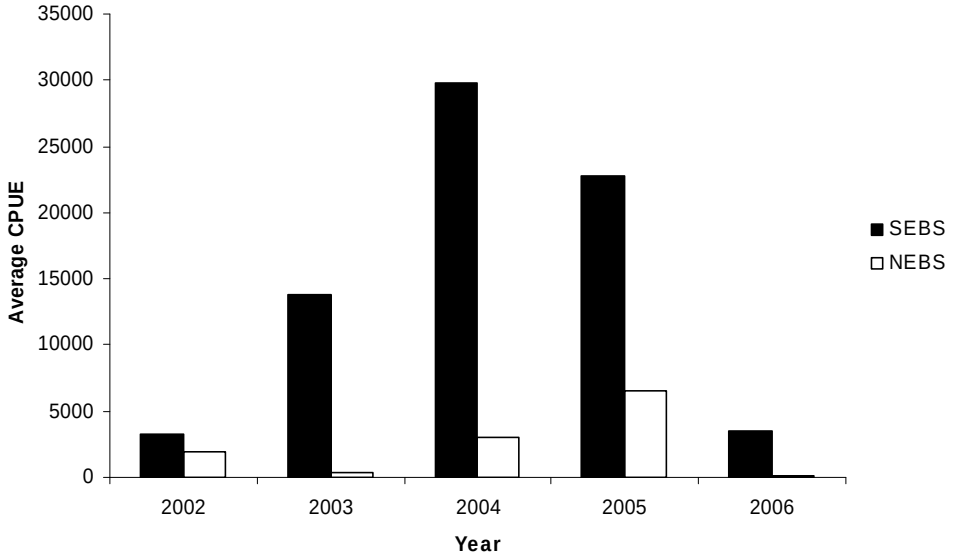
35000
30000
25000
20000
15000
10000
5000
0
Average CPUE
2002
2003
2004
2005
2006
Year
SEBS
NEBS

b

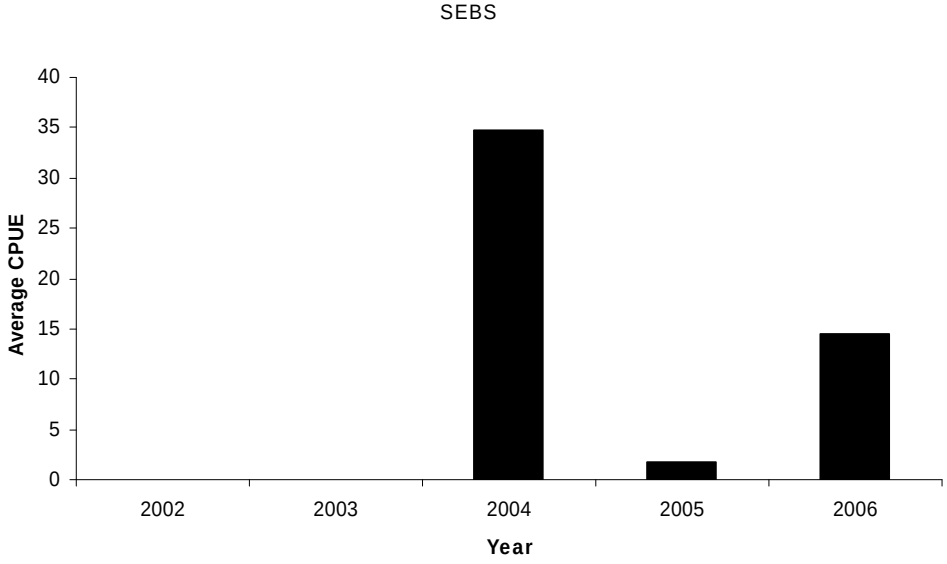
SEBS
40
35
30
25
20
15
10
5
0
Average CPUE
2002
2003
2004
2005
2006
Year

Figure 6

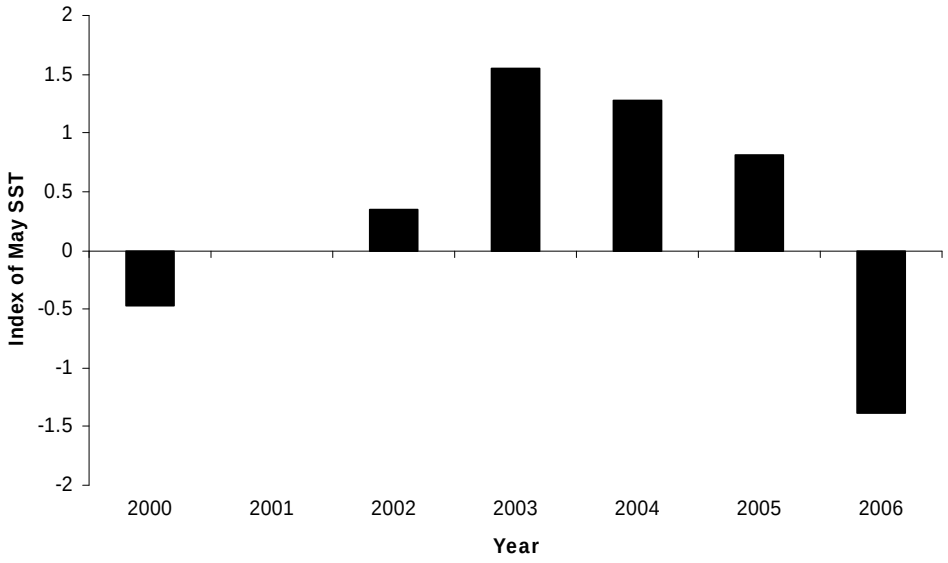
2
1.5
1
0.5
0
-0.5
-1
-1.5
-2
Index of May SST
2000
2001
2002
2003
2004
2005
2006
Year

Figure 7

Appendix 2

Farley, E.V., Jr., J.H. Moss. In press. Growth rate potential of juvenile chum salmon on the eastern Bering Sea shelf—an assessment of salmon carrying capacity. North Pacific Anadromous Fish Commission, Bulletin 5.

GROWTH RATE POTENTIAL OF JUVENILE CHUM SALMON ON THE EASTERN BERING SEA SHELF -- AN ASSESSMENT OF SALMON CARRYING CAPACITY

by

Edward V. Farley, Jr.[1] and Jamal H. Moss

National Oceanic Atmospheric Administration
National Marine Fisheries Service
Alaska Fisheries Science Center
Auke Bay Laboratories, 17109 Point Lena Loop Road, Juneau, AK 99801, USA

[1] All correspondence should be addressed to E.V. Farley, Jr.
email:

Abstract: Spatial and temporal variation in growing conditions for juvenile salmon may determine the survival of salmon after their first year at sea. To assess this aspect of habitat quality, a spatially explicit bioenergetics model was used to predict juvenile chum salmon (*Oncorhynchus keta)* growth rate potential (GRP) on the eastern Bering Sea shelf during years with cold and warm spring sea surface temperatures (SSTs). Annual averages of juvenile chum salmon GRP were generally lower among years and regions with cold spring SSTs. In addition, juvenile chum salmon GRP was generally higher in offshore than in nearshore regions of the eastern Bering Sea shelf during years with warm SSTs; however, the distribution (catch per unit effort) of juvenile chum salmon was not significantly ($p < 0.05$) related to GRP. Shifts from warm to cold SSTs in the northern region do not appear to affect summer abundance of juvenile Yukon River chum salmon, whereas the abundance of juvenile Kuskokwim River chum salmon drops precipitously during years with cold SSTs. From this result, we hypothesize that size-selective predation is highest on juvenile Kuskokwim chum salmon during cold years, but that predation is not as great a factor for juvenile Yukon River chum salmon. Although not addressed in this study, we also hypothesize that the smaller Yukon River chum salmon captured during years with cold SSTs likely incur higher size-selective mortality during winter.

INTRODUCTION

Larger juvenile Pacific salmon (*Oncorynchus* spp.) during their first year at sea have a survival advantage over smaller juvenile salmon from the same cohort (Farley et al. 2007a). Ocean conditions are believed to play a pivotal role in constraining early marine growth of juvenile salmon. For instance, sized-based natural mortality of juvenile coho salmon (*O. kisutch)* was hypothesized to be linked to available nutrients regulating the food supply and hence competition for food (Beamish and Mahnken 2001). Farley et al. (2007b) suggested that bottom-up control of the trophic structure on the eastern Bering Sea (EBS) shelf affected the size and condition of juvenile sockeye salmon (*O. nerka)*. Moss et al. (2005) found that juvenile pink salmon with an above-average growth trajectory during their first summer at sea had higher marine survival rates. Presumably, the above-average growth for juvenile pink salmon would occur during years with higher marine productivity. Thus, linking salmon prey demand to prey supply and their dependence on habitat could provide insight into the complex dynamics among marine productivity and growth and survival of salmon.

A leading hypothesis for ocean productivity on the EBS shelf suggests that spring sea surface temperature (SST) affects prey availability to pelagic consumers. Specifically, cold spring temperatures negatively affect the productivity of prey (Hunt and Stabeno 2002), which will potentially impact salmon growth and survival. Seasonal sea ice extent and timing of ice retreat is believed to affect the timing, magnitude, and persistence of the spring phytoplankton bloom. When sea ice extends to the southern EBS shelf during March and April, an early and short-lived spring phytoplankton bloom occurs in cold water. Cold SST limits copepod growth (Coyle and Pinchuk 2002), thus much of the annual phytoplankton production sinks to the bottom of the ocean. Alternatively, when sea ice is absent during March and April, the bloom occurs substantially later in the season (May and June). The warmer temperatures and later bloom timing allow copepods to graze on phytoplankton, such that secondary production remains in the pelagic system. According to this hypothesis, zooplankton production during

years with reduced sea ice (warm spring SST) is not limited by food availability, providing abundant prey for pelagic fish consumers.

To develop an understanding of the link between juvenile chum salmon prey demand and supply, we used a bioenergetics model to estimate growth rate potential (GRP) over a 4-year period within the EBS shelf as a measure of habitat quality for juvenile chum salmon. The utility of applying bioenergetics models to examine juvenile salmon GRP in marine waters was discussed in Farley and Trudel (in press). Data on juvenile chum salmon and ocean conditions come from BASIS surveys conducted along the EBS shelf during mid-August to early October 2004 to 2007. Sea temperatures and ice extent on the shelf varied during this time period, with warm spring and summer SSTs and reduced sea ice extent during 2004 and 2005 and colder spring and summer SSTs and increased sea ice extent during 2006 and 2007.

Prior information on juvenile chum salmon size and diet data collected during research surveys along the EBS shelf (mid August to October 2000 to 2006) were reported in Farley et al. (in press[**UPDATE]).** The results suggested that shifts in diet and size of juvenile chum salmon occurred between years with warm and cold spring SSTs. The juvenile chum salmon size and diet data presented here include one more year (2007) and are the focal data for the GRP models. We focus on 2004 to 2007 because during these years, the EBS shelf was consistently surveyed during the same time period, sampling the same station grid in the southern and northern EBS (Fig. 1). The EBS shelf was separated into northern and southern regions in order to address stock-specific differences in juvenile chum salmon because Yukon River juvenile chum salmon are distributed in the northern EBS and juvenile Kuskokwim River chum salmon are distributed in the southeastern Bering Sea during fall (Farley et al. 2005). We report the diet and size data for these years; however, the objectives of this study were to compare juvenile chum salmon GRP among years with warm and cold spring SSTs and to examine whether GRP is a useful index of habitat quality for juvenile chum salmon on the EBS shelf. A bioenergetics model was used to test whether (1) GRP was significantly higher during years with warm spring sea temperatures; (2) salmon densities were positively related to GRP; and (3) larger, faster growing salmon occurred during years with higher GRP.

METHODS

Study Area and Sampling Protocols

Stations along the EBS shelf were sampled during August-September, 2004-2007 (Fig. 1). Juvenile chum salmon were collected following methods described in Farley et al. (2005). Fish were collected using a mid-water rope trawl that was 198 m long, with a typical spread of 55 m horizontally and 15 m vertically. The trawl is constructed with hexagonal mesh in the wings and body, and a 1.2-cm mesh liner in the codend. Trawl stations were located along longitudinal meridians spaced every 55.6 km (i.e., along longitudinal meridians at stations spaced every 30 degrees of latitude). The rope trawl was towed at 6.5 to 9.3 km/h with the head rope at or near the surface. Trawl stations were sampled during daylight hours (0730–2100, Alaska Daylight Savings Time) and all tows lasted 30 min and covered 2.8 to 4.6 km. A Seabird SBE-911 conductivity-temperature-depth (CTD) device was deployed at each station to measure the vertical profiles (from near bottom to surface) of ocean temperature. Observed SSTs at 5 m depth taken from CTD profiles were used for bioenergetics modeling. At each trawl station, juvenile chum salmon were selected at random (maximum 50) and standard

biological attributes, including fork length (nearest 1.0 mm) and body weight (nearest 1.0 g) were measured on board.

Regions along the EBS shelf were defined as northern (stations sampled north of 60N, including stations sampled along 60N) and southern (stations sampled south of 60N).

Bioenergetics Model

GRP of juvenile chum salmon over the EBS shelf was estimated using the bioenergetics model developed by Ware (1978) with incorporated modifications to the model developed by Trudel and Welch (2005). This model was parameterized for sockeye salmon and accounts for optimal cruising speed:

$$G_{i,s} = \tau \cdot I_{i,s} - (SMR_{i,s} + ACT_{i,s}) \quad (1)$$

where $G_{i,s}$ is the GRP (cal/s) for juvenile chum salmon during year i at station s, □ is the proportion of food that can be metabolized (Trudel and Rasmussen 2006), $I_{i,s}$ is the feeding rate (cal/s), $SMR_{i,s}$ and $ACT_{i,s}$ are, respectively, the standard metabolic rate (cal/s) and activity costs (cal/s). For simplicity, we assumed that □ was constant and not affected by water temperature (Table 1), as the sum of fecal and urinary losses and specific dynamic action is often nearly constant in bioenergetics models (Trudel and Rasmussen 2006).

The relationship between salmon feeding rate and prey density was assumed to be described by a type II functional response (Holling 1965; Ware 1978):

$$I_{i,s} = ED_{i,s} \cdot \frac{\rho_{i,s}\gamma_{i,s}U_{i,s}}{1 + \rho_{i,s}\gamma_{i,s}h_{i,s}U_{i.s}} \quad (2)$$

where ρ is prey density (g/cm^3), γ is the cross-sectional area of the reactive field (cm^2), U is the optimum swimming speed (cm/s), h is handling time of prey (s/g), and ED is sum of prey caloric content (cal/g_{wet}), and was estimated as:

$$ED_{i,s} = \sum_{z=1}^{p} ED_{i,s,z} \quad (3)$$

where p = the number of prey species z. Consumption rates were equal to zero when no prey were available. The equations for handling time were developed in Farley and Trudel (in press):

$$h = \alpha_4 \overline{W}_i^{CB-1} \quad (4)$$

$$\alpha_4 = \frac{1}{CA \cdot f(T)} \; . \quad (5)$$

where $\overline{W}_i$ is the average chum salmon weight (g), CA and CB are, respectively, the weight coefficient and exponent for maximum feeding rate for chum salmon, and $f(T)$ is the Thornton and Lessem (1978) temperature dependence function for cold-water fish species (see Table 1 for definition and parameters).

The energetic costs associated with the standard metabolic rates and activity costs of juvenile chum salmon were modeled using the empirical models derived by Trudel and Welch (2005). Specifically, standard metabolic rates were modeled as a function of weight and water temperature (ºC):

$$SMR_{i,s} = \alpha_1 \overline{W}_i^{\beta} e^{\varphi T_{i,s}} \quad (6)$$

where α_1, β, and φ are regression coefficients (Table 1). Activity costs were modeled as a function of weight and swimming speed:

$$ACT_{i,s} = \alpha_0 \overline{W}_i^{\delta} U_{i,s}^{\lambda} \quad (7)$$

where α_0, δ, and λ are regression coefficients (Table 1). We used the optimal cruising speed model derived by Trudel and Welch (2005) to estimate the swimming speed of juvenile chum salmon (Table 1).

Prey Biomass

Gut contents from subsamples of juvenile chum salmon at each trawl station were analyzed to characterize prey consumption (Fig. 2). Prey analyses determined that the following prey items were important for juvenile chum salmon (those with percent wet weight greater than 5%): pagurids (northern region only), *Oikopleura* spp., euphausiids, cnidaria, brachyura, amphipods, and fish including age-0 walleye pollock (*Theragra chalcogramma*) and Pacific sand lance (*Ammodytes hexagramous*). The typical size ranges of age-0 pollock and sand lance in the diets of juvenile chum salmon were between 28 to 67 mm total length (TL) and 55 to 80 mm fork length (FL), respectively. Prey that were less than 5% wet weight were lumped into "other fish" and "other zoop" categories.

Fish prey density (g/cm^3) at each station was determined as:

$$\rho_{i,s} = \sum_{z=1}^{f} \frac{N_{i,s,f} \cdot \theta \cdot \overline{W}_f}{\phi \cdot V_{i,s}} \quad (9)$$

where $N_{i,s,f}$ is the number of prey (f = age-0 pollock or sand lance) caught in the trawl at each station, θ is the proportion of prey items captured in trawls that fell within the size range that juvenile chum salmon fed upon (dimensionless), $\overline{W}_f$ is the average weight (g) for each prey item, ϕ is the catchability coefficient (dimensionless), and $V_{i,s}$ is the volume sampled at each station (cm^3). Volume sampled at each station was estimated by multiplying the distance trawled (cm) by the vertical (cm) and horizontal (cm) spread of the net opening. The catchability coefficient (ϕ = 0.016) for age-0 pollock and sand lance was determined following methods described in Farley and Trudel (in press).

The average weight of these prey was 1.7 g for age-0 pollock and 1.2 g for sand lance. Laboratory analyses of subsamples of age-0 pollock taken during the 2005 survey indicated that the average caloric content was 4,424 cal/g_{dry}; caloric content for Pacific sand lance (4,209 cal/g_{dry}) was obtained from Robards et al. (1999). The estimates of catchability, proportion of prey items, caloric content, and weight were held constant for each station, among years.

Zooplankton prey were collected using 65 cm bongo sampler with 505-micron mesh net. The net was towed obliquely to near bottom (max 200 m depth) and the volume of water flowing through the net was measured using a General Oceanics 2030R flowmeter. Zooplankton samples were preserved in a buffered-formalin (5%) solution and processed at the University of Alaska Fairbanks laboratory.

Zooplankton prey density (g/cm^3) at each station was determined as:

$$\rho_{i,s} = \sum_{z=1}^{p} N_{i,s,z} \cdot \bar{W}_{i,s,z} \quad (10)$$

where $N_{i,s,z}$ and $W_{i,s,z}$ are the number and average weight of zooplankton species z (z = 1 to p) at station s during year i.

GRP (cal/s) was converted to cal/d by multiplying $I_{i,s}$ by the number of seconds in a 15-hour day (estimated time juvenile chum salmon spend feeding per day during August and September) and by multiplying $SMR_{i,s}$ and $ACT_{i,s}$ by the number of seconds in a 24-hour day.

Estimated daily GRP (cal/d) at each station s was then expressed as a percentage of body weight (% body weight/d) for each station s by dividing estimated daily GRP (cal/d) by the total energy per fish (cal) as in (Perry et al. 1996):

$$\overline{E}_{i,s} = ED_f \cdot \overline{W}_i \qquad (11)$$

where $\overline{E}_{i,s}$ is the average total energy per fish (cal), ED_f is the caloric content in juvenile chum salmon (cal/g_{wet}), and $\overline{W}_i$ is the average weight (g) of juvenile chum salmon. Annual averages of juvenile chum salmon weight were used as opposed to average weight of these fish at each station because there were stations within a year where no juvenile chum salmon were caught. The caloric content of juvenile chum salmon was determined from subsamples of the juvenile chum salmon caught during the 2004 and 2005 (no data available for 2006 and 2007) surveys using bomb calorimetry and averaged 5,107 cal/g_{dry}. (There was no significant difference in average caloric content of juvenile chum salmon between years; (ANOVA- Fixed effect, F = 1.0, p = 0.32). The units (cal/g_{dry}) were converted to (cal/g_{wet}) by multiplying 5,107 cal/g_{dry} by 23% (W g_{dry}/ W g_{wet}), the average value obtained from the subsample (2004 to 2005) of juvenile chum salmon dried for the bomb calorimetry process. These estimates of growth (% body weight/d) were considered to be juvenile chum salmon GRP on the EBS shelf and were the primary statistic used in subsequent models.

Spring SSTs

Spring SSTs (°C) during May 2002 to 2008 in the southeastern Bering Sea are shown in Fig. 3. Mean May SSTs were averaged over 54°18' N to 60°0' N, 161°12' W to 172°30' W (data from www.beringclimate.noaa.gov). Index values were calculated as the deviations from the mean May SST value (2.33° C) for the 1970-2000 period divided by the standard deviation (0.76° C). Years with cold SSTs were defined as those years when the index values of SSTs were at or below 0 (2006 to 2008); years with warm SSTs were defined as those years when the index values of SSTs were above 0 (2002 to 2005).

Model Applications

The bioenergetics model was used to test the following hypotheses:

Hypothesis 1: GRP is significantly higher during years with warm spring temperatures. This hypothesis was tested using two-way analysis of variance (ANOVA-Fixed Effect) with S-plus software (Insightful, 2001) where year (2004 to 2007) and region (northern and southern) were the categorical variables and GRP was the dependent variable. These data were also pooled by oceanographic domain (see Kinder and Schumacher 1981) and two-way ANOVA was used to test for significant differences between nearshore (coastal domain – depths < 50 m; well-mixed vertical structure, low salinity, warm water temperature, low stratification) and offshore (middle domain – depths > 50 m and < 100 m; strong two-layer vertical structure, moderate salinity, high stratification) domains within each region (northern and southern) among years. If a significant difference (p < 0.05) occurred, a Sidak multiple comparison test was used to calculate the 95% (α = 0.05, 0.01, 0.001) confidence intervals for all pairwise differences between the dependent variable means (Insightful, 2001). The level of

significance between the pairwise differences was determined by examining those confidence intervals that excluded zero for the three values of alpha.

Hypothesis 2: Juvenile chum salmon are distributed in areas of high GRP on the EBS shelf. Within each region, regression analysis was used to examine the relationship between $GRP_{i,s}$ and catch per unit effort ($CPUE_{i,s}$ – defined as the number of juvenile salmon caught during a 30-min trawl haul during year *i* at station *s* and hereon referred to as relative abundance). The natural logarithm of ($CPUE_{i,s}$+1) was used to reduce the wide variability in $CPUE_{i,s}$. Year was used as a factor within the regression analysis and an interaction between relative abundance and year was included to account for year effects. Juvenile chum salmon GRP and relative abundance were also compared graphically by year to provide perspective on the distribution of juvenile chum salmon in relation to regions of high and low GRP on the EBS shelf.

Hypothesis 3: Juvenile chum salmon size and growth rates were significantly higher during years with higher GRP. Differences in annual length within region were determined using two-way ANOVA where year was the categorical variable and length was the dependent variable. Because GRP was generally higher during years with warm spring SST (2004 and 2005) than during years with cold SST (2006 and 2007), the length data were pooled into warm and cold years within each region. Growth rate (mm/day) within each region for warm and cold years was estimated from the slope of the regression of Day of Year on length (dependent variable). The difference in slopes between warm and cold years within each region was determined using analysis of covariance.

RESULTS

Hypothesis Tests

Hypothesis 1. In general, mean annual GRP was positive during 2004 and 2005 and negative during 2006 and 2007 in both regions (Table 2). Juvenile chum salmon GRP differed significantly among years in the northern (ANOVA; $f_{[3,154]} = 43.31$, $p < 0.001$) and southern (ANOVA; $f_{[3,331]} = 40.09$, $p < 0.001$) regions. In the northern region, the pairwise comparison among years indicated that average GRP was significantly higher during 2004 than 2006 and 2007 ($p < 0.001$) and GRP was higher during 2005 than 2006 ($p < 0.001$) and 2007 ($P < 0.01$). Average GRP was also higher during 2004 than 2005 ($p < 0.001$). In the southern region, GRP was significantly higher during 2004 and 2005 than during 2006 and 2007 ($p < 0.001$). These analyses indicate that juvenile chum salmon GRP was higher during warm than cold years in both regions of the EBS.

In the northern region, juvenile chum salmon GRP was positive in the middle domain during all years except 2007 and negative during all years except 2004 in the coastal domain (Table 3). Juvenile chum salmon GRP differed significantly among domains (ANOVA; $f_{[7,288]} = 1814.1$, $p < 0.001$), year (described above) and the interaction between domain and year in the southern region ($p < 0.001$), whereas only the domain (ANOVA; $f_{[7,150]} = 520.6$, $p < 0.001$) and year (described above) were significant and not the interaction term ($p = 0.40$) in the northern region. In the southern region, the middle domain had significantly higher GRP than the coastal domain during all years (2005 and 2006 - $p < 0.001$; 2007 - $p < 0.05$) except 2004. Juvenile chum salmon GRP in the coastal domain of the southern region was significantly higher during 2004 than all other years ($p < 0.001$). In the middle domain of the southern region, juvenile chum salmon GRP was significantly higher during 2004 and 2005 than 2006 and 2007 ($p < 0.001$).

Hypothesis 2. Relative abundance of juvenile chum salmon was highest during the warm years of 2004 and 2005 in the southern region, whereas relative abundance increased during the cold years of 2006 and 2007 in the northern region (Fig. 4). The regression of GRP and relative abundance indicated that the relationship was not significant in the northern (p = 0.30) or southern regions (p = 0.30). These results show that juvenile chum salmon were not distributed in areas of highest GRP during any year. As shown in Figs. 5a-d, the highest catch of juvenile chum salmon generally occurred in water depths < 50 m (coastal domain), an area where GRP was generally at or below zero (Table 3). Areas with the highest GRP occurred offshore in deeper water during each year (middle domain; Table 4); however, the offshore area tended not to have many juvenile chum salmon, especially during the cold years of 2006 and 2007.

Hypothesis 3. Juvenile chum salmon length differed significantly among years in the northern (ANOVA; $f_{[3,2051]} = 623.13$, $p < 0.001$) and southern (ANOVA; $f_{[3,2096]} = 9.32$, $p < 0.001$) regions (Table 4). In the northern region juvenile chum salmon were significantly larger during 2004 and 2005 than during 2006 and 2007 ($p < 0.001$). In addition, juvenile chum salmon were significantly larger during 2004 than 2005 ($p < 0.01$) and during 2007 than 2006 ($p < 0.001$). In the southern region, juvenile chum salmon were significantly smaller during 2005 than during 2004 ($p < 0.001$) and 2007 ($p < 0.01$). These results indicate that juvenile chum salmon were significantly larger during warm years within the northern region, but not within the southern region.

Juvenile chum salmon growth rates were significantly lower ($p < 0.001$) in the northern region during warm years (slope = 0.27 mm/day; regression statistics: F = 5.73, deg (1, 722), p = 0.02) as opposed to cold years (slope = 2.53 mm/day; regression statistics: F = 1384, deg (1,1329), $p < 0.001$). Growth rates of juvenile chum salmon in the southern region were also significantly higher ($p < 0.001$) during cold years (slope = 1.27 mm/day; regression statistics: F = 1533, deg (1, 1491), $p < 0.001$) than warm years (slope = 1.53 mm/day; regression statistics: F = 978.3, deg (1, 605), $p < 0.001$).

A schematic of these results is shown in Table 5 for reference.

DISCUSSION

Our findings suggest a possible connection between GRP of juvenile chum salmon during late summer - early fall and spring SSTs along the EBS shelf. On average, salmon GRP was lower during years with cold rather than warm spring SSTs (supporting Hypothesis 1). However, juvenile chum salmon were not distributed in areas of highest GRP on the EBS shelf. In the southern region, many juvenile chum salmon were distributed in water depths < 50 m (coastal domain), areas on the shelf with significantly lower GRP (opposing Hypothesis 2). Juvenile chum salmon were larger during years with warm rather than cold SSTs in the northern region, but not so in the southern region. In addition, growth rate of juvenile chum salmon was significantly higher during cold rather than warm years in both regions (opposing Hypothesis 3). Juvenile chum salmon were also more abundant during cold years in the northern region, but relative abundance in the southern region declined dramatically during cold years.

The critical-size and critical-period hypothesis for juvenile salmon suggests two periods of high mortality linked to the size (growth rate) of juvenile salmon. The first stage may occur just after juvenile salmon enter the marine environment, where smaller individuals are believed to experience higher size-selective predation (Parker, 1968; Willette et al., 1999). The second

stage is thought to occur following the first summer at sea, when smaller individuals may not have sufficient energy reserves to survive late fall and winter conditions (Beamish and Mahnken, 2001). In our study, juvenile chum salmon were collected at the end of the first summer's growing season. We found that in the southern region, juvenile chum salmon were similar in size among years but their relative abundance dropped dramatically during cold years. These results suggest that perhaps smaller, slower growing individuals during years with lower GRP experienced higher size-selective mortality early in their marine residence. In the northern region, size-selective mortality does not appear to take place during early marine residence. In this case, years with lower GRP had higher relative abundance, suggesting that predation is minimal in the northern regions during years with cold SSTs. However, it is possible that these smaller individuals may experience higher size-selective mortality during their first winter at sea, thus reducing survival later in their marine life history (see Beamish et al. 2004; Moss et al. 2005; Farley et al. 2007b).

We found that juvenile chum salmon growth rates were higher in both regions during years with cold SSTs and reduced GRP. These results appear to be at odds with similar studies of juvenile chum salmon in coastal waters that found that higher growth rates occurred during years with warmer SSTs (Karpenko 1987; Kawamura et al. 2000). We note that juvenile chum salmon were significantly larger during warm years than cold years in the northern region. As marine survival is a function of size for juvenile salmon, perhaps the smaller juvenile salmon dedicated more energy to growth during the latter part of their first summer's growing season. In the southern region, it is likely that smaller, slower growing juvenile chum salmon were not surviving, thus only the faster growing individuals of the population were surveyed. This result is supported by the fact that the relative abundance of juvenile chum salmon in the southern region was much less during years with cold SSTs when compared to years with warm SSTs.

Our goal was to use GRP as an indicator of habitat quality during years with cold and warm spring SSTs rather than to provide precise quantitative estimates of growth rates for juvenile chum salmon. For instance, juvenile chum salmon GRP was negative during some years and shelf habitats indicating that these salmon may be losing rather than gaining weight. The annual estimates of juvenile chum salmon average GRP varied from -1.78% to 3.37% body weight per day for fish that ranged in length between 156 mm to 205 mm FL. Smaller juvenile chum salmon (41 mm FL) fed a varying ration of prey items in an experimental holding tank gained an average of 5.4% body weight (g) per day (LeBrasseur 1969). Larger juvenile chum salmon (90 mm to 160 mm FL) captured in coastal waters off Vancouver Island, British Columbia, Canada, attained daily growth rates between 0.34% to 3.28% (Perry et al. 1996). Juvenile salmon growth rate is size-dependent, and daily growth rate decreases as the fish get larger (Brett 1974). Thus, our highest GRP estimates may not be out of line with experimental estimates, and seem to be in line with marine research estimates of juvenile chum salmon daily growth rate.

Bioenergetics models are particularly sensitive to changes in energy density, composition of stomach contents, and biomass of potential prey (Beauchamp et al. 1989). Our estimates of available prey biomass were generated using a number of assumptions that could potentially lead to a bias of under-over-estimating the number of dominant prey (age-0 pollock and Pacific sand lance) available to juvenile chum salmon on the EBS shelf. For instance, euphausiids make up 20% of juvenile chum salmon diet by wet weight in the southern EBS during cold SST years, yet the bongo nets used to samples these important prey items typically

underestimate euphausiids (Ken Coyle, University of Alaska Fairbanks, Fairbanks, AK, pers. comm.), thereby lowering biomass estimates of euphausiids used in GRP models. Thus, the most plausible explanation for negative GRP is that our estimates of prey biomass were biased low. However, because we maintained these assumptions for all years, comparisons of the relative differences in juvenile salmon GRP would likely provide robust estimates of changes in juvenile chum salmon GRP among the years examined.

Juvenile chum salmon GRP was estimated using average caloric content of juvenile chum salmon collected during 2004 and 2005 (warm years). Caloric content of juvenile chum salmon was not available during 2006 and 2007 (cold years). Decreasing caloric content of juvenile chum salmon increases their estimated GRP. Thus, if caloric content of juvenile chum salmon was lower during cold years, our estimates of juvenile chum salmon GRP could be biased low. However, a recent paper comparing differences in caloric content of age-0 fish on the EBS found that the caloric content of these fish was significantly higher during years with cold SSTs (Moss et al. 2009). Thus, it is likely that juvenile chum salmon caloric content could have been higher during years with cold SSTs, suggesting that our estimates of juvenile chum salmon GRP are biased high.

Our study provides evidence that energetic limitation influences habitat quality on the EBS shelf for juvenile chum salmon during years with cold spring SSTs. Declining GRP in coastal waters is one possible reason why juvenile chum salmon begin to migrate offshore and away from shelf habitats. Our study also highlights differing responses of Yukon *vs.* Kuskokwim River juvenile chum salmon to changing ecosystem states. For instance, shifts from warm to cold SSTs in the northern region do not appear to affect summer abundance of juvenile Yukon River chum salmon, whereas the abundance of juvenile Kuskokwim River chum salmon drops precipitously during years with cold SSTs. From this result, we hypothesize that size-selective mortality from marine entry to late summer is highest in juvenile Kuskokwim chum salmon during cold years, but that size-selective mortality during early marine life is not a factor for juvenile Yukon River chum salmon. Although not addressed in this study, we hypothesize that the smaller Yukon River chum salmon captured during years with cold SSTs and lower GRP likely incur higher size-selective mortality during winter. As such, this work is an instructive case study and is a framework for future research on juvenile salmon energetics in large marine ecosystems.

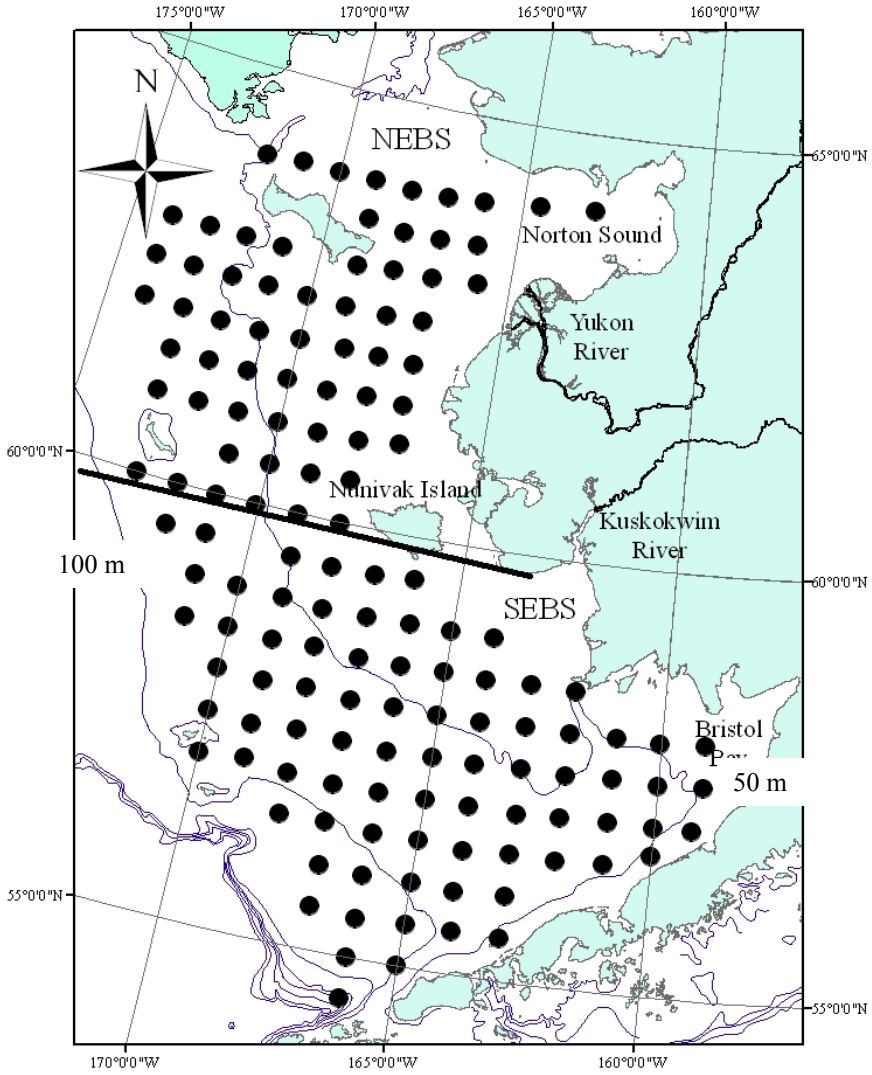

Fig. 1. Area surveyed for juvenile chum salmon during August - September 2004 to 2007, Bering-Aleutian Salmon International Survey (BASIS) research cruises.

a

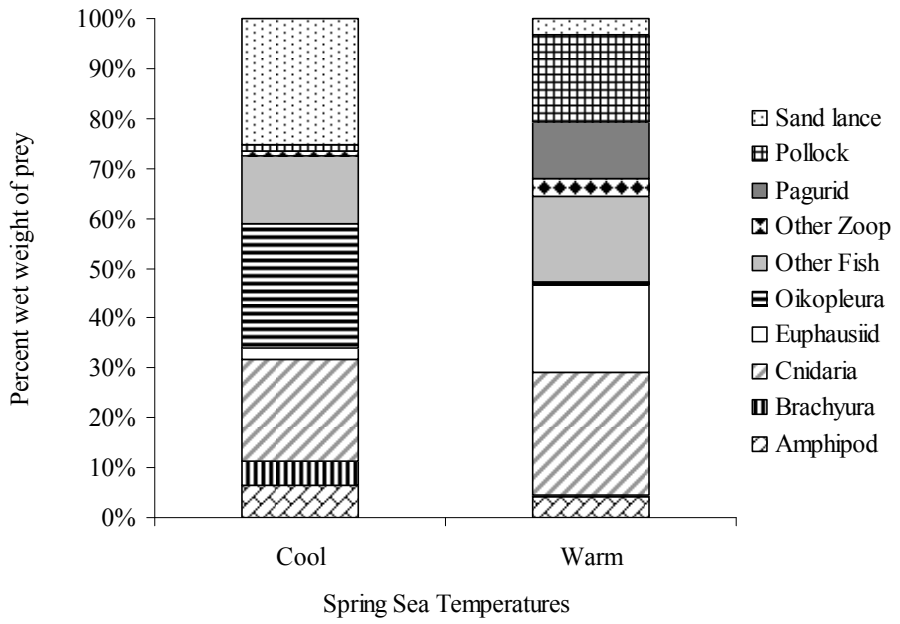
100%
90%
80%
70%
60%
50%
40%
30%
20%
10%
0%
Percent wet weight of prey
Cool
Warm
Spring Sea Temperatures
Sand lance
Pollock
Pagurid
Other Zoop
Other Fish
Oikopleura
Euphausiid
Cnidaria
Brachyura
Amphipod

b

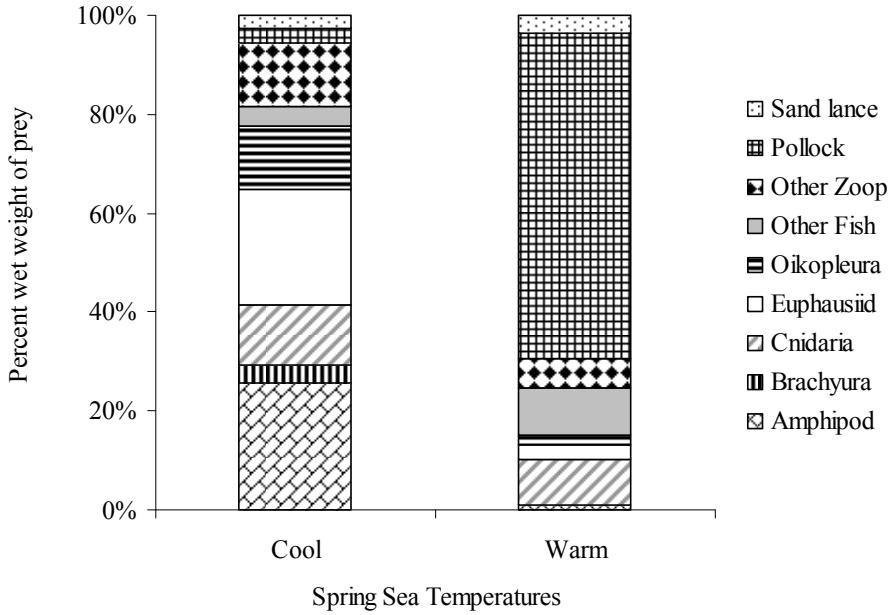
100%
80%
60%
40%
20%
0%
Percent wet weight of prey
Cool
Warm
Spring Sea Temperatures
Sand lance
Pollock
Other Zoop
Other Fish
Oikopleura
Euphausiid
Cnidaria
Brachyura
Amphipod

Fig. 2. Juvenile chum salmon prey composition (percent wet weight) in the a) northern and b) southern regions of the eastern Bering Sea shelf during warm (August to October, 2004 and 2005) and cold (August to October 2006 and 2007) years.

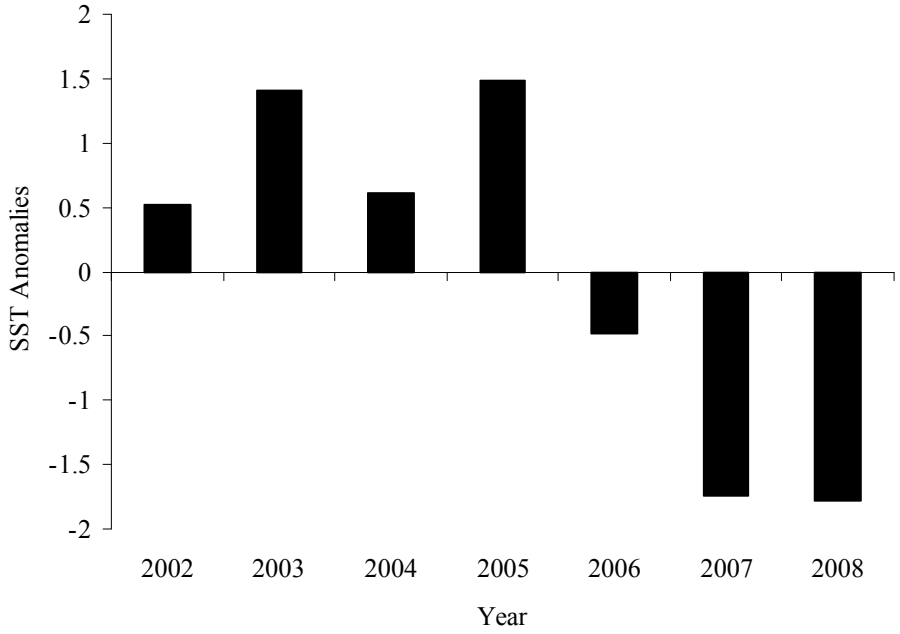

Fig. 3. Anomalies of sea surface temperatures (bar, SSTs,°C) during May 2002 to 2008 in the southeastern Bering Sea (data obtained from http://www.beringclimate.noaa.gov). Mean May SSTs are averaged over the area 54°18' N to 60°0' N, 161°12' W to 172°30' W using data from the National Centers for Environmental Protection and the National Center for Atmospheric Research (NCEP/NCAR) reanalysis project (Kalnay et al. 1996). The anomalies are the deviations from the mean May SST value (2.33° C) for the 1970 - 2000 period normalized by the standard deviation (0.76° C).

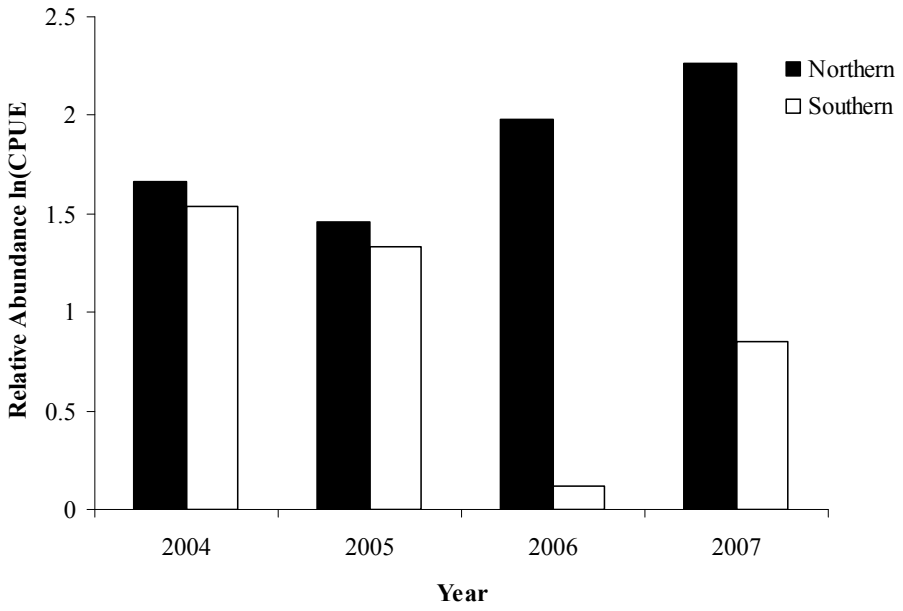

Fig. 4. Relative abundance (natural logarithm of catch per unit effort defined as the number of juvenile chum salmon captured in a 30-min surface trawl) of juvenile chum salmon in the northern (solid bar) and southern (clear bar) regions of the eastern Bering Sea during 2004 to 2007.

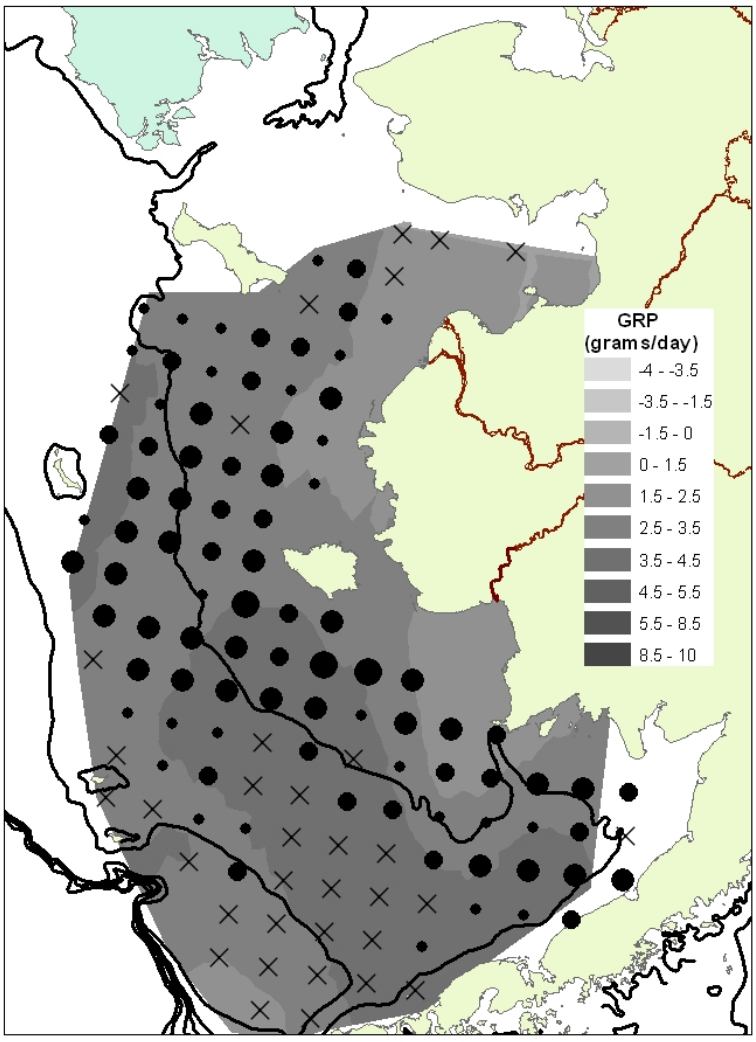

Fig. 5a. Contour plot of juvenile chum salmon growth rate potential (GRP - % body weight per day) in relation to the natural logarithm of catch per unit effort of juvenile chum salmon captured during 2004.

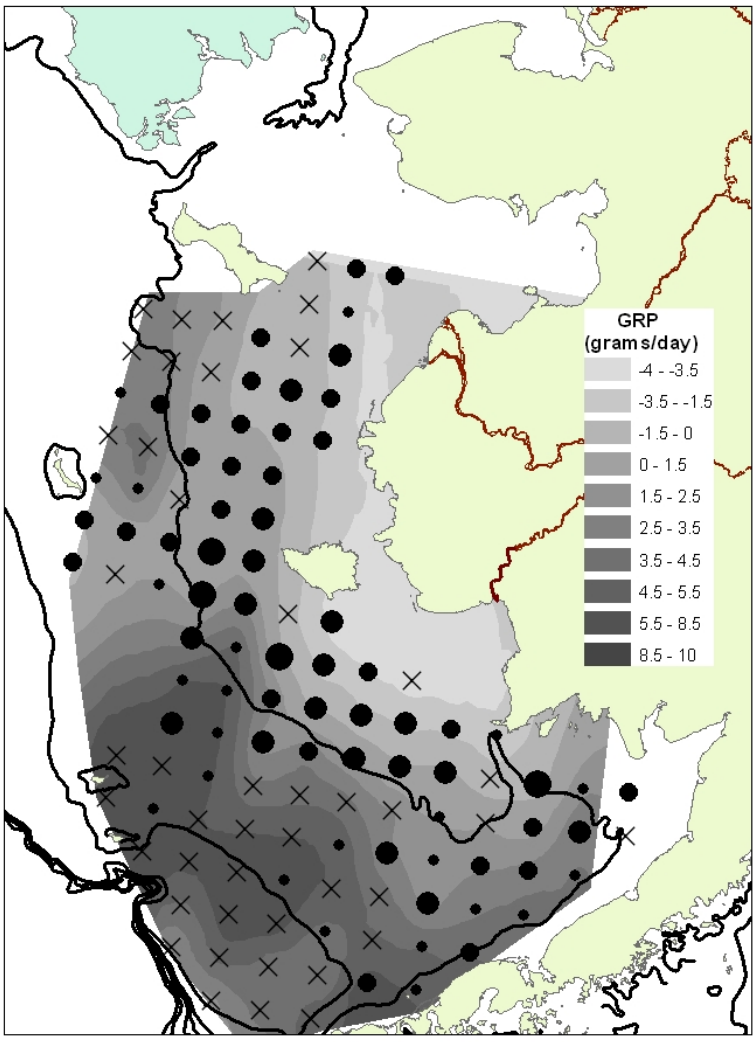

Fig. 5b. Contour plot of juvenile chum salmon growth rate potential (GRP - % body weight per day) in relation to the natural logarithm of catch per unit effort of juvenile chum salmon captured during 2005.

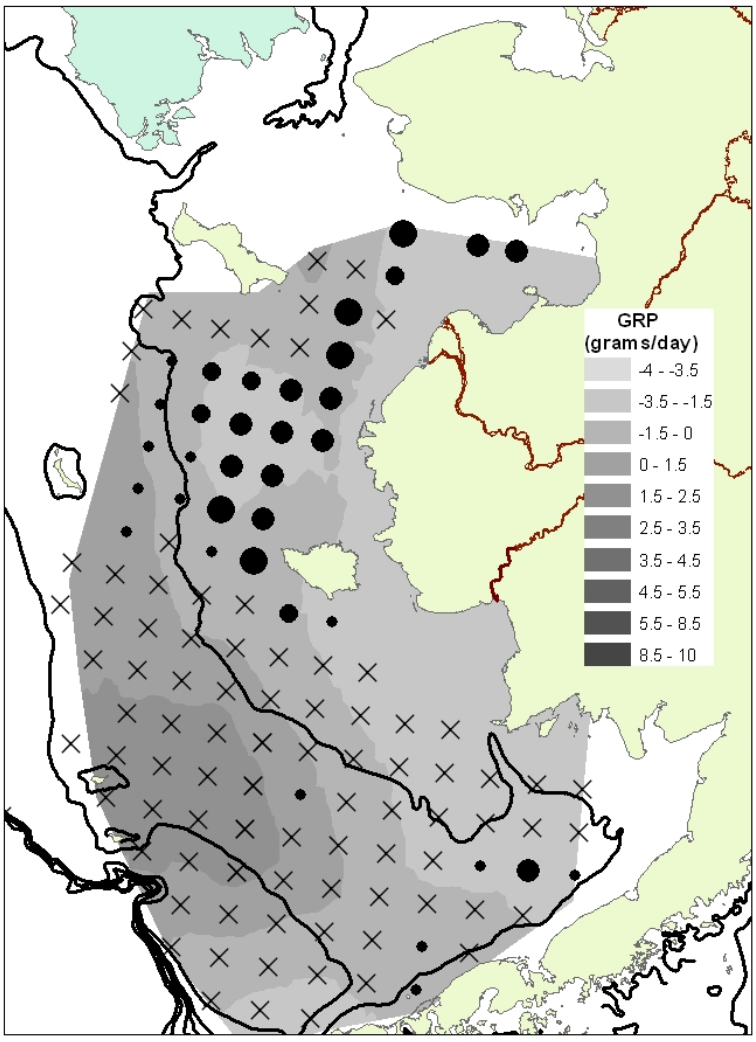

Fig. 5c. Contour plot of juvenile chum salmon growth rate potential (GRP - % body weight per day) in relation to the natural logarithm of catch per unit effort of juvenile chum salmon captured during 2006.

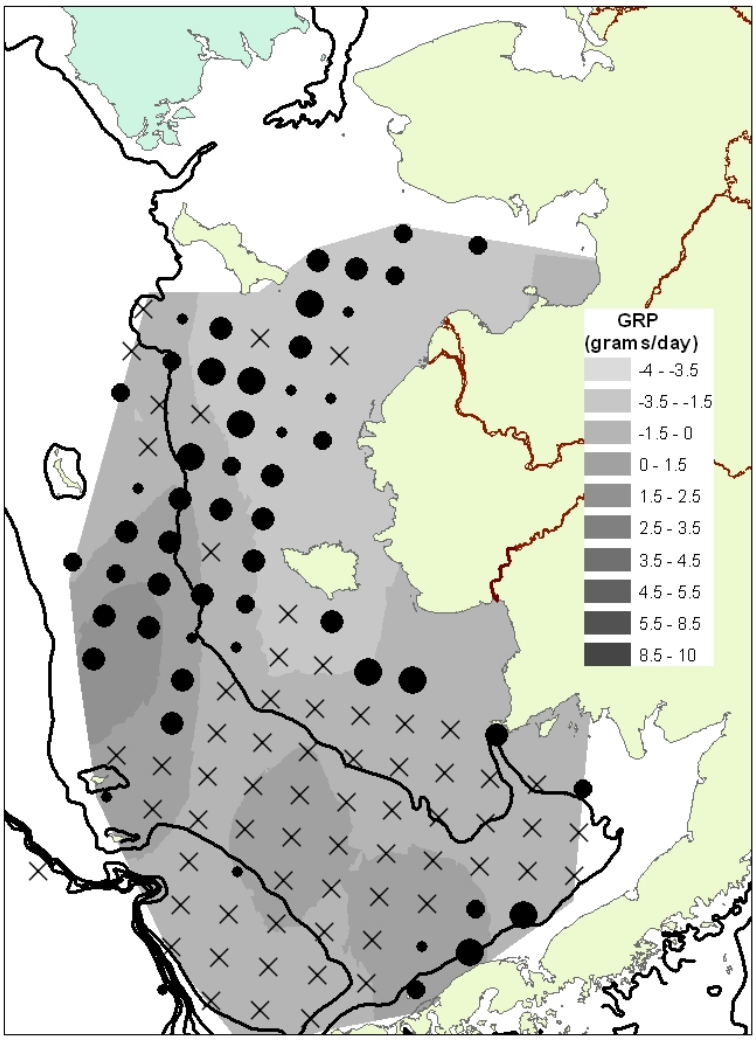

Fig. 5d. Contour plot of juvenile chum salmon growth rate potential (GRP - % body weight per day) in relation to the natural logarithm of catch per unit effort of juvenile chum salmon captured during 2007.

TABLE 1. Definitions of symbols used in the text. Note that subscripts *i* and *s* represent year (*i* = 2004 to 2007) and station and overbars denote mean quantities within the definitions of *i*.

Symbol	Parameter description	Value	Source
ACT	Activity costs (cal/s)		
E	Total energy content of juvenile chum salmon (cal)		
$\mathbf{ED_f}$	Caloric content of juvenile salmon (cal/g_{wet})	1,176	2
$\mathbf{ED_1}$	Caloric content of age-0 pollock (cal/g_{wet})	885	2
$\mathbf{ED_2}$	Caloric content of sand lance (cal/g_{wet})	842	2
$\mathbf{ED_{i,s}}$	Weighted average of caloric content of juvenile salmon prey at year *i* and stations *s* (cal/g_{wet})		
G	Growth rates (cal/s)		
I	Feeding rates (cal/s)		
N	Number of prey caught at a station		
SMR	Standard metabolic rates (cal/s)		
T	Sea surface temperature (°C; 5m below surface)		
V	Volume sampled by the net (cm^3)		
W	Chum salmon weight (g)		
$\mathbf{W_p}$	Prey weight (g)		
□	Catchability coefficient of the net (dimensionless)	0.016	7
□	Proportion of food that can be metabolized (dimensionless)	0.7	1
□	Proportion of prey items captured in the net that is within the range of size range that juvenile salmon fed upon (dimensionless)		

Consumption:

$$I = \frac{\rho\gamma U}{1 + \rho\gamma h U}$$

□ Prey density (cal/cm^3)

□ Cross-sectional area of the reactive field (cm^2)

U	Swimming speed (cm/s)		
h	Handling time (s/cal)		

Cross-sectional area of the reactive field:

$$\gamma = \alpha_3 \cdot W^{\beta 3}$$

□3	Intercept (cm^2)	1	1
□□	Coefficient, □ versus W	0.69	1

Handling time:

$$h = \frac{W^{CB-1}}{ED_p \cdot CA \cdot f(T)}$$

CA	Intercept for maximum feeding rates (g/s)	4.56 E-06	5
CB	Allometric exponent of maximum feeding rate	-0.275	5
$f(T)$	Temperature adjustment for maximum food consumption rates		

Temperature adjustment function:

$$f(T) = K_a \cdot K_b$$

$$K_a = \frac{(0.58 \cdot L1)}{1 + 0.58 \cdot (L1 - 1)} \quad 3$$

$$L1 = \exp(G1 \cdot (T - 3)) \quad 3$$

$G1$ 0.799 6

$$K_b = \frac{(0.5 \cdot L2)}{1 + 0.5 \cdot (L2 - 1)} \quad 3$$

$$L2 = \exp(G2 \cdot (24 - T)) \quad 3$$

$G2$ 0.123 6

Standard metabolic rates*:

$$SMR = \alpha_1 \cdot W^{\beta} \cdot e^{\varphi \cdot T}$$

□1	Intercept (cal/s)	4.76 x10^{-5}	4
□	Coefficient, SMR versus W	0.87	4
□	Coefficient, SMR versus T (1/°C)	0.064	4

Swimming costs*:

$$ACT = \alpha_0 \cdot W^{\delta} \cdot U^{\lambda}$$

□0	Intercept ($cal \cdot s^{-1}$)	1.74 x10^{-6}	4
□	Coefficient, ACT versus W	0.72	4
□	Coefficient, ACT versus U	1.6	4

Swimming speed:

$$U = \omega \cdot W^{\nu} \cdot \exp^{(\kappa \cdot T)}$$

□	Intercept (cm/s)	11.1	4
□	Coefficient, U versus W	0.097	4

□	Coefficient, *U* versus *T* (1/°C)	0.040	4

1. Ware (1978); 2. This study; 3. Beauchamp et al. (1989); 4. Trudel and Welch (2005); 5 Davis et al. (1998); 6 Moss and Farley (Unpub. Data); 7 Farley and Trudel (in press).
*The oxygen consumption rates were converted from mg O_2/h to cal/s using an oxycalorific equivalent to 3.24 mg O_2/cal (Elliott and Davison 1975).

TABLE 2. Annual averages (±SE) of juvenile chum salmon growth rate potential (GRP; % body weight per day) during mid-August – mid-September (southern region) and mid-September to early October (northern region) 2004 to 2007 along the eastern Bering Sea shelf. The number of stations (*n*) is included.

	Northern			Southern		
Year	*n*	GRP	SE	*n*	GRP	SE
2004	42	2.90	0.18	82	3.37	0.20
2005	38	0.58	0.44	81	3.01	0.45
2006	42	-1.04	0.32	89	-0.17	0.30
2007	37	-1.78	0.30	83	-0.25	0.25

TABLE 3. Annual averages (±SE) of juvenile chum salmon growth rate potential (GRP; % body weight per day) within the coastal and middle domains during mid-August – mid-September (southern region) and mid-September to early October (northern region) 2004 to 2007 along the eastern Bering Sea shelf. The number of stations (*n*) is included.

		Coastal			Middle		
Region	Year	*n*	GRP	SE	*n*	GRP	SE
Northern							
	2004	33	2.65	0.21	9	3.81	0.18
	2005	27	-0.16	0.40	11	2.39	0.97
	2006	35	-1.39	0.28	6	0.99	1.21
	2007	32	-1.95	0.25	5	-0.72	1.61
Southern							
	2004	28	2.95	0.37	47	3.75	0.18
	2005	25	-0.12	0.73	46	4.49	0.48
	2006	23	-2.00	0.22	56	0.75	0.40
	2007	27	-1.06	0.31	44	0.55	0.36

TABLE 4. Annual averages (±SE) of juvenile chum salmon length (mm) during mid-August – mid-September (southern Region) and mid-September to early October (northern region) 2004 to 2007 along the eastern Bering Sea shelf. The number of juvenile chum salmon sampled (*n*) is included.

	Northern			Southern		
Year	*n*	Length	SE	*n*	Length	SE
2004	471	205.6	0.97	844	179.9	0.79
2005	253	199.6	1.11	649	172.5	0.88
2006	576	156.2	0.57	30	179.9	3.02
2007	755	193.5	0.90	577	178.1	1.57

TABLE 5. Summary of the hypothesis tests for juvenile chum salmon growth rate potential (GRP), catch per unit effort (CPUE), fork length (FL), and growth rate (GR) within the northern and southern regions of the Bering Sea during years with warm (2004 and 2005) and cold (2006 and 2007) sea surface temperatures. Dash (-) indicates no difference in hypothesis test between warm and cold years.

Region	Hypothesis	Warm	Cold
Northern	GRP	High	Low
	CPUE	Low	High
	FL	Small	Large
	Growth Rate	Low	High
Southern	GRP	High	Low
	CPUE	High	Low
	FL	-	-
	Growth Rate	Low	High

ACKNOWLEDGMENTS

We gratefully appreciate the help of the captains (M. Cavanaugh and S. Brandstitter) and the crew of the F/V *Sea Storm* for their fine efforts and technical assistance in all aspects of the field surveys. We also gratefully appreciate the assistance from Natalia Kuznetsova for on-board diet analyses of juvenile salmon and marine fish collected during BASIS research. Funding for this work was provided by the National Marine Fisheries Service and the Arctic-Yukon-Kuskokwim Sustainable Salmon Initiative, project numbers 45491 and 45557.

REFERENCES

Beamish, R.J. and C. Mahnken. 2001. A critical size and period hypothesis to explain natural regulation of salmon abundance and the linkage to climate and climate change. Prog. Oceanogr. 49: 423-437.

Beamish, R.J., C. Mahnken, and C.M. Neville. 2004. Evidence that reduced early marine growth is associated with lower marine survival of coho salmon. Trans. Am. Fish. Soc. 133:26-33.

Beauchamp, D.A., D.J. Stewart, and G.L. Thomas. 1989. Corroboration of a bioenergetics model for sockeye salmon. Trans. Am. Fish. Soc. 118:597-607.

Brett, J.R. 1974. Tank experiments on the culture of pan-size sockeye (*Oncorhynchus nerka*) and pink salmon (*O. gorbuscha*) using environmental control. Aquaculture 4: 341-352.

Coyle, K.O. and A.I. Pinchuk. 2002. The abundance and distribution of euphausiids and zero-age pollock on the inner shelf of the southeast Bering Sea near the inner front in 1997–1999. Deep-Sea Res. II 49(26): 6009-6030.

Davis, N.D., K.W. Myers, and Y. Ishida. 1998. Caloric value of high-seas salmon prey organisms and simulated salmon ocean growth and prey consumption. N. Pac. Anadr. Fish Comm.Bull. 1: 146-162.

Elliott, J.M. and W. Davison. 1975. Energy equivalents of oxygen consumption in animal energetics. Oecologia 19: 195-201.

Farley, E.V., Jr., J.M. Murphy, J.H. Moss, A. Feldmann, and L. Eisner. In press. Marine ecology of western Alaska juvenile salmon. *In* Pacific salmon: ecology and management of western Alaska's populations. *Edited by* C.C. Krueger and C.E. Zimmerman. Am. Fish. Soc. Symp. 70 pp. #-#.

Farley, E.V., Jr., and M. Trudel. 2009. Growth rate potential of juvenile sockeye salmon in warmer and cooler years on the eastern Bering Sea shelf. J. Mar. Bio. ##:#-#.

Farley, E.V., Jr., J.H. Moss, and R.J. Beamish. 2007a. A review of the critical size, critical period hypothesis for juvenile Pacific salmon. *In* Status of Pacific salmon and their role in North Pacific marine ecosystems. *Edited by* R.J. Beamish and V Radchenko. N. Pac. Anadr. Fish Comm. Bull. 4. pp. 311-317.

Farley, E.V., Jr., J.M. Murphy, M.D. Adkison, L.B. Eisner, J.H. Helle, J.H. Moss, and J. Nielsen. 2007b. Early marine growth in relation to marine-stage survival rates for Alaska sockeye salmon (*Oncorhynchus nerka*). Fish. Bull. 105(1):121-130.

Farley, E.V., Jr., J.M. Murphy, B.W. Wing, J.H. Moss, and A. Middleton. 2005. Distribution, migration pathways, and size of western Alaska juvenile salmon along the eastern Bering Sea shelf. Alaska Fish. Res. Bull. 11(1):15-26.

Holling, C. S. 1965. The functional response of predators to prey density and its role in mimicry and population regulation. Mem. Entomol. Soc. Can. 45:1-60.

Hunt, G.L., Jr. and P.J. Stabeno. 2002. Climate change and the control of energy flow in the southeastern Bering Sea. Prog. Oceanogr. 55:5–22.

Insightful. 2001. S-Plus 6 for Windows guide to statistics. Insightful Corporation, Vol. 1, Seattle, WA.

Kalnay, E., M. Kanamitsu, R. Kistler, W. Collins, D. Deaven, L. Gandin, M. Iredell, S. Saha, G. White, J. Woollen, Y. Zhu, A. Leetmaa, B. Reynolds, M. Chelliah, W. Ebisuzaki, W. Higgens, J. Janowiak, K.C. Mo, C. Ropelewski, J. Wang, R. Jenne, and D. Joseph.

1996. The NCEP/NCAR 40-year reanalysis project. Bull. Am. Meteorol. Soc. 77(3): 437-471.

Karpenko, V. I. 1987. Growth variation of juvenile pink salmon, (*Oncorhynchus gorbuscha*), and chum salmon (*O. keta*), during the coastal period of life. J. Ichthyol. 27(3):117-125.

Kawamura, H., S. Kudo, M. Miyamoto, M. Nagata, and K. Hirano. 2000. Movements, food and predators of juvenile chum salmon (*Oncorhynchus keta*) entering the coastal Sea of Japan off northern Hokkaido in warm and cool years. N. Pac. Anadr. Fish Comm. Bull. 2: 33-41.

Kinder, T.H. and J.D. Shumacher. 1981. Hydrographic structure over the continental shelf of the southeastern Bering Sea. Pages 31–52 *In* The eastern Bering Sea shelf: oceanography and resources. Vol. 1. *Edited by* D. W. Hood and J. A. Calder. Office of Marine Pollution and Assessment, NOAA, Seattle.

LeBrasseur, R.J. 1969. Growth of juvenile chum salmon (*Oncorhynchus keta*) under different feeding regimes. J. Fish. Res. Board Can. 26: 1631-1645.

Moss, J.H., D.A. Beauchamp, A.D. Cross, K. Myers, E.V. Farley, Jr., J.M. Murphy, and J.H. Helle. 2005. Higher marine survival associated with faster growth for pink salmon (*Oncorhynchus gorbuscha*). Trans. Am. Fish. Soc. 134: 1313-1322.

Moss, J.H., and E.V. Farley, Jr., A.M. Feldmann, J.N. Ianelli. 2009. Spatial distribution, energetic status, and food habits of eastern Bering Sea age-0 walleye pollock. Trans. Am. Fish. Soc. 138:497-505.

Parker, R.R. 1968. Marine mortality schedules of pink salmon of the Bella Coola River, Central British Columbia. J. Fish. Res. Board Can. 25:757-794.

Perry, R.I., N.B. Hargreaves, B.J. Wakkell, and D.L. Mackas. 1996. Spatial variations in feeding and condition of juvenile pink and chum salmon off Vancouver Island, British Columbia. Fish. Oceanogr. 5(2): 73-88.

Robards, M.D., J.A. Anthony, G.A. Rose, J.F. Piatt. 1999. Changes in proximate composition and somatic energy content for Pacific sand lance (*Ammodytes hexapterus*) from Kachemak Bay, Alaska relative to maturity and season. J. Exp. Mar. Biol. Ecol. 242: 245-258.

Thornton, K.W. and A.S. Lessem. 1978. A temperature algorithm for modifying biological rates. Trans. Am. Fish. Soc. 107 :248-287.

Trudel, M. and D. W. Welch. 2005. Modeling the oxygen consumption rates in Pacific salmon and steelhead: model development. Trans. Am.Fish. Soc. 134: 1542-1561.

Trudel, M. and J.B. Rasmussen. 2006. Bioenergetics and mercury dynamics in fish: a modeling perspective. Can. J. Fish. Aquat. Sci. 63: 1890-1902.

Ware, D.M. 1978. Bioenergetics of pelagic fish: theoretical change in swimming speed and ration with body size. J. Fish. Res. Board Can. 35:220–228.

Willette, T.M., R.T. Cooney, and K. Hyer. 1999. Predator foraging mode shifts affecting mortality of juvenile fishes during the subarctic spring bloom. Can. J. Fish. Aquat. Sci. 56:364-376.

Appendix 3

Moss, J.H., J.M. Murphy, E.V. Farley, Jr., L.B. Eisner, and A.G. Andrews. In prep. Juvenile pink and chum salmon distribution, diet, and growth in response to the loss of Arctic sea-ice. North Pacific Anadromous Fish Commission, Bulletin 5.

Juvenile Pink and Chum Salmon Distribution, Diet, and Growth in Response to the Loss of Arctic Sea-Ice

Jamal H. Moss[1], James M. Murphy[1], Edward V. Farley Jr. [1], Lisa B. Eisner[1], and Alexander G. Andrews[1]

[1]Ted Stevens Marine Research Institute, Alaska Fisheries Science Center, NOAA Fisheries, 17109 Point Lena Loop Road, Juneau, Alaska, 99801, USA

Moss, J.H., J.M. Murphy, E.V. Farley, L.B. Eisner, and A.G. Andrews. 2009. Juvenile pink and chum salmon distribution, diet, and growth in response to the loss of Arctic sea-ice. North Pacific Anadromous Fish Commission Bulletin 5:**XXX–YYY**.

Keywords: Pink salmon, chum salmon, Chukchi Sea, eastern Bering Sea, bioenergetics, growth.

Abstract: Loss of non-seasonal sea-ice and a general warming trend in the Bering Sea has altered the composition, distribution, and abundance of marine organisms inhabiting the region. Juvenile pink (*Oncorhynchus gorbusha*) and chum (*O. keta*) salmon were found in significant numbers throughout the Chukchi Sea and Bering Strait regions during early autumn 2007 reflecting significant utilization of Arctic marine habitat. Linear models of juvenile pink and chum salmon body size and day of year were parameterized to estimate daily growth rates, habitat specific differences in body size were calculated and contrasted, and growth trajectories for three distinct Arctic habitats simulated using a bioenergetics model. Juvenile Pink salmon inhabiting the eastern Bering Sea were estimated to grow at a rate of 1.17 $mm \cdot day^{-1}$ and juvenile chum salmon were estimated to grow at 1.21 $mm \cdot day^{-1}$. The largest juvenile pink and chum salmon that were encountered during 2007 were distributed in the northern Chukchi Sea. The second largest juvenile pink and chum salmon were located in the southern Chukchi Sea, and the smallest were located in the Bering Strait. Thermal conditions and prey quality the northern Chukchi Sea were most favorable for supporting pink and chum salmon growth, followed by the Bering Strait, and southern Chukchi Sea. The majority of chum salmon encountered in the Arctic were from Alaskan or Russian stocks, and results from this study suggest that these particular stocks will likely benefit from the loss of Arctic sea-ice through experiencing favorable growth rates that support over winter survival.

INTRODUCTION

Loss of non-seasonal sea-ice and a general warming trend in the Bering Sea has altered the composition, distribution, and abundance of marine organisms inhabiting the region (Grebmeier et al. 2006). Juvenile pink (*Oncorhynchus gorbusha*) and chum (*O. keta*) salmon were found in significant numbers throughout the Chukchi Sea and Bering Strait regions during early autumn, reflecting significant utilization of Arctic marine habitat. Marine migration rates play a key role in the distribution of juvenile salmon within the Bering Sea (Farley et al. 2005). Bering-Aleutian Salmon International Survey (BASIS) research cruises have determined that juvenile pink and chum salmon are consistently distributed the greatest distance from shore as compared with other salmon species, reflecting high dispersal rates and minimal utilization of near-shore estuarine habitat. Pink salmon consume large amounts of food in order to sustain rapid growth during the early marine life-history stage (Healy 1980); and offshore movements of chum salmon generally coincide with the decline in nearshore food resources and a period when fish attain a body size that allows for the capture and consumption of prey resources located further from shore (Simenstadt and Salo 1982).

Environmental conditions can limit or enhance growth during the early marine life history stage, which influences over winter survival and recruitment (Moss et al. *in press*, Farley et al. *this issue*). Climate can affect salmon growth and survival directly through physiological influence of water temperature on metabolism; or indirectly through the distribution patterns, migrations pathways, and the availability of prey resources. Thermal conditions and prey quality have been shown to affect juvenile pink salmon growth rates (Cross et al. 2008), which ultimately affects over-winter survival during the first year of marine life (Moss et al 2005). In addition to thermal constraints, there is also evidence that salmon are food limited during offshore migration in the Bering Sea and North Pacific Ocean (Ruggerone et al. 2003, Aydin et al. 2004, Kaeriyama et al. 2004).

All species of pacific salmon are distributed in the epipelagic waters of the eastern Bering Sea during their first summer and fall at sea (Farley et al. *in press*). Early marine growth is known to influence marine survival positively and Pacific salmon run failures are often blamed on unfavorable ocean conditions. Salmon populations that have typically inhabited the Bering Sea are expanding their range to include Arctic waters. The objective of this study is to describe juvenile pink and chum salmon distribution in the Chukchi and Bering Seas, quantify differences in growth by region, and quantify differences in growth attributable to biophysical conditions in Arctic waters. In order to accomplish these goals, linear models of juvenile pink salmon body size and day of year are parameterized to estimate gaily growth rates, habitat specific differences in body size are quantified, and growth trajectories for three distinct Arctic habitats are simulated using a bioenergetics model. New information on the food habits of pink and chum inhabiting the eastern Bering Sea are also reported.

METHODS

Biological Sampling

Juvenile pink and chum salmon were collected in the Bering Strait and Chukchi Sea aboard the fisheries research vessel NOAA Ship *Oscar Dyson* from September 2nd –

September 29th 2007 (Figure 1), using a midwater rope trawl made by Cantrawl Pacific Limited[2] (models 400/580) of Richmond, B.C., Canada. The net is approximately 198 m long, has hexagonal mesh in wings and body, and a 1.2-cm mesh liner in the codend. The net was towed at or near the surface for 30 minutes at speeds between 3.5 and 5 knots at each station. It was then retrieved and the contents emptied into a sorting table on deck. Nekton samples were moved to an onboard laboratory by conveyer belt where standard biological measurements including fork length and body weight were recorded.

Food habits of juvenile pink and chum salmon were examined onboard by removing and pooling the contents of the entire food bolus from the stomachs of up to 10 randomly selected individuals. Stomach contents were weighed to the nearest 0.001g, sorted, and identified to the lowest feasible taxonomic group. Individual prey groups were weighed and divided by the total weight of prey contained in the stomachs and the proportional contributions of each prey group to the diet calculated.

Growth Rate Estimation and Habitat-specific Differences in Body Size

Differences in juvenile salmon average length and body weight according to the type of ocean habitat inhabited can provide insight into how juvenile salmon respond to various conditions. However, a number of confounding factors act to limit direct interpretations of habitat quality to growth rate or body size. The effect of growth during a survey is an important confounding factor in the U.S. BASIS survey, which spanned over 50 days during 2007. To correct for the effect of growth during the survey a simple linear regression model with Gaussian error was used to model length as a function of the day-of-the-year (growth rate term) and habitat type with habitat terms estimated as dummy variables or factors for each type of habitat (Venables and Ripley 1999). The interaction between habitat type and growth rate was not considered as three of the five habitat categories contained a date range of less than five days. This was considered inadequate to describe habitat specific growth rates. Habitat types selected for the analysis included two from the eastern Bering shelf region: Coastal (bottom depth<50 m) and Middle (100 > bottom depth > 50 m), and three from the Arctic region: Bering Strait (64.0-65.5º N), southern Chukchi Sea (66.0-68.0º N), and northern Chukchi Sea (68.5-70.0º N) (Figure 1).

Pink and Chum Salmon Energy Density Estimation

Juvenile pink and chum salmon energy density ($J \cdot g^{-1}$) was estimated using a bomb calorimeter. Pink salmon collected in the eastern Bering Sea from 2003-2007, and chum salmon collected from 2003-2005 were thawed and wiped clean of debris in the laboratory, measured to the nearest 1 mm fork length, and weighed to the nearest 0.001 g. Stomach contents were not removed due to loss of tissue and fluids during the dissection which could cause a greater degree of error in energy density than gut contents (Ciannelli et al. 2002). Whole pink and chum salmon were dried for numerous days at 55 °C using a VWR 1324 gravity convection oven until a change in mass less than 0.01 g was observed. Dried remains were homogenized into a fine powder using a mortar and pestle and then pressed into pellets

[2] Reference to trade names does not imply endorsement by the National Marine Fisheries Service, NOAA.

that were immediately transferred to desiccators maintained at ambient room temperature where they were stored until time of combustion.

Fish pellets were burned in a Parr 1425 semi micro bomb calorimeter and the energy content calculated as,

$$Hg = \frac{TW - f}{m}$$

where, Hg is the gross heat of combustion in calories per gram of sample burned, T is the observed temperature rise in °C, W is the energy equivalent of the calorimeter in cal per ºC, f is the fuse correction measured in calories, and m is the mass of the sample in grams. The conversion of gross heat of combustion into wet weight energy density gives:

$$E_D = 4.186(Hg)\left(\frac{W_d}{W_w}\right)$$

where, E_D is the energy density of the whole fish in $J \cdot g^{-1}$, W_d is the dry weight in g of the whole fish, and W_w is the wet weight in g of the whole fish, Hg is the gross heat of combustion in calories per gram of sample burned, and 4.186 the conversion factor used to convert calories into Joules.

Simulations of Pink and Chum Salmon in the Bering Strait and Chukchi Sea

The Wisconsin bioenergetics model version 3.0 was used to simulate juvenile pink and chum salmon growth trajectories on a daily time-step over a 30-day period in the northern and southern Chukchi Sea, and the Bering Strait region. The model predicted daily growth (mass) rate while accounting for metabolic costs, waste losses, consumer body mass, thermal experience, and food quality (Kitchell et al. 1977). Model simulations were run with a proportion of maximum consumption (P-value) equal to half the physiological maximum (0.5) consumption rate given a specific consumer body size.

$$C = C_{\max} \cdot p \cdot f(T)$$

where C is the specific consumption rate, C_{max} the maximum specific feeding rate, p the proportion of maximum consumption, and $f(T)$ a temperature dependent function. Maximum specific consumption (C_{max}) is the greatest mass of food that can be physiologically consumed during a 24 h period.

$$C_{\max} = CA \cdot W^{CB}$$

where CA is the intercept of an allometric weight function, W is the mass of the fish, and CB the slope of the intercept. Metabolic costs include respiration (R), specific dynamic action (SDA), and activity (ACT). Respiration is calculated as

$$R = RA \cdot W^{RB} \cdot f(T) \cdot ACT$$

where *RA* is intercept of the allometric mass function, *RB* is the slope of the allometric mass function, *f*(*T*) is a temperature dependence function, and *ACT* an activity multiplier. Energy losses due to *SDA*, egestion, and excretion are modeled as a constant proportion of consumption. Model parameters are estimated from laboratory experiments. The parameters used to represent pink and chum salmon in this study were taken from the pink/sockeye parameter set (Beauchamp et al. 1989) provided by the Wisconsin bioenergetics model 3.0 software (Hanson et al. 1997).

The Wisconsin bioenergetics model was used to evaluate regional aspects of growth performance for the northern Chukchi Sea, southern Chukchi Sea and the Bering Strait regions, and was based on region-specific biophysical properties of sea surface temperature and diet composition (Table 1). Sea surface temperature profiles (surface 15 m of the water column) were measured at each survey station with a CTD at 1-m increments and averaged by region. Average proportional contribution of taxonomic groups of prey in juvenile pink and chum diet by region were used to represent diet, as well as literature values for prey energy density and percent indigestible. Consumer body mass at time initial was held constant for the 30-day simulation across all regions. Values for juvenile pink and chum salmon energy densities measured in the laboratory were also used in the model. Model inputs were held constant and the model run on a daily time step in order to assess relative differences in the biophysical conditions of each region on growth.

RESULTS

Spatial Distribution and Growth Rate

High densities of juvenile pink and chum salmon were observed in the Bering Strait and Chukchi Sea relative to the eastern Bering Sea during 2007 (Figure 2). Juvenile pink salmon were estimated to grow at a rate of 1.17 mm·day^{-1} and juvenile chum salmon estimated to grow at a rate of 1.21 mm·day^{-1}over a 6-year period (2002-2007) (Figure 3). During 2007, growth rates for pink salmon were estimated to be 1.18 mm·day^{-1}, and be similar in value to the 6-year mean. Juvenile chum salmon were estimated to grow at a rate of 1.48 mm·day^{-1}, which was 0.27 mm·day^{-1} greater than the 6-year mean. Pink and chum salmon inhabiting the Bering Strait and Chukchi sea were larger on average than those inhabiting the lower latitudes of the eastern Bering Sea during 2007 (Figure 4).

Juvenile Pink and Chum Salmon Food Habits and Energy Density

Juvenile pink and chum salmon fed heavily on fish, squid, and euphausiids in the northern Chukchi Sea (Table 1). Euphausiids remained an important prey item for both species in the southern Chukchi Sea; however fish and squid were not important prey items in terms of diet composition by weight. Rather, crab megalopae was an important prey item for pink salmon, accounting for 69% of the diet by weight in the southern Chukchi Sea region. Juvenile pink salmon food habits differed significantly from chum salmon in the Bering Strait region. Pink salmon primarily preyed upon copepods, crab megalopae, and fish and squid; whereas

chum salmon preyed upon euphausiids and larvaceans. Average juvenile pink salmon (n = 508) energy density with was 4796 $J \cdot g^{-1}$ (STE 26.0), with an average individual wet weight of 50.5 g (STE 1.3). Average juvenile chum salmon (n = 253) energy density was 4679 $J \cdot g^{-1}$ (STE 33.2), with an average individual wet weight of 61.7 g (STE 2.1g).

Bioenergetics Growth Trajectories

Thermal conditions and prey quality the northern Chukchi Sea were most favorable for supporting pink and chum salmon growth relative to the Bering Strait and southern Chukchi Sea. Pink salmon were estimated to grow 29g, and chum salmon to grow 39g over a 30-day simulation for the northern Chukchi Sea. Biophysical conditions in the Bering Strait region were only slightly better for supporting growth (20 $g \cdot 30days^{-1}$) relative to the southern Chukchi Sea ($16g \cdot 30days^{-1}$) (Figure 5). Chum salmon were estimated to grow 21g in Bering Strait and 18g in the southern Chukchi Sea over a 30-day simulation.

DISCUSSION

Climate-induced habitat changes in the Bering Sea have caused a thinning and reduction of sea ice and a northward redistribution of subartic species (Hunt et al. 2002, Overland et al. 2004, Grebmeier et al. 2006). Such climate induced changes may affect feeding and overwintering grounds of salmon by increasing competition (smaller area or ocean waters to inhabit), or enhancing the interactions between international salmons stocks. Simulated growth trajectories for pink and chum salmon inhabiting the northern Chukchi Sea were higher than those for the southern Chukchi Sea and Bering Strait due to a combined affect of warmer sea surface temperature and consumption of higher energy prey items. Sea surface temperature in the northern Chukchi Sea was higher than all other areas sampled in 2007. Higher water temperatures, likely caused by a longer photoperiod during summer months over the shallower Arctic shelf relative to lower latitudes, are more energetically favorable than the cooler waters located over the deeper eastern Bering Sea. The rise in temperature in Arctic waters can be attributed to a lack of sea-ice which would normally act to reflect solar radiation, as darker, ice-free ocean water acts to absorb solar radiation more readily.

Most juvenile chum salmon inhabiting the Chukchi Sea were from Kotzebue Sound stocks (69%); however stocks from Seward Peninsula and Norton Sound (27%) and the Yukon River (3%) were also represented (Kondzela et al. *this issue*). If the absence of non-seasonal sea ice continues, chum salmon stocks within the vicinity of Chukchi Sea will likely continue to experience favorable conditions for supporting growth during the early marine life history phase. Though fewer in number, stocks that actively migrate to the Chukchi Sea will also enjoy favorable growing conditions and this migration pattern would be expected to continue.

Juvenile chum salmon captured in the Bering Strait region were primarily from northern Russia (77%), may have been passively transported from coastal Siberia to the eastern Bering Strait by the Anadyr Current. Other stocks of juvenile chum salmon captured in the eastern Bering Strait region were from Kamchatka (6%), Seward Peninsula and Norton Sound (9%), Yukon River (4%), and the Kuskokwim River (4%) (Kondzela et al. *this issue*).

Juvenile pink salmon were estimated to grow at 1.3 $mm \cdot day^{-1}$ in 2007, an estimate well within the expected range (Cross et al. 2008), however estimates of juvenile chum salmon growth rates were much higher (1.5 $mm \cdot day^{-1}$). Habitat-specific differences in length according

to habitat showed an increasing trend in pink and chum salmon body size from coastal waters to the shelf. Such size differences have been reported for pink and chum inhabiting other regions (Cross et al. 2008, Farley et al. 2005). Chum salmon growth rates were above average in 2007 as compared with mean growth rates from 2002-2007 (1.2 $mm \cdot day^{-1}$) which may be due to seaward migration timing.

Growth trajectories generated from bioenergetics modeling simulations confirmed that biophysical conditions in the northern Chukchi Sea were best for supporting growth, providing further support for higher quality habitat in the Arctic enhancing juvenile salmon growth. It is believed that cold spring sea surface temperatures lead to lower growth and marine survival for juvenile salmon and warmer temperatures lead to higher growth (Farley et al. *in press*), and proven that faster growing juvenile pink salmon experience higher survival to adulthood (Cross et al 2008, Moss et al. 2005). Prince William Sound juvenile pink salmon that migrated from coastal waters onto the continental shelf quickly, and then moved offshore experienced higher survival rates than those that did not (Cross et al. 2008). Prey quality increased as these fish moved from nearshore habitats in PWS to more saline habitats in August (Armstrong et al. 2008). High quality prey items in the northern Chukchi Sea further enhanced juvenile pink and chum salmon growth, and given the potential for high growth rates in the Chukchi Sea, juvenile pink and chum salmon remaining in this region will experience benefits from remaining in shallow shelf habitat.

Juvenile salmon growth may be inhibited or enhanced by ocean conditions due to climate change and variability. Reduced growth may prevent salmon from acquiring a sufficient body size to efficiently feed upon larger and more energy rich prey; thereby causing a trophic feedback loop and increasing competition for zooplankton prey (Aydin et al. 2000). The ability to predict the effects of climate change on the growth and survival of marine organisms is needed, and results from this study suggest that juvenile pink and chum salmon inhabiting the Arctic are currently benefiting from present conditions.

ACKNOWLEDGEMENTS

We thank A. Feldmann, K. Cieciel, and E. Husoe for assistance with data collection and laboratory analyses that supported this study. A. Volkov, and N. Kuznetsova provided pink and chum salmon diet information. We also thank J. Helle for guidance and support of the U.S. BASIS program.

REFERENCES

Armstrong, J.L., K.W. Myers, D.A. Beauchamp, N.D. Davis, R.V. Walker, J.L. Boldt, J.J Piccolo, L.J. Haldorson, and J.H. Moss. 2008. Interannual and spatial feeding patterns of hatchery and wild juvenile pink salmon in the Gulf of Alaska in years of low and high survival. Transactions of the American Fisheries Society 137:1299–1316.

Aydin, K.Y., K.W. Myers, and R.V. Walker. 2000. Variation in summer distribution of the prey of Pacific salmon (*Oncorhynchus* spp.) in the offshore Gulf of Alaska in relation to oceanographic conditions, 1994–98. North pacific Anadromous Commission Bulletin 2:43–54.

Aydin, K.Y., G.A. McFarlane, J.R. King, B.A. Megrey, and K.W. Myers. 2004. Linking oceanic food webs to coastal production and growth rates of Pacific salmon (*Oncorhynchus* spp.), using models on three scales. Deep-Sea Research II 52:757–780.

Beauchamp, D.A., D.J. Stewart, and G.L. Thomas. 1989. Corroboration of a bioenergetics model for sockeye salmon. Transactions of the American Fisheries Society 118:597–607.

Boldt, J.L., and L.J. Haldorson. 2002. A bioenergetics approach to estimating consumption of zooplankton by juvenile pink salmon in Prince William Sound, Alaska. Alaska Fishery Research Bulletin 9(2):111–127.

Ciannelli, L.A., J. Paul, and R.D. Brodeur. 2002. Regional, interannual and size-related variation of age-0 year walleye pollock whole body energy content around the Pribilof Islands, Bering Sea. Journal of Fish Biology 60:1267–1279.

Cross, A.D., D.A. Beauchamp, K.W. Myers, and J.H. Moss. 2008. Early Marine Growth of Pink Salmon in Prince William Sound and the Coastal Gulf of Alaska During Years of Low and High Survival. Transactions of the American Fisheries Society 137:927–939.

Davis, N.D., Myers, K.W., and Ishida, Y. 1998. Caloric value of high-seas salmon prey organisms and simulated salmon growth and prey consumption. North Pacific Anadromous Fish Commission Bulletin 1:146–162.

Davis, N.D. 2003. Feeding ecology of Pacific salmon (*Oncorhynchus spp.)* in the central North Pacific Ocean and central Bering Sea, 1991–2000. Ph.D. thesis. Hokkaido University, Hakodate, Japan. 190 pp.

Farley, E.V., Jr., J.H. Moss, and N. Kuznetsova. *This issue*. Growth rate potential of juvenile chum salmon on the eastern Bering Sea shelf; an assessment of salmon carrying capacity. North Pacific Anadromous Fish Commission Bulletin 5:XXX–YYY.

Farley, E.V., Jr., J. Murphy, J. Moss, A. Feldmann, and L. Eisner. *In press*. Marine ecology of western Alaska juvenile salmon. Proceeding from the Arctic, Yukon, Kuskokwim, Sustainable Salmon Symposium, Anchorage Alaska.

Farley, E.V., Jr., J.M. Murphy, B.W. Wing, J.H. Moss, and A. Middleton. 2005. Distribution, migration pathways, and size of western Alaska juvenile salmon along 454 the eastern Bering Sea shelf. Alaska Fisheries Research Bulletin 11(1):15–26.

Grebmeier, J.M., J.E. Overland, S.E. Moore, E.V. Farley, E.C. Carmack, L.W. Cooper, K.E. Frey, J.H. Helle, F.A. McLaughlin, and S.L. McNutt. 2006. A major ecosystem shift in the northern Bering Sea. Science 311:1461–1464.

Hanson, P.C., T.B. Johnson, D.E. Schindler, and J.F. Kitchell. 1997. Fish Bioenergetics 3.0 for Windows. Center for Limnology, University of Wisconsin-Madison and University of Wisconsin Sea Grant Institute, Madison, WI.

Healy, M.C. 1980. The ecology of juvenile salmon in Georgia Strait, British Columbia, p. 203-229. *In*: W.J. McNeil and D.C. Himsworth (eds.). Salmonid ecosystems of the North Pacific. Oregon State University Press, Corvallis, OR.

Hunt G.L., Jr., P. Stabeno, G. Walters, E. Sinclair, R.D. Brodeur, J.M. Napp, and N.A. Bond. 2002. Climate change and control of the southeastern Bering Sea pelagic ecosystem. Deep Sea Research II 49:5821–5853.

Kaeriyama, M., M. Nakamura, R. Edpalina, J.R. Bower, H. Yamaguchi, R.V. Walker, and K.W. Myers. 2004. Change in feeding ecology and trophic dynamics of Pacific salmon (*Oncorhynchus* spp.) in the central Gulf of Alaska in relation to climate events. Fisheries Oceanography 13:197–207.

Kitchell, J.F., D.J. Stewart, and D. Weininger. 1977. Applications of a bioenergetics model to perch (*Perca flavescens*), and walleye (*Stizostedion vitreum*). Journal of the Fisheries Research Board of Canada 34:1922–1935.

Kondzela, C., M. Garvin, R. Riley, J. Murphy, J. Moss, S. Fuller, and A. Gharrett. *This issue*. Preliminary Genetic Analysis of Juvenile Chum Salmon from the Chukchi Sea and Bering Strait. North Pacific Anadromous Fish Commission Bulletin 5:XXX–YYY.

Moss, J.H., D.A. Beauchamp, A.D. Cross, E.V. Farley, J.M. Murphy, J.H. Helle, R.V. Walker, and K.W. Myers. *In press*. Bioenergetic model estimates of interannual and spatial patterns in consumption demand and growth potential of juvenile pink salmon (*Oncorhynchus gorbuscha*) in the Gulf of Alaska. Deep Sea Research II.

Moss, J.H., D.A. Beauchamp, A.D. Cross, K.W. Myers, E.V. Farley Jr., J.M. Murphy, and J.H. Helle. 2005. Evidence for size-selective mortality after the first summer of ocean growth by pink salmon. Transactions of the American Fisheries Society 134:1313–1322.

Nishiyama, T. 1977. Food-energy requirements of Bristol Bay sockeye salmon *Oncorhynchus nerka* (Walbaum) during the last marine life stage. Res. Inst. N. Pac. Fish. Spec. Vol. pp. 289–320. (In Japanese, English summary)

Overland, J.E., and P.J. Stabeno. 2004. Is the climate of the Bering Sea warming and affecting the ecosystem. Earth and Ocean Sciences 85:309–316.

Ruggerone, G.T., M. Zimmerman, K.W. Myers, J.L. Nielsen, and D.E. Rogers. 2003. Competition between Asian pink salmon (*Oncorhynchus gorbuscha*) and Alaska sockeye salmon (*O. nerka*) in the North Pacific Ocean. Fisheries Oceanography 12:209–219.

Simenstadt, C.A. and E.O. Salo. 1982. Foraging success as a determinant of estuarine and nearshore carrying capacity of juvenile chum salmon (*Oncorhynchus keta*) in Hood Canal, Washington. P. 21–37 *In*: B.R. Melteff and R.A. Nevé (eds.). Proceedings of the North Pacific Aquaculture Symposium. Alaska Sea Grant Report 82–2.

Venables, W.N. and B.D. Ripley. 1999. Modern Applied Statistics and S-PLUS 3rd ed. New York: Springer Verlag.

Tables

Table 1.
Input values for juvenile pink and chum salmon bioenergetics models which were held constant over the 30-day simulation. Model simulations were specific to three regions: the northern Chukchi Sea, southern Chukchi Sea, and the Bering Strait.

	Pink salmon			Chum salmon		
Region	Chukchi North	Chukchi South	Bering Strait	Chukchi North	Chukchi South	Bering Strait
Energy density ($J \cdot g^{-1}$)		4796.36			4679.28	
Start weight (g)	54.77	54.77	54.77	82.56	82.56	82.56
Temperature (ºC)	10.08	9.34	8.65	10.08	9.34	8.65
Diet Comp.						
Copepoda	0.008	0.010	0.228	0.009	0.001	0.042
Amphipoda	0.000	0.005	0.015	0.000	0.057	0.058
Euphausiacea	0.268	0.250	0.130	0.241	0.418	0.361
Pteropoda	0.000	0.002	0.000	0.000	0.000	0.000
Chaetognatha	0.000	0.000	0.010	0.000	0.000	0.004
Appendicularia	0.038	0.005	0.006	0.025	0.150	0.214
Coelenterata	0.000	0.000	0.000	0.000	0.174	0.193
Megalopa	0.075	0.687	0.389	0.032	0.192	0.027
Fish and Squid	0.611	0.041	0.222	0.693	0.008	0.101

Table 2.
Prey energy density and percent indigestible values used in bioenergetic model simulations of juvenile pink and chum salmon growth trajectories.

Prey	Percent Indigestible	Energy Content ($J \cdot g^{-1}$ wet wt.)	Literature Sources
Copepods	9.04	2624.2	Davis et al. 1998, Boldt and Haldorson 2002
Amphipoda	12.99	2465.6	Davis et al. 1998, Boldt and Haldorson 2002
Euphausiids	10.35	3110.2	Davis et al. 1998, Boldt and Haldorson 2002
Pteropoda	10.00	2612.1	Model default value
Chaetognatha	8.50	2213.0	Davis et al. 1998, Boldt and Haldorson 2002
Appendicularia	10.00	3177.2	Davis et al. 1998, Boldt and Haldorson 2002
Coelenterata	10.00	1975.8	Davis et al. 2003, Model default value
Megalopa	8.50	2980.4	Nishiyama 1977, Boldt and Haldorson 2002
Fish + Squid	8.98	5010.6	Nishiyama 1977, Boldt and Haldorson 2002

Figures

Figure 1.

Survey station locations and habitat delineation for the Bering Strait, southern Chukchi Sea, and northern Chukchi Sea.

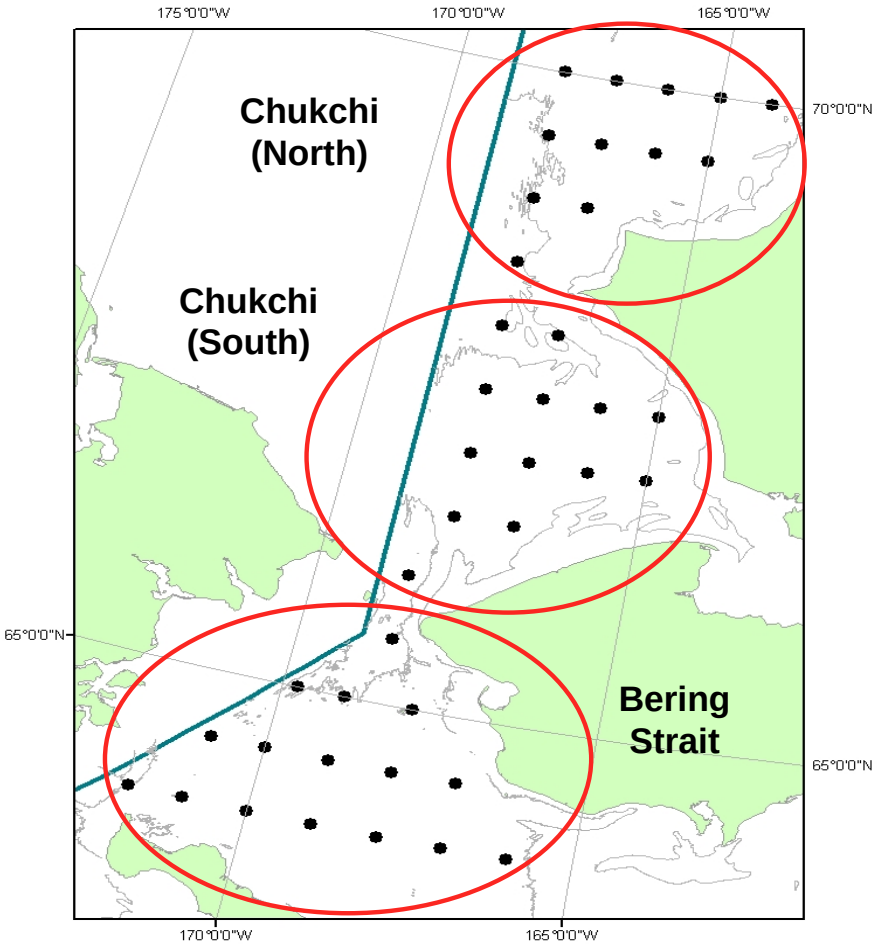

Figure 2.
Relative abundance of juvenile pink and chum salmon inhabiting the eastern Bering Sea, Bering Strait, and Chukchi Sea during late August and early September 2007. Circle size represents catch per unit effort for a 30 minute surface trawl.

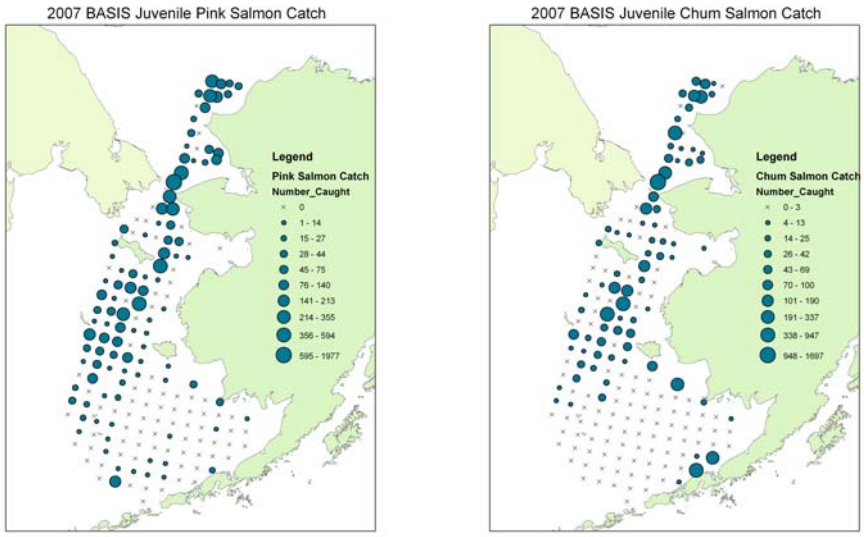

Figure 3.
Linear models representing daily growth of juvenile pink (n = 6828) and chum (n = 8769) salmon collected in U.S. BASIS Surveys from 2002–2007.

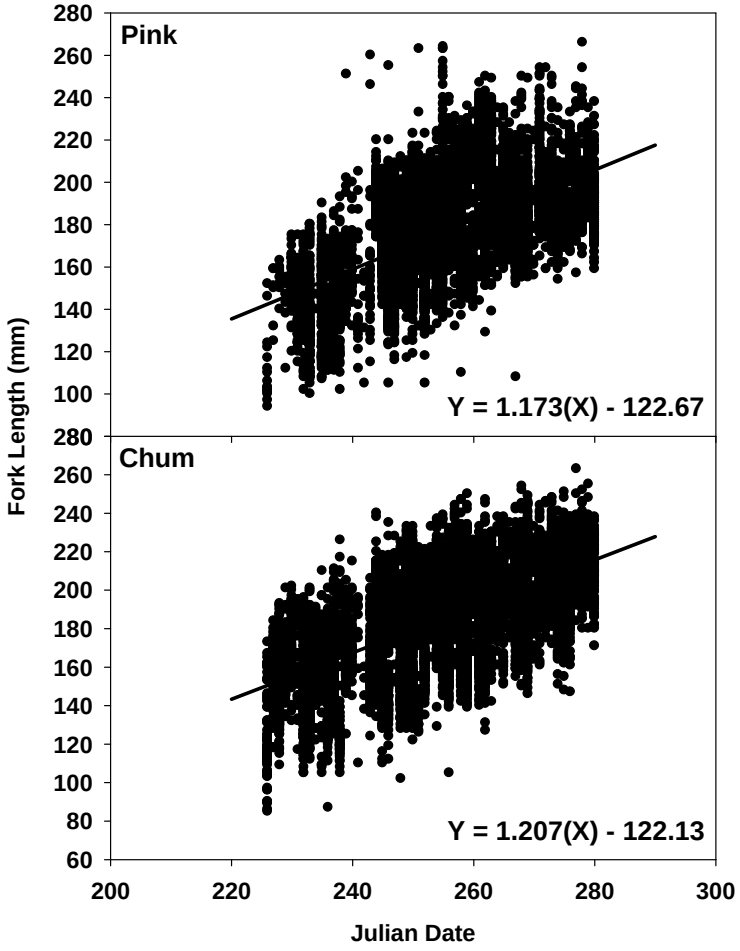

Figure 4.
Differences in estimated average fork length (mm) of juvenile pink and chum salmon by oceanic domain (habitat) during U.S. BASIS cruise in 2007. Standard error estimates of average length are included.

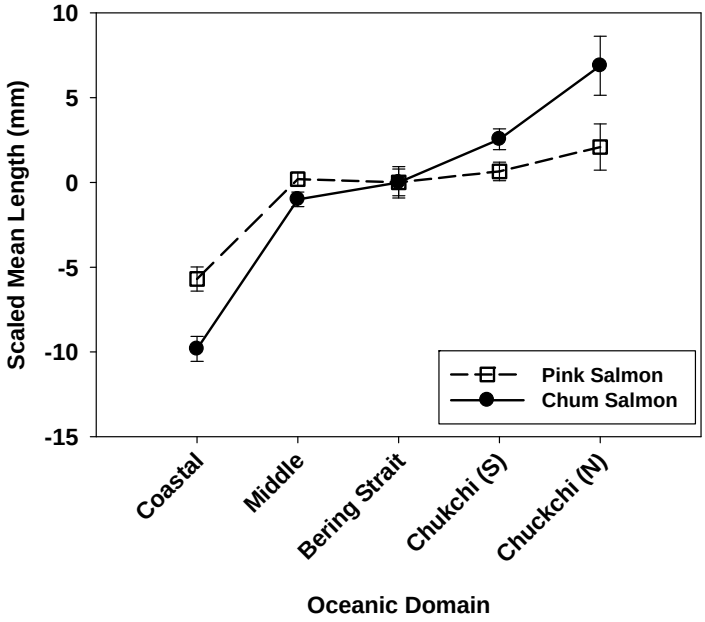

Figure 5.
Growth trajectories for juvenile pink and chum salmon according to region estimated using the Wisconsin bioenergetics model 3.0.

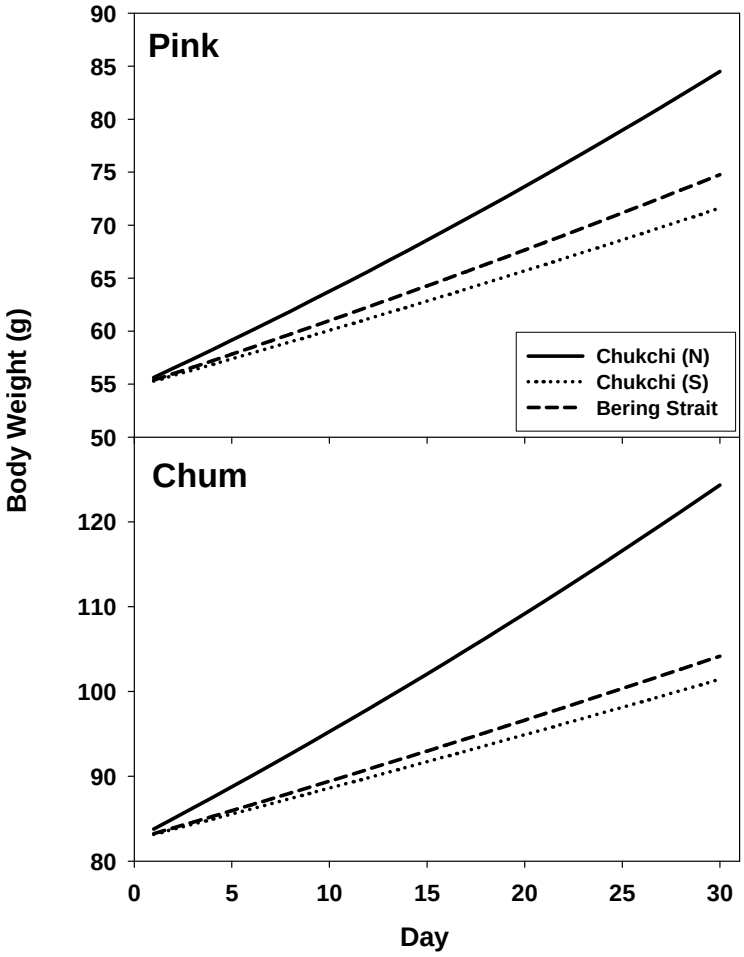

Appendix 4

On temperature and salinity variability over the central eastern Bering Sea shelf

DRAFT MANUSCRIPT

S. Danielson[1]

L. Eisner[2]

T. Weingartner[1]

K. Aagaard[3]

June 2009

(1) Institute of Marine Science, University of Alaska Fairbanks, Fairbanks, AK, USA
(2) Alaska Fisheries Science Center, Juneau, AK, USA
(3) School of Oceanography, University of Washington, Seattle, WA, USA

Abstract

Late summer and early fall temperature and salinity data collected by the Bering-Aleutian Salmon International Survey (BASIS) program are examined in order to better understand the dynamics controlling the temperature and salinity variability of the central eastern Bering Sea shelf waters. Decorrelation length scales are found to be on the order of 100-500 *km* and are generally longer (shorter) in the southern (northern) portion of the domain; the changes from south to north reflect differences in the local circulation fields. Temperature decorrelation length scales are typically longer than the salinity length scales, reflecting differences between the sources and sinks for each parameter. Near surface and near bottom salinity anomalies tend to fluctuate in phase across the central shelf although temperature anomalies fluctuate in phase only in the weakly and unstratified inner shelf waters. Salinities exhibit a broadly weak but locally significant anti-correlation between the coastal and mid-shelf waters. Integrated heat content (HC) and fresh water content (FWC) parameters provide bulk measures of the fluxes required to raise or lower the multi-year mean shelf water temperature and salinity fields to the observed annual values. We find that the HC anomaly is primarily driven by variance in the along-shelf summertime flow field, while the bulk FW anomaly is set by wind-driven transport manifested over the course of the previous winter. In both seasons, the wind forcing is a consequence of the position and strength of the Aleutian Low. Evidence that both the Bering Sea heat and freshwater budgets are experiencing a period of multi-decadal changes comes from observations of significant (at the 99% level) 30 year increasing trends in the winter surface heat flux anomaly and the annual duration of ice-free waters.

1. Introduction

Biological productivity of the eastern Bering Sea (EBS) is well known from its high dollar value commercial fish and crab catches [ref], abundant marine mammal populations [ref] and some of the world's highest documented and potential carbon fixation rates over continental shelves [Walsh et al, others?]. Mechanistic controls of the physical environment that supports this ecosystem are not comprehensively known, in part due to data gaps that span both vast regions of the shelf area and considerable portions of the calendar year. The new and historical datasets described here afford us the opportunity to examine the EBS shelf waters through a fresh lens and over a region that extends from western Bristol Bay as far north as St. Lawrence Island (**Figure 1**). With particular focus on the late summer/early fall time period (mid-August to early October), this manuscript 1) describes spatial and temporal variability associated with the temperature and salinity fields, 2) quantifies and places bounds upon the fresh water (FW) and heat (H) budget partitioning, 3) relates seasonal effects of wind-driven advection to coastal/mid-shelf water mass mixing, replacement and exchange and 4) discusses ramifications of the observations to the nutrient budget and primary productivity over the EBS shelf.

The Bering Sea is a semi-enclosed subarctic sea that links the greater Pacific Ocean with the Arctic Ocean through Bering Strait. It is bounded by the Aleutian Island arc, Siberia and Alaska. The EBS shelf is expansive, extending 800 km in the cross-shelf direction from outer Norton Sound to the continental slope. The shelfbreak extends 1200 km from Unimak Pass to Cape Navarin and is bisected by two distinguished submarine canyons: Bering Canyon (world's longest canyon) and Zhemchug Canyon (world's largest volume of incision) [Normark and Carlson, 2003]. Together, these canyons and the Navarin, Pervenets and Pribilof canyons likely play an important role in setting outer and possibly mid-shelf water properties [Mizobata and Saitoh, 2004; Stabeno et al, 1999, Schumacher and Reed, 1992;…], but our main focus is on the shallower waters overlying the mid and inner shelf regions. Previous studies [Coachman 1986; Kinder & Schumacher 1981] describe the Outer (100-200m), Middle (50m-100m) and Coastal (0-50m) biophysical domains over the southeastern Bering Sea shelf (SEBSS). The northern limit of these zones is not well detailed; Coachman [1986] notes that the boundary between the Coastal and Middle domains (the Inner Front) veers away from the 50m isobaths north of Nunivak Island. Thus, we may require new or additional nomenclature to address regional differences in the biophysical environment represented by our dataset [ref Eisner paper same issue?]. Due to the distribution of the conductivity-temperature-depth (CTD) data under consideration (**Figure 2**), we direct our focus to a region that overlaps both the Middle and Coastal domains and extends from western Bristol Bay to near St. Lawrence Island. For purpose of this paper, we define here the central eastern Bering Sea shelf (CEBSS) as the region that is 1) west of 162 ^{o}W; 2) east of 174 ^{o}W; 3) north of 57 ^{o}N; 4) south of 62.5 ^{o}N; and 5) lies between the 20 *m* and 70 *m* isobaths (see contours in **Figure 2**). This region bounds the maximum extent common to the 2002-2007 CTD survey set. Likewise, we take the inner eastern Bering Sea shelf (IEBSS) to be the area between the 20m isobath and the coast, from Cape Newenham to 62.5 ^{o}N. The EBS shelf north of 56 °N, south of 66 °N and east of Cape Navarin, covers an area of 1.8 x 10^6 km^2 between the 100m isobath and the shoreline, with a mean depth of 43 *m* and a total volume of 7.7 x 10^4 km^3. The CEBSS and IEBSS cover 2.0 x 10^5 km^2 and YY x 10^5 km^2, representing

xx% and yy% of the total EBS 20 – 70 *m* and 0 – 20 *m* regions respectively. Average water depth for the two regions are 45 *m* and *XX m* and their volume encompasses approximately 9.3 x 10^3 km^3 and YY x 10^3 km^3.

The heat content (HC) parameter employed herein is a measure of the amount of heat needed to raise or lower the computed mean CEBSS temperature to the observed value, integrated over the entire CEBSS volume. Likewise, the fresh water content (FWC) parameter is a measure of the volume of fresh water required to be added or removed from the mean CEBSS salinity in order to achieve the observed salinity. In this fashion, consideration of the FW budget employs actual FW volume changes, avoiding the need for reference salinities. Parameters considered below in assessing the HC and FWC budgets include surface heat fluxes, ice melt, river discharge, precipitation (P) and evaporation (E). Mean advective speeds are typically small [refs], but the oceanic transport of heat and fresh water is not negligible. Advective influences include both cross-isobath components (exchange with the nearshore and shelfbreak regions) and along-isobath components (outflow to Bering Strait and inflow from shelf waters derived from Bristol Bay and the Gulf of Alaska [Weingartner et al 2003 and Aagaard et al , Stabenoxxx]), and their distinction is critical. Our observational dataset precludes precise evaluation of most advective components, but we are able to estimate probable magnitudes and present ancillary evidence for the hypothesized advective regime.

The thermal and haline fields both play important roles in setting the location and strength of both frontal systems and the pycnocline, through which nutrient fluxes help maintain primary productivity during the summer. The annual cycle of temperature and salinity changes progresses as follows. North of 60 *°N*, the water column is thermally reset by the end of each winter (HC minimum) back to the freezing point (≈ -1.8 *°C*), coincident with the annual shelf salinity maximum (FWC minimum). These extremes are resultant from the accumulation of dense (cold and salty) water produced by winter freezing. In addition to cooling caused by the seasonal reduction of incident solar radiation, northerly winter winds can promote oceanic heat loss through advection of arctic air masses over the Bering Sea, which increase the air-sea temperature gradient, and through wind driven ice divergence, which creates polynyas and leads and thus enhanced upward surface heat fluxes [Pease; other ref]. Ice melt, delivering low salinity water (~7) to the shelf, occurs continually at the southernmost reaches of the ice extent throughout the winter [ref McNutt or Pease] but the most rapid ablation occurs in May with the seasonal increase of incident solar radiation and the advection of warm air masses from the south [ref Neibauer]. Southerly winds both advect ice northward and increase the melting rate through accelerated sensible and latent heat fluxes [ref]. Melt water, in conjunction with solar heating, helps create the water column stability normally required to initiate a spring phytoplankton bloom [ref]. Through the spring and summer, solar radiation is accumulated in the ocean's surface mixed layer, increasing the strength of thermal stratification. Midshelf waters evolve through the summer toward a strongly stratified 2-layer system, maintained primarily by wind mixing and solar heating in the surface layer and tidal mixing of remnant dense winter water in the lower layer [ref].

We present here data from six years (2002-2007) of late summer to early fall CTD surveys over the EBS shelf (**Figure 3**). Measurements were made between mid August and early October each year as part of the Bering-Aleutian Salmon International Survey (BASIS)

program (**Table 1**). While the BASIS survey's primary goal is to achieve fishery trawls for assessing juvenile salmon and Pollack stocks, the multidisciplinary sampling approach has also garnered extensive physical, chemical and plankton samples. Results from these surveys have been described in Farley [], Coyle [], [etc]. This set of CTD surveys achieves a previously unattained repeated breadth of coverage at this time of year in the EBS. The sampling is not synoptic (40-60 days of ship time per year are required to achieve the broad spatial coverage) but we will show that the late summer/early fall sampling period spans the time when both the fresh water and heat content of the shelf waters are at their annual maximums and that inter-annual variability in both of these parameters is at least as large as the synoptic to mean monthly variability. Though limited in number, the surveys achieve sufficient temporal degrees of freedom to establish statistically robust correlative relations between the temperature and salinity distribution fields and the dynamics likely responsible for their respective setup and maintenance.

In addition to the BASIS CTD data, CTD records from the historical archives at the National Ocean Data Center (NODC) World Ocean Database (WOD) are employed to place the BASIS data within a seasonal climatology context. Atmospheric model output – wind vectors, heat fluxes, pressure – are obtained from the National Center for Environmental Prediction/National Center for Atmospheric Research (NCEP/NCAR) Reanalysis Project 1 output fields. Sea surface temperature records are from the Smith-Reynolds (200x) optimum interpolation Extended Reconstructed Sea Surface Temperature (ERSST) dataset. In-situ weather station records from St. Paul Island are employed for P-E computations. Ice cover data is taken from the passive microwave archive at the National Snow and Ice Data Center (NSIDC). River discharge data is from the United States Geological Service (USGS) streamflow database.

Ultimately, the HC, FWC and nutrient fields all reflect different aspects of the same biophysical environment, mechanistically linked via local and global scale feedback loops but each responding uniquely to the varied forcings. Beyond the descriptive portions, this paper seeks to gain insight into two fundamental questions about the CEBSS waters. First, can we account for observed variability in the HC and FWC fields? Second, how might changes in fluxes or controlling dynamics influence the nutrient distributions and biological productivity? Neither question can be addressed in a fully quantitative fashion but we are able to place bounds on most of the critical parameters. Section 2 describes the data, sources, and methods of data handling. In section 3.1, data extracted from the historical database summarize the mean seasonal and monthly conditions in order to provide temporal context for the BASIS dataset results presented in sections 3.2 and 3.3. Sections 4.1 and 4.2 look at bulk integrations of the HC and FWC fields on seasonal and interannual time frames; section 4.3 addresses long-term trends in the HC and FWC budgets.

2.0 Datasets and Methods

2.1 CTD data

BASIS Conductivity-Temperature-Depth (CTD) data were collected with the following SeaBird Electronics (SBE) instruments and timing: SBE-19 and SBE-19+ (2002), SBE-25 (2003, 2004 & 2005), SBE-917 (2005-2007) and SBE-911 (2005-2007). Instruments were calibrated prior to each season; 2004-2006 salinity measurements were compared to discrete bottle samples as a cross-check on conductivity probe behavior. Temperature, salinity and density profiles were processed using the recommended SeaBird Data Processing subroutines. Final data was binned to 1-m depth levels, plotted and visually inspected for spikes and spurious density inversions. Manufacturer specifications constrain lifetime drift of the temperature probe to less than 0.005 *°C* so we employ this value as our expected accuracy. Experience shows that annual recalibration of the SeaBird conductivity cells generally leads to data with accuracy better than about 0.02 so we employ this value as a rough guide for assessing spikes that need to be cleaned up and as an expected accuracy of the final dataset. Linear interpolation through flagged depth levels was employed to remove problems with magnitudes greater than ~ 0.01-0.02 (*°C* and *PSU*). The CTD ancillary sensor payload changed from year to year, but variously included fluorescence, transmittance, photosynthetically available radiation (PAR) and dissolved oxygen measurements.

To ensure consistent handling of the CTD data from year to year with bulk property computations and gridded map contour plots, we linearly interpolate the temperature and salinity data to a regular 2- or 3-dimensional grid as required. This interpolation ensures comparable volumetric comparisons between years that have differing station layouts and lessens the problems associated with unequal station spacing amongst years. For bulk property comparisons between years, we employ the CEBSS region, which is bounded by the contour in **Figure 2**. The CEBSS region is limited by the largest common domain encompassed by sampling in all years. We can not address the full coastal domain in this manuscript – samples herein extend to only the 20 *m* isobath.

Historical CTD profiles and bottle samples are obtained from the National Ocean Data Center (NODC) World Ocean Database 2005 (WOD-05). These data are screened for errors in position (samples appearing on land and deep samples from a site known to be shallow) or errors in measurement values (unreasonably warm/cold/salty values). Difficult samples to assess were those with reasonable values but perhaps unusual for the collection time of year or location, and egregious outliers are discarded. Our binning method (described below) was designed in part to also help discard outlier or questionable data.

We compute monthly and seasonal mean profiles over a geographic grid with spacing one degree in latitude and two degrees in longitude. Linear interpolations between discrete bottle trip depths are employed to create an approximate full water column profile. All CTD and bottle data are combined into derived profiles to produce a mean monthly representative profile for each grid location in each month of each year, retaining the median temperature and salinity at each depth level. This method has the advantage of discarding outlier casts values, but has the disadvantage over simply taking the mean if a small sample distribution is skewed

away from the true mean. However, we can assess the likelihood of erroneous profiles through examination of the number of samples and observed variance. By creating mean monthly and seasonal profiles before computing the long-term means, we can prescribe an appropriate number of degrees of freedom (DOF = N-2 where N = the number of years represented) and we are ensured that each profile employed in computing the monthly mean is independent, short of multi-year autocorrelation in the temperature or salinity fields.

To evaluate the robustness of these multi-year means, we track the total number of discrete years employed in each grid cell average. For the 20 grid cells whose coverage is more than 50% interior to the CEBSS region, we find that complete coverage is attained with between 11 and 39 years represented for all cells in the May-July and August-October seasonal means; we place a moderate to high level of confidence in these results. The February-April means had one cell with missing data and 15 of the cells had between 3 and 21 samples; we ascribe low to moderate confidence in these values. The November-January means employ zero to 5 years of data, with less than one third of the cells attaining 3 or more samples; one quarter of the cells had no data. The data collected in this time period is so sparse that we are forced to discard the results and focus only on the remaining 3 seasons, keeping in mind that in particular the February-April values may be somewhat skewed by just one or two anomalous measurements within some grid cells. When we employ monthly mean integrations to examine the annual cycle, we lack sufficient spatial data in individual years to create robust error bars so we allow the well resolved BASIS dataset to guide reasonable estimates of probable FWC and HC ranges.

2.2 Ice cover data

Ice cover data are obtained from the National Snow and Ice Data Center (NSIDC) passive microwave satellite archives. The Level 3 data are processed to a ~25 *km* grid. Data from 1988 to the present are daily; from 1978 to 1987 data were collected every other day. Data from 1972-1977 are gappy and so are not employed here. We estimate the number of ice-free days by employing a smoothed concentration-extent time series computed over the Bering Sea south of 66 °*N* and east of 170 °*E*. Assigning a single retreat date to the entire EBS takes an admittedly broad view, but ice decay and growth is relatively rapid and broad scale when conditions exist for the retreat or onset of ice, so we employ fixed a concentration-extent threshold to determine the ice free season duration. The derived annual values are offset by a nearly constant but small amount with varied thresholds chosen within reasonable bounds, so with a few exceptions overall results are insensitive to the choice of threshold value chosen.

2.3 Streamflow data

Daily river discharge data is taken from the US Geological Survey streamflow database for the Yukon and Kuskokwim river stations at Pilot Station and Crooked Creek respectively (http://waterdata.usgs.gov/nwis). Data are provided as quality-controlled products with error flags denoting periods of missing measurements.

2.4 Drifter data

Satellite-tracked oceanographic drifter data from the EBS are employed to examine nearshore-midshelf surface advection fields in the summer and fall. The drifters are cross-shaped Davis drifters drogued to 1 *m* depth. They acquire GPS position fixes every half hour and the data is transferred via email to Fairbanks, AK on a daily basis. After inspection for faulty position or time fixes, the data are converted into vector form and subsequently gridded into 1 degree latitude by 2 degree longitude boxes for grid cells that contain at least 7 drifter-days worth of data.

2.5 Precipitation data

Summary of the day National Weather Service (NWS) precipitation records from St. Paul Island, archived and obtained from the National Climate Data Center (NCDC), are employed to estimate the precipitation over the Bering Sea shelf.

2.6 Sea surface temperature data

Sea surface temperature (SST) data are obtained from the Smith et. al [2008] ERSST product, version ERSST.v3. The gridded fields are constructed from a robust temporal-spatial interpolation scheme applied to the International Comprehensive Ocean-Atmosphere Data Set (ICOADS) SST data. We employ ERSST.v3 because it covers the entire 1979-present passive microwave sea ice concentration dataset. The ERSST dataset is constructed on a 2 degree global grid and monthly time step.

2.7 Atmospheric model fields

Wind vectors, surface pressure fields and surface heat fluxes are taken from the NCEP/NCAR Reanalysis Project 1. We use this product rather than Reanalysis 2 because corrections described below were developed for the Reanalysis 1 results. The Reanalysis computes six-hourly hindcasts of all major atmospheric variables on a ~2.5º global grid from 1948 to the present. The net surface heat flux was created by combining the individual net shortwave, longwave, latent and sensible heat fluxes.

Following the Ladd and Bond [2002] shortwave radiation flux correction for the Bering Sea, we adjust the shortwave fluxes by -70 $W\,m^{-2}$ to reflect the NCEP/NCAR reanalysis' inability to simulate low clouds and fog, but assign a minimum value of 0 $W\,m^{-2}$. Our clipping likely results in a slight underestimate of the solar flux in low light levels. A constant offset bias between years in the handling of the radiation data should not affect results of the anomaly analysis, but it will impact our evaluation of the mean heat flux magnitude. The Ladd and Bond [2002] correction may not apply equally well over our whole domain, given that their analysis shows a much smaller offset at station PAPA, located only XXX km away.

The Reanalysis 1 model performance varies around the globe, but typical evaluations indicate net shortwave root-mean-square (RMS) errors of 30-70 W/m^2 and biases of 5-10 W/m^2 [reference xxxxxx]. A bias of 10 $W\,m^{-2}$ results in an offset of ~$10^{19}\,J$ when integrated over the April-August daylight hours and a $2x10^5\,km^2$ region, or about 4% of the net surface heat flux. Ladd and Bond find good agreement between the winds recorded at mooring M2

and the NCEP wind vectors. Apart from the shortwave flux correction, all other NCEP flux, wind and atmospheric pressure data are employed unmodified.

Some references:

Taylor P.K. editor. 2000. Intercomparison and validation of ocean-atmosphere energy flux fields: Final report of the Joint World Climate Research program and Scientific Committee on Ocean Research working group on air-sea fluxes, World Climate Research Program Report WCRP-112: 303.

Taylor P.K., E.F. Bradley, C.W. Fairall, D. Legler, J. Schultz, R.A. Weller and G.H. White. 2001. Surface fluxes and surface reference sites. In: Observing the Oceans in the 21st Century. C.J. Koblinsky and N.R. Smith, eds. Melbourne, Bureau of Meteorology: 177–197.

Scott, J. D., and M. A. Alexander, Net shortwave fluxes over the ocean, J. Phys. Oceanogr., 29, 3167–3174, 1999.

Quantifying Uncertainties in NCEP Reanalyses Using High-Quality Research Vessel Observations SHAWN R. SMITH, DAVID M. LEGLER,* AND KATHLEEN V. VERZONE1 *Center for Ocean-Atmospheric Prediction Studies, The Florida State University, Tallahassee, Florida*

3.0 Results

3.1 Seasonal Climatology

In order to place the BASIS results (Section 3.2) within an annual cycle framework, we first consider the seasonal climatology. Employing all available CTD data (historical and BASIS data combined), we compile quarterly means of the 0-100m mean temperature and salinity fields across the EBS (**Figure 3**). Insufficient data prevent us from creating a panel for the November-January time period.

Mid-late winter (February-April) is characterized by near-freezing temperatures north of 60N and a high-salinity pool north of 62N. A band of relatively fresh waters extends in the along-shelf direction past St. Matthew Island, the freshest lying just to the northeast of the island. This band may be resultant from fresh shelf water remnant from the previous fall, from ice melt near the edge of the ice pack or along-shore advection. The salty waters surrounding St. Lawrence Island reflect ice formation processes and, consistent with Danielson et al, show no evidence of southward advection of dense water away from the polynya region over the Central shelf domain. Polynya activity in the north can continue into late April, but the heating season typically begins in mid-April and ice cover usually remains well into May (**Table 2**).

In early to mid summer (May-July), waters warm non-uniformly across the EBS with the strongest heating occurring in Norton Sound. Relatively fresh (< 31) coastal waters are observed northward from eastern Bristol Bay, presumably a result of coastal discharge. A salty tongue at approximately the location of Zhemchug canyon protrudes onto the shelf. Given the number of samples taken in the surrounding region, this feature appears to be well resolved and may represent an early summer source of high-nitrate waters to the Outer and Middle shelf domains. We speculate that this intrusion results from the seasonal relaxation of winds that maintain cyclonic stress over the Bering basin and the attendant shelf break front [ref Gawarkewicz papers]. The salty signal just north of Nunivak Island may be biased by the small number of samples within the grid cell.

The late summer/early fall period (August-October) coincides with the BASIS sampling time period and reflects the system's annual HC and FWC maxima. Cross-shelf gradients in density are strongest in this time period and the Inner Front is a well defined feature. Waters inshore of the Inner Front warm to over 8 deg C.

3.3 Late Summer Temperature and Salinity Distributions, 2002-2007

Figure 4 depicts the late summer mean temperature and salinity distributions for 2002-2007 above and below the mixed layer depth (MLD), defined as the depth where sigma-t is 0.10 $kg\ m^{-3}$ greater than the value at 5 m depth. By late summer, surface ice melt plumes are thoroughly mixed, but at nearshore stations river runoff can make selection of a single MLD difficult. In weakly stratified ($\Delta\sigma_t < 0.10\ kg\ m^{-3}$) or vertically homogeneous waters, MLD properties converge.

Along the southeastern shelf, the mean salinity field exhibits gradients in the cross-shelf direction, both above and below the MLD. However, as observed previously by Ohtani [197X], west and north of Nunivak Island, isohalines cross the isobaths: first bulging northwestward offshore of the 30 *m* isobath and then turning northeastward toward Norton Sound. Near and south of St. Lawrence Island, the mean eastward flow carries dense water from the Gulf of Anadyr [ref Schumacher, Danielson]. This saline water of Bering slope origin opposes offshore spreading of fresh coastal waters adjacent to theYukon River and increases the cross-shelf density gradient in Shpanberg Strait where the largest horizontal density gradients (XX $kg\ m^{-3}\ km^{-1}$) in our records are found. The westward bulge of low salinity water centered on 61 ^{o}N may be comprised of Yukon water, Kuskokwim water or other fresh Alaska Coastal Water (ACW) advected from farther south along the coast.

Comment [T1]: Not on the map

The relative position of the 31 isohaline above and below the MLD reveals aspects of the combined effects of stratification, advection and mixing as midshelf and coastal SEBSS waters flow to the north. Offshore of Cape Newenham, the near-bottom 31 isohaline is within 100 *km* of shore and oriented approximately to the west-northwest. Above the MLD, it is oriented to the northwest and the spread between the surface and bottom 31 isohalines is greater than 100 *km*. Approaching 60 ^{o}N, the locations of this isohaline at the surface and at the bottom converge until the water column is nearly unstratified by salinity. North of 60 ^{o}N, they diverge again as the surface fresh coastal lens spreads much farther offshore. This complex behavior is likely explained by the competing roles of mixing, addition of fresh water in Kuskokwim Bay, topographic steering and the shelf-wide pressure gradients set up through northward transport in Bering Strait. Quantifying the details of the mixing taking place here is beyond the scope of this paper, but acknowledging the effects is required to appreciate the fresh water fields we are dealing with. TS Diagram??

Comment [T2]: Seth, are there along-isobath density gradients? I think so and this has dynamical implications vis-à-vis Csanady's theory of pycnobathic currents. It is well to review that theory and see what its implications are for this shelf. I also think that spatial variations in tides come into play and this needs mention here or elsewhere.

In contrast to salinity, the temperature distribution differs greatly on either side of the MLD. Below the MLD, horizontal temperature gradients are generally cross-isobath and a signature of the "cool pool" tongue (remnant winter waters with temperatures < 2 ^{o}C) extends to the southeast, centered about the 70 m isobath. Nearer to shore and where the water column is often well mixed, average late summer temperatures exceed 12 ^{o}C. Above-MLD temperature gradients south of 60 ^{o}N are mostly in the along-shelf direction, whereas north of this the gradients are in the cross-shelf direction. An exception to this occurs in waters inshore of the 30m isobaths and south of Nunivak Island. Here, evidence of enhanced along-isobath flow is seen by the warm tongue that extends northward toward Nunivak Island. As we will discuss in more detail below, this feature may play an important role in isolating the fresher nearshore waters from the midshelf waters farther offshore.

The panels in **Figure 4** show that relative to the along-isobath direction, the mean T and S gradient fields change character between the waters south of Nunivak Island and those to the north. Below the MLD, both the T and S gradient fields are primarily oriented cross-isobath, with the temperature gradient changing sign near the 70m isobath. Above the MLD and south of Nunivak Island, the primary temperature gradient is along isobath whereas the salinity gradient is cross-isobath. North of Nunivak Island, both the temperature and salinity gradients are oriented in the cross-isobath direction, with very little temperature gradient beyond 30m water depth. For the upper layer waters, therefore, advection plays a different role

for the heat and fresh water. Along-isobath advection will not affect the central shelf salt budget, but will impact the heat budget, particularly in the southern portion of the domain where the along-shelf temperature gradient is ~4 *ºC* per 100 *km*. Cross-isobath near-surface advection will affect the salt budget over the whole region but will only impact the heat budget in coastal region of the northern domain. Onshore surface advection in the northern portion of the domain works to increase the cross-shelf density gradient by both the thermal and saline contributions. In the southern portion, onshore advection only increases the density gradient due to the saline contribution. These property gradient fields are important factors that help the advection fields regulate the annual temperature and salinity anomalies. We will return to this subject in Section 4.

In the vertical direction, **Figure 5,** strong thermal stratification exists in all waters outside of the inner front and is strongest in the southeast Bering Sea along the 70m isobath, coincident with the cold pool tongue extending from the northwest. Inshore of the inner front, temperature plays no role in vertical stratification. Salinity contributes to stratification near the Yukon River plume, south of SLI and in western Bristol Bay. There is little contribution by salinity to the vertical stratification, both inshore and offshore of the extensive region between about 58 °*N* and 61 °*N*, suggesting that offshore spreading of low-salinity coastal waters affect stratification in this area at this time of the year. Shelf waters south of XX latitude are typically more strongly stratified, implying that wind events of similar magnitude in the north and the south have different ability to entrain nutrients from below the pycnocline. Interannual variability in the spatial distributions of the thermal and haline compononents to stratification is high, see also Figure XX. For instance, in some years (e.g., 2005) the thermal stratification south of 60 °*N* is much larger than that found north of 60 °*N*, whereas in other years (e.g., 2006) the thermal stratification outside of the Inner Front is nearly constant from south to north.

By interpolating the three-dimensional space of CTD data to an evenly spaced grid, we can make direct water mass type volumetric comparisons between years. **Figure 6** shows the 2002-2007 mean volumetric temperature/salinity (T/S) diagram computed over the domain bounded by the solid contour in **Figure 4** and through three depth layers: 0-20 *m,* 21-40 *m,* and 41-70 *m*. Depth layers are chosen rather than an above/below MLD partitioning in order to enable comparison of equal volumes between years. To account for the entire volume of water within the area, we assume that near-bottom waters not sampled by the CTD have the same properties as those measured at the bottom of the CTD cast. The two-layer stratification regime offshore and well mixed regime onshore both justify use of this approach. As a percentage of the total water column depth, the fraction of water column thus estimated by this method in shallow waters will be greater than in offshore waters. In all, this near-bottom volume accounts for ~10% of the total volume within the domain.

For the 0-20 *m* depth level temperatures range from 5-14 *ºC* and salinities vary from 28 to 32.5. There are however, two major volumetric modes at ~ 6 *ºC*, 31 and at ~8 *ºC*, 31 and a lesser mode near 12 *ºC*, 31.5. The deepest depth level has one major mode at ~ 4 *ºC*, 32, and a secondary mode at ~ 0 *ºC*, 31.5. The deep salinities vary over a narrow range (31-33) and temperatures are mostly between -2 and 6 *ºC*. Mid-level waters occupy nearly the entire range of temperatures seen for the the surface and near bottom horizons (-2 to 12 ºC) but only a

portion of the salinity range (30 to 32.5). This reflects the inability for waters colder than 2 ºC to mix directly with waters whose salinity is less than about 30. The two water types are distantly located from each other: cold waters are offshore and deep; fresh waters are nearshore and shallow. The lack of overlap between the 0-20 *m* and 40-70 *m* water types and the temperature/salinity differences between the two major modes (4 ºC and 1 psu) suggests the strong vertical isolation between the upper and lower layers.

We computed annual anomalies above and below the MLD based on the 2002-2007 mean fields shown in **Figure 4.** The anomaly maps (Figure 7) show the spatial extent, magnitude and sign of the interannual variability. The results indicate that both strong positive and negative temperature and salinity anomalies can extend beyond 200 *km* within a single year. Note that simply classifiying a particular year as "warm" or "fresh" over the Bering Sea shelf as a whole can be misleading unless referenced to a particular shelf subdomain. The most prominent generalizations appropriate to make from the anomaly maps can be summarized as:

1) Across the CEBSS, 2004 was a warm year both above and below the MLD;
2) 2006 and 2007 were cold years below the MLD except for the nearshore region north of Nunivak Island in 2007;
3) 2005 had both extensive regions of cold and warm anomalies (but note that data between PI, SMI and NI were somewhat sparse this particular year);
4) Waters north of NI were fresh in 2002;
5) Salinity anomalies appear to fluctuate out of phase between the nearshore region and the mid-shelf region.

The boundaries between positive and negative anomalies are often coincident with identified bio/geo/physical domain boundaries like the inner front, although this is not always the case, as seen with the 2005 temperatures below the MLD. We do not have the temporal data required to determine whether this reflects a transition between two states, a temporary breakdown of the traditionally defined domain boundaries and associated dynamics or synoptic-scale aliasing. Below, we examine the statistical significance of these distribution patterns, cautioning that synoptic scale fluctuations may impede making definitive conclusions. First, however, we will show how the anomaly fields manifest themselves within volumetric T/S anomaly plots.

We can infer some of the mechanics involved with water mass modification that has taken place over the course of the summer through inspection of annual volumetric T/S diagram anomaly plots (not shown). Lacking data that describe the winter's end conditions, a first-order assumption is that the shelf-wide water column is comprised primarily of water similar in type to the dominant mode 40-70 *m* water found at the end of summer. This assumption neglects temperature and salinity variations that may be found in coastal waters, but may reflect the offshore water column reasonably well. Whereas 2006 and 2007 both exhibit mixing along a line that indicates mid-depth warming and freshening, the warm and salty year of 2002 shows primarily warming in the mid-depth layer.

3.4 Vertical and Horizontal Correlations of Temperature and Salinity

To evaluate whether the anomaly patterns shown in **Figure 7** are statistically robust features and to help us relate these patterns to the driving physics, we employ an ensemble of correlation maps, **Figure 8** and **Figure 9**. With only N = six data points, we are left with N-2= 4 degrees of freedom (DOF) so significance at the 95% level requires a cross-correlation magnitude of at least 0.81. The yellow contours in **Figure 8** outline regions of statistical significance (both positive and negative) using this criterion.

Figure 8a depicts the correlation at each grid point between the temperatures above the MLD with the temperatures below the MLD for the 2002-2007 time series. The significant vertical temperature correlations are restricted primarily to waters within and near the inner front. This pattern reflects the fact that in shallow depths the water column is strongly mixed by tides and winds and this intense nearshore mixing transmits the local summer heating signal through the whole water column. Offshore, correlations degrade in deeper waters and in the region just south of SLI. This isolation between the surface mixed layer and the deep layer implies that the upper layer evolves separately from the lower layer once late spring stratification overtakes winter mixing. A suggestion of (nonsignificant) anti-correlation between upper and lower outer shelf waters (mostly deeper than 70m total water column depth east and southeast of the Pribilof Islands) supports a notion of possible positive feedback between the cold pool extent and the ability of the upper water column to re-stratify in the spring [ref Stabeno, Coach].

Salinity, on the other hand, is significantly correlated in the vertical direction in both nearshore and offshore regions (**Figure 8b**). Thus, over much of the eastern shelf salinity anomalies above and below the MLD fluctuate in phase with one another on an interannual basis. Exceptions to this are found near and south of SLI, western Bristol Bay and the outer southeast shelf region. We suggest that these regions show no correlation due to the influence of Anadyr and Yukon waters near SLI, alongshore advection of coastal water masses from Bristol Bay and shelf-basin exchange over the outer shelf respectively.

Figure 9 depicts the horizontal correlations of the anomaly fields for the above- and below-MLD time series between each marked point with all other points in the same domain. The correlation maps indicate that: 1) Correlated regions are much broader than the station spacing, indicating that the BASIS sample grid is sufficient to resolve coherent anomalies with length scales of greater than ~50-100 km. 2) The de-correlation scale for temperature anomalies generally exceeds the scale of the salinity anomalies in the southern portion of the domain, reflecting differences in the controlling source and sink terms. 3) The decorrelation length scale for temperatures in the southern portion of the domain (O 200-500km) is greater than the temperature decorrelation scale in the north (O 100-200 km). These differences reflect differences between the broadscale along-isobath advection typical of the SEB in opposition to the cross-isobath advection observed between St. Lawrence Island and Nunivak Island. 4) Salinity is generally anti-correlated between the nearshore and mid-shelf regions though the extent of the significant regions is limited and patchy (e.g., 9K and 9L). 5) In contrast to salinity, correlated temperatures span both coastal and mid-shelf regions in both the south and the north (9E and 9H). This suggests that broadscale surface heat fluxes drive the temperature anomalies while the nearshore salinity anomalies are largely driven by coastal

runoff and freshwater dispersal patterns. 6) Alongshore salinity anomalies are generally in phase from C. Newenham to the Yukon River although the correlation is not generally significant over large distances (9L and 9N). The shorter alongshore salinity correlation length scales may reflect the local influence exerted by the Yukon and Kuskokwim river outflows.

What effect does the sampling scheme have on our results? Since we are interested in characterizing the interannual variability, with our small number of independent samples we require the synoptic noise level to be small. Presuming that the interannual synoptic variability is uncorrelated on an annual basis, we conclude that the mere existence of the observed large-scale coherent patterns suggests that the high frequency signals are small with respect to the interannual signal. In addition, mooring records from prior deployments [ref Stabeno, Danielson, Kinder, Schumacher] depict typical synoptic variability at discrete depth levels and we see that many high frequency fluctuations are indeed relatively small and ephemeral. The long time period required to complete the survey has the additional affect of smoothing synoptic scale variability. Seasonal and monthly integrations shown in Section 4 will also suggest that the seasonal and monthly variability are the same order or smaller than the interannual differences.

Comment [T3]: Another way to characterize this is to examine the temporal variability in summer from our SLIP moorings. This gives you an idea of the variance at a particular depth for particular months. You could use that data to quantify the variance in a signal at one spot for a particular month. How does that variability then compare with the interannual anomalies?

In summary, we find that the broad extent of significant T and S horizontal correlations shows that the station spacing employed by the BASIS survey does in fact capture significant large-scale features. Likewise, the interannual fluctuations have probably not been obscured by seasonal or synoptic variability over the time required to complete the surveys. In the vertical direction, above- and below-MLD salinity anomalies vary in phase with each across most of the central shelf whereas the temperature anomalies vary in phase only within and near to the Inner Front. In the horizontal plane, temperature anomalies are correlated over distances of ~500 km or more. Coastal salinity anomalies operate weakly out of phase with offshore salinity anomalies. This final and somewhat surprising result provides insight to the dynamics driving the greater EBS shelf and we will investigate it in detail below.

4.0 Discussion

By integrating the observed temperature and salinity fluctuation over the CEBSS volume, can we learn anything about the dynamics of the bulk heat and FW fields? Employing detailed accounting of the various heat and FW sources and sinks, we will attempt to bound the relevant parameters, ultimately showing that both surface heating and along-isobath wind driven transport are related to the summer's end HC while the previous winter's cross-isobath Ekman transport is primarily responsible for setting up the FWC anomaly. All of the driving mechanisms are influenced by the large-scale atmospheric pressure distributions associated with the Aleutian Low. Scaling arguments, dynamical considerations and flux balances allow us to estimate advective contributions to the HC and FWC budgets.

4.1 Seasonal variability

Employing the historical CTD database again, we integrate the mean quarterly water column (**Figure 3**) in order to compute the FWC and HC over the CEBSS region. Anomalies are computed with respect to the mean of the three resolved seasons. The FWC and HC

parameters are both at a minimum in late winter and largest in the August-October time period, exhibiting a range of ~ 101 km^3 and 2.6 x 10^{20} J respectively. Similar computations made on monthly mean grids indicate a March-August range of ~150 km^3 and 3.0 x 10^{20} J respectively, but these values may be biased due to the few number of late winter CTD samples. Nonetheless, the two values provide upper and lower expected bounds for the seasonal changes in FWC and HC. Summing the various non-advective heat and FW source terms between April and the end of August (**Table 3**) shows us that 1) ice melt and P-E are not sufficiently large to account for the observed seasonal increase in FWC; 2) river discharge is large enough to provide substantial FW inputs but we cannot presently show that the coastal waters are able spread out into the CEBSS region fast enough (see below); 3) the net surface heat flux can account for the seasonal increase in heat content, within the accuracy of the computations; 4) the historical data and the use of estimated winters end HC standing stock (described below) give similar magnitudes and probable ranges for the seasonal heat accumulation. Employing the summer's end HC variance to estimate the range across seasons is justified through analysis of the ERSST time series at the grid point 60N/170W. Autocorrelation of this monthly time series over the 1979-2008 period shows that the decorrelation time period for temperature anomalies is ~ 2 years. Importantly, and consistent with our observations below, the FWC and HC interannual variability (**Table 4** and **Table 5**) is not small with respect to the expected seasonal variability.

4.2 Interannual variability

4.2.1 Fresh Water Anomalies

Integration over the CEBSS volume shows the how the bulk FWC varies on an interannual basis (**Table 4**). Recognizing that the salinity anomalies vary out of phase between the nearshore and offshore regions, the bulk of the volume is contained in regions with water depths greater than 30m so the integrations primarily reflect conditions offshore. With respect to the mean 2002-2007 salinity field, the summer's end CEBSS volume exhibits a range of 140 km^3 FW between the freshest and saltiest years. Thus, within the CEBSS volume alone (which accounts for ~10% of the EBS shelf volume), inter-annual FW standing stock variability is an appreciable fraction – 20% – of the 700 $km^3\,yr^{-1}$ range of FW exported through Bering Strait annually [Woodgate and Aagaard, 2005]. With an estimated residence time of ~3 years on the Bering Shelf, this implies that the central Bering shelf is a significant high latitude buffer of fresh water (Peterson, et al, 2006; Aagaard and Carmack,) and processes that redirect or modify the shelf waters could influence the North Pacific's impact on the Arctic Ocean. This presentation of course neglects differential contributions to the Bering Strait outflow from Anadyr and Shpanberg Straits and we have sidestepped consideration of the residence time of waters in the IEBSS region. Below, we will consider the magnitudes of the various source terms in order to attempt an accounting for the observed magnitude of FWC variability. We will need to separate the contributions from seasonal and interannual changes in the possible source terms.

Directly input to the IEBSS, the Yukon (202 $km^3\,yr^{-1}$) and Kuskokwim (38 $km^3\,yr^{-1}$) rivers provide the largest point sources of fresh water to the eastern shelf. Coastal discharge increases rapidly from low winter-end values (Yukon, 900-1500 $m^3\,s^{-1}$; Kuskokwim, 170 -450

$m^3\ s^{-1}$) to the annual maximum (Yukon, 13000-33000 $m^3\ s^{-1}$; Kuskokwim, 2000 -11000 $m^3\ s^{-1}$) in May or June. Integrated over the April-August months, these two rivers typically discharge 152 km^3, with a range of about ± 30 km^3. Most of this fresh water probably departs the Bering Sea through Bering Strait [Coachman et al 1975; …, Aagaard et al, 2006], although perhaps after first mixing with central shelf waters south of St. Lawrence Island [Danielson, et al, 2006]. Due to the paucity of data inshore of the 20 *m* isobaths, the frontal, stratification and advective regimes within the expansive IEBSS area have not been described in detail. Using sediment plumes as tracers for brackish waters, examination of satellite imagery suggest the existence of frontal systems during summer months. We speculate that these fronts result in coastal trapping of the river discharge, impeding cross-shelf spreading of the coastal low salinity waters. This summer circulation scheme is supported by recently collected oceanographic drifter data, **Figure 10**, showing that mean gridded surface vectors from June through August are directed predominantly along-isboath and toward the north. In contrast, the fall and winter vectors show predominantly westward transport. We conclude that despite the large volume of FW discharged by the rivers, the current year's outflow and its variability have little direct influence on the summer's end CEBSS salinity; this is also supported by the non-significant cross-correlation between the discharge time series and the shelf FWC time series (**Table 4**).

We estimate the precipitation and evaporation over the CEBSS region by scaling precipitation records collected on St. Paul Island to the CEBSS region and evaporation by employing the Reanalysis skin temperature and latent heat flux estimates. We find that for the April-August time period, P-E for the CEBSS region is 23 km^3 on average, with interannual variability on the order of ± 4 km^3 (**Table 3**).

Sea ice FWC anomalies are estimated from the ice extent (**Table 2**) at the start of the summer's heating season. Passive microwave satellite sea ice measurements provide surface area estimates of ice cover but not thickness. Estimating that typical Bering Sea winter end ice thickness is ~0.5 *m*, (R. Gradinger, pers. comm. (Rolf and I have plans to estimate some ranges as well in late July)), we can make a crude estimate of the FWC held by the sea ice by assigning a bulk salinity of 7 to the ice melt (ref). As with coastal runoff, the sea ice FWC anomalies do not correlate with the summer's end CEBSS FWC anomalies nor are they large enough to account for the observed anomaly variance (**Table 4**). Melting an ice pack with area of 1.0 x 10^5 km^2 (representing the northern half of the CEBSS region), thickness of 0.5m, and bulk salinity of 7 (refs) would deposit the equivalent of 50 km^3 of fresh water at the top of the CEBSS water column. Such a fresh water input is capable of freshening the underlying water column by 0.25 if distributed uniformly (as in a stormy spring) or by 1.2 if mixed over only the upper 10m (as in a calm spring with a warm, fresh surface lens). Using the expected range of winter's end ice thickness and extents, the probable FW contribution from winters end melting of the ice pack is in the range of XX-YY km^3.

Comment [SLD4]: Check all the computations in this paragraph

What about the role of advection to the seasonal increase in FWC? Long-term mooring records report sluggish mean flows along the eastern Bering Sea shelf [refs], with magnitude on the order of 1-5 $cm\ s^{-1}$. For an along-isobath distance of 250 km, a 2 $cm\ s^{-1}$ flow results in a flushing time of 250 km /.02 $m\ s^{-1}$ = 145 *days*, and we see that the winter-end water masses of the southeast Bering shelf likely remain within the CEBSS at the end of summer, but water in

the northern portion of the domain at the end of winter are likely gone by the end of summer. The late winter salinity distribution (**Figure 3**) shows that early summer northward advection would promote replacement of the saline waters found near St Lawrence Island (**Figure 3**) with fresher waters from farther south. Using $\Delta S \sim 0.5$ and assuming that southern shelf waters are replaced by those with similar salinity, we find that along-shore advection can account for a seasonal increase of ~50 km^3 FW. With on average 38 km^3 available from P-E, 46 km^3 from ice melt and 50 km^3 from advection, it appears that our expected range of 101-150 km^3 is roughly balanced, without need to move large volumes of river discharge offshore. However, the interannual variability in summer's end standing stock (**Table 4**) does not appear to be reflected in the variability of the ice melt and P-E source terms.

Since we cannot account directly for the observed interannual oceanic FWC anomalies, we turn the analysis to indirect comparisons via time series correlations. A number of likely environmental time series were examined (wind fields integrated over various time periods and regions, lagged ice extent and retreat time series, lagged river discharge integrations). One dataset stands out with a strong and statistically significant correlation: cross-shelf Ekman transport derived from the along-shore winter winds and integrated over the preceding October-May time period. This mechanism works on the shelf system in the fashion most amenable to influencing salinity modifications: transport is forced along the direction of the largest salinity gradients and begins at the time of year when the gradients are maximal. The fall winds winds help erode the frontal structure at the same time that decreased discharge rates are less able to maintain the frontal system. Additional regressions performed with the transport computed over slightly varying integration periods (e.g., varying the start and end integration months backward and forward in time) give similar results.

The winter cross-isobath transport vs. FWC correlation has a value of $r = -0.95$; and $p = 0.0037$. The sign convention indicates that anomalously strong winds in the alongshore direction (from the north in the northern portion of the domain and from the northwest in the southern portion) precede a summer with an anomalously fresh shelf. This result is somewhat counter-intuitive, because strong winter winds with a northerly component promote enhanced polynya activity on south-facing coastlines and can advect cold air masses from the arctic, thus leading to strong heat ocean to atmosphere heat fluxes and shelf salinization. Danielson et al 2006 estimate, however, that only ~25% of the winter saline production comes from the polynyas themselves and only found evidence that this high salinity water is advected northward, not southward. Rodinov et al. [2007] show that northerly winds in the eastern Bering can also be the result of storm systems displaced eastward into the Gulf of Alaska and that these systems can recirculate warmer southerly air masses over the Bering Shelf. Years with the greatest positive FWC anomalies coincide with the years that experienced the largest westward component of transport over the eastern shelf; these years had low pressure centered over the northern Gulf of Alaska (**Figure 11**). Ignoring shallow-water effects, Ekman transport of fresh water from the coastal region could supply 58 km^3 of fresh water when integrated over the 2006 winter season (**Table 3**) assuming a cross-shelf salinity gradient of 1 between the nearshore and offshore regions. Likewise, winter eastward transport in 2005 could have removed 67 km^3 of FW; both of these values are of the proper magnitude to account for the observed summer's end FWC anomaly.

Other possibilities exist to form the mechanistic link between alongshore winter winds and the summer's end FWC, but we are unable to reliably quantify their effects herein. Strong downwelling winter winds could set up an alongshore barotropic northward flow (as described below for the transport of heat) and thus flush the coastal water more readily from our system. Or, it is possible that the wind-FWC relationship is merely a correlative one and the differences are generated within the ice formation/melting conveyor belt or other circulation features dependent upon the 3-dimensional flow field and its interaction with topography. Analysis of numerical model results may provide insight to the dynamics at play, and we will extend this line of research in future efforts.

Distributed across the CEBSS volume, 150 km3 FW reflects an equivalent of X meter FW and a net salinity change of about 0.70. The CEBSS volume is ~9,300 km^3 with a mean salinity of ~32 (**Figure 3**). Across the IEBSS (volume ~480 km3), typical late summer salinities are probably less than 30. Mixing the two volumes thoroughly would result in a water mass with salinity 31.9. If inshore waters are completely depleted with respect to nitrate but offshore has 10 [μM] then mixing would result in final water mass of 9.5 [μM], a 5% decline in nitrate available for primary production. A much greater relative impact would be felt by the inshore waters, which start the winter nitrate depleted. Complete mixing of coastal and midshelf waters could bring as much as 9.5 [uM] to the IEBSS. Thus, important questions remain: what is the nutrient load for coastal waters at the end of winter? What is the interannual variability in nutrient levels here and what effect might large variability have upon the ecosystem? The coastal nutrient environment could be highly sensitive to the presence or lack of cross-shelf winter exchange. Though probably nutrient depleted for much of the summer, in the early summer the IEBSS must provide sufficient food resources to support juvenile salmon for their transit from the fresh water out into the CEBSS. The drifter data and trawl records of Farley et al [XX] both suggest that the transit through the IEBSS region may take at least 1-2 months (check this), thus leaving the smolt highly dependent upon the food supply that they encounter.

4.2.2 Heat Content Anomalies

The heating season onset (**Figure 12**) takes place in the spring when the daily mean net surface heat flux over our focus area changes sign from negative (oceanic heat loss) to positive (oceanic heat gain). To maintain a consistent time period of comparison between years, we take April 1st to be a date near the spring equinox at which to begin the surface heat flux integration. Integrating onward from each individual year's heating season onset does not appreciably change our results because net daily fluxes near the equinox are small. Following the same arguments given above about the summer flushing of the northern portion of the domain due to along-isobath advection, we find that the region of greatest ice extent variability in the winter (waters south of 60 °*N*) coincides with the domain encompassing water that remains over the CEBSS at the end of summer. Thus it is the waters south of 60 °*N* that have the greatest impact on the heating seasons' HC anomaly.

Lacking 2002-2007 springtime CTD survey data, we estimate the annual winter's end heat content (**Table 3** and **Table 5**) in the following manner, taking advantage of the nearly homogeneous water column at this time of year (Stabeno et al, 2001, 2002). Over the mean

March and April shelf area that is occupied by sea ice with concentration > 30%, we impose a near-freezing water column mean temperature of -1.5 °*C* and over the region not covered with sea ice we impose a water column temperature of +3 °C. {USE +2} The former value is likely good to within .5 °*C*; the latter is probably good to within +/- 2 °*C,* based on ERSST April data and NOAA mooring M2 results (Hunt et al. , Stabeno et al, 2002). Convection and intense winter wind stirring can mix shelf beyond 70m depth so these values are applicable throughout the water column. Although this simple linear model is a gross oversimplification, the temperature differential based on these error estimates is probably accurate to better than a factor of two. If the mean ice extent in the month of May is chosen to initialize our heating season's start heat content, the winter's end heat content anomaly is significantly correlated with the summer's end anomaly, but in neither case does the winter's end HC variance account for more than 30% of the summer's end HC anomaly.

Comment [T5]: I think you need to show this and maybe compute things for the range in temps., e.g. +/-2C

Integrating the Reanalysis surface heat flux between the start of the heating season (April 1st) and the end of August, we find a significant correlation to the oceanic HC anomaly (**Table 3** and **Table 5**). While the summer heat flux provides the vast bulk of the mean heat content, the summer surface flux anomaly represents only about 10% of the HC anomaly. We turn to advective contributions to support the difference.

The summer mean along-isobath velocity (*v)* can be estimated on an annual basis by balancing each summer's end (*se*) heat content with estimates of the winter's end (*we*) heat content and the cumulative surface heat flux (*s*) over the heating season: [Need to add the latent heat of melting term in here. Small, but might as well include it]

$$(1) \quad Q_{se} = Q_{we} + \int_{we}^{se} Q_s dt + \int_{we}^{se} v \frac{\partial Q}{\partial y} dt$$

Computation of the alongshore heat content gradient is achieved by integrating the heat content in the waters north of 60N and in the waters south of 60N. Absent springtime CTD data, we estimate Q_{we} as described above. We find that the heat gradient at winter's end is similar in magnitude to the heat gradient at the end of summer. We use the two values to estimate a probable range of possible velocities and assume that *dQ/dy* is constant from spring through summer . Potential errors in the computation should be small: 1) cross-shelf transport is neglected in summer and we have shown the cross-shelf thermal gradients to be appreciable in the north. However, the drifter data suggest that cross-isobath flow in summer is restricted by the presence of frontal systems; 2) We assume all surface heat flux goes into warming the ocean and ignore any effect of heat driving ice melting. The two estimates of *dQ/dy* result in the range of velocities given by the red and blue symbols in **Figure 13**. We see that the along-isobath velocity required to maintain balance in the heat equation is less than 2 $cm\ s^{-1}$ and that both northward and southward mean flows are predicted.

Another component of advection that we can estimate is the surface Ekman transport. Compensating return flows support differential heat advection in the surface and subsurface waters; the magnitude will be dependent upon both the vertical and the along-isobath temperature gradients. Considering only the surface Ekman flux and integrating from April through August, we find that the along-isobath transport computed across 60 °N is significantly correlated with the summer's end HC anomaly, whereas the cross-isobath transport is not. Assuming an Ekman depth equal to a typical mid-shelf summer mixed layer

depth (~20m), the mean along-shelf Ekman velocity is .1 $cm\ s^{1}$, and the 2002-2007 range is between -1 and +1 $cm\ s^{-1}$ (**Figure 13**). The atmospheric factors responsible for the correlation between the velocity and HC anomaly are evident in the sea level pressure and transport vectors presented in the right-hand two columns of **Figure 12**. In 2004, the warmest year encountered during the BASIS surveys, an anomalously (?) deep Aleutian Low developed over the western Bering Sea while anomalously (?) high pressure sat over the Alaskan mainland, resulting in strong northward transport over the shelf. The coldest two years, 2006 and 2007, had mean westward/southwestward transport over the shelf resulting from a split Aleutian Low pattern manifested by closed sea level pressure contours both in the northern Gulf of Alaska and the western Bering Sea.

Much of the central Bering Shelf is within the e-folding distance for the barotropic Rossby radius of deformation ($R_o = (gH)^{1/2} f^{1} \sim$ 100-250 km). In this case, an alongshore barotropic flow can also result from sealevel set-up and set-down driven by geostrophically balanced pressure gradients:

$$(2) \quad V = \frac{h\tau^{y}}{r\rho},$$

where the along-isobath transport V is a consequence of the along-isobath wind stress τ^{y}. We take the frictional damping coefficient r (10^{-3}), water depth h (45 m) and density ρ (1024 $kg\ m^{-3}$) to represent reasonable values. Integrated between April and the end of August, we find a range of velocities supported within +/- 2.5 cm/s for the years 2002-2007 (**Figure 13**, green symbols). For greater or smaller values of r, this velocity range would scale accordingly.

Comment [T6]: This may be a little high for this water depth.

Interestingly, all three methods of estimating the along-isobath summer heat transport show similar magnitude in their interannual changes. Balancing the HC anomaly equation, the Ekman transport estimates and the barotropic flow estimates all suggest the possibility of either net northward or southward flow over course of the summer. Large positive HC anomalies coincide with years that exhibit strong northward advection of heat. We are unable to separate the probable impact of Ekman vs. along-isobath barotropic flows and the velocities in either case may be sufficient to maintain heat balance. Refining uncertainty in the surface heat flux field and assessing the impact of cross-isobath flows is also critical to gaining fuller understanding of the CEBSS heat budget.

4.3 Decadal scale trends

Interannual variance in the maximum southerly extent of ice and near-freezing waters depends in part on the year-to-year variability of winter winds. In low ice extent years, this is resultant from a westward shift and deepening of the Aleutian Low [Overland & Pease, 1982; Niebauer and Day, 1989]. Examining passive microwave satellite records extending back to 1979, we find a similar wind/ice relation along with a 28 year increasing trend ($r^2 = 0.24$; p value=0.008; trend = 8 days per decade) of the ice-free season length (**Figure 14**). This trend is consistent with other observations of decreasing ice cover noted across the arctic [ref] and the Bering Sea itself [ref Hunt et al 2002; Stabeno 2001, Jewett et al, submitted] and is accompanied by both an earlier onset of spring melting and a delayed onset of winter ice formation. Thus, we have indications that the neither the heat nor FW budgets of the EBS may be in steady state over the modern satellite record time period. In addition to the increase in

mean duration of the ice-free season, we find that the variance of this parameter has increased threefold between the 1979-1991 and 1992-2007 time periods. Ramifications of a longer ice-free production season with higher interannual variance are unclear but potentially significant for the greater ecosystem.

Despite the changes observed in the ice-free season duration, we do not observe a statistically significant change in a) the maximum areal extent, b) the date that the maximum ice extent is attained (Figure 5a) or c) the mean areal extent of sea ice over the 1979-2007 record. Ice pack ablation is dependent upon initial ice thickness and areal extent, atmospheric heat fluxes and oceanic heat fluxes. Consistent with the observed reduction in ice cover days, inspection of the 1979-2008 Reanalysis results at the grid point closest to 60°*N*/170°*W* indicates that there exists a significant positive trend in the cooling season (October-March) net surface heat flux anomaly ($r^2 = 0.26$; $p = 0.0037$; trend = 9.7 $W\,m^{-2}$ per decade). Integrated over the 6 month period, an increase of 30 $W\,m^{-2}$ is $9*10^{19}$ J in total. Spring and summer surface heat fluxes over the same time period show no significant trend. Oceanic contributions to water column heat content and impact on ice growth are not well known because neither water column temperature nor velocity measurements cover the satellite record time period. Monthly ERSST anomaly time series from the 60°*N*/170°*W* grid point exhibit a highly significant ($r^2 = 0.14$; $p < .0001$; trend = 0.1 °C per decade) linear increase in sea surface temperature over the same time period, however a significant trend is not found when SSTs are integrated cross the entire CEBSS region.

Evidence from the ice records and the Reanalysis output both point to a probable reduction in the total ice volume found at winter's end. How an ice melt season shortened by two or three weeks and accompanied by an earlier onset of ice-free waters affects this shelf's overall productivity is unknown, but such a change in shelf habitat during the dynamic spring period suggests the possibility of meaningful ecosystem ramifications [e.g., Hunt 2002].

4.4 Summary and Conclusions

The BASIS CTD dataset has enabled this investigation of the EBS shelf physical system and have been able to place results within a broader context through the use of many ancillary datasets and historical data. We observe evidence of decadal-scale changes in both the heat and FW budgets: an increase in the duration of ice-free waters and a decrease in the winter ocean-atmosphere heat flux. Compilation of HC and FWC budget on an annual basis suggests that the summer's end HC anomaly is primarily related to along-isobath advection, while the summer's end FWC anomaly appears to be related to winter cross-isobath advection. The multi-year repeated occupations of the BASIS grid allows us to compute decorrelation length scales for a large portion of the EBS shelf and we find indications that the shelf-wide temperature and salinity fields operate in distinctly different fashions from one another. Whereas the temperature fields above and below the MLD are correlated only within the Inner Front, the two salinity fields are correlated over the middle shelf as well. However, in the horizontal dimensions, temperature decorrelation length scales are greater and the salinity field exhibits weak but significant anti-correlation between the nearshore and offshore regions.

Pressure systems that propagate across the Bering Sea impact ocean conditions, through regulation of incident sunlight via the cloud cover distribution and the wind driven mixing and advection. Modulation of these forcing parameters occurs with the passage of individual storms, varying about a mean seasonal state. Inspection of monthly mean surface Ekman transports (**Figure 15**) shows that particularly in the months of October and November, shelf surface flows are driven cross-isobath (westward). In addition to carrying coastal waters to the mid-shelf region, this process may have the ability to remove fresh water from the shelf itself, influencing the ultimate flux of FW northward through Bering Strait.

Although we have been able to bound portions of the HC and FWC budgets over the CEBSS, many aspects of the system remain beyond precise quantification. In particular, the bulk heat and FW flux estimates provide only rough bounds on the advective components. In the Bering Sea, advection is influenced by numerous factors that we cannot address without a concerted numerical modeling effort. For example, the CEBSS is characterized by low relief, exceedingly small bottom slopes (O[10^{-4}]), and relatively unchanging isobath orientations while the IEBSS is characterized by extensive regions of shallow water and a coastline whose orientation with respect to the prevailing winds varies from south to north. The EBS shoreline extends toward the northeast from Unimak Pass to inner Bristol Bay and then exhibits long (O[100 *km*]) alternating southward and westward facing shorelines as it winds around Bristol Bay, Kuskokwim Bay, and the Yukon-Kuskokwim delta until it reaches Norton Sound. The length scale of these shoreline segments is on the order of and slightly less than that of the synoptic atmospheric length scales (O[100-500 *km*]) so we can expect that the coastal circulation response to wind events relative to the cross-shore/along-shore conventions will vary as a function of distance along the coast [Yankovsky et al. ala BEST proposal, and other good coastal wind driven papers]. Varying nearshore responses will naturally promote circulation divergence fields, leading to cross-isobath exchange.

We hope that the balances constructed herein will help enable the operators of numerical simulations the ability to diagnose the dynamics of heat and FW fluxes within their models. It is possible that numerical model investigations will alleviate some of the problems associated with incomplete datasets, but field data are also required. Results from the National Science Foundation and North Pacific Research Board co-sponsored Bering Ecosystem Study (BEST) and Bering Sea Integrated Research Program (BSIERP) initiatives will take the first steps, with the net addition of CTD survey results along with mooring array records. The BEST mooring array should shed light on some of the important items left unresolved in this manuscript, including especially the flow fields and T/S evolutions on sub-synoptic through seasonal time scales. Most importantly, however, we find that lack of data from the broad shelf expanse inshore of the 20 *m* isobath limits our ability to assess the fate of the large fresh water fluxes in this region and better assess the coastal nutrient dynamics regime, a place where juvenile salmon may spend a significant period of time before making their way to the midshelf domain. We hypothesize that variability in winter's cross-shelf exchange can impact the springtime nutrient load over the inner shelf and that the resultant production can ultimately play a role in determining the success of individual year class salmon.

5.0 Acknowledgements

S. Danielson and T. Weingartner would like extend their appreciation to all of the BASIS program scientists for their willingness to undertake this collaborative effort in analyzing this large dataset and for the engaging exchanges between the Juneau and Fairbanks sites. S. Danielson received financial support from the Bering Sea Fisherman's Association, grant #XXX. Thanks to K. Ciecel for CTD data processing. R. Gradinger provided useful estimates of the winters end average sea ice thickness and salinity.

6.0 References

Next task. This will also lead to some filling in of results and discussion points.

7.0 Tables and Figures

Year	Start Date	End Date	Number of CTDs
2002	20 August	7 October	154
2003	21 August	8 October	129
2004	14 August	30 September	143
2005	14 August	6 October	90
2006	17 August	20 September	137
2007	15 August	8 October	166

Table 1: Summary of 2002-2007 BASIS CTD survey timing and coverage. The number of CTDs reported reflect only those taken over the EBS shelf: additional stations were occupied north of Bering Strait in some years. The integration domain covers a shelf area of 2.0 x 10^5 km^2 between the 20 *m* and 70 *m* isobaths, encompassing a volume of ~9,300 km^3. Mean water depth within this domain is 45 *m*.

Year	CEBSS Mean April Ice Extent (km^2)	Maximum Ice Extent Date	Ice Retreat Date	Heating Season Start Date (-165°W, 57.5°N)	Heating Season Start Date (-170°W, 62.5°N)
2002	32500	20 February	18 May	6 April	22 April
2003	35600	26 March	6 May	2 April	16 April
2004	50100	2 April	11 May	10 April	9 April
2005	67800	9 April	21 May	17 April	23 April
2006	87700	4 February	31 May	27 April	3 May
2007	70600	24 March	24 May	1 April	28 April

Table 2: Summary of the 2002-2007 spring ice and surface heat flux conditions. The date of maximum ice extent and mean retreat date are computed for the greater EBS shelf area, while the ice extent column is given for the CEBSS region only. The heating season start dates are shown for one southerly and one northerly grid point.

Parameter	Mean	Range
ΔFWC1	101	57-173
Sea Ice FWC	41	18-62
Σ(P-E)	23	19-25
Σ(River Discharge)	152	132-189
ΔHC1	260	213-305
ΔHC2	250	216-269
Σ(Surface Heat Flux)	244	228-258
Latent Heat of Melting	13	6-21

Table 3. Spring to fall mean seasonal changes in the FWC and HC standing stocks and estimates of the various non-advective flux terms summed over the April 1 to August 31 time period. Units are km^3 for FWC and $EJ=10^{18}$ J for HC values. Minimum and maximum values from the 2002-2007 time period give expected ranges. The mean quarterly composites given in Figure 3 form the basis for ΔFWC1 and ΔHC1 and the accompanying min/max ranges reflect the interannual variability found in the BASIS (summer's end) data. The ΔHC2 estimate comes from the fall HC as measured in the BASIS dataset and spring HC estimated from the ice extent; the min/max ranges reflect variability found in the spring HC parameter. Heat required to melt ice is taken for fresh water ice, so the value reported is a slight overestimate. Heat required to raise the ice temperature to the freezing point is neglected.

		Summer's End FWC	Ice FWC	May-August River Discharge	October-May Cross-shore Ekman Transport
		(km^3)	**(km^3)**	**(km^3)**	**($x10^3\ m^3\ s^{-1}$)**
Anomalies	**2002**	-44.0	-14.2	-9.5	35.9
	2003	-14.0	-2.7	-9.0	1.58
	2004	4.0	12.3	-5.3	5.08
	2005	-48.0	3.1	38.0	103
	2006	72.0	5.0	6.4	-98.7
	2007	30.0	-3.5	-20.3	-46.4
V		2112	82	414	
R			0.4	0.31	**-0.95**
P			0.44	0.55	**0.0037**

Table 4: Annual anomalies of the 2002-2007 summer's end FWC, FWC of sea ice at the end of winter, FWC of May-August Yukon and Kuskokwim net discharge, and October-May cross-isobath Ekman transport. The oceanic FWC values are computed over the focus domain outlined in Figure 4. The bottom three rows show variance (v), correlation coefficients (r) and p-values (p) for the anomalies. The correlation and p-values summarize cross-correlation computations between the ocean FWC anomaly with columns 4-6. Correlations significant at the 95% level are in boldface type. The variance is not reported for the Ekman transport computations because it is not directly comparable to the FWC and HC variances. The cross-shore winter Ekman transport is based on NCEP reanalysis winds and computed across the along-shore line segments connecting the following three points: (62.5 *°N,* 167.5 *°W*), (60 *°N*, 167.5 *°W*) and (58.5 *°N*,162 *°W*). The sign of the transport follows the convention that offshore (westward) transport is negative and onshore (eastward) transport is positive.

		Summer's End HC	Winter's End HC	April-August Surface Heat Flux	April-August Along-isobath Ekman Transport
		(EJ)	**(EJ)**	**(EJ)**	**($x10^3$ m^3 s^{-1})**
Anomalies	**2002**	12.0	19	8.6	5.9
	2003	28.0	14	5.7	7
	2004	45.0	0.5	14.0	35
	2005	3.0	8.7	-7.0	-8.5
	2006	-42.0	-8.6	-16.0	-32
	2007	-47.0	-34	-5.0	-7.5
V		1330	382	127	
R			0.73	**0.85**	**0.85**
P			0.969	**0.0335**	**0.0336**

Table 5: Annual anomalies of the 2002-2007 summer's end oceanic HC, winter's end oceanic HC, April-August net surface heat flux and April-August along-isobath Ekman Transport. The ocean HC anomalies are computed over the focus domain outlined in Figure 4. The bottom three rows show the variance (v), correlation coefficients (r) and p-values (p) for the anomalies. The correlation and p-values summarize cross-correlation computations between the oceanic HC anomaly with the anomalies in columns 4-6. Correlations significant at the 95% level are in boldface type. The variance is not reported for the Ekman transport computations because it is not directly comparable to the HC variances. 1 EJ = 10^{18} J. The summer Ekman transport is computed across latitude 60°N between Nunivak and St. Matthew islands. The sign of the transport follows the convention that northward transport is positive. The winter's end HC anomaly is estimated from ice cover during the months of March and April as described in the text.

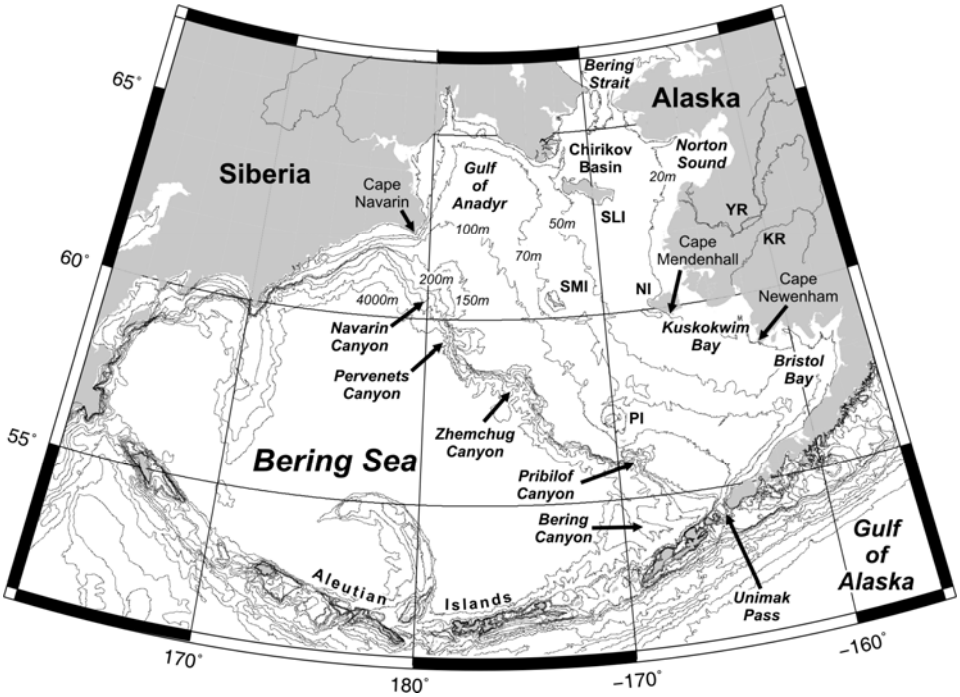

Figure 1. Map of the Bering Sea labeled with place and feature names employed in the text. Abbreviations include: YR = Yukon River; KR = Kuskokwim River; SLI = St. Lawrence Island; SMI = St. Matthew Island; PI = Pribilof Islands; SS = Shpanberg Strait. The Arctic Ocean lies to the north of Bering Strait and the greater Pacific Ocean lies south of the Aleutian Islands. Depth contours are plotted at the following depth levels: 20m, 50m, 70m, 100m, 150m, 200m, 500m, 1000m, 2000m, 3000m, 4000m, 5000m and 6000m.

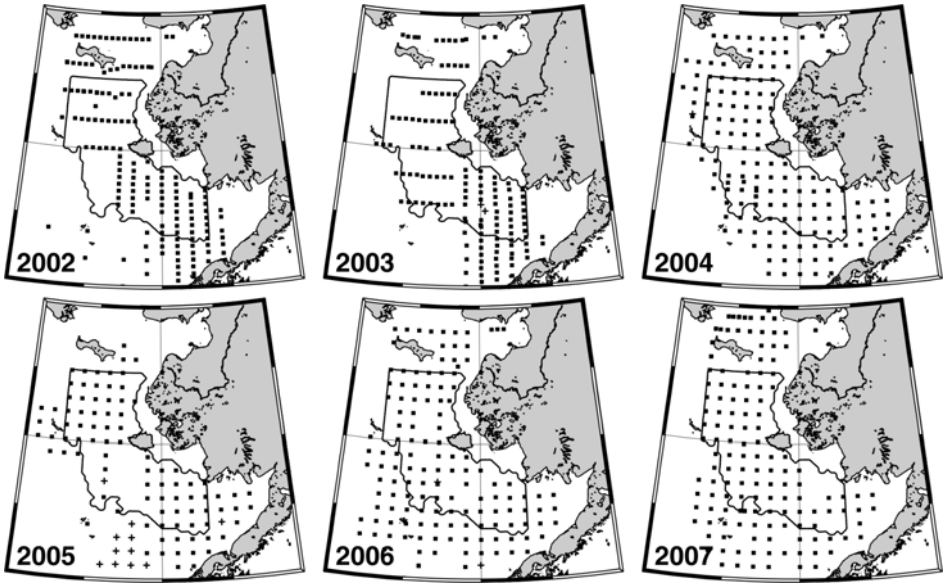

Figure 2. 2002-2007 CTD station coverage over the eastern Bering Sea shelf. The region that bounds heat and freshwater integrations is denoted in each panel by a thin contour. Squares show locations of good temperature and salinity data; plus signs show locations of good temperature data only. Nominal station spacing of ½° latitude (56 km) is achieved in 2004-2007 across most of the focus domain; west of Nunivak Island in 2002 and 2003 the station spacing is 1° of latitude, or about 111 km. Map bounds are located at 65N, 55N, 174W and 156W.

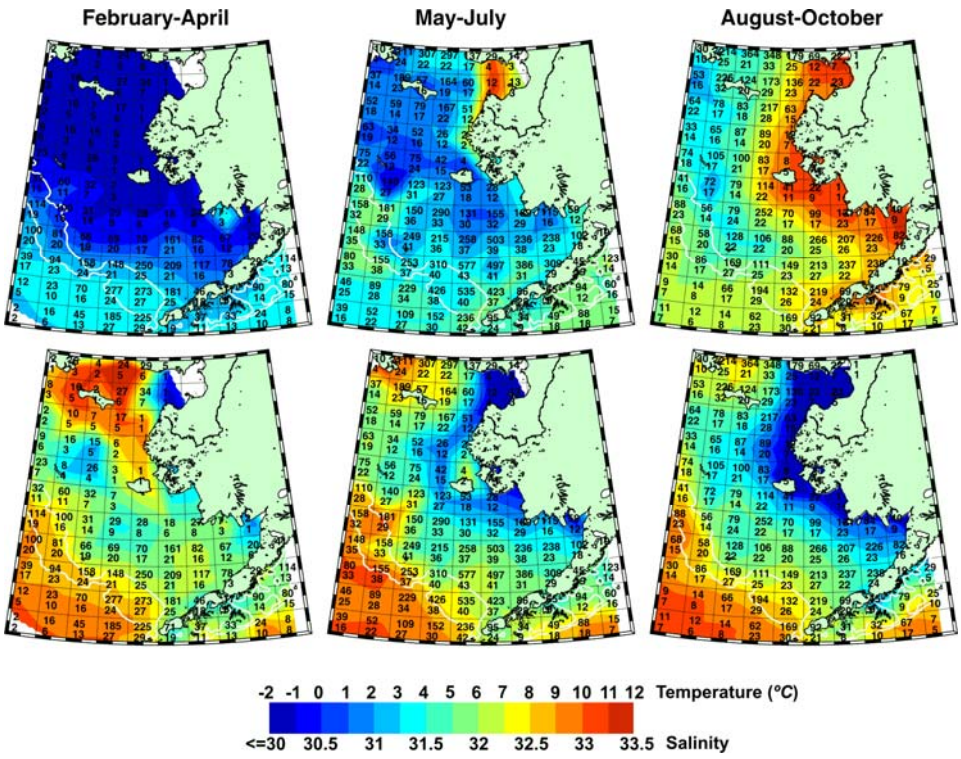

Figure 3. Mean 0-100m temperature (top row) and salinity (bottom row) in the eastern Bering Sea during the months indicated. Data are a combination of the historical NODC data and the BASIS CTD data. Data are gridded in 1º latitude by 2º longitude cells. The upper number in each cell indicates the total number of casts in each quarter; the lower number denotes the number of years represented by these casts. Note the existence of some cells with no or few data points. Data are first binned into annual mean values within each cell in order to ensure equal weighting between years. White contours denote the 100m and 200m isobaths. . Map bounds are located at 65N, 54N, 175W and 155W.

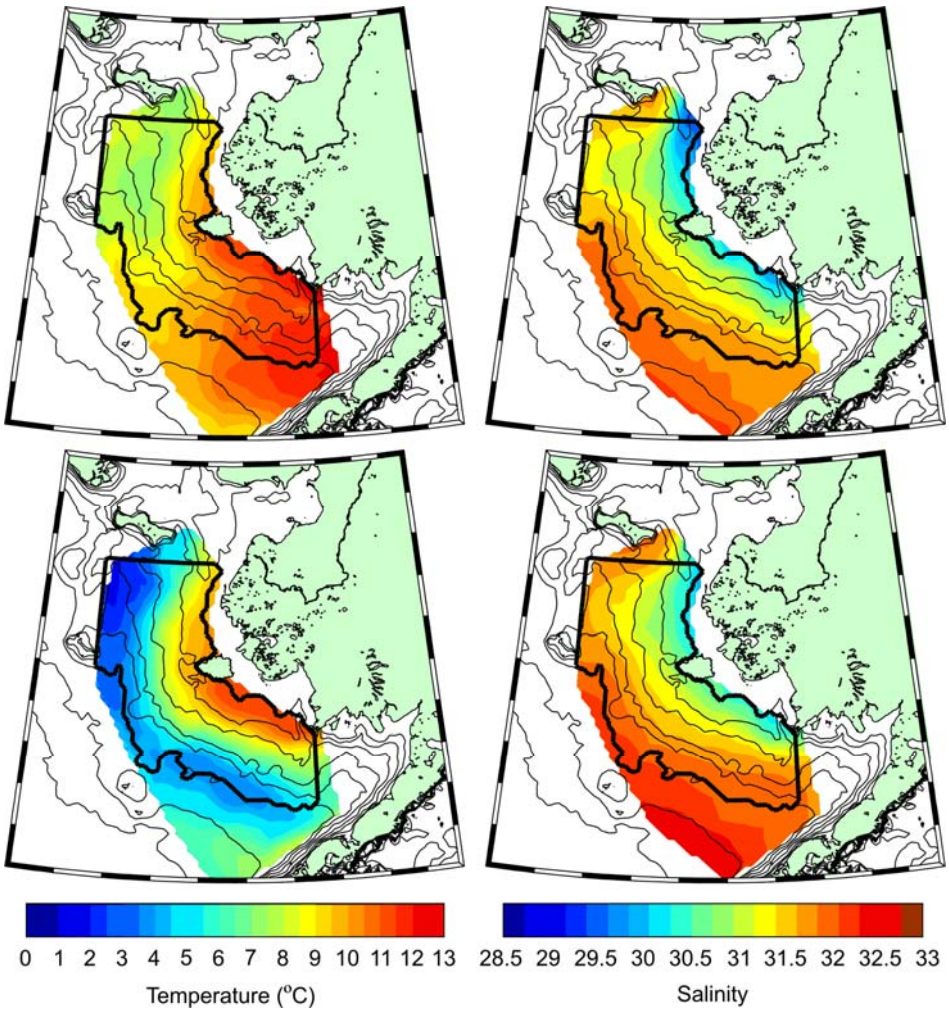

Figure 4. 2002-2007 mean distributions of temperature (left) and salinity (right) above (top) and below (bottom) the mixed layer depth. The mixed layer depth is defined as depth where the density exceeds that measured at 5m depth by 0.1 kg m^{-3}. Depth contours are plotted at the following levels: 20m, 30m, 40m, 50m, 60m, 70m, 100m and 200m. The thick contour denotes the integration region employed in the heat and fresh water content computations below. . Map bounds are located at 65N, 55N, 175W and 156W.

FIX COLOR BARS

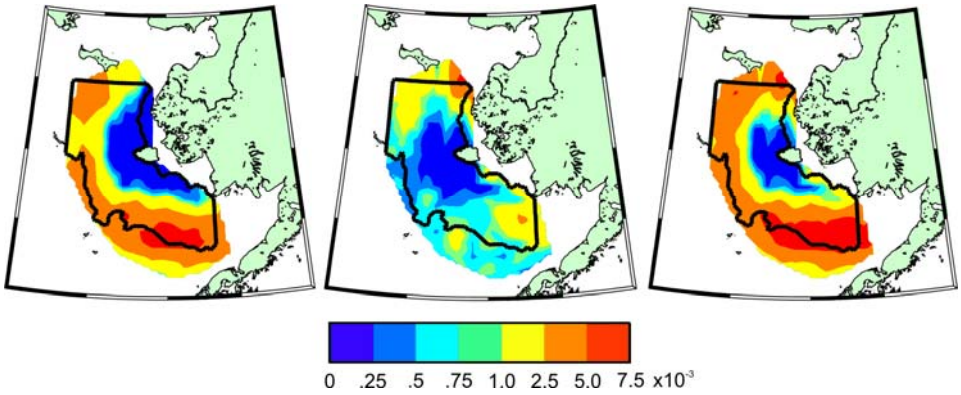

Figure 5. 2002-2007 mean maximum water column Brunt-Vaisala frequency computed by holding the salinity constant at the water column mean (left); by holding the temperature constant at the water column mean (center); and by allowing both temperature and salinity to vary (right). Note the nonlinear color scale. Vertical temperature homogeneity exists in a broad arc encircling Nunivak Island; thermal stratification generally dominates in waters beyond the inner front. Salinity induced stratification is low between the latitudes of C. Newenham and about 61 °N. Salinity induced stratification is highest offshore of the Yukon River. South of SLI and in western Bristol Bay, stratification due to salinity is typically about one-half to one-fourth that of the stratification due to temperature. Map bounds are located at 65N, 55N, 175W and 156W.

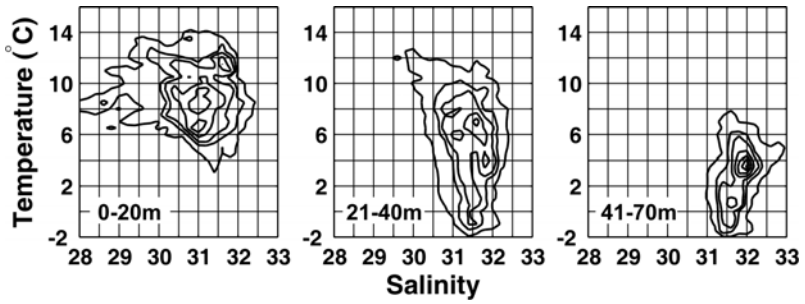

Figure 6. 2002-2007 mean volumetric T-S diagram for the CEBSS region (outlined with a thick contour in Figure 4) and over depth levels 0-20m, 21-40m and 41-70m. Volume contours are drawn at 0, 10, 20, 40, 60, 80, 100 and 120 km^3 levels. The volume encompassed by each depth range is approximately 4300, 3300 and 1700 km^3 respectively. The integration is performed over cells with dimensions of ΔT=0.5 ºC and ΔS = 0.2.

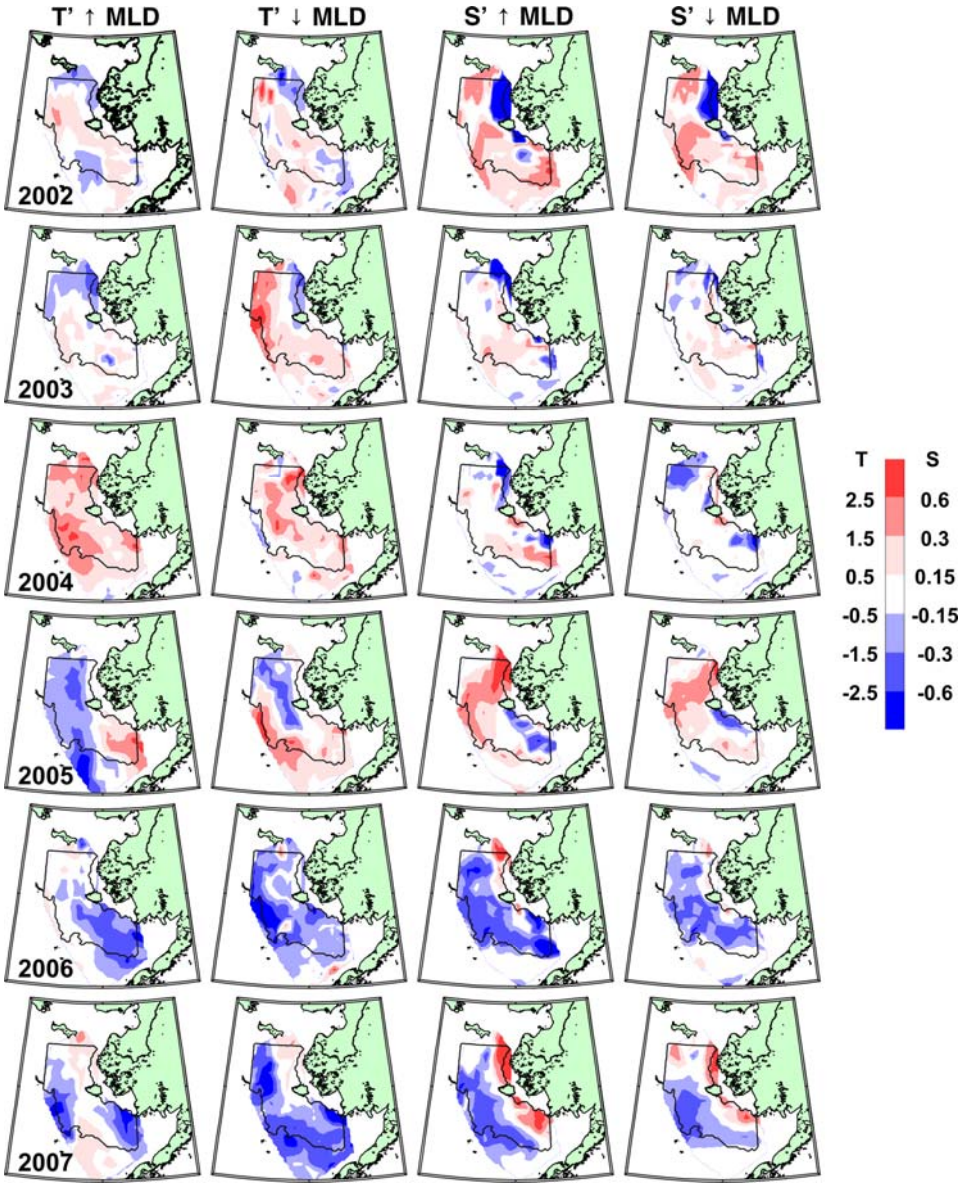

Figure 7. Temperature and salinity anomalies above (↑) and below (↓) the mixed layer depth (MLD = depth where $\sigma_t = \sigma_t$ @ $5m + 0.1\ kg\ m^{-3}$). Anomalies are computed in temperature and salinity units with respect to the multi-year means shown in Figure 4. Blue (red) colors indicate that the temperature/salinity anomalies are warmer/saltier (cooler/fresher) than the mean fields. . Map bounds are located at 65N, 55N, 175W and 156W.

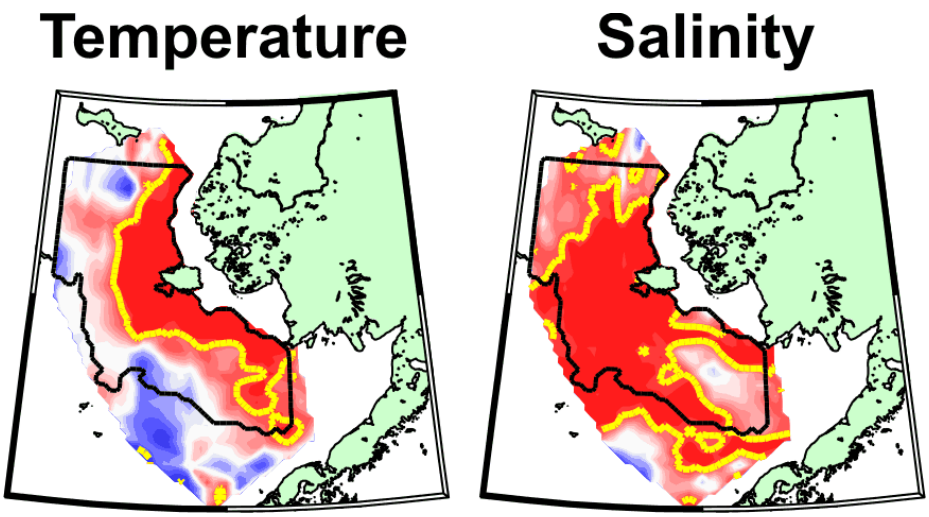

Figure 8. Temperature (left) and salinity (right) correlation maps, showing the temporal correlation between values above the MLD with values below the MLD at zero lag. Red indicates positive correlation; blue indicates negative. Yellow contours denote significance at the 95% confidence level (r = +/- 0.81) and the black contours outline the CEBSS region. Map bounds are located at 64N, 55N, 156W and 173W.

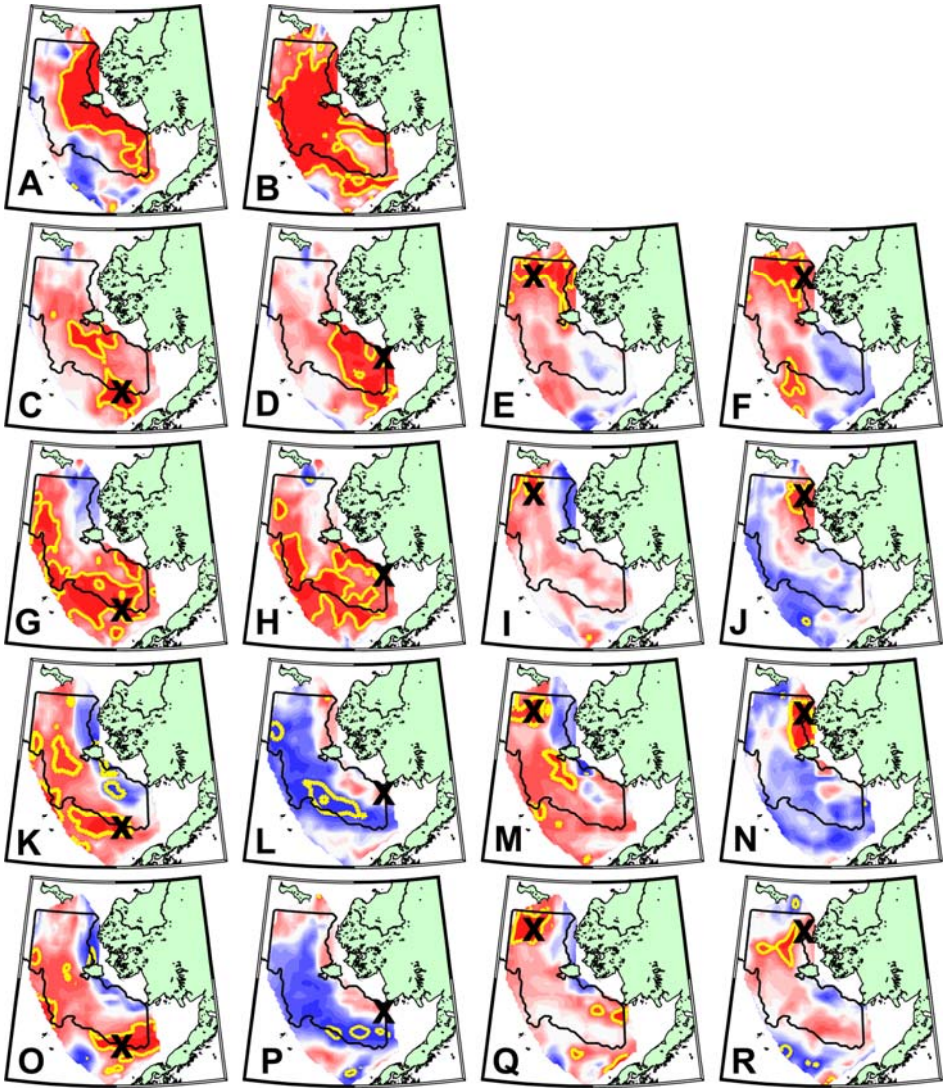

Figure 9. Temperature and salinity horizontal correlation maps. Correlations are computed at zero lag between the point marked by an "X" on each panel and all other grid points for: 1) Temperatures above the MLD (C-F); 2) Temperatures below the MLD (G-J); 3) Salinity above the MLD (K-N) and 4) Salinity below the MLD (O-R). Color scheme as in Figure 8. Map bounds are located at 64N, 55N, 156W and 173W. NOTE: This figure had panels A+B broken out into Figure 8. Final version will be a 4x4 panel, relabeled with panels C-R going to A-P.

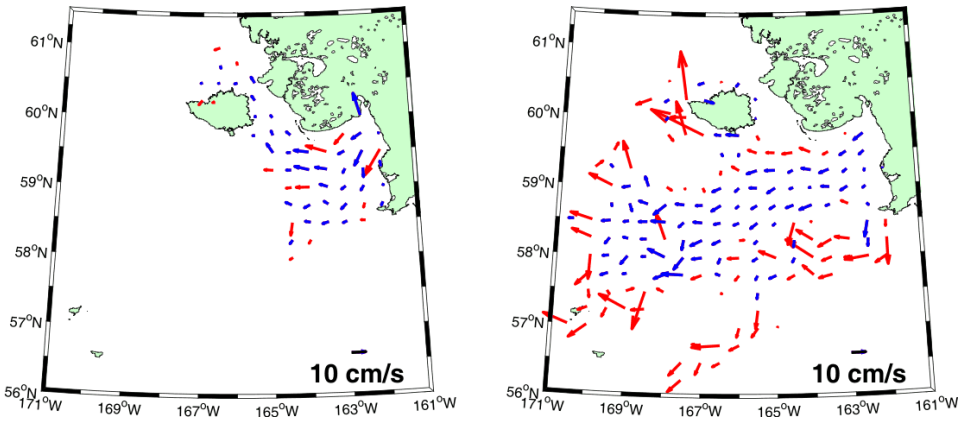

Figure 10. Mean seasonal flow patterns derived from oceanographic drifters for June-August (left) and September-January (right). Note implied convergence in western Kuskokwim Bay and enhanced northward flow at many grid points in the summer months, whereas in the fall and winter months the flow is more uniformly directed westward. Blue vectors denote grid cells with at least seven drifter-days worth of data; red vectors contain less than seven drifter-days of data.

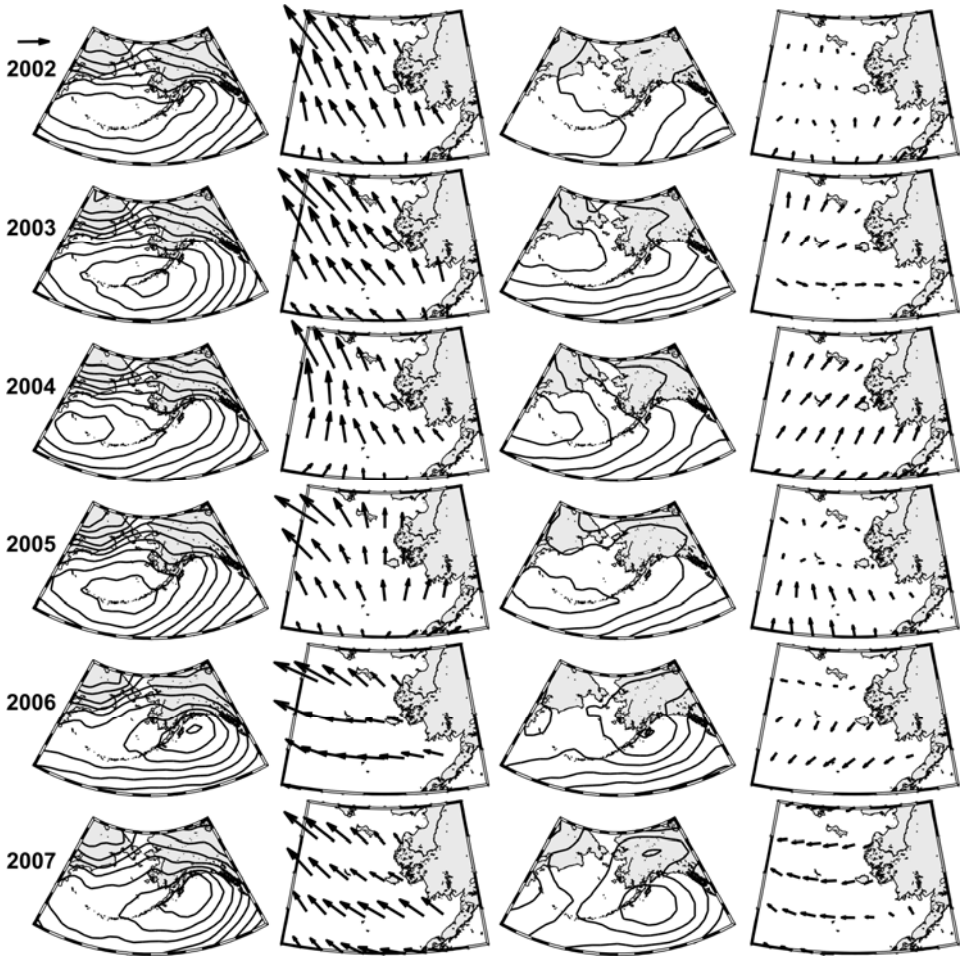

Figure 11. October-May mean sea level pressure contours and Ekman transport vectors (left-hand two columns) and the same parameters for the April-August (right-hand two columns). Pressure contours are drawn at 2 millibar increments; high pressure exists in the southeast corner of all pressure maps; closed contours are all low pressure cells. The scale vector (upper left corner) has a magnitude of 540 $kg\ m^{-1}\ s^{-1}$. Cross-shelf transport over the winter months is significantly correlated at the 95% level with the following summers end FWC anomaly (r^2= 0.90, p=0.004). Along-shelf transport in the summer months is correlated with the summers end HC anomaly (r^2= 0.72, p=0.004).

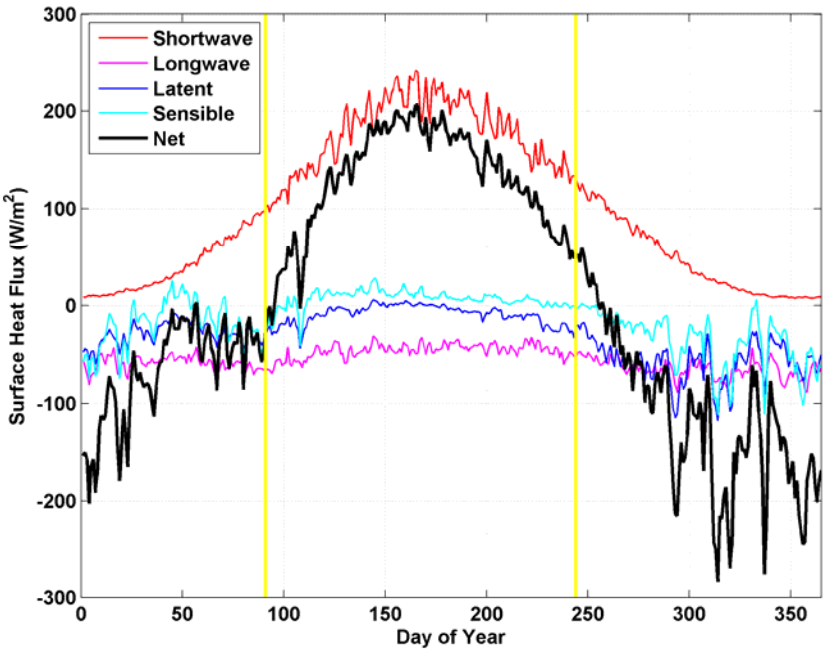

Figure 12. Annual mean cycle of surface heat fluxes for the CEBSS region over the years 2002-2007. [NOTE: Ladd/Bond correction not applied here, need to rethink that.] April 1st and September 1st are denoted with vertical yellow bars. The heating season begins on the date near April 1 when the net surface heat flux crosses from negative (oceanic heat loss) to positive (oceanic heat gain).

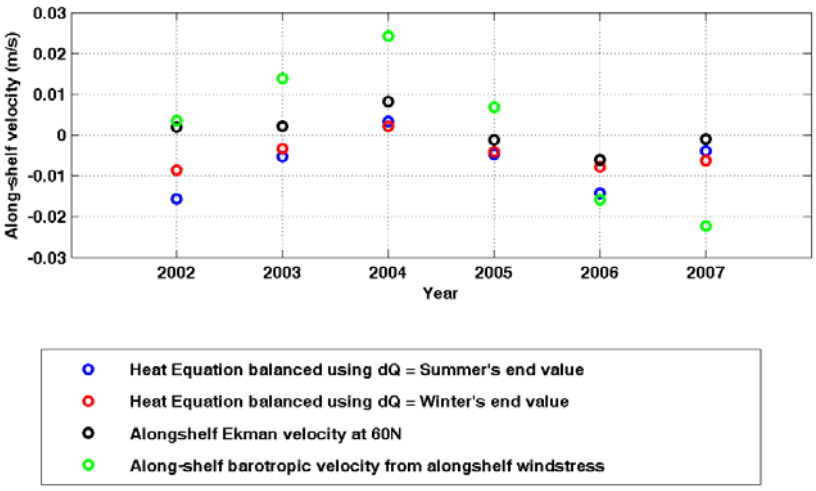

Figure 13. Along-shelf velocities estimated by balancing the heat equation (blue and red), by computing the mean summer surface Ekman transport (black) and by computing the mean along-shelf barotropic transport (green). [NOTE: I've got maybe too many figures in this paper. Could replace this figure with a table.] [To do: estimate the compensating Ekman flux in the bottom layer; this will likely reduce the black values magnitudes somewhat.]

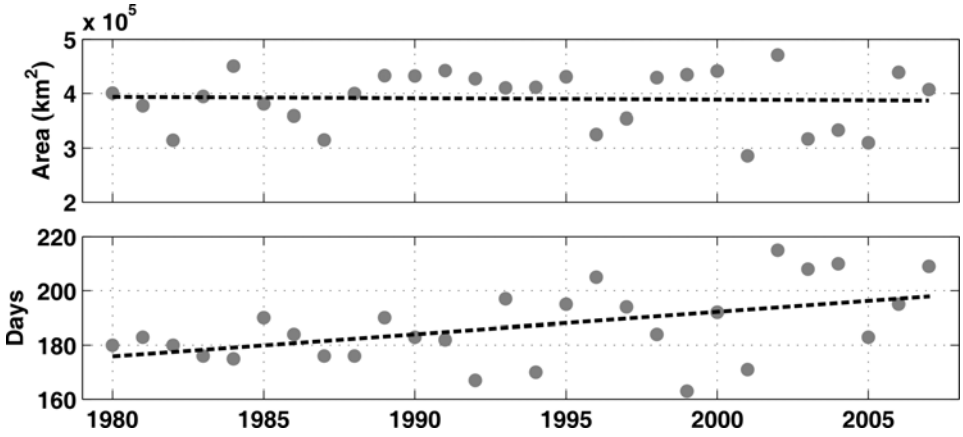

Figure 14. Time series (1979-2007) of sea ice annual maximum areal extent (upper panel) and duration of ice-free waters (lower panel) computed over the Bering Sea east of 170 ºE and south of Bering Strait. Plots are derived from passive microwave satellite data obtained from the National Snow and Ice Data Center (NSIDC). The areal extent computation is made for the winters of 1979/80 through 2006/07. The ice free-water duration computation is made for each individual calendar year with a threshold of $5x10^4$ km^2. The dashed lines show the best fit linear trends, indicating an 8 day per decade increasing slope for the ice-free season length. This slope is significantly different from zero at the 95% confidence level ($r^2 = 0.24$, $p = 0.008$). Estimates of the 1) maximum ice extent, 2) the day of year that the maximum ice extent is attained (not shown) and 3) the mean annual ice extent (not shown) all exhibit no significant trend.

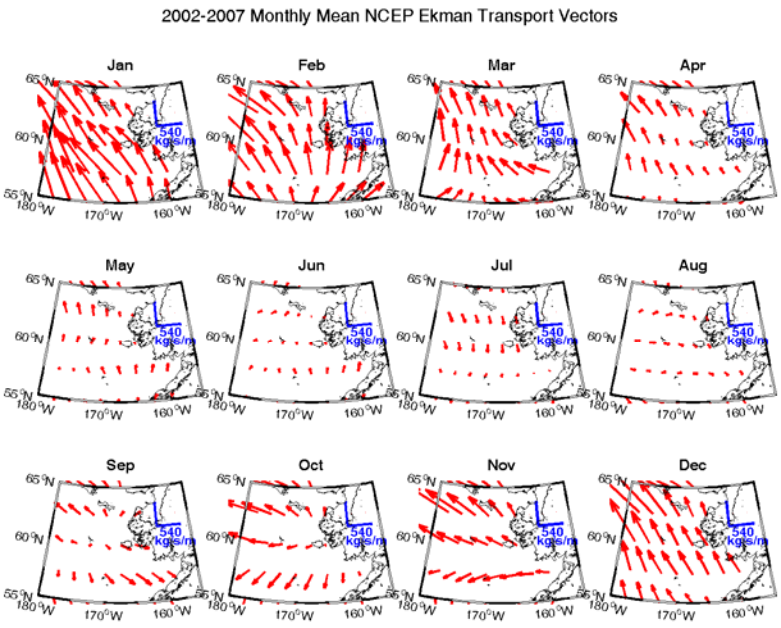

Figure 15. Monthly mean Ekman Transport computed from NCEP winds over 2002-2007. Note the large westward transport that develops in Oct/Nov. May-Aug have distinctly smaller magnitudes, April & Sept are transition months between the light summer winds and strong winter winds. Dec-April have a pronounced northerly component. Shelf waters may be lost to the basin in October and November.

Alternate/Additional Figures:

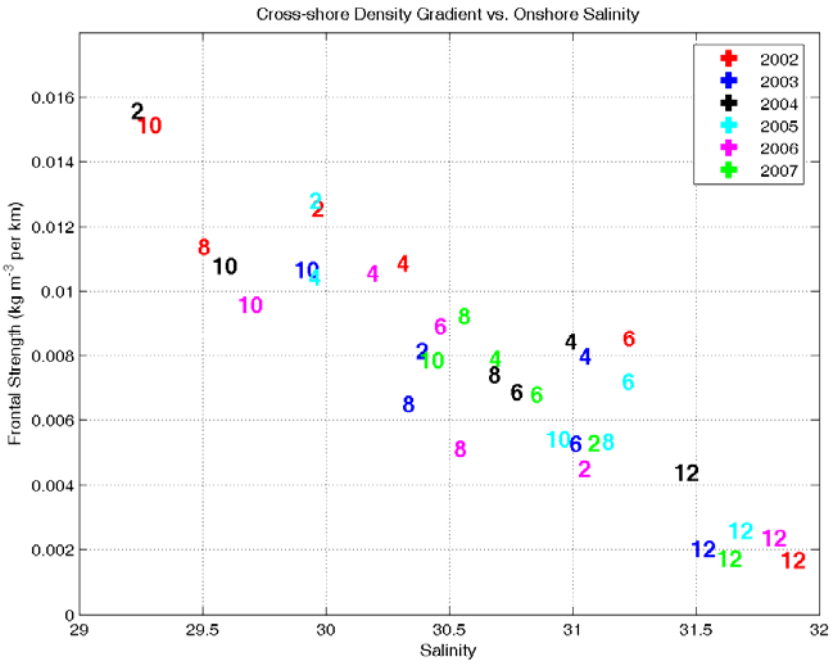

Figure AA. Cross-shore density gradient vs. onshore salinity values measured at the station pairs along the coast. Stations 2, 4, 6, 8 and 10 have the nearshore stations near C. Newenham, C. Mendenhall, 60 N, 61N and 62N. Station 12 is near the Alaskan panhandle. The offshore stations are ~ 200km offshore.

Appendix 5
#25-O-05

Stock-Structured Distribution of Western Alaska and Yukon Juvenile Chinook Salmon from United States BASIS surveys, 2002-2007

James M. Murphy*[1], William D. Templin[2], Edward V. Farley, Jr.[1], and James E. Seeb[3]

1 Ted Stevens Marine Research Institute, Auke Bay Laboratories, Alaska Fisheries Science Center, NOAA Fisheries, 17109 Point Lena Loop Road, Juneau, AK 99801, USA; E-mail, Jim.Murphy@noaa.gov
2 Gene Conservation Laboratory, Division of Commercial Fisheries, Alaska Department of Fish and Game, 333 Raspberry Road, Anchorage, Alaska 99518, USA
3 University of Washington, School of Aquatic and Fishery Sciences, Box 355020, Seattle, WA 98195, USA

ABSTRACT

We describe migratory patterns of western Alaska and Yukon Chinook salmon (*Oncorhynchus tshawytscha*) using stock-structured distribution data from United States Bering-Aleutian Salmon International Surveys (BASIS), 2002-2007. Juvenile Chinook salmon were distributed within water depths less than 50 m and their highest densities were found close to river mouths of primary Chinook salmon-producing rivers in the eastern Bering Sea (Yukon, Kuskokwim, and Nushagak rivers) through their first summer at sea. This reflects a later marine dispersal from freshwater entry points than typically found in Gulf of Alaska stream-type Chinook salmon and resulted in the presence of juvenile Chinook salmon in shallow, non-trawlable habitats during the surveys. Stock mixtures of juvenile salmon in the northern shelf region (north of 60°N) did not support significant northward migration of stocks from the southern shelf, reflecting limited mixing of salmon from different production regions during their first summer at sea. Recoveries of coded-wire tagged Yukon River Chinook salmon near the Bering Strait provide evidence that Yukon River Chinook can extend north into the Bering Strait and Chukchi Sea.

Keywords: Bering Sea, Chinook salmon, distribution, juvenile, migration, stock structure

INTRODUCTION

Migratory corridors used by Chinook salmon and their distribution within the corridors provide key information on the early marine ecology and life-history strategies of juvenile salmon important to their growth and survival (Brodeur et al. 2000). Juvenile Chinook salmon (*Oncorhynchus tshawytscha*) from western Alaska and Yukon, Canada enter the marine waters of the eastern Bering Sea during the spring and summer and migrate along the coast of western Alaska during their first summer in the ocean (Healey et al. 1991). An understanding of the underlying migratory patterns of salmon is also required to interpret and apply research survey data to population studies (Farley et al. 2005).

Although much of the historical work on salmon migration has relied on tagging and marking research (Hartt and Dell 1986; Orsi and Jaenicke 1996; Farley et al. 1997; Courtney et al. 2000), genetic methods have expanded the ability of research surveys to define migratory behavior of salmon in the ocean (Seeb et al. 2004; Templin et al. 2005). Recent developments in single nucleotide polymorphism (SNP) markers and genetic baselines provide efficient and accurate assignment of Chinook salmon to freshwater origin (Smith et al. 2005; Templin et al. 2005). SNP data can be collected and scored very rapidly compared to other genetic markers, thus increasing its power and efficiency to discriminate stock origins.

Farley et al. (2005) initially described migratory pathways of juvenile Chinook salmon in the eastern Bering Sea using information on the body size structure of juveniles. Reconstructing migration corridors from size data capitalizes on the fact that much of the variability in juvenile size reflects the time of ocean entry. Dispersal patterns of juvenile salmon from points of ocean entry are apparent in the spatial distribution of size with the largest juvenile salmon (earliest out-migrants) distributed the greatest distance from their point

of ocean entry. In the following analysis, migratory patterns of juvenile western Alaska and Yukon Chinook salmon are described using information on ocean distributions and freshwater origin from coded-wire tags and genetic stock identification methods.

METHODS

Juvenile Chinook salmon were collected with surface rope trawls during the U.S. Bering-Aleutian Salmon International Survey (BASIS) surface rope trawl surveys on the eastern Bering Sea shelf from 2002-2007 (Table 1). Start dates of the survey ranged from August 14 to August 21; end dates ranged from September 20 to October 8 (Table 1.). Variation in start and end dates each year reflected changes in vessel availability and survey coverage and design. Initial survey design (2002 and 2003) used transect-based sampling along latitude and longitude lines (Farley et al. 2005). A grid-based sampling design with stations at each degree of longitude and 30 minutes of latitude was used from 2004 to 2007.

Juvenile Chinook salmon and other pelagic fish were collected with surface rope trawls built by Cantrawl Pacific Limited of Richmond, British Columbia[3]. Trawls were 198 m long, had hexagonal mesh in wings and body, and included a 1.2-cm mesh liner in the codend (Murphy et al. 2003). Trawls were towed at the surface at an average speed of 4.3 knots, resulting in an average vertical mouth opening of 14 m and horizontal mouth opening of 58 m. Sampling depths were slightly deeper than the vertical opening as the center of the trawl often was just below the surface during the trawl deployment. Water depths shallower than 20 m were considered non-trawlable and were not sampled. Nor'eastern Trawl Systems 5-m alloy doors with 60-m bridal lengths were deployed typically 360 m astern of the boat. Buoys were secured to the wing-tips and center of the headrope to help keep the trawl at the surface and

[3] Reference to trade names does not imply endorsement by the National Marine Fisheries Service, NOAA.

wingtip buoy wakes were monitored to ensure the headrope was maintained at the surface during the tow. Trawl speeds were adjusted to keep the trawl at the surface and trawl doors in the water. A Simrad FS900 net sounder was used to monitor the fishing dimensions and trawl geometry during each tow. All trawls were towed astern of the vessel for 30 minutes at each station. Catch per unit of fishing effort, CPUE, was used to describe salmon spatial distributions and the standardized unit of fishing effort was effort during a 30 minute trawl set. Average area swept by the trawl at each station was 0.25 km^2.

Stations were sampled between 07:30-21:00 hours (Alaska Standard Time), and typically four stations were sampled each day. Stations were sampled during daylight with the exception of the first station of each day. The first station of the day was sampled just after sunrise, and occasionally would occur during sunrise depending on the schedule set for vessel operations by the chief scientist. Salmon catch rates from the crepuscular time-period were not significantly different from other daylight samples (Farley et al. *In press*). Sample dates differed by location due to the order in which stations were sampled during the survey. Average sample dates were estimated with a weighted average date with weights provided by the catch at each station.

Standard research trawl protocols were used to process trawl catch. All salmon were sorted and counted by species and life-history stage; all juvenile Chinook salmon were examined for a missing adipose fin. Snouts were removed from juvenile Chinook salmon with a missing adipose fin and examined for the presence of a coded wire tag at the Auke Bay Laboratories in Juneau, Alaska. Individual lengths and weights were collected from a subsample of up to 50 Chinook salmon and genetic samples were collected from these fish.

Kriging models implemented in ArcGIS software package (ESRI 2006) were used to construct the spatial distribution map of juvenile Chinook salmon on the eastern Bering Sea shelf. The spatial mean was removed with a local polynomial regression model and the spatial covariance was of juvenile Chinook salmon was modeled with a spherical variogram (Cressie 1991). The spatial model was used to estimate the distribution of juvenile Chinook salmon in non-trawlable habitats with the addition of boundary conditions. Boundary conditions were created by adding with zero catch data on land at spatial scales matching the survey sampling grid.

Freshwater stock origins of juvenile Chinook salmon were determined from coded-wire tag (Jefferts et al. 1963) recoveries and from genetic stock identification analysis. Coded-wire tags were assigned to freshwater origin using the coast-wide mark database maintained by the Pacific States Marine Fisheries Commission (http://www.rmpc.org/) and by coded-wire tag release information provided by the Whitehorse Rapids fish hatchery (YRJTC, 2009).

A coast-wide baseline of 42 SNP genetic markers for Chinook salmon (updated from Templin et al. 2005) was used to assign freshwater origin of juvenile Chinook salmon. SNP data were obtained from 1,356 juvenile Chinook salmon following the methods of Seeb at al. (2009), and stock mixtures were estimated for three locations on the eastern Bering Sea shelf. Mixed stock proportions at each location were estimated using conditional maximum likelihood models implemented in the SPAM 3.7 mixed-stock software program (Debevec et al. 2000). Accuracy of mixed stock assignment to freshwater origins considered in this analysis was greater than 90% using the 42-SNP baseline (Templin et al. 2005).

Chinook salmon outside of the eastern Bering Sea are were not assumed to be present in the area sampled by U.S. BASIS survey during their first summer at sea; therefore, only

Chinook salmon stocks from eastern Bering Sea river systems were considered in the mixed stock analysis. Genetic analysis was only completed on the juvenile life-history stage of Chinook salmon (Chinook salmon during their first summer at sea). Stock groups included in the analysis were: the Upper Yukon River stock group, the Middle Yukon River stock group, the Coastal Western Alaska stock group, and an 'Other' stock group (Fig. 1). The Coastal Western Alaska stock group included the Lower Yukon Chinook salmon stocks and all other western Alaska stock groups outside of the Yukon River except the upper Kuskokwim River and North Alaska Peninsula stock groups. For simplicity, these two stock groups were combined into a single 'Other' stock group. The Lower Yukon stock group included Alaskan tributary streams draining the Andreafsky Hills and Kaltag Mountains; the Middle Yukon stock group included Alaskan tributary streams in the upper Koyukuk River and Tanana River basins; the Upper Yukon stock group included Canadian tributary streams draining the Pelly and Big Salmon Mountains (Lingnau and Bromaghin 1999).

Juvenile mixtures in the northern shelf region (north of 60°N) were compared with expected adult mixtures in the Yukon River. Expected adult stock mixtures were estimated by the average mixtures present in commercial and subsistence harvests in the Yukon River (DuBois and DeCovich 2008). These estimates were not corrected for potential stock selective harvest.

RESULTS

Juvenile Chinook salmon were primarily distributed within water depths less than 50 m through their first summer at sea (middle of August through the middle of October) and the highest densities of juvenile Chinook salmon were found close to river mouths of primary

Chinook salmon-producing rivers in the eastern Bering Sea (Yukon River, Kuskokwim River, Nushagak River) (Fig. 2). Juvenile Chinook salmon were distributed as far north as the Chukchi Sea and the southern extent of their distribution occurred along the north shore of Bristol Bay. The migratory corridor of juvenile Chinook salmon was broader in the northern shelf (north of 60°N) than the southern shelf region. Peak densities of juvenile Chinook salmon occurred in the shallowest water depths sampled during the survey. Significant numbers of juvenile Chinook salmon were estimated to be present in water depths shallower than could be sampled by the trawl gear (20 m).

Average sample dates of the genetic mixtures differed due to the order in which stations were sampled during the survey (Table 2). The average sample date of mixtures 1, 2, and 3 were: August 24, September 24, and September 10, respectively. The average sample date of mixtures 2 and 3 combined was September 16.

Stock mixtures differed by region and location (Table 2). In the southern Bering Sea shelf (mixture 1), 94% of the juvenile Chinook salmon were classified as the Coastal Western Alaska stock group. In the northern Bering Shelf, mixture 2 contained 45% Upper Yukon, 23% Middle Yukon, and 29% Coastal Western Alaska stocks. Mixture 3 was similar to mixture 2 with 44% Upper Yukon, 26% Middle Yukon, and 29% Coastal Western Alaska. Stock proportions from mixtures 2 and 3 combined, were 45% upper Yukon, 24% Middle Yukon, and 30% Coastal Western Alaska stocks.

Stock proportions between juvenile populations and adult harvests were similar enough to discount significant bias due to incomplete sampling of the juvenile population. The proportion of the Coastal Western Alaska stock group in the juveniles from the northern shelf region (mixtures 2 and 3 combined, 30%, SD = 3%) was slightly higher than the proportion in

the harvest (21%, SD = 8%), but within the range expected for Yukon River harvests. The proportion of the Middle Yukon River stock group in the juvenile population (24%, SD = 3%) was similar to the proportion observed in the harvest (23%, SD = 10%). The proportion of the Upper Yukon stock group in the juvenile population (45%, SD = 3%) was lower than the average proportion in the harvest (56%, SD = 8%), but not significantly lower.

Coded-wire tags all matched tag codes from the Whitehorse Rapids Fish Hatchery located near Whitehorse, Yukon. Coded-wire tag codes from juvenile Chinook released by the Whitehorse Rapids Fish Hatchery in 2002 included release location codes (Table 3). Tag codes from 2007 only included information on agency and year of release. However, as no other tagged Canadian juvenile Chinook entered the ocean in the Bering Sea in 2007, it was possible to assign origin to the Whitehorse Rapids Fish Hatchery.

Coded-wire tags were recovered at the mouth of the Yukon River and just south of the Bering Strait (Fig. 4). Coded-wire tags from 2002 were recovered near the mouth of the Yukon River at 63°N and at 64.1°N. Coded-wire tags recovered from 2007 were all recovered just south of the Bering Strait at 65.2°N, confirming the presence of a northward migration corridor for juvenile Yukon Chinook salmon.

All coded-wire tagged juveniles were age-0 (or fall-type Chinook), a known life-history feature of Chinook salmon produced from the Whitehorse Rapids Fish Hatchery. The size of hatchery juveniles (125-193 mm; 18-79 g) were significantly smaller than the average size of juvenile Chinook salmon captured during the survey (213 mm, 127 g) and hatchery juveniles still had visible parr marks at the time of capture (average date of September 10). The presence of parr marks on hatchery juveniles indicates an ocean entry date much later than most wild juvenile Chinook salmon on the eastern Bering Sea shelf.

DISCUSSION

The estuarine and early ocean habitats of juvenile salmon in the Bering Sea differ from juvenile habitats in the Gulf of Alaska. Juvenile salmon occupy a broad shallow shelf with relatively stable waters in the Bering Sea. In the Gulf of Alaska, juvenile salmon occupy habitats ranging from a network of narrow corridors associated with fjords in Southeast Alaska, to the narrow shelf and highly dynamic waters of northern California (Brodeur et al. 2000; Orsi et al. 2000). Migratory corridors of juvenile salmon in summer are largely thought to be constrained to epipelagic waters over the continental shelf once they reach the open ocean in the Gulf of Alaska (Brodeur et al. 2000; Fisher et al. 2007; Orsi et al. 2000). Juvenile salmon migratory corridors in all open ocean regions are most likely defined by oceanographic, not bathymetric features; however, the close association of these features in the Gulf of Alaska (Mundy 2005) often results in the use of the continental shelf to describe juvenile salmon migratory corridors**.** The broad continental shelf of the Bering Sea provides the opportunity to investigate biological and physical features such as water mass types and frontal regions that structure migratory pathways of juvenile salmon.

Juvenile Chinook salmon were primarily distributed within water depths less than 50 m through their first summer at sea (middle of August through the middle of October) and the highest densities of juvenile Chinook salmon were found close to river mouths of primary Chinook salmon producing rivers in the eastern Bering Sea (Yukon River, Kuskokwim River, and Nushagak rivers). This reflects a later dispersal from freshwater entry points than typically found in Gulf of Alaska stream-type Chinook salmon (Fisher et al. 2007). This is likely the

combined effect of later ocean entry dates and lower migration rates of juvenile Chinook salmon on the eastern Bering Sea shelf.

Foraging behavior of salmon within the Coastal Domain may play a key role in defining juvenile Chinook salmon habitat and dispersal rates during their first summer at sea. The Coastal Domain is typically found in water depths shallower than 50 meters on the eastern Bering Sea Shelf (Schumacher and Stabeno 1998) and is associated with reduced water column stability, tight pelagic-benthic coupling, and high benthic productivity (Grebmeier et al. 2006). These structural components of the Coastal Domain favor forage fish species such as capelin and Pacific sand lance, which are the principal prey of juvenile Chinook salmon (Farley et al. *In press*). It is possible that feeding behavior of Chinook salmon on these forage fish species may be contributing to a delayed dispersal from the Coastal Domain. An apparent preference for the Coastal Domain is also seen in coho salmon (Farley et al. 2005) which also preferentially feeds on the forage fish species in the Coastal Domain.

The adequacy of the U.S. BASIS survey design for juvenile Chinook salmon populations differed by region. The broad migratory corridor of juvenile Chinook salmon and later survey sampling dates in the northern Bering Shelf region resulted in most juvenile Chinook from this region present within trawlable habitats (> 20 m). The narrow migratory corridor and earlier sampling dates in the southern shelf region resulted in a higher proportion of the juvenile population present in non-trawlable habitats and higher spatial variance in the catch data. The inability to distinguish between primary stock groups contributing to the southern shelf index area also limits our ability to evaluate how well the survey data reflects juvenile Chinook salmon stocks in this region. Improvements to the juvenile Chinook salmon data from the southern shelf region would be possible with finer scale sampling within the

Coastal Domain, gear modifications to improve sampling capabilities in shallow water habitats, later sampling dates, and improved stock discrimination.

Similarity in stock mixtures from both strata in the northern region supports a limited northward migration of southern stocks. If the presence of southern stocks was the primary factor contributing to differences in the juvenile and adult harvest mixtures, the southern stocks would need to be equally present in both strata. This is unlikely given the apparent dispersal rates of the juvenile Chinook salmon in the eastern Bering Sea.

Comparisons between stock proportions of the juvenile population in the northern shelf region and historic Yukon River harvests also did not support significant northward migration of southern stocks. If significant numbers of juvenile Chinook salmon from southern shelf were migrating north, the estimated proportions of the Coastal Western Alaska stock group would be significantly higher in the northern shelf region than expected for Yukon River Chinook salmon. The proportion of Coastal Western Alaska stocks in the northern shelf region was within the range expected for the Yukon River.

Coded-wire tag recoveries during the survey provide evidence that the distribution of Yukon River Chinook salmon can extend northward through the Bering Strait. Survey designs that include portions of the Bering Strait and Chukchi Sea will improve sampling coverage of the Yukon River Chinook salmon stocks and the Chukchi Sea needs to be considered as rearing habitat for at least a portion of Yukon River Chinook salmon stocks. Coded-wire tagged Chinook salmon near the Bering Strait were all recovered in 2007—an exceptionally warm summer (Moss et al. *This volume*). Temperature, time of ocean entry, and seasonal currents may all be important factors determining the proportion of juvenile Yukon River Chinook salmon that migrate northward into the Bering Strait and Chukchi Sea.

Life-history differences between wild and hatchery fish can result in different distributions of hatchery and wild Yukon River Chinook salmon; therefore it is not appropriate to characterize the distribution of wild juveniles with coded-wire tag recoveries alone. However, life-histories of wild and hatchery Yukon River Chinook salmon are not completely unique. Although Yukon River Chinook are characterized as stream-type Chinook salmon (Gilbert 1922), several unmarked or wild juvenile Chinook were similar in size or smaller than hatchery Chinook and also had visible parr marks, indicating the presence of fall-type or freshwater age-0 juveniles in wild populations. This emphasizes the importance of freshwater age plasticity in stream-type Chinook salmon as part of their natural life history variation and not simply an artifact of hatchery rearing (Beckman and Dickhoff 1998).

The following conclusions can be made concerning the U.S. BASIS survey data as it applies to juvenile Chinook populations on the eastern Bering Sea shelf. The timing of the survey, ocean entry dates, and the width of the Coastal Domain on the eastern Bering Sea shelf are all believed to impact the proportion of juvenile Chinook populations present in non-trawlable habitats during the survey. The effect of non-trawlable habitat on survey data can be large particularly in the southern shelf region and corrections for non-trawlable habitat are needed. U.S. BASIS survey data from the northern shelf region will primarily apply to Yukon River Chinook salmon populations; however, stock identification data will still be needed to monitor stock contributions to this region. Yukon River Chinook salmon distributions can extend through the Bering Strait and into the Chukchi Sea; complete coverage of Yukon River Chinook salmon will require sample coverage in the Bering Strait and southern Chukchi Sea.

ACKNOWLEDGMENTS

We thank the captains and crew of the F/V *Sea Storm* F/V *Northwest Explorer*, and the NOAA ship *Oscar Dyson* for their excellent support of the field surveys. We thank Jamal Moss, Lisa Eisner, Kris Cieciel, Angela Feldman, Alex Andrews, and Erik Husoe from the Auke Bay Laboratories, and Natalia Kuznetsova and Oleg Ivanov from the TINRO-Centre in Vladivostok, Russia for their support on U.S. BASIS surveys. We thank Andy Barclay and Judy Berger from the Gene Conservation Laboratory for their support with laboratory analysis of genetic mixtures. Principal funding support for this work was provided by the Alaska Fisheries Science Center NOAA/NMFS, the Alaska Department of Fish and Game, and the Alaska Sustainable Salmon Fund: projects 45491 and 45484.

REFERENCES

Brodeur. R. D., G. W. Boehlert, E. Casillas, M. B. Eldridge, J. H. Helle, W. T. Peterson, W. R. Heart, S. T. Lindley, and M. H. Schiewe. 2000. A coordinated research plan for estuarine and ocean research on Pacific salmon. Fisheries. 25:7-16.

Beckman, B. R. and W. W. Kickhoff. 1998. Plasticity of smolting in spring chinook salmon: relation to growth and insulin-like growth factor-I. J. Fish Bio. 53:808-826.

Courtney, D. L., D. G. Mortensen, J. A. Orsi, and K. M. Munk. 2000. Origin of juvenile Pacific salmon recovered from coastal southeastern Alaska identified by otolith thermal marks and coded wire tags. Fish. Res. 46:267-278.

Cressie, N. A. C. 1991. Statistics for Spatial Data. John Wiley and Sons, New York. 920 pp.

Debevec, E. M., R. B. Gates, M. Masuda, J. Pella, J. Reynolds, and L. W. Seeb. 2000. SPAM (version 3.2): statistics program for analyzing mixtures. J. Hered. 91(6):509–510.

DuBois, L., and N. A. DeCovich. 2008. Origins of Chinook salmon in the Yukon River Fisheries, 2005. Alaska Department of Fish and Game, Divisions of Sport Fish and Commercial Fisheries, Fish. Data Ser.No. 08-02.

Enviornmental System Research Institue (ESRI). 2006. ArcGIS: Release 9.2 (software). Redlands, California: Environmental Systems Research Institute, 1999-2006.

Farley, E.V., Jr., J.M. Murphy, B.W. Wing, J.H. Moss, and A. Middleton. 2005. Distribution, migration pathways, and size of Western Alaska juvenile salmon along the eastern Bering Sea shelf. Alaska Fish. Res. Bull. 11:15-26.

Farley, E.V., J.M. Murphy, J.H. Moss, A. Feldmann, and L. Eisner. *In press*. Marine ecology of western Alaska juvenile salmon. Am. Fish. Soc. Symp.

Fisher, J., M. Trudel, A. Ammann, J. Orsi, J. Picoolo, C. Bucher, E. Casillas, J. Harding, R. MacFarlane, R. Brodeur, J. Morris, and D. Welch. 2007. Comparisons of the coastal distributions and abundances of juvenile Pacific salmon from central California to the northern Gulf of Alaska. Am. Fish. Soc. Symp. 57: 31-80.

Gilbert, C. H. 1922. The salmon of the Yukon River. U. S. Bureau of Fisheries Bulletin 38:317-332.

Grebmeier, J.M., J.E. Overland, S.E. Moore, E.V. Farley, Jr., E.C. Carmack, L.W. Cooper, K.E. Frey, J.H. Helle, F.A. McLaughlin, S.L. McNutt. 2006. A major ecosystem shift in the northern Bering Sea. Science 311:1461 - 1464.

Hartt, A. C., and M. B. Dell. 1986. Early oceanic migrations and growth of juvenile Pacific salmon and steelhead trout. Int. North Pac. Fish. Comm. Bull. 46.

Healey, M. C. 1991. Life history of Chinook salmon. Pages 311–394 *in*. Pacific salmon life histories. Edited by C. Groot and L. Margolis. UBC Press, Vancouver.

Jefferts, K. B., P. K. Bergman, and H. F. Fiscus. 1963. A coded wire identification system for macro-organisms. Nature (Lond.) 198:460-462.

Lingnau, T. L., and J. F. Bromaghin. 1999. Origins of Chinook salmon in the Yukon River fisheries, 1997. Alaska Department of Fish and Game, Division of Commercial Fisheries, Regional Information Rep. 3A99-09, Anchorage.

Mundy, P. R. 2005. The Gulf of Alaska: biology and oceanography. University of Alaska, Alaska Sea Grant College Program, Fairbanks.

Murphy, J., O. Temnykh, and T. Azumaya. 2003. Trawl Comparisons and Fishing Power Corrections for the F/V *Northwest Explorer*, R/V *TINRO*, and R/V *Kaiyo Maru* During the 2002 BASIS Survey. (NPAFC Doc. No. 677) 25 p.

Moss, J. H., J. M. Murphy, L. E. Eisner, and E. V. Farley. *This volume*. Growth, size, and diets of juvenile pink and chum salmon in response to loss Arctic sea ice. North Pac. Anadr. Fish Comm. Bulletin 5.

Orsi, J. A., and H. W. Jaenicke. 1996. Marine distribution and origin of pre-recruit chinook salmon, *Oncorhynchus tshawytscha*, in southeastern Alaska. Fish. Bull. 94:482-497.

Orsi, J. A., M. V. Sturdevant, J. M. Murphy, D. G. Mortensen, and B. L. Wing. 2000. Seasonal habitat use and early marine ecology of juvenile Pacific salmon in southeastern Alaska. Pages 111-122 in J. H. Helle, Y. Ishida, D. Noakes, and V. Radchenko, editors. Recent changes in ocean production of Pacific salmon. North Pacific Anadromous Fish Com. Bull. 2.

Seeb, J. E., C. E. Pascal., R. Ramakrishnan and L. W. Seeb. 2009. SNP genotyping by the 5'-nuclease reaction: advances in high throughput genotyping with non-model organisms. A. A. Komar (ed.), Methods in Molecular Biology, Single Nucleotide Polymorphisms, 2nd Edition. Humana Press (*chapter 18 in press*).

Seeb, L. W., P. A. Crane, C. M. Kondzela, R. L. Wilmot, S. Urawa, N. V. Varnavskaya, and J. A. Seeb. 2004. Migration of Pacific Rim chum salmon on the highseas: insights from genetic data. Environ. Biol. Fish. 69:21-36.

Schumacher, J. D., and Stabeno, P. J. 1998. Continental shelf of the Bering Sea. Pages 789-822 in The Sea: Vol. 1, The global coastal ocean: regional studies and synthesis. Wiley, New York

Smith, C. T., W. D. Templin, J. E. Seeb, and L. W. Seeb. 2005. Single-nucleotide polymorphisms (SNPs) provide rapid and accurate estimates of the proportions of U.S. and Canadian Chinook salmon caught in Yukon River fisheries. N. Amer. J. Fish. Man. 25:944-953.

Templin, W. D., C. T. Smith, J. E. Seeb, and L. W. Seeb. 2005. SNPs provide high-throughput resolution for migratory studies of Chinook salmon. (NPAFC Doc. 908) 10 p. Alaska Department of Fish and Game, 333 Raspberry Road, Anchorage, AK, USA 99518.

Yukon River Joint Technical Committee (YRJTC). 2008. Yukon River salmon 2007 season summary and 2008 season outlook. Regional Information Rep. No. 3A08-01, Anchorage.

Yukon River Joint Technical Committee (YRJTC). 2009. Yukon River salmon 2008 season summary and 2009 season outlook. Regional Information Report No. 3A09-01, Anchorage.

Table 1. Number of surface trawl stations sampled during U.S. BASIS surveys on the eastern Bering Sea shelf by year and vessel, 2002-2007.

Year	Vessel	Start Date	End Date	Number of Trawl Stations
2002	*F/V Sea Storm*	20-Aug-02	07-Oct-02	152
	F/V Northwest Explorer	08-Sep-02	06-Oct-02	44
2003	*F/V Sea Storm*	21-Aug-03	08-Oct-03	151
2004	*F/V Sea Storm*	14-Aug-04	30-Sep-04	143
2005	*F/V Sea Storm*	14-Aug-05	06-Oct-05	127
2006	*F/V Sea Storm*	14-Aug-06	20-Sep-06	105
	F/V Northwest Explorer	21-Aug-06	04-Sep-06	53
2007	*F/V Sea Storm*	15-Aug-07	08-Oct-07	136
	NOAA Ship *Oscar Dyson*	05-Sep-07	26-Sep-07	50

Table 2. Estimated stock mixtures of juvenile Chinook salmon (with 95% confidence intervals) collected during U.S. BASIS surface trawl surveys on the eastern Bering Sea shelf by region and location, 2002-2006. Average sample dates and DNA sample sizes are included.

					Stock Group			
Stock Mixture	Region	Location	Average Sample Date	Sample Size	Coastal Western Alaska	Middle Yukon	Upper Yukon	Other
1	Southern Bering Shelf	< 167°W	24-Aug	819	0.94 (0.88-0.98)	0.00 (0.00-0.00)	0.01 (0.00-0.10)	0.05 (0.01-0.12)
2	Northern Bering Shelf	60°N<>62° N	24-Sep	238	0.29 (0.21-0.36)	0.23 (0.16-0.30)	0.45 (0.38-0.53)	0.03 (0.00-0.08)
3	Northern Bering Shelf	62°N<>64.5 °N	10-Sep	299	0.29 (0.24-0.34)	0.26 (0.20-0.31)	0.44 (0.38-0.50)	0.01 (0.00-0.03)

2/3	Northern Bering Shelf	60°N<>64.5°N	14-Sep	537	0.30 (0.26-0.35)	0.24 (0.19-0.29)	0.45 (0.40-0.50)	0.01 (0.00-0.42)

Table 3. Coded-wire tag recoveries from juvenile Chinook salmon captured during U.S. BASIS surface trawl surveys on the eastern Bering Sea shelf, 2002-2007. Release information provided by the Whitehorse Rapids Hatchery (YRJTC, 2009).

		Release Data		Recovery Data				
Freshwater Origin	Tag Code	Date	Weight (g)	Date	Latitude	Longitude	Length (mm)	Weight (g)
Whitehorse Rapids Hatchery: Michie Creek	185061	2-Jun-02	3.2	4-Oct-02	63.0°N	166.0°W	155	49
Whitehorse Rapids Hatchery: Michie Creek	185106	10-Jun-02	3.2	3-Oct-02	64.1°N	164.5°W	193	79
Whitehorse Rapids Hatchery: Wolf Creek	185102	2-Jun-02	3.1	3-Oct-02	64.1°N	164.5°W	153	43
Whitehorse Rapids Hatchery	18	2007	--	13-Sep-07	65.2°N	168.1°W	176	58
Whitehorse Rapids Hatchery	18	2007	--	13-Sep-07	65.2°N	168.1°W	125	18
Whitehorse Rapids Hatchery	18	2007	--	13-Sep-07	65.2°N	168.1°W	179	58

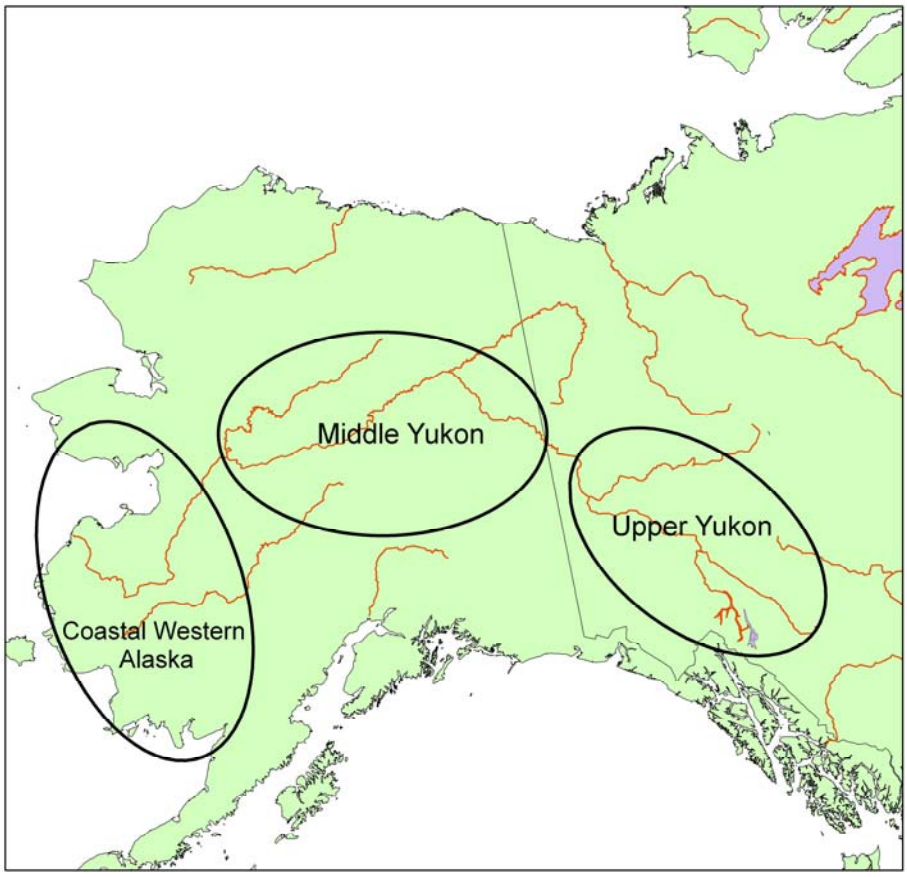
Middle Yukon
Upper Yukon
Coastal Western
Alaska

Figure 1. Approximate locations of regional genetic stock groups of juvenile Chinook salmon (Coastal Western Alaska, Middle Yukon, and Upper Yukon) captured during U.S. BASIS surface trawl surveys on the eastern Bering Sea shelf.

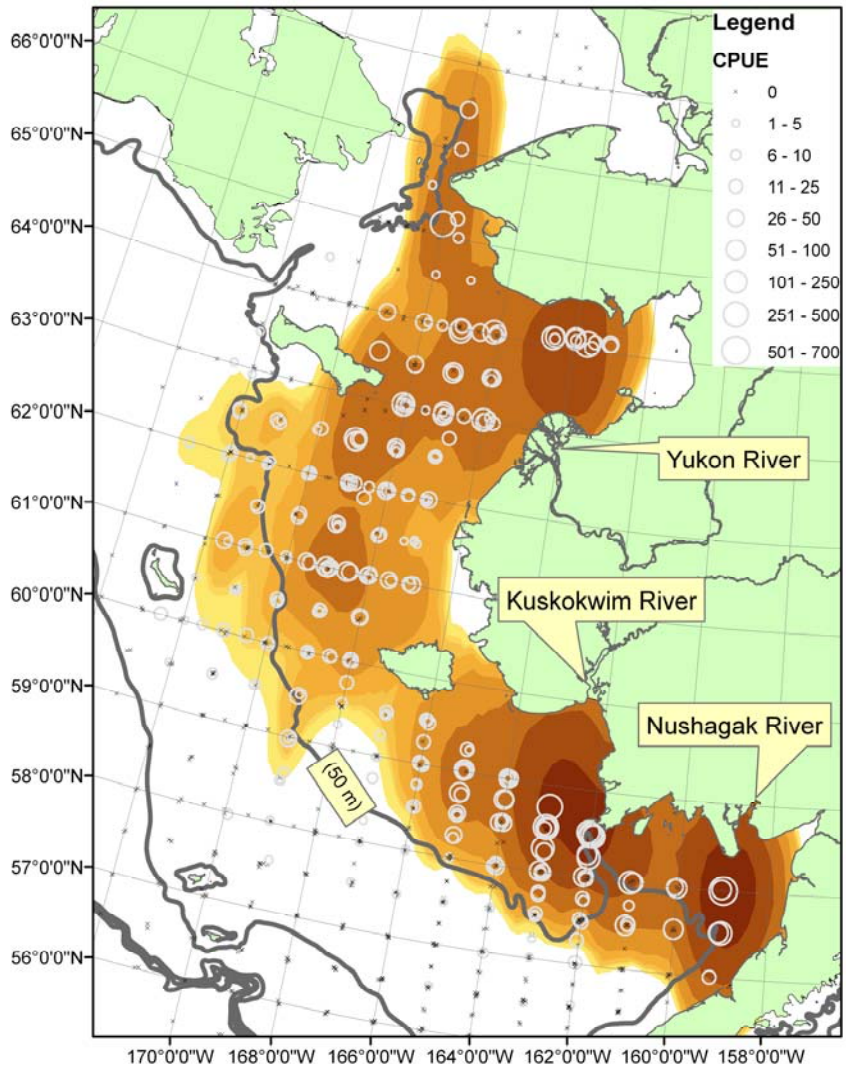

Figure 2. Distribution of juvenile Chinook salmon during U.S. BASIS surface trawl surveys on the eastern Bering Sea shelf (mid August to early October), 2002-2007. Distribution is based on catch per unit of effort (CPUE) with a 30-minute trawl haul used as the standard unit of effort.

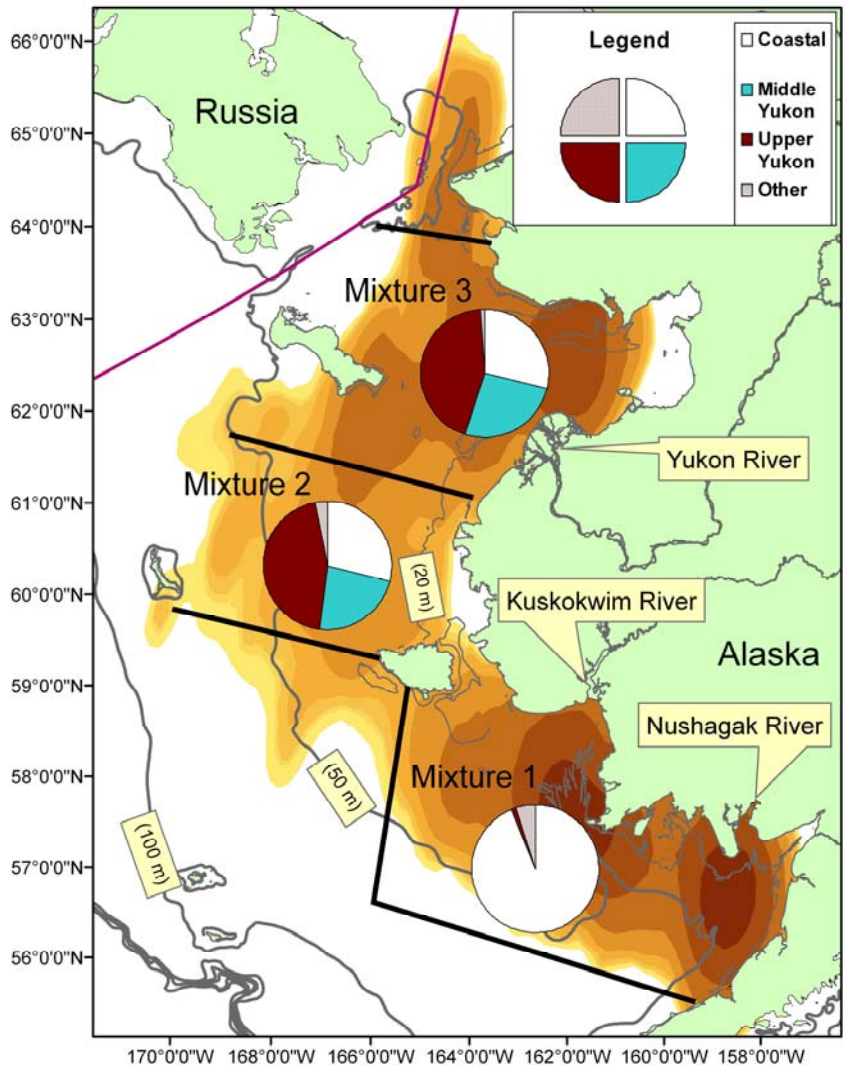

Figure 3. Genetic stock mixtures of juvenile Chinook salmon (Coastal Western Alaska, Middle Yukon, Upper Yukon, and 'other' stock groups) captured during U.S. BASIS surface trawl surveys on the eastern Bering Sea shelf (mid August to early October), 2002-2006. Mixtures are overlaid on a map of juvenile Chinook distribution and black bars identify the spatial extent of each mixture.

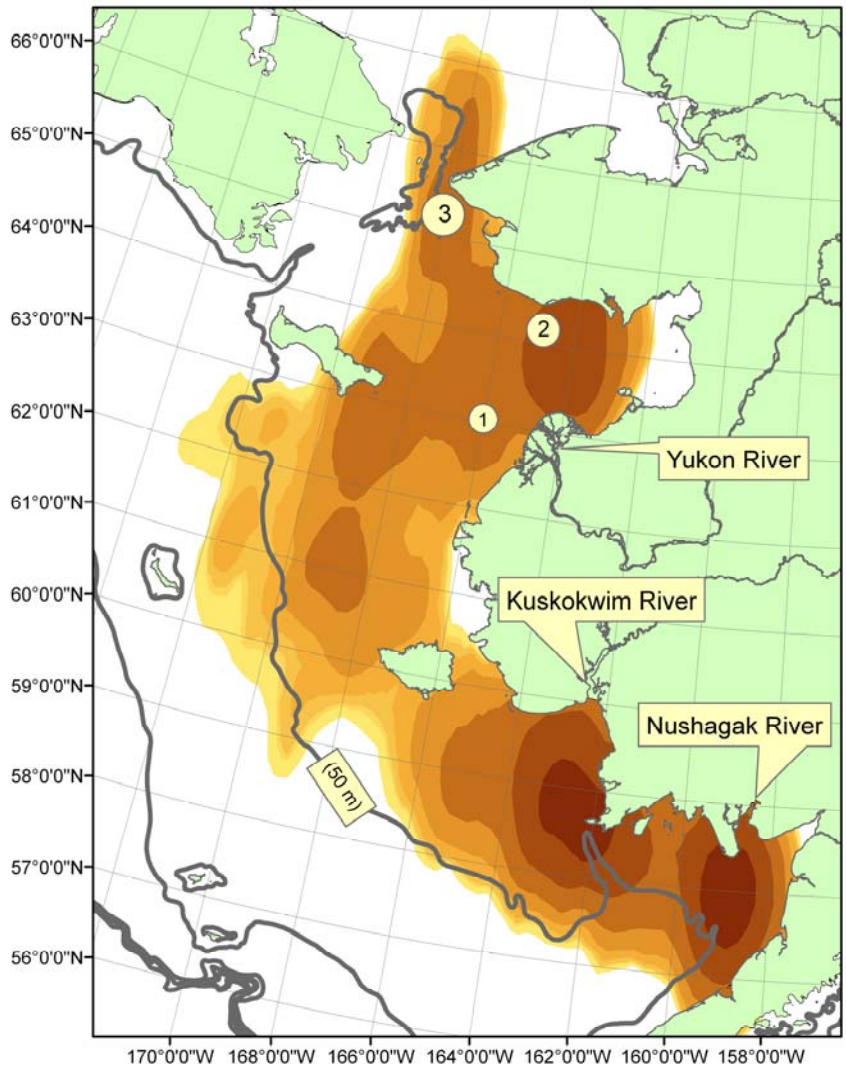

Figure 4. Locations of coded-wire tag recoveries of Whitehorse Rapids hatchery Chinook salmon from the Yukon River during U.S. BASIS surface trawl surveys on the eastern Bering Sea shelf (mid August to early October), 2002-2007. Circles indicate coded-wire tag recovery locations and are overlaid on a map of juvenile Chinook distribution. Numbers in circles indicate the number of coded-wire tags recovered at each location.

Appendix 6

Effects of Temperature and Body Size on Juvenile Chum Salmon (*Oncorhynchus keta*) Consumption Rate

JAMAL H. MOSS* AND EDWARD FARLEY JR.

Auke Bay Laboratories, Alaska Fisheries Science Center, National Oceanic and Atmospheric Administration
17109 Point Lena Loop Road, Juneau, AK, 99801, U.S.A.

Abstract.— Temperature is a controlling factor that governs the rate of biochemical reactions and influences the activity level of fish. Little is currently know about the influence of temperature on the feeding rates of juvenile salmon; information which could provide insight into the influence of biophysical factors on feeding ecology and behavior. Utilizing bioenergetics models in research focused on understanding biophysical mechanisms that influence salmon ecology is growing, which has resulted in a need for species- and life stage-specific model parameters to generate accurate predictions. The effect of temperature and body size on the consumption rate of juvenile chum salmon (*Oncorhynchus keta*) was investigated for individuals of similar body size to those within their first summer in the marine environment to address these concerns. Juvenile chum salmon ranging 50–100mm (FL) in size were fed live mysid shrimp (*Mysidopsis bahia*) to satiation over a 24-hour period. Feeding trials were conducted across a range of temperatures (3.5–23.0º C), that were held constant during a given trial. Weight dependence on specific consumption took the form of a decreasing power function. Temperature dependence on specific maximum consumption took the form of a cool and coldwater species. Maximum consumption increased rapidly from 3-8.5 ºC, and demonstrated a slight decrease between 8.5-23 ºC. Bioenergetics model simulations run with the newly estimated parameters predicted lower growth rates than the existing model most commonly used to estimate growth for juvenile pink (*O. gorbuscha*), chum, and sockeye salmon (*O. nerka*).

Introduction

Temperature is a controlling factor that governs biochemical reactions, metabolism, and activity level in fish (Fry 1971). Little information is currently available about the influence of thermal experience on juvenile salmon feeding rates, which could provide insight into the influence of biophysical factors on feeding ecology and growth. It has been well documented that Pacific salmon (*Oncorhynchus spp.*) increase their likelihood for survival by growing quickly (Moss et al. 2005, Beamish and Mahnken 2001), and are thus required to balance energy intake with energy costs associated with water temperature, fish size, ration size, and physical activity (Groot et al. 1995). As juvenile chum salmon grow during early marine residence they move offshore (LeBrasseur 1969) and feed on larger, more energy rich zooplankton species (Birman 1969). Brett et al. (1969) examined the effect of reduced ration on the relationship between specific growth rate and temperature for 7-12 month year-old sockeye salmon (*Oncorhynchus nerka*), and Shelbourn et al. (1973) did so for 0.5-5.2 sockeye

salmon. However, with the exception of these few investigations, experimental studies exploring the mechanisms of temperature and feeding behavior that affect growth in salmon fry (Groot et al.1995) have not been conducted.

Bioenergetics models have been used to quantify fish growth (Brandt et al. 1992, Mazur et al. 2007), consumption (Ciannelli et al. 1998), and bioaccumulation rates of toxins (Barber et al. 1991). These models are recognized as powerful tools for exploring the non-linear effects of temperature, prey quality, and body size on fish growth (Madenjian et al. 2004, Mazur et al. 2007). The practice of borrowing parameters from closely related species and life stages is common (Ney 1993), however, this practice has been criticized (Trudel et al. 2004, Trudel and Welch 2005) and the importance of developing species- and life stage-specific models from targeted laboratory experiments has been stressed (Orsi et al. 2004). Recent research focused on the juvenile life history stage has resulted in a need for model parameters specific to the early ocean life history stage (Orsi et al. 2004); however performing laboratory experiments necessary to parameterize these models can difficult (Trudel et al. 2004).

Specific applications of bioenergetics models to scientific investigations concerning juvenile Pacific salmon ecology have focused on the quantification of prey consumption (Brodeur et al. 1992, Boldt and Haldorson 2002, Orsi et al. 2004), growth rate (Beauchamp et al. 1989, Cross et al. 2005), and the assessment of habitat quality (Rand 2002, Farley and Trudel 2009). Bioenergetics models parameterized for salmon have been primarily developed from the adult life stages, and substituting parameters derived solely from juvenile salmon responses would likely increase model accuracy of simulations generated for juveniles, and advance understanding of juvenile Pacific salmon ecology.

Bioenergetics models are based on the laws of thermal dynamics where the energy consumed by a fish must balance the energy lost through physiological processes and growth. Somatic fish growth is influenced by prey availability (Boisclair and Legget 1989, Mazumder and Edmundson 2002) prey quality (Davis et al. 1998), and temperature (Mazur et al. 2007). Energy acquired through prey consumption is allocated to metabolic costs, lost through activity, egestion, or excretion. Energy remaining after these costs are satisfied is available for somatic and gonadal tissue growth, unless an energy deficit exists, which would result in weight loss. The terms of this energy budget can be measured directly in laboratory experiments designed to measure metabolism, activity, maximum specific consumption rate, and energy lost through waste products. Model generated estimates of prey consumption have been corroborated with independently derived field estimates for sockeye salmon (Beauchamp et al. 1989), lake trout (Madenjian et al. 2000), and largemouth bass (Rice and Cochran 1984). In contrast, other studies have found substantial discrepancies between model output and independent estimates from field estimated food consumption (Chipps and Wahl 2008).

A sensitivity analysis performed on the sockeye salmon bioenergetics model revealed that the intercept of the dependence of consumption on weight, the proportion of maximum consumption, and the proportion of maximum consumption in the temperature dependence function at low temperatures were among the most sensitive parameters (Beauchamp et al. 1989). Therefore, the main objective of this study were to first quantify the effect of

temperature and body size on maximum specific consumption rate for juvenile chum salmon (*O. keta*). Newly estimated parameters from the laboratory experiments were then used to predict the growth of juvenile chum salmon of comparable in size during their first summer in marine waters using the Wisconsin bioenergetics model (Hewett and Johnson 1992).

Methods

Fish husbandry.— Juvenile chum salmon were transported from the Douglas Island Pink and Chum Inc. hatchery to the National Oceanic and Atmospheric Administration Auke Bay Marine Station located in Juneau, Alaska, in plastic 18.9 L buckets supplied with battery powered air pumps and stones. Fish were immediately transferred to raceways upon arrival that were supplied with a constant flow of water upon arrival, where fish were allowed a three week acclimation period before feeding experiments were initiated. During the acclimation period fish were fed pelletized fish feed that was dispensed by a battery-operated feeder at a rate of 4% body weight in addition to live mysid shrimp (*Mysidopsis bahia*) daily.

Feeding experiments.— Individual fish were weighed and transferred from raceways to 7.6 L white opaque plastic buckets (hereafter referred to as experimental arenas) that were contained in a temperature-controlled water bath. Each experimental arena was supplied with oxygen via an air pump and stone, and covered with a fine mesh screen to prevent fish from escaping. Heating and cooling elements were placed in the water bath and incrementally adjusted every few hours over a 24-h period until a desired experimental water temperature was obtained; and then adjusted once more to maintain the desired temperature for a particular experimental trial. Experimental subjects were allowed a 48-h acclimation period prior to an experimental trial, during which time fish were denied food. A natural photoperiod was maintained from the time fish arrived to the laboratory until the experimental trials ceased.

Juvenile chum salmon utilized in feeding experiments ranged from 1.0-6.5 g and 50–100mm fork length (FL) in size; and were acclimated to five different temperatures ranging between 3.5-23.0 °C. Experimental arenas were opaque, 2-gallon buckets that were covered with a fine mesh screen and supplied with oxygen. Temperature was held constant during feeding trials, and fish were fed live mysid shrimp in excess over a 24-hour period. Each juvenile chum salmon was presented with a biomass of mysids that accounted for approximately 12% of its body weight. Fifty mysids were weighed just prior to an experiment in order to calculate the average weight of a single mysid, which was then used to determine the number of mysids to add to the experimental arena. This pre-determined amount of mysids were then transferred to a small beaker of water and added to an experimental arena containing a single juvenile chum salmon. The experiment was initiated once the prey was added. Chum salmon were removed from the experimental arenas 24-hours later, measured (FL and weight), and euthanized. Mysids remaining in the experimental arena that were not consumed during the trial, were collected by straining arena water through a sieve, and enumerated immediately. Thus, the amount of mysids consumed over the 24-h period calculated by

$$C = M_I - M_F$$

where, C is the weight of mysids consumed over a 24-h period, M_I is the weight of mysids added to the experimental arena initially, and M_F is the weight of mysids remaining at the end of the experiment. Mysids not consumed during the trial were converted to a biomass estimate by multiplying the average weight calculated prior to the experiment by the number remaining after the trial.

Consumption Rate Models of Pacific Salmon.— *Maximum specific consumption is typically fit to a power function (Hanson et al. 1997).*

$$C_{\max} = CA \times W^{CB}$$

Where C_{max} is maximum specific consumption rate ($g \cdot g \cdot d^{-1}$), CA is the intercept of the allometric mass function, and CB the slope of the allometric function. To simplify the parameterization, the temperature where C_{max} is highest for most sizes of fish is first identified, and the weight-dependence function for consumption at that temperature parameterized. For any other temperature, the weight-dependent C_{max} would be reduced by the temperature-dependant function of consumption that varies from 0.0 to 1.0.

In the most common application, the bioenergetics model estimates consumption by iteratively fitting the proportion of maximum consumption required to satisfy the change in body mass observed over a specified time interval for fish of a given size under a specified temperature regime (Hanson et al. 1997).

$$C = C_{\max} \times P \times F(T)$$

Where C is the model estimate of consumption, C_{max} is the maximum specific consumption, P the proportion of maximum specific consumption, and $F(T)$ a function of temperature. Total consumption is estimated by iteratively fitting the proportion to maximum consumption until a required change in body mass specified by the user is reached.

Parameter estimation and curve fitting.— Specific consumption rate was plotted against body size and a curve was fit to data by least squares. Curve fitting was done for data collected at the temperature where consumption was highest for all sizes of juvenile chum salmon. The response of specific consumption rate to temperature was characteristic of a response for cool- and cold-water species (Thornton and Lessem 1978). The Thornton-Lessem response is the combination of two sigmoid curves, with one curve fit to the portion of the data where consumption increases with temperature and the other curve where consumption decreases with temperature (T) where

$$f(\mathrm{T}) = \mathrm{K_A} \cdot \mathrm{K_B}$$

$\mathrm{K_A} = (\mathrm{CK1} \cdot \mathrm{L1})/(1+\mathrm{CK1} \cdot (\mathrm{L1}-1))$
$\mathrm{L1} = e^{(\mathrm{G1} \cdot (\mathrm{T}-\mathrm{CQ}))}$
$\mathrm{G1} = (1/(\mathrm{CTO}-\mathrm{CQ})) \cdot \ln((0.98 \cdot (1-\mathrm{CK1}))/(\mathrm{CK1} \cdot 0.02))$
$\mathrm{K_B} = (\mathrm{CK4} \cdot \mathrm{L2})/(1+\mathrm{CK4} \cdot (\mathrm{L2}-1))$

$L2 = e^{(G2*(CTL-T))}$

$G2 = (1/(CTL-CTM))\cdot\ln((0.98\cdot(1-CK4))/(CK4\cdot 0.02))$

3.5g chum salmon were used to estimate temperature-dependent consumption parameters. Specific parameters estimated from this curve were CTO and CTM, the temperature at which 98% of maximum consumption occurs; and CQ, the temperature where consumption is a small fraction (CK1) of peak consumption. The warmest experimental temperature was designated as CTL, a temperature warmer than CTO and CTM where consumption is a reduced fraction (CK4).

Model simulations.— The Wisconsin bioenergetics model (Hanson et al. 1997) was run using the pink/sockeye salmon model parameters provided with the model software; and then run once more with the newly estimated parameters for temperature and weight dependence on maximum specific consumption substituted. Model input consisted of biophysical data collected from juvenile chum salmon migrating through Icy Strait, Alaska to the Gulf of Alaska during their first year of life (Orsi et al. 2004). This data included prey composition in diet by weight, chum salmon energy density, and thermal experience during June 28th-August 30th 2001. Prey energy density estimates were borrowed from literature sources (Cross et al. 2005). Proportion of maximum consumption (P-value) was set at a rate of 1.0 for generating estimates of growth; where juvenile pink and chum salmon are believed to feed at near maximum rates during early marine life (Cross et al. 2005). The model was run at a daily time step for 63 days period. Percent differences in growth and consumption between the two models were calculated and reported.

Results

Juvenile chum salmon consumption rates were highest at 8.5ºC. Specific consumption gradually decreased from temperatures greater than 8.5 ºC to the warmest experimental temperature of 23.0 ºC (Figure 1). The temperature dependent response of specific consumption was characteristic of cool- and cold-water species (Thornton and Lessem 1978). Absolute consumption ($g\cdot d^{-1}$) increased with body size for all temperatures. Parameters CTO and CTM represent the temperature where 98% of maximum consumption is achieved, and were set at to the observed maximum of 8.5 ºC (Figure 1). We designated CQ = 3.0º as the temperature at which consumption was a small fraction (CK1 = 0.3761) of peak consumption, as it was the coolest experimental water temperature utilized in the study. The warmest experimental temperature was designated as CTL = 23.0ºC, a temperature warmer than CTO and CTM where consumption was some reduced fraction (CK4 = 0.8923) of peak consumption.

The effect of weight on specific consumption at each experimental treatment temperature was characteristic of a decreasing power function (Figure 2). Weight dependence on maximum consumption was calculated at the optimal feeding temperature for juvenile chum salmon which was 8.5ºC. The intercept of mass dependence for a 1g fish at the optimum water temperature was 0.1298, with a coefficient of mass dependence of -0.2881 (Table 1).

We used an initial start weight of 8.5g, which was the average juvenile chum body weight in Icy Strait during June 2001 as reported by Orsi et al. (2002). Observed average body was reported to be 32.1g on average by Aug 30th 2001. Our model predicted that juvenile chum would grow to a size of 22.4g by August 30th, assuming near maximum prey consumption rates. This difference in size suggests that model simulations using the temperature and weight dependent functions specific to juvenile chum salmon may have under estimated growth. The adult sockeye/pink model predicted a body size of 85.6g on Aug 30th, and likely over estimated growth.

Discussion

A series of feeding to satiation experiments over a 20ºC range of water temperatures and body size yielded valuable information on interrelationships between prey consumption rate, temperature, and body size for juvenile chum salmon. Results from this investigation and can be applied to field data and be used to infer the affect of biophysical conditions on the growth and prey consumption of juvenile chum salmon. Experiments designed to quantify the physiological and behavioral aspects of feeding can offer insight into potential constraints on growth and survival of juvenile salmon in the ocean (Moss et al. 2005, Farley et al. 2005, 2009), and until the present time, model parameters specific to juvenile chum salmon did not exist. Existing models have been constructed using adult and sub-adult life history stages of other species have been substituted.

Temperature and size dependence on juvenile chum salmon oxygen consumption and metabolic rate were not included as part of this study. Oxygen consumption and metabolic rate of fingerling sockeye increase exponentially with temperature (Brett 1964, 1970). Assuming that fingerling sockeye salmon demonstrate a similar response to juvenile chum salmon, energetic demand increases with temperature. Temperature dependent feeding rate increased rapidly from low temperatures and peaked at 8.5 ºC. Feeding rate then gradually decreased from 8.5 - 23.0 ºC. Therefore, juvenile chum salmon must allocate a greater amount of energy to metabolic costs when experiencing temperatures above 8.5, while their food consumption rate gradually decreases. Diel vertical migrations are a strategy that fish use to regulate metabolic rate and maximize food conversion efficiencies. However, information on the temperature and size dependence on juvenile chum salmon metabolic rate would be needed to accurately assess an energy budget that would reveal the combined effects of water temperature and body size on energy assimilation.

Orsi et al. (2004) reported that the total amount of prey consumed by juvenile chum salmon was relatively insensitive to temperature when estimated using a bioenergetics model. The shape and form of the temperature dependence on maximum specific consumption parameterized in this study shows that feeding rates only slightly decline with increasing temperature above 8.5 ºC. Seasonal growth was underestimated when the Wisconsin model was run on daily time-step increments using substituted biophysical parameters specific to juvenile chum salmon. Average body size predicted by the model was 70% of the juvenile

chum salmon migrating through Icy Strait during 2001. This discrepancy may be due to higher than the model overestimating metabolic costs.

Given the information on seasonal body sizes of juvenile chum salmon, the existing adult sockeye/pink bioenergetics model likely overestimates growth and the combined juvenile chum adult sockeye/pink model like underestimates growth. Laboratory experiments designed to capture the effect of temperature and size on metabolism and egestion, and excretion are need to further refine the juvenile chum salmon bioenergetics model and provide more accurate predictions of growth.

Acknowledgments

We thank Cara Rodgveller, Erik Husoe, Jacqeline Mitchell, and Angela Feldmann for their assistance with laboratory trials. We also thank Rick Focht and Douglas Island Pink and Chum Inc. for providing juvenile chum salmon. This research was funded in part by the Alaska Yukon Kuskokwim Sustainable Salmon Initiative.

References

Barber, M.C., Suarez, L.A. and Lassiter, R.R. 1991. Modeling bioaccumulation of organic pollutants in fish with an application of PCBs in Lake Ontario salmonids. Canadian Journal of Fisheries and Aquatic Sciences 48:318-337

Beamish, R.J. and Mahnken C. 2001. A critical size and period hypothesis to explain natural regulation of salmon abundance and the linkage to climate and climate change. Progress in Oceanography 49:423−437.

Beauchamp, D.A., D.J. Stewart, and G.L. Thomas. 1989. Corroboration of a bioenergetics model for sockeye salmon. Transactions of the American Fisheries Society 118:597-607.

Boisclair, D. and W.C. Leggett. 1989. The importance of activity in Bioenergetics models applied to actively foraging fishes. Canadian Journal of Fisheries and Aquatic Science 46:1859-1867

Birman, I.B. 1969. Distribution and growth of young Pacific salmon of the genus *Oncorhynchus* in the sea. Journal of Ichthyology 9:651-666.

Boldt, J.L., and L.J. Haldorson. 2002. A bioenergetics approach to estimating consumption of zooplankton by juvenile pink salmon in Prince William Sound, Alaska. Alaska Fisheries Research Bulletin 9(2):111-127.

Brandt, S.B., Mason, D.M., & Patrick, E.V. 1992. Spatially-explicit models of fish growth rate. Fisheries 17**:**23–35.

Brett, J.R. 1964. The respiratory metabolism and swimming performance of young sockeye salmon. Journal of the Fisheries Research Board of Canada 21:1183-1226.

Brett, J.R., J.E. Shelbourn, and C.T. Shoop. 1969. Growth rate and body composition of fingerling sockeye salmon, *Oncorhynchus nerka*, in relation to temperature and ration size. Journal of the fisheries Research Board of Canada 26:2363-2394.

Brett, J.R. 1970. Fish – the energy cost of living. P. 37-52 *In:* W.J. McNeil (ed.). Marine aquaculture. Oregon State University Press, Corvallis.

Brodeur, R.D., R.C. Francis, and W.G. Pearcy. 1992. Food consumption of juvenile coho salmon on the continental shelf off Washington and Oregon. Canadian Journal of Fisheries and Aquatic Sciences 49:1670-1685.

Chipps, S.R., and D.H. Wahl. 2008. Bioenergetics modeling in the 21st Century: Reviewing new insights and revisiting old constraints. Transactions of the American Fisheries Society 137:298–313.

Ciannelli, L., R.D. Brodeur, and T.W. Buckley. 1998. Development and application of a bioenergetics model for juvenile walleye pollock. Journal of Fish Biology 52:879-898.

Cross, A.D., D.A. Beauchamp, J.H. Moss, K.W. Myers, J.L. Armstrong, J.L. Boldt, N.D. Davis, L.J. Haldorson, and R.V. Walker. 2005. Modeling bioenergetics of juvenile pink salmon in Prince William Sound and the coastal Gulf of Alaska. Deep Sea Research II 52:347-370.

Davis, N.D., K.W. Myers, and Y. Ishida. 1998. Caloric value of high-seas salmon prey organisms and simulated salmon ocean growth and prey consumption. North Pacific Anadromous Fish Commission Bulletin 1:146-162.

Farley, E.V., Jr., and M. Trudel. 2009. Growth Rate Potential of juvenile sockeye salmon in warm and cool years on the eastern Bering Sea shelf. Journal of Marine Biology 10p.

Farley, E.V., Jr., J.M. Murphy, B.L. Wing, J.H. Moss, and A. Middleton. 2005. Distribution, migration pathways, and size of western Alaska juvenile salmon along the eastern Bering Sea shelf. Alaska Fishery Research Bulletin 11(1):15-26.

Fry, F.E.J. 1971. The effect of environmental factors on the physiology of fish. P. 1-98 *In:* W.S. Hoar and D. J. Randall (eds.) Fish physiology. Volume 6. Environmental relations and behavior. Academic Press, New York.

Groot, C., Margolis, L. and W.C. Clarke. 1995. Physiological ecology of Pacific salmon. University of British Columbia Press, Vancouver, Canada.

Hanson, P.C., T.B. Johnson, D.E. Schindler, and J.F. Kitchell. 1997. Fish bioenergetics 3.0. University of Wisconsin Sea Grant Institute, Technical Report WISCU-T97- 001, Madison.

Hewett, S.W., and B.L. Johnson. 1992. *Fish Bioenergetics Model 2*: *An upgrade of a generalized Bioenergetics Model of Fish Growth for Microcomputers*. Madison, WI: University of Wisconsin Sea Grant Institute.

Lebrasseur, L.J. 1969. Growth of juvenile chum salmon (*Oncorhynchus keta*) under different feeding regimes. Journal of Fisheries Research Board of Canada 26:1631-1645.

Madenjian, C.P., O'Connor, D.V., and D.A. Nortrup. 2000. A new approach toward evaluating fish bioenergetics models. Canadian Journal of Fisheries and Aquatic Sciences 57:1025-1032.

Madenjian, C.P., O'Connor, D.V., Chernyak, S.M., Rediske, R.R., and O'Keefe, J.P. 2004. Evaluation of a chinook salmon (*Oncorhynchus tshawytscha*) bioenergetics model Canadian Journal of Fisheries and Aquatic Sciences 61:627-635.

Mazumder, A., and J.A. Edmundson. 2002. Impact of fertilization and stocking on the trophic interactions and growth of juvenile sockeye salmon (*Oncorhynchus nerka*). Canadian Journal of Fisheries and Aquatic Sciences 59:1361-1373.

Mazur, M.M., M.T. Wilson, A.B. Dougherty, A. Buchheister, and D.A. Beauchamp. 2007. Temperature and prey quality effects on growth of juvenile walleye Pollock *Theragra chalcogramma* (Pallas): a spatially explicit bioenergetics approach. Journal of Fish Biology 70:816-836.

Moss, J.H., D.A. Beauchamp, A.D. Cross, K. Myers, E.V. Farley, Jr., J.M. Murphy, and J.H. Helle. 2005. Higher marine survival associated with faster growth for pink salmon (*Oncorhynchus gorbuscha*). Transactions of the American Fisheries Society 134:1313–1322.

Ney, J.J. 1993. Bioenergetics modeling today: growing pains on the cutting edge. Transactions of the American Fisheries Society 122:736-748.

Orsi, J.A., E.A. Fergusson, W.R. Heard, D.G. Mortensen, M.V. Sturdevant, A.C. Wertheimer, and B.L. Wing. 2002. Survey of juvenile salmon in the marine waters of Southeastern Alaska, May-September 2001. North Pacific Anadromous Commission Doc. 630. Auke Bay Laboratory, Alaska Fisheries Science Center, National Marine Fisheries Service, NOAA, U.S. Dept. Commerce, 11305 Glacier Highway, Juneau, AK 99801-8626, USA, 51p.

Orsi, J.A., A.C. Wertheimer, M.V. Sturdevant, E.A. Fergusson, D.G. Mortensen, and B.L. Wing. 2004. Juvenile chum salmon consumption of zooplankton in marine waters of southeastern Alaska: a bioenergetics approach to implications of hatchery stock interactions. Reviews in Fish Biology and Fisheries 14:335-359.

Rand, P. S. 2002. Modeling feeding and growth in Gulf of Alaska sockeye salmon: implications for high seas distribution and migration. Marine Ecology Progress Series 234:265-280.

Rice, J.A., and P.A. Cochran. 1984. Independent evaluation of a bioenergetics model for largemouth bass. Ecology 65:732-739.

Shelborn, J.E., J.R. Brett, and S. Shirahata. 1973. Effect of temperature and feeding regime on the specific growth rate of sockeye salmon fry (*Oncorhynchus nerka*), with a consideration of size effect. Journal of the Fisheries Research Board of Canada 30:1191-1194.

Thornton, K.W., and A.S. Lessem. 1978. A temperature algorithm for modifying biological rates. Transactions of the American Fisheries Society 107:284-287.

Trudel, M., D.R. Geist, and D.W. Welch. 2004. Modeling the oxygen consumption rates in Pacific salmon and steelhead: an assessment of circulation models and practices. Transactions of the American Fisheries Society 133:326-348.

Trudel, M., and D. W. Welch. 2005. Modeling the oxygen consumption rates in Pacific salmon and steelhead: Model Development. Transactions of the American Fisheries Society 134:1542-1561.

Tables:

Table 1. Newly estimated parameters representing the temperature and body weight dependence on maximum prey consumption for juvenile chum salmon.

Symbol	Parameter description	Value
CA	Intercept of mass dependence for a 1g fish at the optimum water temperature	0.1298
CB	Coefficient of mass dependence	-0.2881
CQ	Lower water temperature at which the temperature (≤CTO)	3
CTO	Temperature corresponding to 0/98 of the maximum consumption	8.5
CTM	Temperature (≥CTO) at which dependence is still 0.98 maximum consumption	8.5
CTL	Temperature at which dependence is some reduced fraction (CK4)	23
CK1	Lower temperature at which temperature dependence is a small fraction	0.3761
CK4	Maximum consumption rate	0.8923

Figures

Figure 1.

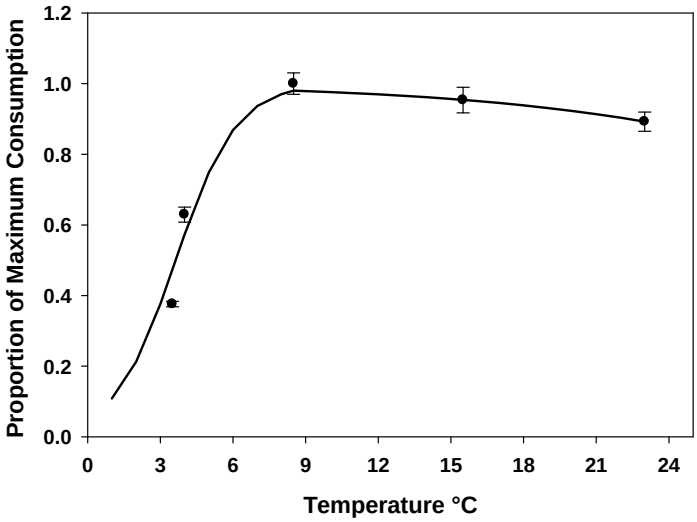

The proportion of the physiological maximum consumption rate for juvenile chum salmon from feeding on mysid shrimp prey over a 20 ºC range in temperature. Data points and error bars (1 SE) represent average maximum consumption estimates obtained from laboratory feeding rate experiments. The cure fit to the data is temperature dependence for cool- and cold water species function obtained from Thorton and Lessem (1978).

Figure 2.

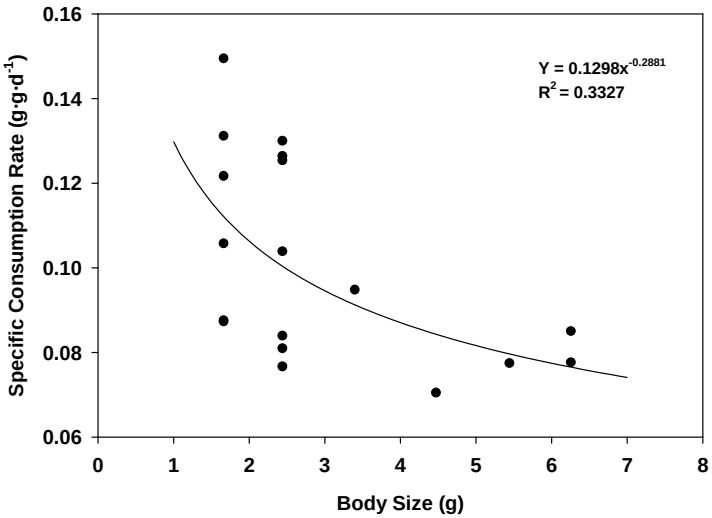

Juvenile chum salmon specific consumption rate estimates generated from maximum feeding rate experiments conducted at 8.5ºC; the temperature at which daily feeding rates were observed to be highest.

Figure 3.

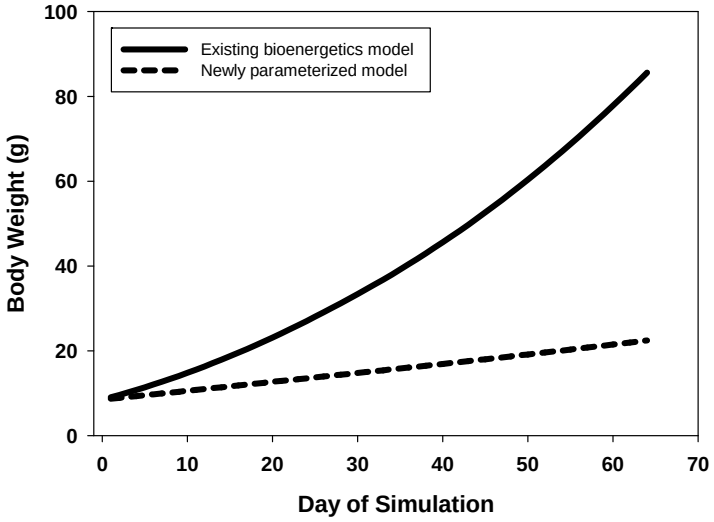

Juvenile chum salmon prey consumption estimates generated using the adult sockeye/pink salmon model (solid line) and with the substitution of the newly estimated temperature and weight dependence parameters for juvenile chum salmon (dashed line). Proportion of maximum consumption was fixed at 1.0 and model input data specific for juvenile chum salmon migrating through Icy Strait July – September 2001 acquired from Orsi et al. (2004).

Appendix 7
Estimates of ocean entry and marine growth rates of western Alaska juvenile chum salmon (*Oncorhynchus keta*) using otolith microstructure and otolith chemistry.

James M. Murphy[1], Edward V. Farley Jr.[1] and Jamal H. Moss[1]

[1] Auke Bay Laboratories, Alaska Fisheries Science Center, NOAA Fisheries 17109 Pt. Lena Loop Rd Juneau, AK

ABSTRACT

Juvenile chum salmon (*Oncorhynchus keta*) otoliths collected during U.S. Bering-Aleutian Salmon International Survey (BASIS) research on the eastern Bering Sea shelf were used to estimate ocean entry dates and marine growth rates of western Alaska chum salmon. Otolith strontium (Sr:Ca molar ratio) was used to separate marine and freshwater growth regions in juvenile otoliths, and daily growth increments were counted within the marine portion of the otolith to estimate ocean entry dates. Average entry dates in the northern shelf region (north of 60°N) were estimated at June 27 in 2006 and July 7 in 2007. Average entry date for juveniles captured in the southern shelf region (south of 60°N) was estimated to be June 17 in 2007. In general, estimates are similar to observed entry dates; however, adequate comparisons to observed ocean entry dates will require information on origin and life-history type. Exponential growth rate models were fit to daily weight-at-age data and marine growth of western juvenile chum salmon was estimated to be 5% body weight per day, similar to growth rates of chum salmon fry in nearshore habitats. The ability of western Alaska juvenile chum salmon to maintain a growth rate of 5% through their first summer at sea likely reflects the importance of longer feeding periods (day lengths) available to western Alaska juvenile salmon.

INTRODUCTION

Chemical and structural features of fish otoliths enable precise reconstruction of age, growth, and migration of fish species (Campana 1999). In anadromous fish species such as juvenile salmon, otolith strontium (Sr) can be used as natural marker of migration between freshwater and marine habitats (Zimmerman 2005, Aria and Hirata 2006). Daily periodicity of otolith increment formation in juvenile chum salmon (Saito et al. 2007) enables daily age and growth studies to be completed on juvenile chum salmon (Volk 1984). Combining otolith microchemistry and microstructure studies provide a powerful tool in reconstructing life-history patterns of chum salmon such as ocean entry timing and marine growth rates of juvenile chum salmon.

Otolith growth is initiated in embryonic fish by the formation of the primordia. Daily metabolic rhythms result in daily growth increments in the otolith, made up of an incremental unit and a check unit (Campana and Nielsen 1985). Increments consist of needle-like aragonite microcrystals of calcium carbonate ($CaCO_3$) precipitated onto the otolith surface within an otolith protein matrix. Checks contain fewer aragonite microcrystals and a higher proportion of organic protein matrix. These chemical differences result in higher light transparency and lower light reflectivity within checks. During periods of active growth, increments are thick with well-defined differences between increments and checks. During slow growth periods, increments are finer with less distinction between increments and checks.

Chemical similarity of strontium and calcium (both are divalent cations) results in the replacement of calcium ions with strontium ions within the $CaCO_3$ crystaline structure of otoliths. Therefore, ambient Sr:Ca molar ratios play a key role in defining Sr:Ca molar ratios

in otoliths (Zimmerman 2005). As Sr:Ca molar ratios are generally higher in marine than freshwater habitats otolith Sr:Ca molar ratios can be used to define the transition between freshwater and marine habitats in anadromous fish species (Zimmerman 2005).

In the following analysis we combine data on otolith microstructure and microchemistry to estimate the time of ocean entry and early marine growth rates of juvenile western Alaska chum salmon. Marine growth rates and the time of ocean entry are key life-history parameters of juvenile chum salmon needed to evaluate how freshwater and marine impact the marine ecology of juvenile chum salmon.

METHODS

Sample collection

Juvenile chum salmon were collected during U.S. Bering-Aleutian Salmon International Survey (BASIS) surface trawl surveys. BASIS surveys were conducted aboard the F/V *SeaStorm* and F/V *Northwest Explorer* in 2006 and aboard the F/V *Sea Storm* and the NOAA Ship *Oscar Dyson in 2007* (Table 1). BASIS survey started on August 14 and ended on September 20 in 2006; and started on August 15 and ended on September 26 in 2007. The trawls used to capture juvenile chum salmon were built by Cantrawl Pacific Limited of Richmond, British Columbia[4], were towed at the surface at an average speed of 4.3 knots with Nor'eastern Trawl Systems 5-m alloy doors, 60-m bridal lengths and included a 1.2-cm mesh liner in the codend.

Surface trawl catches were sorted by species and the total catch in numbers and weight of juvenile salmon were measured at each station. Biological data were collected from all juvenile salmon when catches were below 50 individuals per haul. When catches exceed 50, a

[4] Reference to trade names does not imply endorsement by the National Marine Fisheries Service, NOAA.

random sample of 50 juvenile chum salmon was selected for biological data measurements. Heads were removed from a subsample of juvenile chum salmon and frozen for later removal of otoliths in the laboratory.

Sagittal otoliths were removed, cleaned, rinsed in deionized water and stored dry in micro-centrifuge tubes until thin sectioning. Either the left or the right sagittal otolith was selected for thin sectioning and an additional cleaning step was completed prior to mounting by a brief immersion in 1% hydrochloric acid and mechanical removal of any biological residue using a fine tip dissecting probe followed by a rinse in deionized water. Otoliths were dried in 96 well plates tissue culture plates until thin sectioning.

A total of 1406 chum salmon otoliths were collected during U. S. BASIS surveys in 2006 and 2007 (Table 1). Limited samples sizes of otoliths collected during previous years resulted in their use as training samples in the development of otolith preparation techniques and chemical analysis. A large percentage of otoliths from 2006 were also used as part of the training set, therefore a limited sample size was available for ocean entry analysis during 2006. Otoliths selected for analysis of ocean entry date differed slightly in 2006 and 2007 due to differences in available sample sizes. During 2006, all otoliths not included in the training set were used in the analysis of ocean entry; therefore the 36 otoliths analyzed in 2006 reflect a random sample of juvenile salmon captured during the survey. All otoliths collected in 2007 were available for the analysis of ocean entry and a length stratified subsample was used to select otoliths for the analysis of ocean entry (Table 1).

Otolith preparation and analysis

Thin sections of juvenile salmon sagittal otoliths were prepared for microstructure and chemistry analysis along the sagittal plane. The approach used to complete the thin section is a critical step in the analysis of ocean entry timing. It was obvious from the training otoliths that poor technique will result in significant error in the interpretation of chemistry data and render microstructure of the otolith unreadable or subject to large errors. Otoliths were mounted to petrographic slides using thermoplastic cement (Crystalbond^{TM} 509 Clear) with the medial surface (sulcus-side) down onto petrographic glass slides. The lateral surface of the otolith was ground and leveled along the sagittal plane to the depth of the primordia with a Histolic Precision Grinding Fixture (Buehler Ltd. Lake Bluff, Illinois) and lapped by hand on a LaboPol-21 polishing machine (Struers, Inc., Cleveland Ohio) using 1200 and 4000 grit wet-dry sandpaper under flowing water and briefly polished with 8000 grit micro-mesh polishing cloth.

The primary method used to complete the otolith thin section included flipping and mounting otoliths onto a batch slide with a 1 inch diameter spot size of thermoplastic cement (30 juvenile chum otoliths were mounted to each batch slide). The medial surface was subsequently ground and polished to uniform thickness (approximately 50 microns) using a Histolic slide holder with 1200 and 4000 grit wet-dry sandpaper and polished with 8000 and 12000 grit micro-mesh polishing cloths. Leveling and polishing of the otolith thin section was completed by hand lapping and a digital micrometer to ensure a uniform thickness of the otolith thin section.

Several thin sections from 2007 were also prepared by flipping onto coverslips and completing the thin section on individual otoliths in a manner similar to Zimmerman (2005). Once the thin section was complete, the coverslip, with the thin section, was transferred to a

common batch slide. Otoliths from 2006 were also flipped and the medial surface was thinned to a common reference thickness using the Histolic holder before transferring to a batch slide. Otoliths were flipped a second time when transferred to a batch slide and was ground and polished to the same reference depth to remove the Crystalbond adhesive. This preparation enabled chemistry data to be collected from lateral surface of the otolith and was not continued in 2007 due its sensitivity to variations in slide thickness.

Otolith elemental analysis was completed on an Agilent 7500ce inductively-coupled mass spectrometer (ICP-MS) (Agilent Technologies, Inc. Santa Clara, CA) interfaced with a New Wave UP213 laser ablation induction system (New Wave Research, Fremont, CA) at the University of Alaska's Advanced Instrumentation Laboratory in Fairbanks, Alaska. Prior to analysis the ICP-MS cones were cleaned and the shield torch removed. The sample line from the laser to the ICP-MS was replaced and the New Wave standard ablation sample chamber was cleaned. All ablations occurred in an argon atmosphere. The instrument was tuned for operation by setting the laser power to 100%, sample depth to 5 microns, spot size to 100 microns, pulse frequency to 10 Hz, and a scan speed to 10 microns/second. The ICP-MS instrument response was then tuned using masses 9, 139, and 238 to maximize the signal and obtain stability with the relative standard deviations (RSDs) less than 5%. Doubly charged ions were tuned to less than 0.1% at 119/238, and oxides tuned with 254/238 to less than 5%. Fractionation was monitored on 232/238 and adjusted with tuning parameters to be greater than 70% but less than 100%. The following were typical values for the ICP-MS parameters:

Plasma Conditions	
RF Power	1200 W
RF Matching	1.62 V
Carrier Gas	1.18 L/min
Ion Lenses	
Extract 1	3 V
Extract 2	-97.5 V
Omega bias-ce	-18V
Omega Lens-ce	-0.2V
Cell Entrance	-26V
QP Focus	3V

The ICP-MS was configured to monitor a standard set of otolith isotope masses. These included: Mg^{24}, Mn^{55}, Ca^{42}, Ca^{43}, Sr^{86}, Sr^{86}, and Sr^{88}. Ca^{43}, Sr^{88}, and Mn^{55} isotopes were used in this analysis to estimate molar ratios of strontium (Sr) and manganese (Mn) to calcium (Ca) to correct for ablation effects. Strontium molar ratios (Sr:Ca) were used to identify the transition from freshwater to marine habitats in juvenile chum salmon. Although otolith Sr:Ca molar ratios are not thought to contain enough sensitivity to identify ambient salinity levels, they can be used to reconstruct the timing of chronology of migration in juvenile salmon between freshwater and marine habitats (Zimmerman 2005). Strontium molar ratios, Sr:Ca, (mmol/mol), were defined as:

$$Sr:Ca = \frac{N_{Sr88}}{\alpha N_{Ca43}} * 1{,}000$$

Where N_{Sr88} and N_{Ca43} are the mass spectrometer counts of Sr^{88} and Ca^{43} in the sample, and α (mol/mol) is a calibration term calculated from the NIST 610 standard reference material used to scale the ratio of isotope counts to elemental molar ratios, and is defined as:

$$\alpha = \frac{C_{Ca} W_{Sr} Nstd_{Sr88}}{C_{Sr} W_{Ca} Nstd_{Ca43}}$$

Where $Nstd_{Sr88}$ and $Nstd_{Ca43}$ are the average mass spectrometer counts of Sr^{88} and Ca^{43} in the NIST610 standard, and W_{Sr} and W_{Ca} are the molar weights (g/mol) of Sr and Ca, and C_{Ca} and C_{Sr} are the concentration (ug/g) of Sr and Ca, respectively. NIST certified concentrations of Ca (85,762.9 ug/g) and Sr (515.5 ug/g) (Pearce et al. 1997) and molar weights of Ca (40078 ug/mol) Sr (87620 ug/mol) were used to convert isotope ratios to elemental molar ratios.

Otolith manganese was used as a chemical reference of the otolith center. Ca^{43}, and Mn^{55} isotopes were used to calculate molar ratios of otolith manganese Mn:Ca (mmol/mol) in a manner similar to otolith strontium describe above. Otolith manganese is believed to provide an indicator of physiological development in fish otoliths and can be useful to chemically define the location of the primordia (Brophy et al. 2004). NIST certified concentrations of Mn (485 ug/g) and a molar weight of Mn (54938 ug/mol) were used to convert isotope ratios to elemental molar ratios (Pearce et al. 1997).

Otoliths were ablated with the laser along a transverse (dorsal to ventral) cross-section that passed through the otolith primordia. Identical laser ablation parameters were used on both the otolith and the NIST610 standard. Focal depth of the laser was set a 5 microns below the surface, and the laser output was set at 80% power and pulse frequency of 10 Hz with a round spot size of 25 microns, and a laser speed of 5 microns/sec. Laser transects were pre-ablated at 40% power and pulse frequency of 10 Hz, with a 50 micron spot size, and at a speed of 25 microns/sec. A 30 second laser warm-up time was used as an argon blank prior to sampling and a second argon blank was provided by permitting the ICPMS to monitor isotope levels in the chamber after each otolith was ablated. Isotope counts within both argon blanks were used to estimate background levels of each isotope and background levels were subtracted from the isotope counts of the otolith and standard prior to calculating molar ratios.

Chemical reference points of ocean entry were identified as the location of rapid increase in otolith strontium. The start and end points of the increase in otolith strontium were identified along the ventral and dorsal sections of the otolith, and the otolith center was identified by the spike in manganese. A running median filter (supsmu) was applied to the chemistry data to assist in identifying the position of chemical reference points. The supsmu filter is part of the Splus (TIBCO Palo Alto, California) statistical library. A span parameter of .01 was used which provided a filter of approximately 3 data points). Reference distances of ocean entry were calculated from the otolith center (Mn spike) and from the edge (start of transect). Chemical reference points and microstructure data were combined using a Leica DMD 180 microimaging device (Leica Microsystems, Bannockburn, IL) at 20x and 40x magnification with a polarized light filter. Center reference distances were used to identify ocean entry points on the otolith when a clear center reference was available; otherwise ocean entry points were referenced from the otolith edge. For some otoliths, increments were not countable between the start and end positions of the rapid increase in otolith strontium (assumed to be the time period associated with smolting). When increments were not countable with confidence, an average number of increments during this period was assumed.

Features associated with a marine entry check (Saito et al. 2007) were noted when chemical reference points were added to the otolith microstructure. Entry checks were classified into three categories: 1) no visible entry check, 2) entry check present but not identifiable without the aid of chemistry reference, 3) entry check visible and identifiable.

Exponential growth models were fit to daily weight-at-age data and used to estimate early marine growth rates of juvenile chum salmon. Exponential growth models define growth as:

$W_i = \alpha e^{\beta A_i}$

where W_i and A_i are the weight (g) and age (d) of the ith fish, respectively. The model was log transformed and fit by linear regression as:

$\ln(W_i) = \ln(\alpha) + \beta A_i + e_i$.

The parameter $\beta(x10^2)$ can be used as an estimate of growth rate in units of % body weight per day (Ricker 1979).

RESULTS

Otoliths from a total of 157 chum salmon were analyzed for ocean entry, 36 from collections in 2006 and 121 from collection in 2007. The remaining otoliths collected during 2006 were used as part of the training set. The 121 chum salmon otoliths examined from 2007 were part of a length-stratified subsample of all available otoliths. Otoliths from 2006 were from the northern Bering Sea shelf region (north of 60N and south of 64.5N); otoliths from 2007 were from both the northern and southern Bering Sea shelf regions. Otoliths were collected from approximately 25-30% of the fish processed for biological samples and approximately 10-12% of the otoliths were analyzed for ocean entry.

The location of an abrupt increase in Sr:Ca molar ratios was used as reference point to identify the transition from freshwater to marine habitats (Fig. 1). Sr:Ca molar ratios in nearly all otoliths increased from freshwater reference levels (0.5 to 1 mmol/mol) to marine reference levels (2 to 3 mmol/mol). A number of otoliths contained high strontium levels (2 mmol/mol) during the freshwater period, but strontium levels dropped to typical freshwater reference levels after exogeneous feeding, suggesting the elevated strontium levels were partially due to

maternal contributions. Several otoliths contained asymmetry in Sr:Ca molar ratios, with elevated freshwater Sr:Ca ratios typically along the ventral plane. For these otoliths, reference points were identified on the dorsal plane and ventral reference points were assigned to the same growth increments as the dorsal plane.

Most otoliths contained a spike in Mn:Ca molar ratios in the center of the primordia (Brophy et al. 2004). Absence of a Mn:Ca spike was believed to be the result of otolith preparation. Chemical and visual center reference points were checked by ensuring dorsal and ventral ocean entry points were set to the same growth increments on the otolith; misalignment was often due to the presence of multiple primordia. Mn:Ca molar ratios were also typically elevated just prior to ocean entry and at ocean entry. Elevated Mn:Ca at these locations are believed to be associated with exogenous feeding and smoltification (Fig. 2).

Sr:Ca molar ratios were compared with patterns in otolith microstructure to determine how well the location of ocean entry can be defined using otolith growth patterns. In general, the identification of growth features associated with ocean entry was a particularly challenging task in samples collected during the BASIS survey due to the mixture of stocks present in the BASIS survey as significant stock-specific growth patterns were present. However, the location of salt water entry was readily apparent in growth histories for some chum salmon, particularly in the northern Bering Sea shelf (Fig. 2).

In the northern shelf, 58% of the chum salmon in 2006 and 65% of the chum salmon in 2007 had a visible and identifiable entry check (assumed to be a smolting check) in microstructure growth. An additional 35% of the chum salmon in 2006 and 30% in 2007 had entry checks but required the use of chemistry data to identify its location. Only 6% of the

chum salmon in 2006 and 5% in 2007 did not have a visible ocean entry check in the northern shelf.

In contrast, only 17% had visible and identifiable ocean entry check in the southern Bering Sea shelf. A similar 31% had entry checks that could be identified with the assistance of chemistry data. However, 44% of the otoliths did not have an identifiable entry check. This assignment was subjective and is strictly based on our own interpretation of the clarity of entry check. A focused effort on a single stock would improve the interpretation and identification of entry checks using otolith microstructure.

Microstructure growth increments were assumed to be daily in the chum salmon otoliths analyzed in this study. This assumption was based primarily on the validation of daily increment formation in juvenile chum salmon completed by Saito et al. (2007). Subdaily increments were also present in otoliths. Subdaily increments occurred primarily during the early marine period of rapid growth (shortly after strontium levels reached marine reference levels). Fine-scale adjustments to focal depth while counting increments were used to resolve daily and sub-daily increments. Sub-daily increments were typically more visible on the ventral side of the otolith due to relatively longer ventral axis and wider increment spacing. Counts were made on both the sides of the otolith when there was potential confusion between daily and sub-daily increments.

Resolving daily increments during the very early marine period (between the location where Sr:Ca molar ratios began to increase from freshwater reference levels and the location where they reached marine reference levels) presented some difficulty for some chum salmon otoliths, particularly when a distinct ocean entry check was present in microstructure growth. Counts were not completed in this period unless increments could be clearly resolved. When

increments were not clearly visible, the average increment number within this period was used (average of 11 increments or 11 days). During 2006, increment counts within this region were completed on 75% of the otoliths. During 2007, increment counts were completed on 31% of the otoliths from the southern shelf and 16% of the otoliths from the northern shelf. An unknown level of error is introduced by using an average number of increments during this period, and could introduce bias in the counts if the visibility of the increments is correlated with the duration of this initial marine stage.

Ocean entry dates were calculated by subtracting the total marine increments from the capture date (Table 2). The average number of marine increments in juvenile chum salmon otoliths in 2006 was 74. All otoliths examined for ocean entry during 2006 were from the northern shelf. In 2007, the average number of marine increments in the northern shelf was 79, and the average number of increments in the southern shelf was 85. These counts resulted in an average ocean entry date in 2006 of June 26, and ranged from June 5 to July 12. During 2007, the average ocean entry date in the northern shelf was estimated to be July 4, with a range from June 19 to July 25. The average entry date in the southern shelf was earlier at June 17, with a broad range from May 24 to July 18.

Daily age data were combined with weights to estimate marine growth rates of western Alaska chum through exponential weight-at-age models (Ricker 1979). Given the difficulty in estimating daily increments during the initial smolting period for some juvenile chum salmon, growth rates were calculated for total marine growth (Fig. 3; A) and for marine growth after Sr:Ca molar ratios reached marine reference levels (Fig. 3; B). Marine growth rates were estimated to be 5.1% body weight per day for both growth models. Standard error of the

estimates were similar at 0.34%, and 0.36% body weight per day for total marine growth and for marine growth after Sr:Ca molar ratios reached marine reference levels.

DISCUSSION

Otoliths provide a powerful tool for life-history studies of fish through the analysis of chemical and growth histories (Campana 1999). A clear understanding of growth history is often required to interpret chemical histories; however, chemical histories may also be used to improve the interpretation and understanding of growth histories, such as ocean entry checks in otolith microstructure (Saito et al. 2007).

Preparation of the otolith surface is one of the first critical first steps for both chemical and microstructure growth studies. Significant error can be introduced in the interpretation of both chemistry and growth stemming from the initial otolith preparation stage; a clear understanding of these sources of error is needed to define appropriate tradeoffs of preparation time and the quality of the prepared otolith surface. The batch approach developed for this analysis worked well for the purposes of defining ocean entry but may not necessarily be optimal for other applications. Laser parameters used in this analysis was set up through comparisons of discrete (spots) and continous (transect) sampling completed as part of the training set. However, the training set was completed with the ICP-MS shield torch off resulting in lower sensitivity and lower isotope counts in the training set. With higher sensitivities, optimal spot size for life-history chemical traces may be smaller (7- 15 microns) than the spot size used in this analysis.

Daily increments during the initial marine or smolting period were difficult to resolve in some juvenile chum salmon otoliths, particularly from juvenile chum in the northern Bering Shelf region during 2007. Improved preparation techniques and/or image processing may be required to resolve daily increments during this period. The Leica DMD180 was used not because of the quality of the image or optics but because of the ability to adjust focal depth to resolve increment structure while marking distance references and annotating growth rings. Microscopes with higher quality optics and/or real-time camera displays may be required to resolve increment structure during the initial marine period.

Sr:Ca molar ratios provided a clear signature of ocean entry in nearly all otoliths examined for ocean entry. Maternal contributions to juvenile chum salmon otolith chemistry and/or freshwater strontium levels resulted in elevated freshwater Sr:Ca molar ratios in some juvenile chum; however, Sr:Ca ratios typically dropped to freshwater reference levels at exogeneous feeding. Identification of the relative contribution of freshwater strontium or maternal influence will require additional information on strontium isotope concentrations.

Mn:Ca proved to be useful in establishing a chemical reference point of the primordia (Brophy et al. 2004). It was necessary to validate that the chemical and visual locations of the primordia agreed by ensuring Sr:Ca molar ratio reference points were set to the same growth interval. When visual and chemical reference points of the primordial did not agree it was typically the result of the laser transects crossed multiple primordia. In addition to elevated Mn in the otolith primordia, Mn was also elevated in growth checks occurring at the time period expect for exogenous feeding and ocean entry. Typically the growth checks were to close enough together to prevent them from being identified as separate events. However, when enough sufficient distance (time) was present between the growth checks Mn was

elevated in both periods (Fig 2). If Mn is primarily under physiological control (Brophy et al. 2004), otolith Mn may be elevated during these times periods due to the physiological demand of 'buttoning up' and smoltification.

Due to the mixed stock nature of samples collected during the BASIS survey, the detection and identification of entry checks is subject to a higher degree of error than studies focused on a single stock. Identification rates of entry checks in otolith microstructure is expected to be higher for studies on a single stock (Saito et al. 2007) than the detection rates reported here due to stock-specific growth and life-history patterns. However, it is also true that otolith microstructure growth patterns associated with ocean entry for any one given stock will not necessarily apply to other stocks of salmon.

The higher identification rate of entry checks observed northern Bering Shelf may be associated with unique estuarine habitats of the Yukon River (only 6% did not have an apparent ocean entry check in the northern Bering Shelf, whereas 44% of the chum salmon from the southern Bering shelf did not have an apparent ocean entry check). Chum salmon typically spend up to three weeks in coastal estuarine habitats and are considered second only to Chinook salmon in their estuarine dependence (Salo, 1991). Martin et al. (1987) suggested that the shallow estuarine habitats and high discharge levels of the Yukon River resulted in high dispersal rates of juvenile chum salmon from nearshore estuarine habitats of the Yukon River. Rapid dispersal from freshwater to marine habitats may result in a much more distinctive ocean entry check in juvenile chum salmon from the Yukon River. Martin et al. (1987) also noted that juvenile chum salmon entering marine habitats at smaller sizes and later entry dates were more susceptible to dispersal from coastal estuarine habitats and suggested that summer chum salmon, due to their smaller size and later ocean entry date would be more

susceptible to dispersal from estuarine habitats (Martin et al. 1987). Unique aspects of estuarine habitats of the Yukon River may result in unique smolting processes and early marine growth patterns of Yukon River chum salmon. Similarly, size dependent dispersal rates from nearshore habitats will result in differential nearshore habitat utilization patterns, smoltification, and early marine growth patterns in summer- and fall-type chum salmon. Additional work linking otolith growth and chemistry with genetic stock identification will help clarify life-history characteristics of summer and fall-type chum salmon.

Estimates of average entry date were 10 and 17 days earlier for juvenile chum salmon captured in the southern Bering Sea (June 17) than the northern Bering Sea (June 27 and July 4). Average entry date estimated for the southern Bering Sea was similar to peak outmigration dates observed for the Kuskokwim River (Chris Zimmerman, personal communication). Average entry dates estimated for northern Bering Sea juvenile chum were 9 and 16 days later than the observed peak entry date (June 18) for the Yukon River in 1986 (Martin et al. 1987). Errors associated with increment counts during the initial marine or smolting period could be contributing to underestimates of daily ages of juvenile chum salmon in the northern Bering Sea region. However, changes in the relative production of summer and fall chum salmon could alter average ocean entry dates due to differences in ocean entry dates of the two life-history types (Martin et al. 1987). Similarly, later ocean entry dates could also reflect contributions of chum salmon stocks other than the Yukon if ocean entry dates for other stocks enter the marine environment later than Yukon River chum salmon. Information on origin and life-history type is needed before mixed-stock ocean entry dates estimated here can be adequately compared to observed ocean entry dates.

Estimates of marine growth rate (5% body weight per day) were similar to the range observed for chum salmon fry in nearshore waters (4-6%) (see review by Salo 1991). The ability of western Alaska juvenile chum salmon to maintain a growth rate of 5% through their first summer at sea likely reflects the importance of longer feeding periods (day lengths) available to western Alaska juvenile salmon (Martin et al. 1987).

ACKNOWLEDGEMENTS

Chris Zimmerman and Randy Brown provided assistance and guidance with otolith preparation techniques and with the interpretation of otolith chemistry data from the ICPMS. Karen Spaleta and Ken Severin at the Advanced Instrumentation Laboratory at the University of Alaska, Fairbanks provided support and assistance with the operation of their ICPMS. Luke Carrothers, Matt Keyes, and Nate Bickford provided assistance with the initial otolith training sets. Eric Husoe and Jeanette Gann assisted with otolith extraction and sample management. Angela Feldman, Kris Cieciel, and Lisa Eisner assisted with field collections. Funding support for this work was provided by the Alaska Sustainable Salmon Fund (AYKSSI Projects 45491 and 45557).

LITERATURE CITED

Aria, T., and T. Hirata. 2006 Determination of trace elements on otoliths of chum salmon Oncorhynchus keta by laser ablation-ICP-mass spectrometry. Fish. Sci. 72: 977-984.

Brophy, D., T. E. Jeffries and B.S. Danilowicz. 2004. Elevated manganese concentrations at the cores of clupeid otoliths: possible environmental, physiological, or structural origins. Mar. Biol. 144: 779–786.

Campana, S. E. 1999. Chemistry and composition of fish otoliths: pathways, mechanisms and applications. Mar. Ecol. Prog. Ser. 188:263-297.

Campana, S. E. and J. D. Neilson. 1985. Microstructure of fish otoliths. Canadian Journal of Fisheries and Aquatic Sciences 42: 1014–1032.

Martin, D.J., C.A. Simenstad, D.A. Milward, E.C. Volk, M.L. Stevenson, P. Nunes, M. Savoie, and R.A. Grotefendt. 1986. Distribution, seasonal abundance, and feeding dependencies of juvenile salmon and non-salmonid fishes in the Yukon River Delta. Final Report, Outer Continental Shelf Environmental Assessment Program, Research Unit 660, Dames & Moore, Seattle.

Pearce N.J.G., Perkins W.T., Westgate J.A., Gorton M.P., Jackson S.E., Neal C.R. Chenery S.P. (1997) A compilation of new and published major and trace element data for NIST SRM 610 and SRM 612 partially certified glass reference materials. Geostandards Newsletter: The Journal of Geostandards and Geoanalysis. 21: 115–144.

Ricker, W. E. 1979. Growth rates and models, p. 677-743. *In* W. S. Hoard, D. J. Randall, and J. R. Brett [ed.] Fish Physiology. Vol. 8. Academic Press, New York, NY.

Saito, T., T. Kaga, J. Seki, and T. Otake. 2007. Otolith microstructure of chum salmon *Oncorhynchus keta*: formation of sea entry check and daily deposition of otolith increments in seawater conditions. Fish. Sci. 73: 27-37.

Salo, E. O. 1991. Life history of chum salmon (on…). p. 233-309. In C. Groot and L. Margolis [ed.] Pacific Salmon Life Histories U.B.C. Press, Vancouver Canada

Volk, E. C., R. C. Wissmar, C. A. Simenstad, and D. M. Eggers. 1984. Relationship between otolith microstructure and the growth of juvenile chum salmon (Oncorhynchus keta) under different prey rations. Can. J. Fish. Aquat. Sci. 41: 126-133.

Zimmerman, C. E. 2005. Relationship of otolith strontium-to-calcium ratios and salinity: experimental validation for juvenile salmonids. Can. J. Fish Aquat. Sci. 62: 88–97.

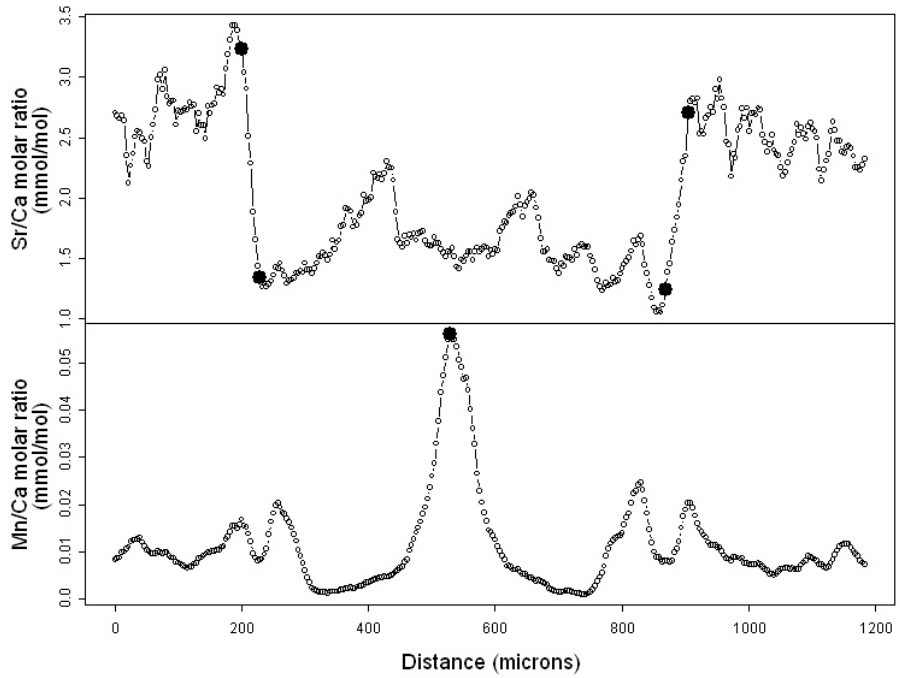

Fig. 1 Otolith molar ratios of strontium (Sr/Ca) and manganese (Mn/Ca) in juvenile chum salmon 547 captured during U.S. BASIS surveys on the eastern Bering Sea shelf. Points highlighted in Sr/Ca molar ratios identify initial marine entry and the point when Sr/Ca ratios reach full marine reference levels. The highlighted point in Mn/Ca ratios identify the chemical center of the otolith associated with embryonic activity. Additional peaks in Mn/Ca are thought to correspond with exogenous feeding and smoltification. The juvenile chum salmon was captured offshore of the Yukon River at latitude 63N and longitude 168W on 9/20/2007 with a fork length of 196 mm.

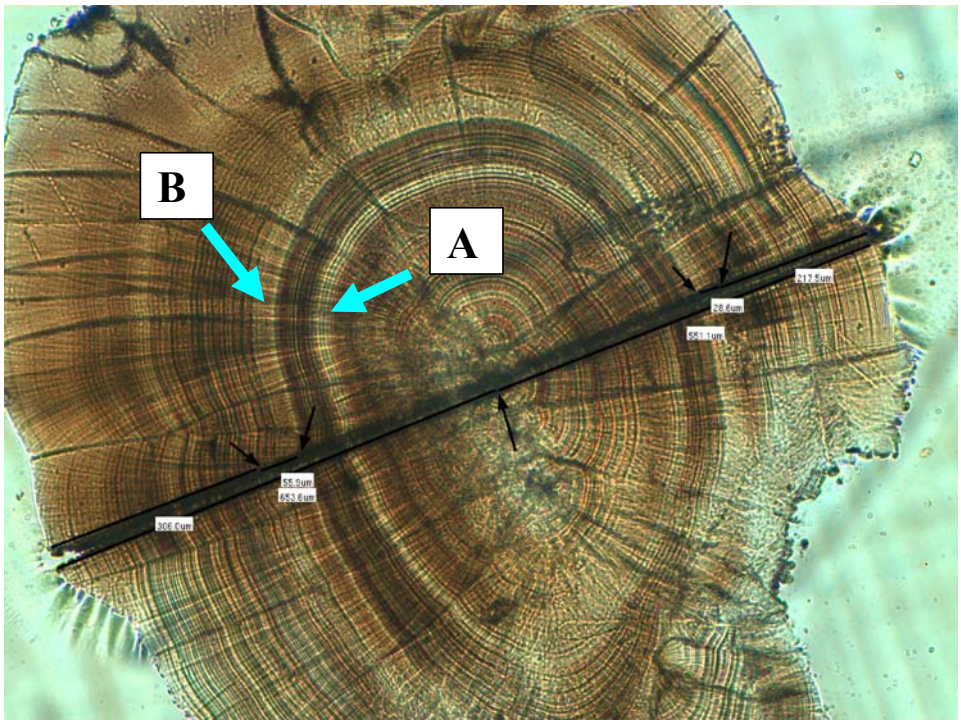

Fig. 2 Otolith microstructure growth patterns of juvenile chum salmon 547 captured during U.S. BASIS surveys on the eastern Bering Sea shelf. Black arrows indicate chemical reference points from Fig. 1 of otolith center (Mn/Ca molar ratios) and start and end of ocean entry (Sr/Ca molar ratios). Large arrows identify ocean entry (B) and exogeneous feeding (A) checks. The juvenile chum salmon was captured offshore of the Yukon River at latitude 63N and longitude 168W on 9/20/2007 with a fork length of 196 mm.

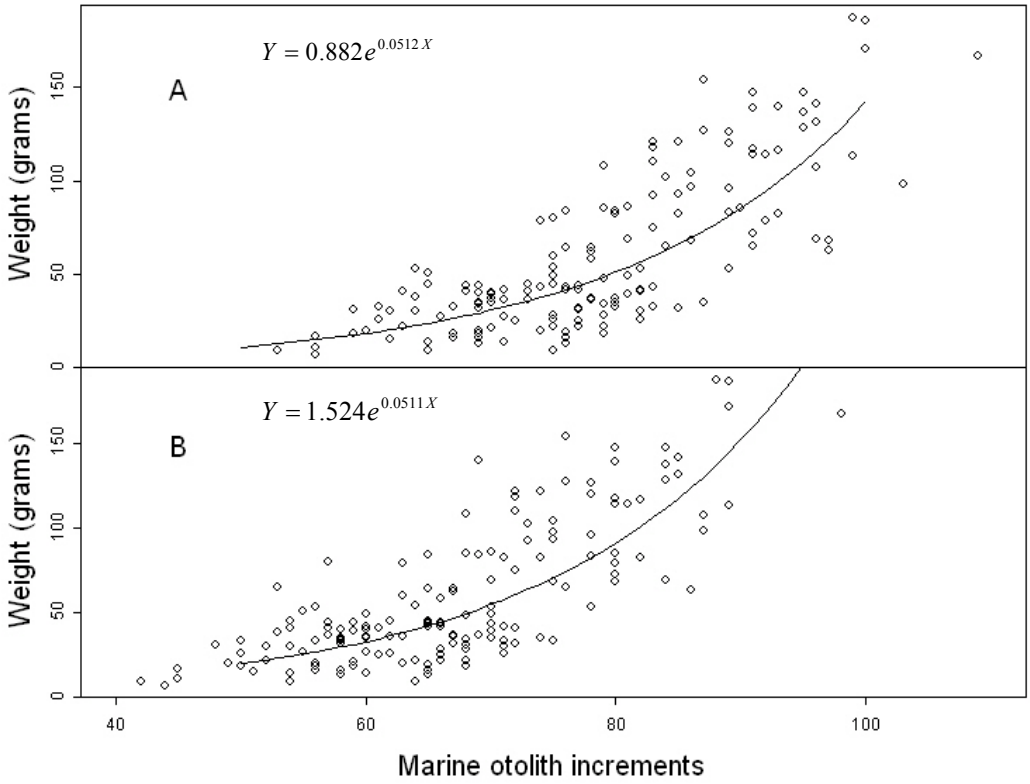

Fig. 3 Relationships between body weight and the number of otolith increments within the marine growth region of juvenile chum salmon captured during U.S. BASIS surveys on the eastern Bering Sea shelf during 2006 and 2007. Exponential growth models are fit to total marine otolith increments (A) and marine increments after smolting (B) or once otolith Sr:Ca molar ratios reach marine reference levels. Assuming increments are deposited at daily intervals, both exponential growth models provide estimates of growth rate of 5.1% body weight per day.

Table 1. Number of surface trawl stations, catch of juvenile chum salmon, number of lengths and otoliths collected, and the number of otoliths used for ocean entry estimates from U.S. BASIS surveys on the eastern Bering Sea shelf by year and region during 2006 and 2007. The eastern Bering Sea shelf was divided into two regions: southern (latitudes less than 60° N) and northern (latitudes greater than 60° N and south of 64.5° N).

Year	Region	Stations	Catch	Length Sample	Otoliths Collected	Otoliths Used for Ocean Entry Estimates
2006	Southern Bering Sea Shelf	113	198	88	33	--
	Northern Bering Sea Shelf	45	1002	586	308	36
	Total	158	1200	647	341	36
2007	Southern Bering Sea Shelf	108	2331	732	508	54
	Northern Bering Sea Shelf	47	1981	731	559	67
	Total	155	4312	1463	1067	121
Total		313	5512	2137	1408	157

Table 2. Lengths, sample sizes, average and standard deviation of the number of marine increments, average sample date and the estimated average, minimum, and maximum ocean entry dates of juvenile western Alaska chum salmon captured during U.S. BASIS surveys on the eastern Bering Sea shelf by year and region during 2006 and 2007. The eastern Bering Sea shelf was divided into two regions: southern (latitudes less than 60° N) and northern (latitudes greater than 60° N and south of 64.5° N). Ocean entry dates are based on the assumption that otolith increments are formed on a daily basis during the first summer at sea. Average values by region in 2007 are a weighted average with weights provided by the length sample size within each length strata.

Year	Region	Fork Length (mm)	Otolith Entry Sample	Length Sample	Average Marine Increments	StDev Marine Increments	Average Sample Date	Average Entry Date	Minimum Entry Date	Maximum Entry Date
2006	Northern Bering Sea Shelf	153.44	36	587	74.00	6.97	9/9/2006	6/27/2006	6/5/2006	7/12/2006
2007	Northern Bering Sea Shelf	140-160	12	137	70.08	7.49	9/18/2007	7/10/2007	6/26/2007	7/23/2007
		160-180	13	129	72.85	5.73	9/21/2007	7/10/2007	6/28/2007	7/25/2007
		180-200	14	164	79.29	5.44	9/22/2007	7/5/2007	6/24/2007	7/20/2007
		200-220	13	212	83.85	4.39	9/23/2007	7/1/2007	6/21/2007	7/13/2007
		220-240	13	80	88.62	5.14	9/22/2007	6/26/2007	6/19/2007	7/3/2007
		240-260	2	9	96.50	3.54	9/26/2007	6/21/2007	6/19/2007	6/24/2007
		Average			78.98		9/21/2007	7/4/2007		
	Southern Bering Sea Shelf	80-120	20	50	66.05	7.65	8/15/2007	6/10/2007	5/28/2007	6/23/2007
		120-160	11	189	74.36	7.45	8/27/2007	6/13/2007	5/24/2007	7/18/2007
		160-200	10	238	90.90	5.47	9/8/2007	6/9/2007	5/20/2007	6/30/2007
		200-240	9	246	93.33	5.83	10/1/2007	6/29/2007	6/11/2007	7/15/2007
		240-280	4	9	101.00	5.83	10/6/2007	6/27/2007	6/20/2007	7/3/2007
		Average			85.87		9/11/2007	6/17/2007		